Design and Development of Gasification Processes in Fluidised Bed Chemical Reactor Engineering

Thesis Submitted to Cardiff University in Fulfilment of the Requirements for the Degree of Doctor of Philosophy in Chemical Engineering-Reactor Design

By

Mohammed Hussein Ahmed Al-hwayzee

B.Sc. Chemical Eng. & M.Sc. Chemical Eng.

School of Engineering - Cardiff University

Cardiff, Wales, United Kingdom

September 2016

DECLARATION

This work has not previously been accepted in substance for any degree and is not concurrently submitted in candidature for any degree.

Signed ……..….. (**Mohammed H. A. Al-hwayzee**) Date 30/09/2016

STATEMENT 1

This thesis is being submitted in partial fulfilment of the requirements for the degree of Doctor of Philosophy (PhD).

Signed ……..…. (**Mohammed H. A. Al-hwayzee**) Date 30/09/2016

STATEMENT 2

This thesis is the result of my own independent work/investigation, except where otherwise stated. Other sources are acknowledged by explicit references.

Signed ……..… (**Mohammed H. A. Al-hwayzee**) Date 30/09/2016

STATEMENT 3

I hereby give consent for my thesis, if accepted, to be available for photocopying and inter-library loan, and for the title and summary to be made available to outside organisations.

Signed ……..…. (**Mohammed H. A. Al-hwayzee**) Date 30/09/2016

ABSTRACT

This thesis focuses on studying and investigation the effects of the hydrodynamic and operating parameters in the air-biomass gasification in a bubbling fluidised bed gasifier under low temperature (<800ºC) conditions and evaluating the potential of the gasification of two solid biomass waste materials, Iraqi date palm wastes and sawdust pinewood. These parameters are air flowrate, particle size of the sand bed material, biomass particle size, static bed height, air equivalence ratio, bed temperature, number of holes in distributor plates and biomass fuel type.

A design study was conducted to provide preliminary data for designing and constructing a large lab-scale fluidised bed column, diameter D=8.3cm, for cold and hot fluidisation experiments. Cold fluidisation experiments were conducted to provide the fluidisation behaviour data for the sand, biomass and their mixture.

The design and cold fluidisation results have shown a compatible finding in the following: 1) the design parameter U_{mf} has shown that, it increases as sand particle size increases. 2) It was not affected by static bed height. In addition, cold fluidisation results show that: sand has a high fluidisation quality compared to pure biomass and sand-biomass mixture and there is no effect of the bed static height on the U_{mf}.

In general, the studied parameters on the air-biomass gasification performance have shown that: 1) air flowrate has a considerable effect, 2) as sand and biomass particle size increases a weakened gasification was achieved. 3) The static height effect has been observed due to the location of the biomass feeding position thereby affecting reactant residence time. 4) For equivalence ratio range (0.2-0.4) the lowest value provided optimum gas composition and LHV values, whereas the highest value ER= 0.43 provided highest (CCE), CGE) and (GY). 5) No significant effect was seen for bed temperature between 360 to 465ºC. 6) A considerable effect has been shown for the distributor plate configuration.

Finally, the results has shown that SPWB has potential compared to IDPWB for energy generation. However, additional simulation, optimization and experimental studies on the bubbling fluidised biomass gasification for a broad range of operating and hydrodynamic parameters are hereby suggested.

DEDICATION

To my Imam Al Hujjah Ibnu Alhassen (ajtf)

I am your soldier

To my parents ……

To my wife ….. my love

To my lovely daughters…..

Safa, Amenah, Nusk and Gherked

To my brothers and Sisters

ACKNOWLEDGEMENTS

Foremost, I would like to praise and thank my GOD (ALLAH) for helping me to complete this thesis.

I would like to extend my thanks to the Iraqi Government-Ministry of Higher Education and Scientific Research, in particular Kerbala University for granting the opportunity to study and complete the PhD. Thanks for the staff of the Iraqi cultural attaché in London for their help during my stay in the UK.

The words are not sufficient to express my gratefulness and deepest thanks to my supervisor, Dr. Richard Marsh for his continuous supervision, positive discussions, important ideas through this research work and his various support along my study. Again I repeat my grate thank for him.

I would like also to thank the staff of School of Engineering and the staff of the Mechanical Engineering Work Shop. Special thanks for Mr Malcolm Seaborne and other technical staff for their technical supports during experimentation. My thanks for Dr. Julian Steer for his help and support.

I must also thank Mr Hussein, the director of the project of the Organic Fertilizer Preparation and Mushroom Cultivation - Karbala City-Iraq and other staff for their help for providing my research an Iraqi date palm wastes biomass material IDPWB.

I wish also to thank all the staff of the Research Office, Finance Office and the IT staff in School of Engineering for their help during my study period.

I would like to present my thanks for the staff of the Cardiff University Student Support for their helps and advice.

I am greatly indebted to my devoted wife. My gratefulness for her love, care, encourage, support, patience in best and worse conditions. My, thanks to my lovely daughters Safa, Amenah, Nusk and Gherked who have suffered the most during my absence in their most needed times. My apology for them.

Finally, my deepest thanks and gratitude to my big family, brothers, sisters and my relatives for their helps, supports and prayers.

TABLE OF CONTENTS

Contents

LIST OF ABBREVIATIONS

BFB	=	Bubbling Fluidised Bed	
BFBG	=	Bubbling Fluidised Bed Gasifier	
BFBR	=	Bubbling Fluidised Bed Reactor	
BSI	=	British Standard International	
CC	=	Carbon Conversion	
CCE	=	Carbon Conversion Efficiency	%
CGE	=	Cold-Gas Efficiency	%
CFB	=	Circulating Fluidised Bed	
CFBC	=	Circulating Fluidised Bed Combustor	
CFBG	=	Circulating Fluidised Bed Gasifier	
CFBR	=	Circulating Fluidised Bed Reactor	
CH_4	=	Methane gas	
CO	=	Mono carbon oxide	
CO_2	=	Di-carbon oxide	
db	=	Dry basis condition	
DCFB	=	Dual Circulating Fluidised Bed	
EFB	=	Empty Fruit Branch	
ER	=	Equivalence Ratio	
FCFB	=	Fast Circulating Fluidised Bed	
Ga	=	Galileo number	
GSR	=	Gasifier Solid Residue	
GY	=	Gas yield	Nm^3db/kg feed
H_2	=	Hydrogen gas	
H_2O	=	Water	
HHV	=	High Heating Value	MJ/Nm^3db
ICE	=	Internal Combustion Engine	
IDPWB	=	Iraqi date palm waste biomass	
LHV	=	Low Heating Value	MJ/Nm^3db
MAFR	=	Mass Air Fuel Ratio	
$(MAFR)_{actual}$	=	Actual Mass Air Fuel Ratio	
$(MAFR)_{stoichio}$	=	Stoichiometric Mass Air Fuel Ratio	
N_2	=	Nitrogen gas	
O_2	=	Oxygen gas	
PGC	=	Producer Gas Composition	
R1-R16	=	Reaction Number	
S/B	=	Steam to biomass ratio	
SPWB	=	Sawdust pinewood biomass	
T	=	Temperature	
TGA	=	Thermo Gravimetric Analysis	
TWH	=	Tera Watt-hour	

NOMENCLATURE

ALPHABETIC SYMBOLS

A, A_c	=	Cross-sectional area	
Ar	=	Arechimed	dimensionless
C1, C2	=	Constants	
D, *D*	=	Fluidised bed column diameter	mm, cm, m
dp	=	Particle diameter	µm, mm
$\bar{d}_p$	=	Mean particle diameter	µm, mm
g	=	Acceleration gravity	cm/s^2, m/s^2
H	=	Height of the total fluidised bed (bed + freeboard)	mm, cm, m
H_s	=	Static bed height	mm, cm, m
L, L_m H_s	=	Height of the fixed (static)bed	mm, cm, m
L_f , H_f	=	Height of the bed at fluidisation conditions	mm, cm, m
L_{mf}, H_{mf}	=	Height of the bed at minimum fluidisation	mm, cm, m
K1, K2	=	Constants	
$\dot{m}_{biomass}$	=	Biomass mass rate	g/min, kg/hr
$\dot{m}_{air}$	=	Air mass rate	g/min, kg/hr
N_{dens}	=	Orifice density= No of orifices in distr. plate/A_c	N_{orf}/cm^2
N_{orf}	=	No of orifices (holes) in distributor plate	
R	=	Universal gas constant = 8.314	m^3 .Pa/^{o}K.kmol
$Re_{p.mf}$	=	Particle Reynold number at minimum fluidisation	dimensionless
t_{distr}	=	Thickness of the distributor plate	cm, mm
t	=	Time	s, min, hr
Tset	=	Setting Temperature of gasifier heater and air-	^{o}C
T_{preset}		Setting Temperature of air-preheater	^{o}C
U_b	=	Bubble rise velocity	cm/s, m/s
$U_{b,ms}$	=	Bubble rise velocity at slugging regime	cm/s, m/s
U_{fi}	=	Initial fluidisation gas velocity	cm/s, m/s
U_{mb}	=	Minimum bubbling gas velocity	cm/s, m/s
U_{mf}	=	Minimum fluidisation gas velocity	cm/s, m/s
U_{ms}	=	Fluid velocity at which the slugging regime occurs	cm/s, m/s
U_o	=	Superficial gas velocity	cm/s, m/s
U_t	=	Particle terminal velocity	cm/s, m/s
$\dot{V}_{air}$	=	Air volumetric flowrate	cm^3/s, m^3/s

GREEK SYMBOLS

α	=	Volume of the wake per volume of bubbles	dimensionless
δ	=	Fraction of the total bed occupied by the bubbles	dimensionless
ΔP_{bed}	=	Pressure drop across the bed	mbar
ΔP_{distr}	=	Pressure drop across the distributor plate	mbar
ε, ε_s	=	Voidage of the static bed	dimensionless
ε_{mf}	=	Voidage of the bed at minimum fluidisation	dimensionless
ε_f	=	Voidage of the bed at fluidisation conditions	dimensionless
μ	=	Fluid dynamic viscosity	Kg/m.s
ρ_f	=	Density of fluid	g/cm^3, kg/m^3
ρ_g	=	Density of gas	g/cm^3, kg/m^3
ρ_s, ρ_p	=	Density of solid particle	g/cm^3, kg/m^3
ρ_b	=	Bulk density of the solid material	g/cm^3, kg/m^3
ϕ_s	=	Particle sphericity	dimensionless

Chapter 1

Introduction

1.1 Background

The expansion of human activity since the Industrial Revolution has increased for fossil type energy sources, especially petroleum derivatives due to their easy transport and storage. Given that fossil resources have been formed over millions of years, it is not possible to replenish its reserves especially if compared to the current of consumption rate, so this type of energy is considered non-renewable. Recent crises have included fuel prices, depletion of this fuel in the near future, problems of the pollution of the environment and rising surface temperatures, known as global warming. All the above have been causing great concern for humanity and promoting many countries in the world represented by developed countries to move to reduce these environmental problems. This has included prioritisation of renewable and environmentally clean energy sources to protect the planet and to avoid possible human catastrophe. Although many of these countries possess fossil fuel energy such as oil, natural gas and coal, the impacts of climate change should be mitigated including the use of renewables. These renewable energy sources include solar energy, wind energy, hydro energy, underground thermal energy and biomass. Bioenergy includes bio-ethanol alcohol (biofuels) which can be produced from the fermentation of sugars, starches and other plants, biodiesel which can be produced from vegetable oil (such as soybeans) and biogas which can be produced from plants, sewage waste, as well as wood and cellulosic material combustion as a source of thermal energy.(Demirel 2012)

Global studies generally indicate that the countries of the world are generally moving towards the use of renewable energy, particularly biomass energy, which has nowadays become a strong alternative and considered a new effective source of energy. As stated in the International Energy Agency report in 2009, bioenergy accounted about 68.6% of the total primary energy consumption in the renewable energy domain and this, in turn, accounted for about 9% of the total primary energy overall amenities. This means that biomass formed 6.2 % of that total as shown in Figure 1.1(Eea 2011) , while in 2012, this percentage became about 10% (International Energy Agengy 2014)

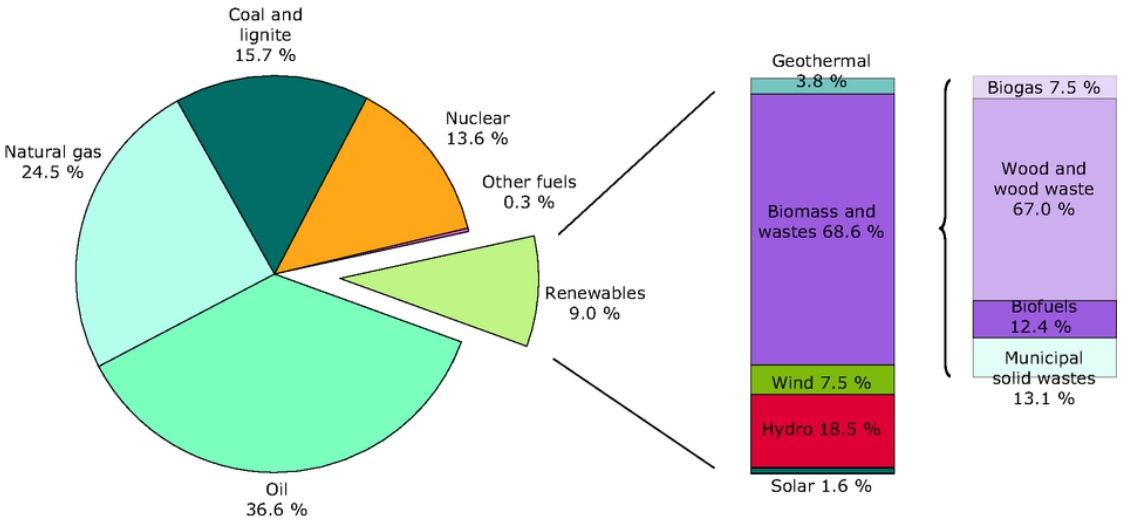

Figure 1. 1 Total primary energy consumption by energy source in 2009, EU-27 (Eea 2011)

The study provided by the International Energy Agency on the entire global consumption for the use of biomass energy in the production of electric stated that the global energy consumption in 2009 was 290 TWh, equivalent to 1.5% of world electricity production. In addition, according to the study forecasts this percentage will increase each year slightly until it expected to be 7.5% in 2050, which correspond 3100 TWh (Eisentraut and Brown 2012).

As mentioned above, climate change is one of the largest environmental risks. It has occurred as a result of increase greenhouse gas emissions since the beginning of the Industrial Revolution. These emission gases are mostly composed of water vapour, carbon dioxide, methane, nitrous oxide, ozone, which play a major role in the Earth's surface heating. One of the advantages uses of biomass fuels that they do not lead to an increase in the greenhouse gases, where plants absorb carbon dioxide in the atmosphere by photosynthesis and when they are burned so they come out the same amount that has been absorbed (Demirel 2012)(Basu 2010). This is called carbon cycle as shown in Figure 1.2. Therefore, the cultivation of plants leads to the closure of the carbon cycle, and hence there is no increase in carbon dioxide levels in the environment.

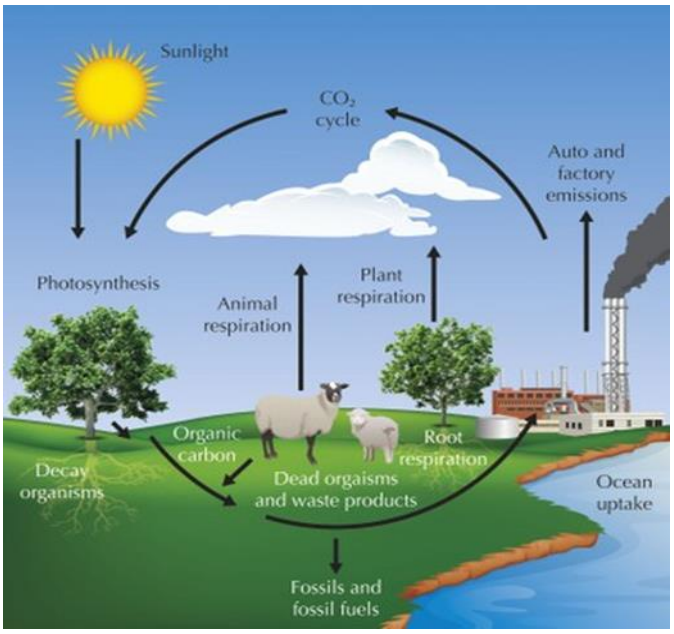

Figure 1. 2 The carbon cycle (http://thefrogpad.weebly.com/general-ecology.html," n.d.)

The stored chemical energy in biomass material can be released as heat by combustion. Biomass can also be converted to producer gases by gasification, partial oxidation, or by pyrolysis with no oxidation. These producer gases can be used as fuel for energy generation and for the creation of new chemical compounds for example in Ficher-Tropsch synthesis. There are three thermal-chemical conversion process mainly, combustion, gasification and pyrolysis processes.

1.2 Gasification and biomass gasification

Gasification technology is a thermo-chemical process that can convert biomass fuels such as crop residues, sewage sludge and municipal wastes into a fuel gas which could be utilised for applications including electricity generation, heating and chemical products. The gasification process is a partial oxidation reaction, which can convert a solid biomass fuel to a gaseous fuel using an air-fuel ratio less than 1 at specific conditions of temperature and pressure. Many chemical reactions occur at high temperature and at specific equivalence ratio, air fuel ratio, throughout this process leading to the final desired product (Christopher Higman 2003).

Biomass gasification process can be categorised in three processing steps: upstream processing step, (which includes biomass reduction size, drying and preparation of gasifying agents), gasification process step, and downstream process step, (which includes producer gas clean-up and reforming and gas utilisation). (Kumar et al. 2009).

The process step of the biomass gasification is the heart of the process. It includes thermal-chemical conversion of biomass fuel to an energy rich combustible gaseous product in controlled conditions using different gasifying agents such as air, O_2-air, O_2, air and/or steam and air and/or CO_2. Unlike the combustion process where biomass oxidation is completed in one-step, the biomass fuel in the gasification process undergoes a series of physical transformation process and chemical reactions within the gasifier. These processes are shown in Figure 1.3-a and b:

- **Drying:** Where the moisture content of the solid biomass fuel evaporates, leaving dry biomass and releasing steam which may contribute in later chemical reactions.
- **Pyrolysis:** This occurs when the solid biomass is exposed to elevated temperature in the gasifier. Volatile materials are released by the pyrolysis process, which precedes the gasification process, at low temperature (350-700^{o}C) as initial biomass conversion. This step includes devolatization of volatile materials and thermal breakdown of weaker chemical bonds of larger hydrocarbon molecules in solid biomass. The low temperature volatile vapours consist of gaseous species mainly hydrogen and methane, large condensable molecules (phenol and acids) called primary tars, which are characterised by oxygenated compounds that give the primary tar its high reactivity, and a solid chars (a material containing mainly coal and ash). In the presence of a gasifying agent and a relatively high temperature environment (700-850 ^{o}C), secondary gas-phase reactions including (cracking, reforming, combustion, and CO shift) of primary tars are initiated producing combustible gases and secondary tars (phenolic and olefins). At higher temperatures (850-1000^{o}C), tertiary conversion of secondary tars to **p**oly **a**romatic **h**ydrocarbons (PAHs) also occur and soot formation is observed (Morf et al. 2002)(Piriou 2009).
- **Combustion:** Within the gasification environment some of the char and of the volatile products combust partially with a limited amount of oxygen to produce CO_2, CO, H_2O and the required heat to sustain the gasification reactions.
- **Gasification:** where char residues, pyrolysis tars (primary, secondary and tertiary tars) and pyrolysis gases are partially oxidised at high temperature (600-1500^{o}C) using the required gasifying agents to produce a producer gas mainly hydrogen (H_2), carbon monoxide (CO), carbon dioxide (CO_2), methane (CH_4) and traces of ethane and propane. Also, char and tar are the result of incomplete reaction of biomass (Chhiti and Kemiha 2013) .

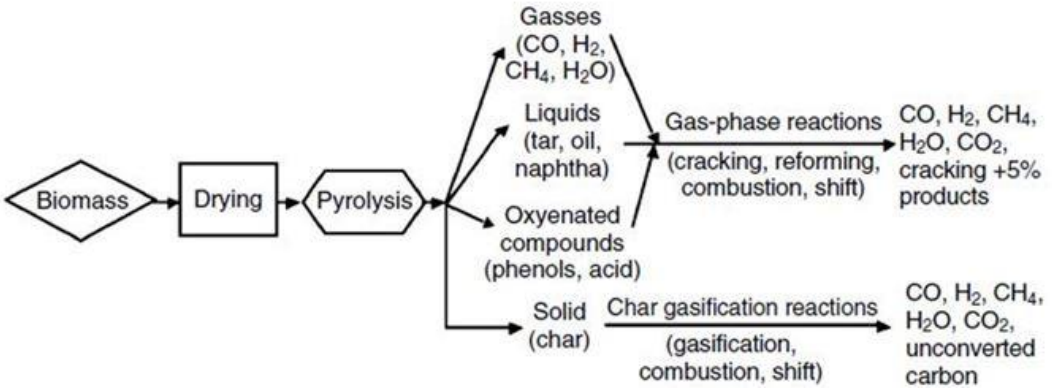

a) Process sequence for gasification of biomass solid fuel (P. Basu2010) (Christopher Higman 2003)

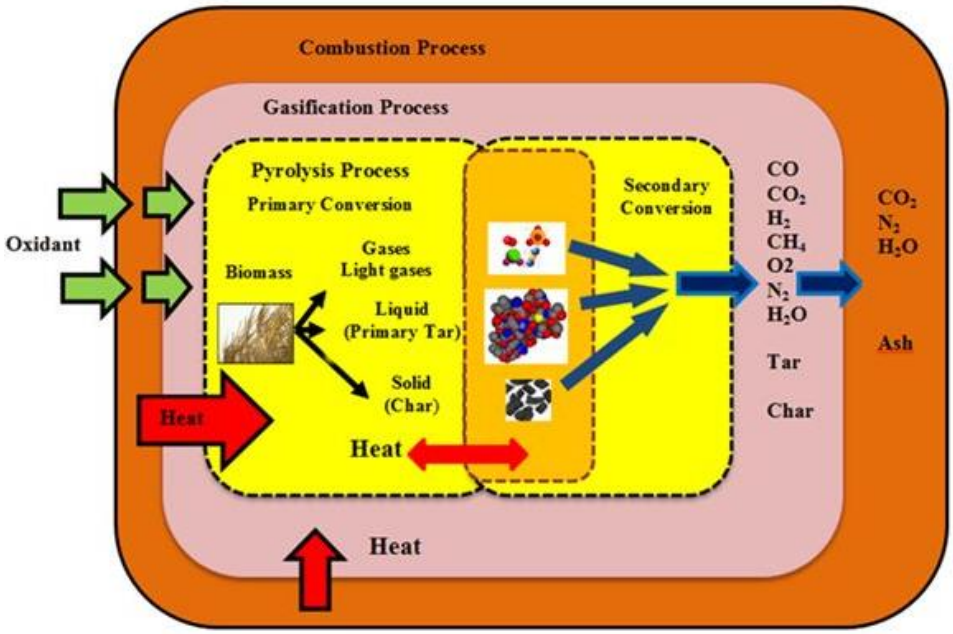

b) Schematic representation of three thermochemical process (Redrawn)-(Arena 2012), (Gómez-barea et al. 2011).

Figure 1. 3 Schematic of biomass gasification process (a and b)

As mentioned above, during the gasification step different thermal process are taking place. In addition, depending on operating conditions, several exothermic and endothermic chemical reactions take place in the gasifier. Due to the reversibility of the gasification reactions, the direction of the reaction and its conversion require a knowledge in thermodynamic and reaction kinetics. The thermodynamic equilibrium of the gasification reactions imposes a high effect on the thermal efficiency and the producer gas composition.

1.3 Fluidised Bed Reactors

Chemical reactors are used in chemical processes to convert raw materials to new product materials at specific conditions, such as temperature, reactants concentration and pressure. There are different types, configurations and designs of reactors depending on the nature of the process and the factors affecting the process efficiency. One class of these reactors is the fluidised bed reactor, which is used in gas-solid reactions especially in a process involving a thermo-chemical conversion process. In the last ten years, fluidised bed reactor technologies have generated research interest in biomass gasification processes because of advantages in temperature uniformity and control, excellent fuel flexibility and high heat and mass transfer rates (Alauddin et al. 2010)(Siedlecki et al. 2011).

Basically, fluidised bed is a packed bed through which fluid flows at such a high velocity that the bed is loosened and the particle-fluid mixture behaves as though it is a fluid. Thus, when a bed of particles is fluidised, the entire bed can be transported like a fluid, if desired. This phenomenon has been utilised to obtain excellent contact of the solid and fluid and the solid and wall due to a vigorous agitation. This condition means that nearly uniform temperatures through the bed, high heat and mass transfers and high reaction rates (for process with chemical reaction) can be maintained. For these reasons thermochemical processes such as solid biomass and coal gasification, combustion and pyrolysis have been carried out using fluidised bed reactors (Basu 2006) (Christopher Higman 2003).

In the case of a fluidized bed gasifier the fuel, solid fuel biomass or coal, is gasified in a bed of small particles (inert or catalytic bed material or both) fluidized by a suitable gasification medium gas. There are two principal types of fluidised bed gasifier; bubbling fluidised bed and circulating fluidised bed, which are presented in Chapter 2 in details.

1.4 Energy in Iraq

Energy resources in Iraq mainly rely on fossil fuels including predominantly oil, followed by natural gas. Iraq is the world's third-largest oil exporter. Iraq ranked fifth and thirteenth in the sequence of the world's oil and natural gas reserves, respectively. Sources of energy available from fossil fuels are considered the mainstay of the Iraqi economy where the export of oil is currently constituted 95% of state revenue. At the

moment, all sectors such as electricity, industry, transport, buildings rely mostly on fossil energy sources mainly oil.

According to the central scenario presented by the International Energy Agency on energy in Iraq as shown in Figure 1.4, 90% of Iraqi electricity comes from fossil energy sources, oil and gas. The remaining 10% is from renewable energy i.e. hydropower represented a contribution of 5 TWh and will contribute 5% in 2035, while for solar energy the scenario considered that this energy would contribute 50MW in 2035. With regard to wind and biomass energies, the scenario reported that the wind speed in Iraq is relatively low, and the resources of biomass material are moderate so the scenario and within the study period this was not considered on a large scale.

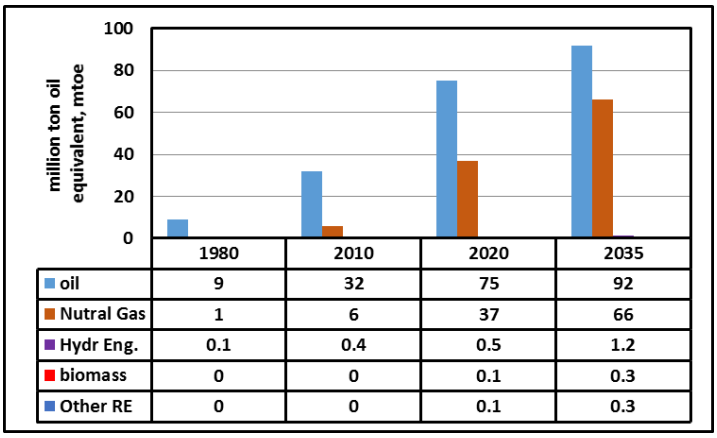

	1980	2010	2020	2035
oil	9	32	75	92
Nutral Gas	1	6	37	66
Hydr Eng.	0.1	0.4	0.5	1.2
biomass	0	0	0.1	0.3
Other RE	0	0	0.1	0.3

Figure 1. 4 Primary energy demand by fuel in Iraq, in million ton oil equivalent (International Energy Agency 2012)

So according to this scenario, the contribution of renewables will be small compared to the fossil fuels oil and natural gas. Given the high carbon emissions from Iraqi's industries, the desire of the main sectors to decrease their dependency on fossil fuels and to make use of renewable energy resources, many official research centres have been recently established in Iraqi ministries to upgrade the Iraqi contribution in renewable energies. These ministries are the ministry of electricity, ministry of industry and minerals and ministry of higher education and scientific research.

1.5 Iraqi Biomass Energy-Date Palm Wastes

The wastes and residues of plants and other agricultural products can be considered as biomass resources. The date palm wastes are one of these biomass wastes. Since Iraq is the original palm frontrunners and is one of the Arabic countries in the production of

dates, it is logical that Iraq should take serious steps towards bio-energy sources from date palm trees.

Iraq has suitable climate conditions for this tree cultivation. Palm trees are usually tall (tall stem), with no branches, and enormous leaves, or fronds, at their tops as shown in Figure (1.5). Date palms can be grown on large tracts of land and vast stretches of middle to the south of Iraq.

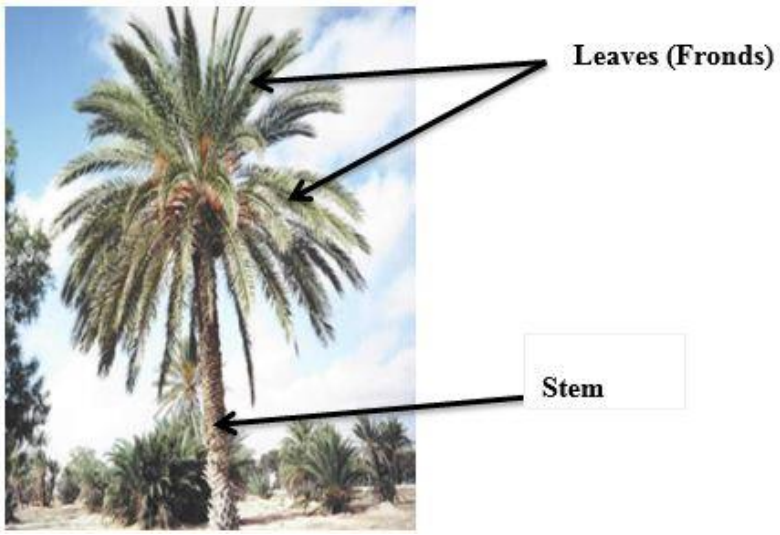

Figure 1. 5 Single date palm tree showing its stem, leaves (fronds).

Statistical studies indicate that Iraq possesses large numbers of date palm trees. A study published by Dr. Abdul-Basit Auda, (Anon 2011c) reported that Iraq has a wide production of these tree approximately 16 million trees and are distributed in many Iraqi states as shown in Figure 1.6 (Anon 2011c). Also, the date palm tree of old trees can be short-lived to about 100 years and more (Ali 2010).

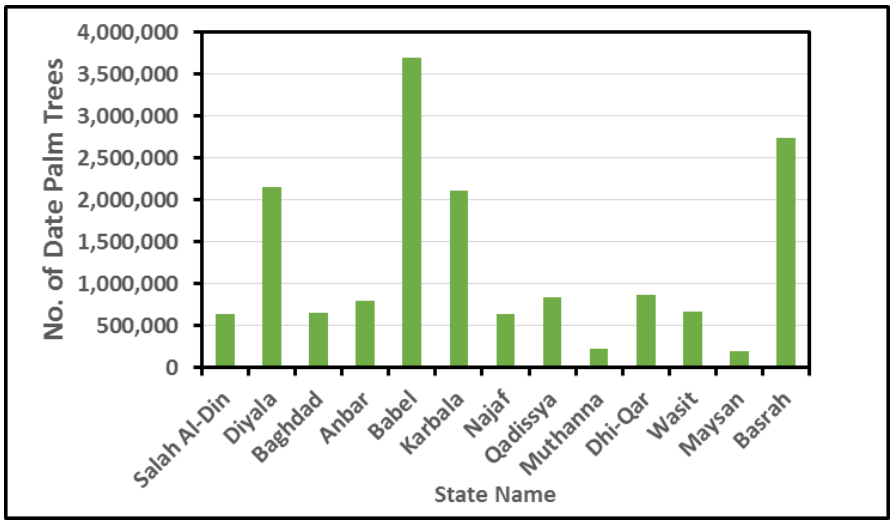

Figure 1. 6 Production of Iraqi date palm trees by states in Iraq in1998 (Anon 2011c)

Studies reported that the single one date palm tree like any tree need to be cleaned and pruned once a year, leaving significant amounts of wastes, approximately 25-50 kg per tree. These wastes are; dry leaves, leaf bases, fibres generated as a result of the growth, as well as parts bearing the fruit (date) of the palm, which is called raceme, as shown in the images below, Figure 1.7 (AHMED F. ZABAR 2012). In Iraq, in the past, the dry waste of these residues is not considered to have significant economic value. They were destroyed by burning or utilising as fuel in cooking operations and some local industries. Sometimes their stems was used in house roofs building. All these above factors enhance the sustainability of using these Iraqi date palm wastes.

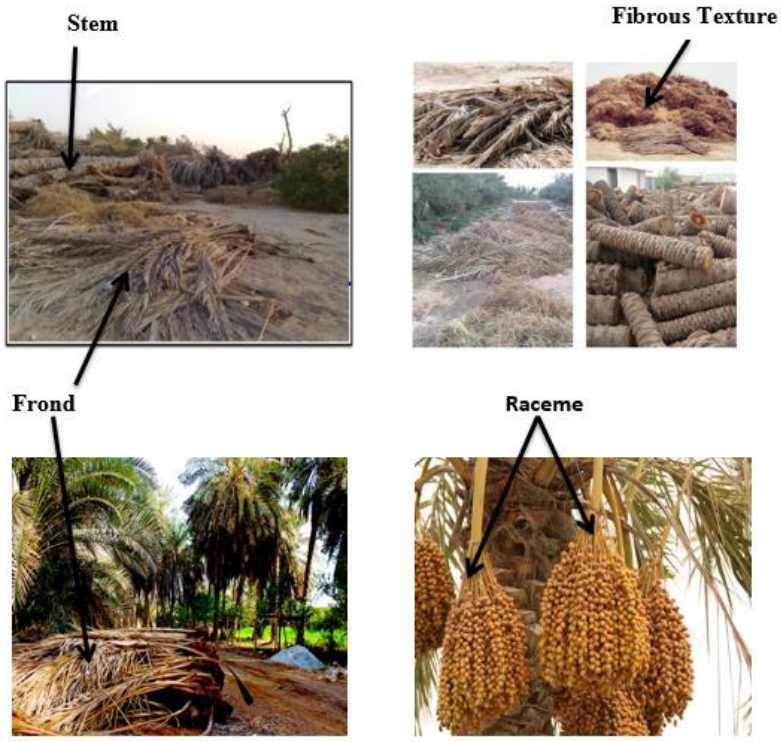

Figure 1. 7 Waste materials of Iraqi date palm trees

In recent years, the Iraqi government represented by Ministry of Agriculture has tried to take advantage of these wastes and residues as much as possible for using as an organic fertiliser. Some of the research centres have been established for this purpose. These centres currently cover only a small percentage of these wastes compared to the large quantities of such waste.

It can be concluded that these Iraqi date palm residues can be preliminary considered as one of the varieties of the biomass solid fuel which can be utilised to obtain a clean gaseous fuel in Iraq which can be used in many fields and applications, thereafter it will be one of those major biomass renewable energy sources. In order to see the feasibility

of these residues in biomass gasification, these residues were chosen as one feedstock material in this study.

1.6 Motivation and Aims

The design and development of low-carbon gasification processes are still at immature stages. There is still a lot of basic scientific information lacking in the technical literature. This study will be concerned with the investigation of fluidization parameters on biomass gasification in order to produce fundamental data for the enhanced understanding of fluidised bed gasifier design. The principal aims of this study are:

1) To provide a basic database for air bubbling fluidised bed biomass gasification.
2) To design and develop an air fluidised bed gasifier.
3) To study the effect of the bubbling fluidised bed hydrodynamic parameters on the gasifier performance.
4) To evaluate the feasibility of the Iraqi date palm residues as a biomass feedstock in biomass gasification and hence will contribute to support renewable bioenergy in Iraq.
5) To evaluate the gasifier performance at low gasification temperature.

1.7 Research Hypothesis

The drive to increase renewable energy production and displace the use of fossil fuels has caused an increase in interest in biomass gasification. The performance of the biomass gasification reactors to obtain high quality syngas still needs further development and modification. The fluidised bed reactor, especially the bubbling fluidised bed reactor, is one of these reactors that should be studied for improvement in terms of operating method and energy consumption. This study aimed to deal the following research hypotheses:

(a) Designing, building and constructing a hot air bubbling fluidised bed gasifier close to a pilot plant scale, rather than lab-scale, to give a practical indication for industrial gasifier performance.
(b) Studying the hydrodynamic parameters of the bubbling fluidised bed gasifier in isothermal conditions i.e. as a cold fluidised bed to provide primary data for fluidised operation under hot gasifying condition.
(c) Using Iraqi date palm biomass wastes comparing to sawdust pinewood material, which is an abundant biomass material in UK and its high chemical specifications

enhance its potential using in gasification processes as a feedstock biomass material. This will give a reliable indication to use the Iraqi date palm wastes as a biomass material source for renewable energy generation in Iraq.

(d) Whether the number of holes in perforated distributor plate, expressed as a distributor open area, has any effect on the bed hydrodynamic and consequently on the gasifier performance.

1.8 Layout of the thesis structure

The following Chapters have structured the thesis:

Chapter 1: In this chapter, the general overview on the energy conservation and climate change are highlighted. Energy resources are discussed, and alternative approaches to reducing sources contributing to the climate change are presented. The aims of the current research, hypotheses and thesis structure are also described.

Chapter 2: In this chapter, the overview on the biomass gasification is provided. Factors affecting gasification process, gasifier performance and syngas quality are discussed in detail. The development of the fluidised bed reactor from coal feedstock to biomass is highlighted. In addition, Factors affecting minimum fluidisation velocity are discussed as well.

Chapter 3: This chapter presents the theoretical design of the experimental rig especially the fluidised bed gasifier, air box section, distributor plate section and reactor bed and freeboard sections. Design equations and steps of design calculations for these sections are also presented.

Chapter 4: In this chapter, the materials and methods of characterisation that were performed on the biomass materials, pine wood sawdust and Iraqi date palm residues, and quartz sand are described. In addition, all equipment and accessories for cold and hot rigs are presented.

Chapter 5: This chapter details the experimental layout and describes procedures that were used during the fluidised bed hydrodynamics and biomass gasification. The parameters of interest and operating conditions for all experimental tests are explained in detail

Chapter 6: This chapter displays and discusses the experimental results obtained from this study from cold fluidisation rig. Fluidised bed hydrodynamic under different experimental tests are discussed.

Chapter 7: This chapter displays and discusses the experimental results obtained from this study from biomass gasification hot rig. Gasification product gas composition and gasifier performance for different operating and hydrodynamic parameters under different experimental tests are discussed.

Chapter 8: In this chapter, the findings from experimental undertaken in this study are concluded. The recommendations for future work in the field of fluidised bed biomass gasification to improve the gasifier performance and syngas composition and heating value are highlighted and proposed.

Chapter 2

Theory and Literature Review

2.1 Introduction

In this chapter, a biomass gasification system and its expected reactions (around 10-14 reactions) are described and reviewed. Gasifier design, an important factor that affects the gasification process, is presented in Section 2.3.1, where the main type of the fluidised bed gasifiers is reviewed. Due to their interest in this study, definition, characterisations and drawbacks of two common types of fluidised bed gasifier, bubbling and circulating, are offered in some detail. In Section 2.4, the gasification of biomass in fluidised bed reactor is presented and in Section 2.4.1 the factors that noticeably affect the fluidised bed gasifier performance for biomass gasification such as biomass feedstoke type, operating temperature, gasifying agents, equivalence ratio, and bed material are highlighted and explained. Also, the hydrodynamic factors of bubbling fluidization that affect the biomass gasification process are also highlighted and reviewed in Section 2.4.2. To be more acquainted with the fluidisation phenomenon, the classification of four groups for solid particles and the types of fluidization regimes are defined in Sections 2.5.2 and 2.5.3, respectively. The important design parameter, minimum fluidisation velocity U_{mf} is identified and highlighted in Section 2.5.4. Furthermore, the methodology of the experimental measuring and theoretical estimation of U_{mf} velocity is presented in detail. Also, the fluidisation of single biomass and binary mixtures are explained in Section 2.5.5. Finally, Section 2.5.6 reviews the factors that affect the design parameter U_{mf}.

2.2 Biomass Gasification Reactions

As mentioned in Chapter 1- Section 1.2 during the gasification step several chemical reactions occur among the hydrocarbons in the fuel (mainly char), steam, carbon dioxide, oxygen, and hydrogen in the gasifier, in addition to chemical reactions among the released gases. Table 2.1 presents typical reactions for biomass gasification process. This table shows the reaction number of each reaction, the chemical equation, the heat of reaction, which indicates reaction type, exothermic or endothermic, and the name of reaction. The understanding of the gasification physical processes and chemical reactions are essential in the gasification process design and operation

Table 2. 1 Main reactions in heterogeneous and homogeneous phase during the solid biomass gasification process (Arena 2012)

Reaction No	Reaction classification and equation	Heat of Reaction MJ/kmol	Reaction Name
	Biomass Pyrolysis		
R2.1	Biomass ⟶ Char+ Tar + H_2O + Light gas ($CO+CO_2+CH_4+H_2+ O_2 + N_2+ \ldots$)	**>0**	Biomass devolatilisation
	Oxidation Reactions		
R2.2	$C+ ½ O_2 \longrightarrow CO$	**-111**	Carbon partial oxidation
R2.3	$CO + ½ O_2 \longrightarrow CO_2$	**-283**	Carbon monoxide oxidation
R2.4	$C + O_2 \longrightarrow CO_2$	**-394**	Carbon oxidation
R2.5	$H_2 + ½ O_2 \longrightarrow H_2O$	**-242**	Hydrogen oxidation
R2.6	$CnHm + n/2\ O_2 \longleftrightarrow nCO + m/2H_2$	**Exothermic**	CnHm partial oxidation
	Gasification reactions involving steam		
R2.7	$C + H_2O \longleftrightarrow CO + H_2$	**+131**	Water-gas reaction
R2.8	$CO + H_2O \longleftrightarrow CO_2 + H_2$	**-41**	Water- gas shift reaction
R2.9	$CH_4 + H_2O \longleftrightarrow CO + 3H_2$	**+206**	Steam methane reforming
R2.10	$CnHm + nH_2O \longleftrightarrow nCO + (n + m/2)H_2$	**Endothermic**	Steam reforming
	Gasification reaction involving Hydrogen		
R2.11	$C + 2H_2 \longleftrightarrow CH_4$	**-75**	Hydrogen gasification
R2.12	$CO + 3H_2 \longleftrightarrow CH_4 + H_2O$	**-227**	Methanation
	Gasification reaction involving carbon dioxide		
R2.13	$C + CO_2 \longleftrightarrow 2CO$	**+172**	Boudouard reaction
R2.14	$CnHm + nCO_2 \longleftrightarrow 2nCO + m/2\ H_2$	**Endothermic**	Dry reforming
	Decomposition reaction of tars and hydrocarbons		
R2.15	$pCxHy \longrightarrow qCnHm + rH_2$	**Endothermic**	Dehydrogenation
R2.16	$CnHm \longrightarrow nC + m/2H_2$	**Endothermic**	Carbonization

- Note that C_xH_y represents tars and C_nH_m represents hydrocarbon with a smaller number of carbon atoms.

The chemical reactions of gasification can proceed to different extents depending on the gasification conditions of temperature, pressure, and the feedstock type. The most significant gasification reactions are:

2.2.1 Water-gas reaction (R2.7)

This is a heterogeneous (gas-solid), reversible and an endothermic reaction. Due to its products CO and H_2 gases, it is considered a principal gasification reaction. According to their equilibrium graphs, it is not so extensively affected by temperature as the Bouduard reaction, especially above 800^{o}C.

2.2.2 Boudouard reaction (R2.13)

This is a heterogeneous (gas-solid), reversible reaction and highly endothermic reaction. In this reaction CO gas is produced by reacting CO_2 gas with char at high temperature and low pressure, at least 700^{o}C in atmospheric pressure. At one atmosphere, its equilibrium graph shows that above 700^{o}C, CO gas concentration increases significantly when the temperature increases. The rate of this reaction is insignificant below 1000^{o}K (Basu 2010).

2.2.3 Water-gas shift reaction (R2.8)

This is a homogeneous (gas-gas), reversible and low exothermic reaction. This reaction is used to adjust H_2 to CO ratios in producer gas or syngas for many end products or to set the H_2 gas volume % to meet the downstream process requirements (Basu 2010). This reaction can operate with different catalysts between 205^{o}C and 482^{o}C (Laboratory 2016).

2.2.4 Methanation reaction (R2.12)

This is a homogeneous (gas-gas), reversible and a highly exothermic reaction. However, it is preferred at low temperature and high pressure. Due to its higher heating value comparing with CO or H_2, CH_4 is the desired gas in combustion process applications.

2.2.5 Steam methane reforming reaction (R2.9)

This is a homogeneous (gas-gas), reversible and a highly endothermic reaction. It progresses very slowly and requires relatively low temperature and catalyst. To occur and due to its enthalpy, this reaction requires a high amount of energy. It is a limited reaction due to the low concentration of CH_4 in the gasifier.

2.3 Key factors affecting the gasification process

There are many factors that affect the gasification process, producer gas quality (composition, production of H_2, CO, CO_2 and CH_4, free tar content and heating value) and the performance of gasification (represented by gas yield, carbon conversion efficiency, and total heating value efficiency). Generally, these factors are reactor design, origin feedstock of fuel, operating conditions such as equivalence ratio, temperature, pressure and gasifying agent (medium). In addition, for each type of gasifier design, there are additional factors that affect the gasification process and reactor performance.

2.3.1 Gasifier design

Reactor design is crucial for gasification efficiency, composition and heating value of the product gas, and also for tar formation. Practically, according to the gas-solid contact method, three main categories of gasifier used for biomass gasification are (Basu 2010)(Siedlecki et al. 2011):

I- Fixed-Bed (Moving-Bed) Gasifiers.
- Updraft
- Downdraft
- Crossdraft

II- Entrained flow gasifiers.

III- Fluidised Bed Gasifiers:
- Bubbling fluidized bed gasifier (BFBG).
- Circulating fluidized bed gasifier (CFBG).

Despite the fact that these gasifiers apply analogous principles for biomass fuel conversion, but their operations and performances are different.

2.3.1.1 Fluidised bed gasifiers:

As mentioned in Chapter 1-Section 1.3, fluidised bed reactors can be used for thermochemical gas-solid reaction processes. For a fluidized bed gasifier the fuel, solid fuel biomass or coal, is gasified in a bed of small particles (inert or catalytic bed material or both) and fluidized by a suitable gasification medium gas (Basu 2010). There are two principal types of fluidised bed gasifier.

I. Bubbling fluidized bed gasifier (BFBG):

The oldest bubbling fluidised bed gasifier for coal gasification was developed by Fritz Winkler in 1921 (Basu 2010). Basically, as shown in Figure 2.1 a and b, the BFBG simply comprised of an air blower, gas plenum (gas box), the distributor plate, screw feeders for solid fuel and bed material feed, fluidized bed with freeboard column unit and cyclone separator unit (Engineering 2011).

When the agent gas introduces through the distributor plate and passes upward through the gasifier bed, at a specific velocity bubbles are formed within the bed which rise and grow in size until they reach the surface material bed where they burst (Sadaka 2010). The little amount of solid materials are carried along with bubbles in wake, and when the bubbles burst at the surface of the bed, the carried particles fall downward by gravity. They flow again upward along with newly formed bubbles. Just this portion of the process, wake portion movement, is responsible for mixing the bed materials, fuel particles, and gasifying agent. This boiling state gives nearly uniform temperature, high heat and mass transfer that is characteristic of fluidized bed reactors (Harriott 2003)(Tzeng 2007)(Basu 2006).

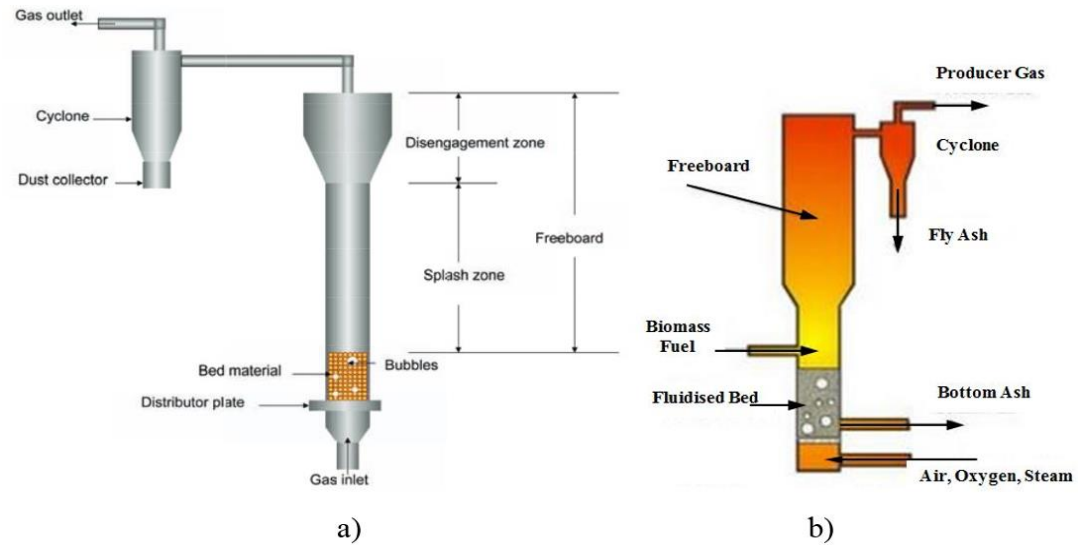

Figure 2. 1 A simple sketch of bubbling fluidised bed gasifier: a) (Sadaka 2010), b) (Patel 2014)

❖ Characteristics of the bubbling fluidised bed gasifier

This design operates at low fluid superficial velocity, typically less than 1m/sec. Although it is often operated at atmospheric pressure, but also can operates under pressurized conditions, which will further increase the throughput. Owing to the low residence, time of the fuel and low char's reactivity the char conversion is low.

The uniform temperature distribution, high mixing and high heat and mass transfer are applicable throughout the gasifier. Carbon with some fine bed material and ash are entrained in the gas product, trapped, and separated out in a cyclone. BFBG has high flexibility and suitability for the gasification of solid biomass fuel regarding both particle size and different types of materials. This design results in lower cost and less maintenance. It is suitable for scaling up. (Gautam 2010)(Tzeng 2007) (Ciferno and Marano 2002)(Brown 2006).(Siedlecki et al. 2011)(Puig-Arnavat et al. 2010).

❖ **Drawbacks of the bubbling fluidised bed gasifier**

Particulates elutriate as the product gas increases the solid load in the cyclone and filter. The issue of the weakness of the interaction and mixing of the species when the conversion of the char is low due to the low residence time of the fuel, the slow reactivity of the char and un-recycled trapped solid materials.

At higher temperatures above 900-950^{o}C and when the biomass fuels have a high content of ash, potential ash melting will occur causing stickiness of particles leading to the agglomeration phenomena causing bed de-fluidization and thereby the gasifier. (Cirad 2009) (Puig-Arnavat et al. 2010) (Siedlecki et al. 2011).

II. Circulating fluidized bed gasifier (CFBG):

❖ **Simple (classical) circulating fluidized bed**

This general circulating fluidized bed abbreviated as CFB, has been used as a common term since the 1970s and for gas-solid process applications CFB technology dates back to the 1960s (Yang 2003). This gasifier type works at a high superficial gas velocity beyond bubbling and turbulent fluidization regimes. It is also known as fast fluidization under certain conditions (see Section 2.5.3.5). At this critical point, known as the transition boundary velocity, the bed particle entrainment occurs. This is called a transport or transition velocity. Beyond this point, the bed fluidisation cannot be continued without entrained solids recycling. The typical gas velocity range is 2-12 m/sec and particle rate flux range is 10-1000 kg/m^2.sec, so that there is not an interface distinguishing between a dense bed and a dilute region above. By this point, a CFB is differentiated from a bubbling fluidized bed BFB (Siedlecki et al. 2011)(Yang 2003) (Ciferno and Marano 2002)(Klein 2002).

Figure 2.2 shows a schematic diagram of CFBG gasifier. As a result of gas high-velocity the entrained solid particles will separate, re-circulate and return back to the reactor through an external particle flow system, which usually consists of one or more cyclones, a standpipe and a valve or seal (Yang 2003) (Ciferno and Marano 2002)

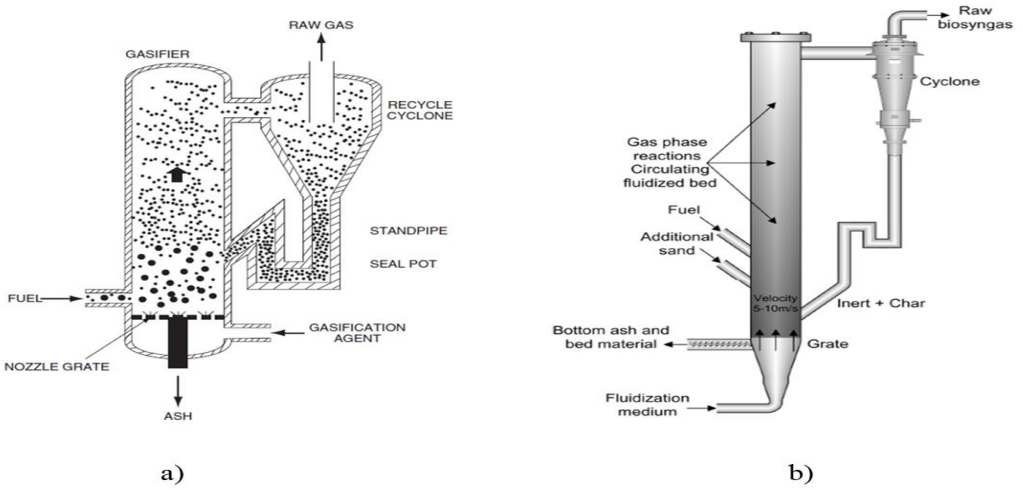

Figure 2. 2 Classical circulating fluidized bed gasifier-direct heating: a) Lurji Gasifier (Christopher Higman 2003), b) Classical type (Siedlecki et al. 2011)

There are two types of circulating fluidized bed (Siedlecki et al. 2011) (Christopher Higman 2003):

❖ **Fast circulating fluidized bed FICFB (Indirectly Heated Unit):**

Sometimes is called Dual or Twin Circulating Fluidized Bed Reactor DCFB. The operation of this gasifier is based in which the gasifier vessel is divided into two distinct fluidization; reactors, which are operated at two different gas velocities as shown in Figure 2.3, one of them is a bubbling fluidized gasifier BFBG, where usually the steam is an agent gas while the other reactor (combustor) is a simple circulating fluidized bed combustor CFBC, usually air is an agent gas. Some of its features are available in (Puig-Arnavat et al. 2010). The design aimed to avoid mixing of gasification products with those from the combustion in order to obtain high purity hydrogen. In the combustor heat generated, due to char combustion raises the bed material temperature. After leaving combustor, it is captured by a cyclone and then recirculated into the BFBG to supply the required heat for char gasification endothermic reactions using steam as an agent gas (Siedlecki et al. 2011) (Brown 2006)(Christopher Higman 2003).

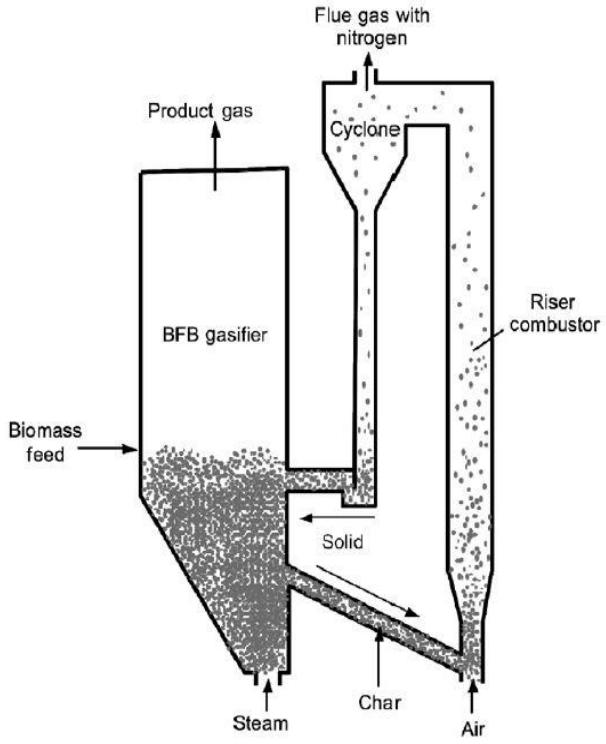

Figure 2. 3 Twin (dual) fluidized bed gasifier (Basu 2010)

❖ **Characteristics of the circulating fluidised bed gasifier**:

If height of the bed is significantly high, then long and controllable residence time of particles can be achieved. It can be operated at pressurized conditions. Also at higher velocities, typically 2-12 m/sec leading to higher velocities of the recirculation and violent gas-solid contact and mixing. This will give high heat and mass transfers and reaction rates which causing higher overall carbon conversion. This is suitable for large-scale systems and has very good scale-up potential. Its ability and flexibility to gasifying different types and particle sizes of feedstocks with different compositions and moisture content, especially biomass and wastes, of which the size, shape, and fluidizing characteristics, are harder to control than coal. The energy throughput per unit cross-sectional area of gasifier is higher than for BFBG.

❖ **Drawbacks of circulating fluidising bed:**

The reactor height significantly increases their cost. The process control mechanism is more complex in comparison to its BFB counterpart. As with BFB, because the ash content and temperature limitation, bed agglomeration is a possibility. As a result of long circulation loop, gradients of temperature occur in the solid flow axis direction.

Tar conversion is still not high, but it is little higher than BFBG gasifier. (Sadaka 2010) (Tzeng 2007) (Siedlecki et al. 2011)(Klein 2002)(Ciferno and Marano 2002) (Yang 2003).

2.4 Gasification of biomass in the bubbling fluidised bed gasifiers BFBGs

As mentioned in previous sections fluidised bed gasifiers enhance the gasification reaction rate and conversion efficiencies (mainly carbon and thermal efficiency) due to high heat and mass transfer, excellent mixing and high contact of gas-solid fuel. In addition, the use of the bed material as a medium of heat transfer and catalyst, will highly contribute to tar reduction and improve the producer gas quality. These specifications encourage researchers to use the bubbling fluidised bed gasifier for biomass gasification studies.

Jeremiáš et al., 2009) evaluated the effect of the addition of the gasifying agent CO_2 to the main gasifying agent steam in bubbling fluidised bed gasifier and various bed materials on the performance of allothermal gasifier.(Lv et al. 2004) developed a small scale bubbling fluidised bed gasifier to study the effects of pine sawdust biomass gasification parameters. They investigated the effects of gasifier temperature, equivalence ratio, steam-biomass ratio, pine sawdust particle size on the gasifier performance represented by gas composition, producer gas LHV and carbon conversion. To show the potential of implementing air-bubbling fluidised bed gasifiers in rural electrification projects for biomass agricultural wastes, a wood chips biomass gasification in a large size of BFBG was performed by (Lim and Alimuddin 2008). They monitored the gasifier performance in terms of its thermal output. In their review paper, (Alauddin et al. 2010) presented 27 various research paper, for the dated period between 1995 and 2009, which were conducted in gasification of lignocellulosic biomass, (agricultural residues, herbaceous crops , forestry residues, waste paper and other wastes (municipal and industrial), etc.) in bubbling fluidised bed gasifier for renewable energy development. These data were presented as a table in four fields for each research paper: system configuration and operation parameters, investigated parameters, optimum obtained results and reference. In their conclusion, they stated that researchers confirmed that fluidised bed gasifiers have a great potential to perform the gasification of this type of biomass. In recent years, the investigators and studies have been conducted and investigated in lignocellulosic biomass gasification for renewable

energy development specifically by fluidised bed gasifiers such as: (Lahijani and Zainal 2011) investigated the gasification of palm empty fruit bunch (EFB) biomass in a pilot scale air-blown bubbling fluidised bed to examine the ability of EFB biomass for renewable energy uses. Their results show the potential of their biomass for bioenergy production factories. Similarly (Kim et al. 2013) investigated the efficiency of the production of a gas fuel for a syngas-engine power supply from woody solid fuel biomass using a gasification technology by air-blown bubbling fluidised bed gasifier. They found that the caloric value of the producer gas (above 4.7 MJ/Nm^3) was satisfied for syngas engines. (Tilay et al. 2014) carried out various experiments in non-catalytic biomass gasification for syngas production using two types of the gasifire, lab-scale fixed-bed and pilot-scale bubbling fluidised bed. The feedstock biomass was called canola meal, which is one of by- product of solvent extraction of canola oil industry in Canada. They studied the effect of various gasification parameters, mainly temperature, equivalence ratio ER and three different gasifying agents steam, O_2, and CO_2, on the gasifier performance. From their experimental results for both gasifiers, they found that canola biomass could be considered as one of the potential sources for syngas production. In addition, those results show the ability to use the data for further processes design and canola gasification scale-up at industrial applications.

2.4.1 Factors affecting biomass gasification process in bubbling fluidised bed gasifiers

In general, design and operation of any gasifier entail a high comprehension of the effect of biomass feedstock types and operation parameters, and hydrodynamic parameters for fluidised bed gasifiers, on the performance index of the gasification system. The main task of most biomass gasification research is to better these indices by improving the producer gas composition, gain a significant gas lower heating value LHV, lowering tar content and promoting the cold gas efficiency, gas yield and carbon efficiency (Alauddin et al. 2010). It should be noticed that for any gasification process the maximum value of those indices could not be achieved together at the same time.

2.4.1.1 Biomass feedstock

Biomass feedstock flexibility is one factor that plays a key role in the gasifier design and performance. The physical and chemical properties of biomass feedstock are important in establishing operating conditions of, specifically bubbling fluidised bed

gasifiers. Chemical properties can be known according to any standard methods using analysis tools, mainly proximate analyses, heating value LHV and. ultimate analyses These analyses are detailed in Chapter 4-Section, 4.3.2.1, 4.3.2.2 and 4.3.2.3, respectively. These analyses can also be used to carry out calculations related to the process design and performance (Christopher Higman 2003). Figure 2.4 shows the general formula of those analyses (Siedlecki et al. 2011).

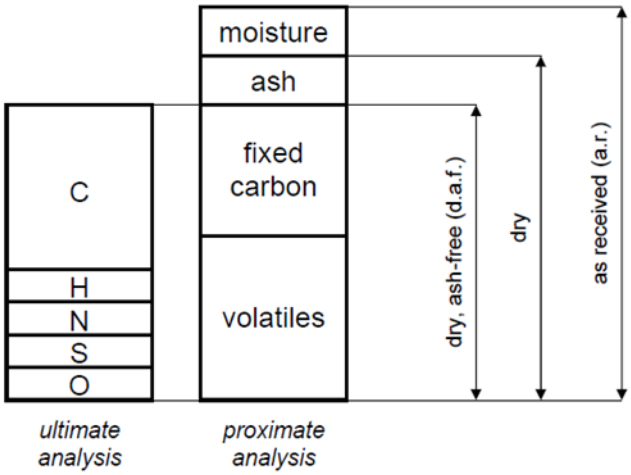

Figure 2. 4 General composition and main chemical elements in typical solid biomass fuels (Siedlecki et al. 2011)

In addition, the Figure shows the basis on which the analysis is based on such as **d**ry **a**sh-**f**ree basis (**daf**), **d**ry **b**asis (**db**) and **a**s **r**eceived basis (**ar**). These bases are critical to the state for any analysis. (Legonda 2012) established a standard analysis of solid biomass fuel as shown in Table 2.2.

Table 2. 2 Typical proximate, ultimate and trace element analysis of biomass (Legonda 2012)

Proximate Analysis		Trace Elements (ppm)			
Moisture content (wt %)	6-10	As	0-5	Ti	10-214
Ash (wt % db)	1-15	Ba	0-125	V	0-9
Volatile matter (wt %)	61-76	Cd	0-1	Zn	11-162
Fixed carbon (wt %)	13-21	Co	0-9	Al	19-5001
Calorific value (MJ/kg)	16-20	Cr	2-23	Si	1-46000
		Cu	1-128	Ca	650-23301
Ultimate Analysis (wt %)		Mn	17-1052	Mg	160-7613
C	38-58	Mo	0-7	Fe	26-4867
H	5-8	Ni	0-60	K	400-25000
O	32-47	Pb	1-86		
S	<0.4	P	75-2900		
N	0-2	Na	24-3497		

Volatile matter content is a measure of the reactivity of the solid fuel, where reactivity is a measure of chemical activity of substances and a tendency of material to undergo a chemical reaction. Therefore, a solid biomass, which has higher volatile material content are more reactive and can be easily converted into gas with a low amount of char-producing. Also, this biomass char is highly porous, and this property can increase the rate of gasification. Although a biomass which has a high content of volatile matter can be gasified easier, but at the same time, its producer gas has a high tar yield which is a problem in biomass gasification process downstream and producer gas quality making its removal difficult not easy (Basu 2006)(Basu 2010).

Moisture content: It is an important physical property of a given biomass solid fuel which highly affects the design and operation of the gasifier. Moisture content in biomass varies in the interval 3-63% (Vassilev et al. 2010). Most the steam reactions in gasification processes are endothermic as shown in reactions R2.7, R2.9 and R2.10, Table 2.1 except reaction R8, which is an exothermic reaction. For high moisture content of solid biomass fuel, a significant amount of heat is required for moisture evaporation comparing with a small amount of heat which can be obtained by exothermic reaction heat R2.8, -41MJ/kmol. This will reduce the thermal energy inside the gasifier. Thereafter, this can hinder the endothermic reactions resulting in a low quality of producer gas, its low heating value LHV and composition (Basu 2010) (Kirsanovs et al. 2014). Also, this may increase methane composition and lower hydrogen content due to exothermic hydrogen gasification reaction R2.11. This reaction occurs because of the production of H_2 in the presence of CO by water-gas shift reaction (R2.8) due to high moisture content (Kirsanovs et al. 2014) (Radwan 2012). High moisture content, above 30%, causes ignition difficulties. In addition, it reduces the temperature achieved in the oxidation zone resulting in incomplete cracking of hydrocarbons which are released by pyrolysis reactions (Kirsanovs et al. 2014) (Radwan 2012). This will increase the percentage of undesired materials, e.g. tar products downstream. Many researchers studied the effect of moisture for several biomass solid fuels on the low heating value of biomass fuel itself (Marsh et al. 2008) and (Molino et al. 2015). They found that low heating value of each fuel proportion inversely with the moisture content.

On the other hand, some moisture content in the feedstock is desirable because it can contribute in enhancing steam reforming reactions, R2.9 and R2.10, and char gasification, R2.7, at higher temperature. Also, for syngas composition adjusting, steam

with a required value of steam-fuel ratio or as gasifying agent is widely used in industrial gasification applications (Vassilev et al. 2010).

Ash content: It is another important issue especially in bubbling fluidized bed gasifiers, which affects the practical operation of the gasifier. It does not effect on the producer gas composition directly. Chemically, ash content is an inorganic solid material, which is mainly composed of metal oxides and some of their salts. Ash content can be measured by proximate analysis for biomass (Siedlecki et al. 2011) and (Basu 2006). The issues and negative effects of the ash content lies in the following: 1) a high amount of ash will reduce the heating value of the solid fuel. 2) When the ash contains a high amount of alkali oxides and salts, which are promoted in the existence of chlorine and especially with high silica content in bed material forming eutectic materials (sticky compounds) of low melting points about 770^{o}C for alkali-silicates (K_2O-SiO_2), whereas it is lower for K_2O-CaO-SiO_2. These materials lead to agglomeration phenomena especially in high temperature bubbling fluidized bed gasifiers causing a bed material defluidisation and therefore gasifier shutdown (Siedlecki et al. 2011)(Radwan 2012).

Recently research has been conducted to study the effect of lignocellulosic biomass composition (as a feedstock) on the performance of gasification and pyrolysis process. (Hlavsová et al. 2016) evaluated the effect of the composition of nine herbaceous plants on the products (gases, liquids and solid char) distribution from pyrolysis using a fixed bed reactor. They found that product distribution were affected by chemical and biochemical composition of biomass fuel, liquid, and char secondary reactions. (Lv et al. 2010) investigated the effect of six types of natural biomass and acid-washed biomass, represented by their three compositions, cellulose, lignin and AAEM species (**A**lkali and **A**lkaline **E**arth **M**etals), on gasification and pyrolysis properties using a TGA analyzer and fixed bed reactor. They concluded that interaction between AAEM-cellulose-lignin is responsible on the activity of biomass gasification. Also, they observed that the pyrolysis rate was higher when the cellulose content was raised. Whereas the pyrolysis rate for biomass with higher lignin content became slower. In their research paper, (Barmina et al. 2013) stated that when various lignocellulosic biomass are used for fuel gas production, detailed experimental research is needed to evaluate the influence of the differences in their chemical and elemental composition on gasification and combustion processes.

2.4.1.2 Air gasification agent (medium)

Many gasifying agents have been used in the gasification process. These agents are typically air, oxygen, steam, CO_2, H_2, and combination of them in required ratio. The gasification product gas can be classified according to its lower heating value (LHV). The value of LHV of the producer gas depends on the type of gasifying agent employed as illustrated in Table 2.3 (Cirad 2009) (Radwan 2012).

Table 2. 3 Classifications of producer gas according to lower heating value (Cirad 2009)

LHV level	LHV, MJ/Nm^3	Gasifying agent
Low	4 – 6	using air and air/steam
Medium	12 – 18	using O_2/ steam
High	40	using H_2

The main oxidation reactions during the biomass gasification process using air as gasifying agent, as a source of oxygen, are R2.2 to R2.6 have been shown in Table 2.1.

Lee, Kim, & Song, (2002) revealed in their experimental study, air/steam gasification of an Australian bituminous coal in a fluidised bed, that with increasing air/coal ratio (1.6 – 3.2) at 850^{o}C, carbon conversion and gas yield, were increased from 0.3 to 0.42 and 0.25 to 0.425Nm^3/kg, respectively, whereas the calorific value (LHV) decreased from 2.7MJ/kg to 1.6MJ/kg. In addition, the composition of product gas was significantly affected by increasing the air/coal ratio; H_2 varied from 9.5% to 5.5%, CO from 5.9% to 4.5%, CH_4 from 2% to 1.4%, while CO_2 increased from 7.0% to 8.9%.

(Devi et al. 2002) showed in their review that the effect of the gasifying agent on the product gas composition, especially tar formation, depends on the equivalence ratio. The review reported that the product gas composition by (vol. %) produced from air gasification in the fluidised bed at 800^{o}C and at ER= 0.35, was CO= 14%, H_2= 10%, CO_2= 15%. The tar content decreased considerably with increasing ER to values typically of 2 g /Nm^3 being obtained. (Narvaez et al. 1996) reported that the gasification of pine sawdust with air at 800^{o}C and with the ER raise to 0.45 gives tar content of about 2-7 g/Nm^3. ER strongly influences the product gas quality and is more significant at higher temperatures. Moreover, 30% of the tar concentration was decreased when ER increased from 0.22 to 0.32 at 700^{o}C. The decrease was mainly attributed to the conversion of phenol. Most of the phenol can be converted at values of ER= 0.27 and 700^{o}C.

(Siedlecki et al. 2011) confirmed in their review that the effect of ER on the main output parameters such as tar yield, cold gas efficiency (CGE), carbon conversion (CC), and the reactor temperature (T) take the trends illustrated in Figure 2.5 As can be seen the trends are similar to those previously reported. The Figure shows that increase an ER leads to increase oxygen, which leads to increase combustion of the char and product gas and thereby leads to increase the carbon conversion and reactor temperature. This means the yield of the combustible producer gases and thereby the cold gas efficiency will decrease. Finally, as ER increases the yield of the tar will decrease due to tar cracking and oxidation reactions.

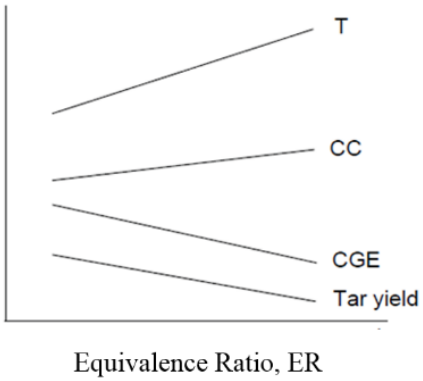

Figure 2. 5 Effect of the variation of ER on the main process parameters (Siedlecki et al. 2011)

2.4.1.3 Temperature

Temperature is an essential parameter in the gasification process. Due to the thermal-chemical reactions, temperature plays an important role in accelerating the rate of the endothermic and exothermic reaction of gasification process, tar cracking and char conversion. Its effects revealed in producer gas quality, gas yield and low heating value LHV.

For biomass fluidized bed gasification, the temperature range lies between nearly 650^{o}C and 950^{o}C. The effect of the temperature parameter on gasification performance depends on various factors mainly: 1) the type of gasifying agent, 2) Equivalence ratio, which in turn depends on the method of the source of the heat supply, externally or internally, where for internal heating ER will affect temperature, whereas for external heating the controlling temperature is not affected by ER. 3) Biomass fuel moisture content. 4) The heat loss from the system. (Gautam 2010) (Siedlecki et al. 2011).

(Cao et al. 2006) investigated experimentally the performance of a proposed tar-free biomass gasification process conducted by a lab-scale air-sawdust biomass fluidized

bed gasifier under autothermic conditions. They studied the effect of temperature variations at the top (freeboard) and the bottom (dense) regions of gasifier on the tar reduction in producer gas. Regarding tar reduction, they observed when the bottom temperature was at 651^{o}C and the top temperature increased firstly to 750^{o}C, to 854^{o}C, to 898^{o}C and finally to 934^{o}C, the tar content in producer gas was 1227mg/Nm^3, 21mg/Nm^3, 15.98mg/Nm^3 and 12.34mg/Nm^3, respectively. On the other hand, there was no improvement in the tar reduction when top temperature increased to 850^{o}C. They found that at the optimum temperatures, upper region was 860^{o}C and bottom region was 750^{o}C the carbon conversion efficiency and cold gas efficiency could reach above 87.1% and 56.9%, respectively. In air-polypropylene gasification in bubbling fluidized bed reactor, (Xiao et al. 2007) studied the effect of operating parameters, ER (i.e. temperature effect), static bed height, and fluidisation velocity on gas composition, producer gas LHV, and product yield (gas, tar and char) distribution. They found a strong effect of ER ranging from 0.2-0.45 (i.e. temp (approximately) = 700^{o}C – 900^{o}C) at U/U_{min}= 3.0 and H_s=200mm on the product gas distribution. When ER increased the gas yield increased from 76.1 to 94.4 wt %, whereas tar decreased dramatically and reached to 0.5 wt% at ER= 0.4. In addition, the char yield decreased from 15.9 to 5.0 wt %. This effect of ER on gas, tar and char yield was attributed to the temperature effect and this in turn attributed to primary pyrolysis at high bed temperature, higher secondary cracking temperature which led to tar cracking reactions. In addition, a higher gasification temperature promoted the endothermic char gasification reactions mainly Boudouard and water - gas shift, R2.13 and R2.8, respectively, Table 2.1. When ER (also temperature) increased (for the same range), HHV was decreased significantly from 11.35 to 5.17 MJ/Nm^3, whereas the composition of CO_2 increased significantly, from 7.0 to 16 vol %. This was due to the combustion reactions. For CO and H_2 their content trend initially increased with ER and then decreased. For the former it increased dramatically from 20% to 22.5 at ER=0.25 and then decreased dramatically to 14.5 % at 0.45, whereas for the latter increased gradually from 4.5 % to 5.5 % at ER=0.35 then decreased gradually to 4.5 % at ER=0.45. CH_4 decreased slightly from 6 % to 4 %. A similar investigation was conducted by (Ghani A.K. et al. 2009) for air gasification of two biomass agricultural wastes (coconut shell and palm kernel shell) by a lab-scale bubbling fluidized bed to study the potential of those biomass for hydrogen production. For the temperature effect, they found that for two biomass, gas yield and low heating

value increased as temperature increased. The same effect was obtained for CO and H_2 composition, whereas opposite effect was obtained for CH_4 composition.

2.4.1.4 Equivalence Ratio, ER

Equivalence ratio is an important factor in biomass gasification, where it is directly related to air or O_2 amount and flowrates, biomass feeding amount and gasifier temperature. This parameter, sometimes called " air ratio or air factor" and, sometimes is represented by the symbol λ (Lambda) (Siedlecki et al. 2011). It is a dimensionless factor that relates the actual and the stoichiometric amounts of the reactants of the thermal conversion process. This relation has been described and defined by Equation 3.25 in Chapter 3. ER value specifies the type of the thermal process. ER=0.0 refers to pyrolysis process, 0.0 < ER< 1.0 to gasification process and ER > 1.0 to combustion process. ER is highly related to the reactor temperature. When ER increases (i.e. amount of oxygen increases and vice versa or the amount of fuel reduces and vice versa). This oxygen increase will permit to combust the product gas and char, thereby reactor temperature will increase and subsequently will affect the product gas quality and process performance (Xiao et al. 2007)(Ghani A.K. et al. 2009)(Basu 2010)(Siedlecki et al. 2011). These affects have been shown in Figure 2.5. According to producer gas specifications needed and uses especially in fluidized bed gasifiers to achieve optimum conditions, the typical values of ER vary from 0.2 to 0.4. The selected range of ER value for most air or oxygen biomass fluidized bed gasification studies lies in this range (Siedlecki et al. 2011) (Basu 2006)(Basu 2010)(Makwana et al. 2015). For ER values less than 0.18, gasification process will approach pyrolysis (i.e. low reaction temperature and higher tar content in producer gas), whereas for ER >0.45 a low quality of producer gas will produce (Makwana et al. 2015)(Basu 2010)(Basu 2006)(Alauddin et al. 2010).

2.4.2 Hydrodynamic factors

2.4.2.1 Static bed height

The effect of bed height for air-polypropylene gasification on the performance of the bubbling fluidized bed gasifier was investigated by (Xiao et al. 2007). For a fixed values of ER=0.3 and the ratio of air superficial velocity to minimum fluidisation velocity U_o/U_{mf} = 3.0, the effect of three values of static bed height 100, 200, 300 mm were studied. They showed this effect was not significant on the gas composition. CO and

CO_2 reached maximum values for bed height of 200mm, whereas H_2 remained almost constant. CH_4 and heavier hydrocarbons dropped slightly with the increase of bed height. The higher heating value fell steadily as bed height increased. They attributed this to the decrease of hydrocarbon because of the bed height increase the residence time increase, where at high temperature zone the cracking reactions of hydrocarbon were enhanced. On gas yield there was no significant effect. (Ghani A.K. et al. 2009) studied the effect of bed static height from 15cm to 35cm (with 5cm increment) at fixed fluidization velocity ratio and ER for two biomass materials -air gasification in a fluidized bed gasifier. They concluded that static bed height does not affect significantly the gasification process. They showed that increasing the bed height would increase the residence time of gases and the reactions of hydrocarbon cracking especially in the high temperature dense bed. On the other hand, too high bed height gave an unfavorable effect because of large bubble formation (slug fluidisation). Their results showed generally a significant increase when bed height increased from 15cm to 30cm, whereas this decreased from 30cm to 35cm.

2.4.2.2 Gasifying agent (fluid) velocity

For the same study of (Xiao et al. 2007), the effect of air superficial velocity (expressed in U_o/U_{mf} ratio from 2 to 4) on the gas composition at fixed ER and bed height values was studied. As fluidization velocity increased CO, H_2 and CnHm gases decreased whereas CH_4 was slightly increased and CO_2 dramatically increased. This was attributed to the high quantity of air available, which leads to rapid exothermic and combustion reactions, hence a higher amount of CO_2 in the producer gas. Increasing fluidisation velocity decreased the gas yield. For the same study mentioned in bed height effect, Section-2.4.2.1(Ghani A.K. et al. 2009), the effect of three fluidisation velocity ratios 2.2, 2.8, and 3.33 was investigated. The trend of gas LHV for two biomasses decreased dramatically as velocity ratio increased. A similar trend was found for gas yield for coconut shell biomass, while an opposite trend was found for palm kernel shell biomass. For producer gas composition, increasing the ratio caused a decreasing trend for CO and H_2 components, whilst an increasing trend for CO_2 and CH_4 gases. Most of studies have discussed the effect of air flowrate its equivalence ratio relationship. According to its definition, ER is considered from the measuring of the air (or oxygen) flowrate (Kumar et al. 2009). There has been no any research studies taken on the effect of agent gas, in a fluidized bed gasifier, on gasification performance with

hydrodynamic aspects. What should be taken into account is that gas flow rate must be more than the minimum fluidisation flowrate conditions. (Kumar et al. 2009) reported that increasing air flowrate leads to an increase in temperature and in turn higher biomass fuel conversion and quality of producer gas, which is a positive effect. This air increase will lead to increasing in the combustion reactions, which in turn decreases the heating value of the producer gas. For this reason, the ER value has a limited range (from 0.2 to 0.45). Also higher air flowrate affect biomass conversion due to its short residence time. The effect of ER has been discussed in the previous section. It should be noted that in the above studies for fluidisation flow effect, they kept ER values constant by altering the biomass flow rate when airflow increased or decreased.

2.4.2.3 Biomass particle size

Many researchers studied the effect of biomass particle size on the gasification process in fluidized bed reactors. In their experimental study on biomass air-steam fluidisation gasification, (Lv et al. 2004) explored the effect of biomass (pine sawdust) particle size, their average size 0.75, 0.53, 0.38, 0.25mm, on gasification performance, gas yield, gas LHV, carbon conversion efficiency and gas composition at specific operating conditions. Their results showed that all performance parameters increased as particle size decreased. They attributed that CH_4, CO, and C_2H_4 were more influenced by smaller particle than larger particles, except CO_2 produced less. They concluded that for biomass producer gas quality and yield the small particles were more preferable than large size. They explained that reaction kinetics is a controlling step for pyrolysis process when smaller particle sizes are used, whereas gas diffusion is a controlling step when large particles are used due to the diffusion of the product gas. In their study, (Ghani A.K. et al. 2009) confirmed this fact when they studied the particle size effects in air gasification of three types of agricultural residues for H_2 production. They proved that H_2 composition and its yield decreased when biomass particle size increased from 0.1mm to 5mm. For air fluidisation gasification of empty fruit bunch for H_2-rich production, (Mohammed et al. 2011) found that smaller biomass particle size produced more CH_4 and CO and less CO_2, while for H_2 its composition remained approximately constant for particle sizes <0.3mm and 0.3-0.5mm then decreased dramatically for particle size 0.5-1mm. This is agrees with above study (Lv et al. 2004). In addition, LHV and total yield of the producer gas increased as biomass particle size decreased, while char and tar yield decreased. They attributed these findings to the increase of

temperature gradient inside the large particles causing a lower temperature than the surface. Finally, they concluded that the smallest size gave maximum producer gas yield, while the second range, 0.3-0.5mm gave highest LHV and optimum gas composition of producer gas.

From their experimental study on H_2 - rich producer gas by steam gasification of biomass in a research-scale fluidized bed, (Fremaux et al. 2015) investigated the effect of three particle sizes. These sizes are 0.5-1 mm (small), 1-2.5 mm (medium) and 2.5-5 mm (large) of wood residue biomass on H_2 yield and tar content in producer gas at temperature=900^{o}C and at different *S/B* ratio(by wt), varied from 0.5 to 1. They found that small size improved H_2 yield and clearly at high *S/B* ratios (0.8-1). They cited two reasons. The first one related to decreasing heat transfer resistance with decreasing particle size and the second one due to diffusion limitations of volatile materials formed. Moreover, (Mohd Salleh et al. 2015) investigated the influence of the bio-char particle size of EFB (empty fruit bunch) biomass material, in the range $\geq$ 0.2mm and $\leq$ 2mm, on carbon conversion and producer gas; yield, composition and high heating value in an air-blown fluidized bed gasifier at 800^{o}C. Their results indicated that when particle sizes decreased the H_2 and CO compositions, producer gas yield, high heating value and carbon conversion increased and a slight increase in CH_4. In their meta-study in biomass gasification conversion process, (Nguyen et al. 2015) emphasized that this process is highly affected by shapes and size of biomass feedstock particles. They cited a study, which observed that when the biomass particle size decreased the composition of H_2 plus CO and H_2/CO ratio increased.

2.4.2.4 Fluidised bed material

Fluidized bed reactors usually use a bed material capable of performing the fluidization process. The main tasks of any bed material used in any thermo-chemical reaction, such as gasification, are:

- During the gasification process, the bed material should remain inert with reactant materials at the process conditions.
- It can operate at high temperature. Furthermore, it has a high specific heat capacity and can store heat, which can be used to gasify the biomass fuel to drive the endothermic reactions.
- The material can transfer heat between the particles itself and biomass solid-fuel particles. By this method large temperature peaks will be avoided, also a uniform

temperature distribution in the reactor can be achieved (Siedlecki et al. 2011)(Christopher Higman 2003)(Harriott 2003)(Daizo and Levenspiel 1991).

Inert and natural silica sand material is considered as a bed material, which has been used in the fluidized bed gasification process. Since the mid- 1980s, interest in the subject of catalysis for biomass gasification has grown because of the need to produce a high quality producer gas from the biomass gasification process to increase its economic feasibility (David Sutton, Brian Kellehr 2001). Beside the above tasks, the catalysts employed in this process have an important effect on gasification process, mainly:

1- Catalytic activity on some of the gasification reactions. This effect is mostly desirable to increase the rate of tar conversion, enhance the product gas quality and reduce methane concentration. All these effects lead to improve the gasifier performance.

2- Interaction with the fuel constituents at a certain temperatures results in a change of physical properties. For this case the other important problem that can be observed is agglomeration, which is an undesirable phenomenon leading to de-fluidization (Siedlecki et al. 2011).

Because of these influences, the choice of the bed material is considered an important parameter in the gasifier design. This requires special bed material characteristics and properties, such as (Siedlecki et al. 2011) (David Sutton, Brian Kellehr 2001):

The main materials which can be potentially used as catalytically active materials either as in-bed additives or even bed materials in fluidised bed gasifier are: Dolomites (Ca $Mg(CO_3)_2$), limestone (calcites) ($CaCO_3$), magnesites ($MgCO_3$) and olivine ($(Mg^{+2},Fe^{+2})_2SiO_4$)(Siedlecki et al. 2011).

2.5 Fluidisation phenomena and fluidised bed

When a fluid flows upward through a packed bed of solid particles, at a specific velocity the drag force of the fluid holds the particles medium and a continuous motion of solids particles is formed producing a loosened suspension bed. This bed is called a fluidised bed. It behaves like a fluid, which can flow through pipes and valves. These phenomena can be used in wide applications to obtain high mixing and agitation of the fluid-solid particles, which produces an excellent contact between the solids and the solids itself, the fluid and the column wall. A uniform temperature distribution throughout the reactor, a high mass and heat transfer and its ability to operate in a continuous state are

the main advantages which make fluidised bed reactors one of the widely used in industrial applications. Many applications can be applied by this phenomenon for physical and chemical processes. For the former such as: water moving through sand bed, water-zeolite ion exchange, drying and cooling of powders in food, pharmaceuticals and polymer industries, granulation and pneumatic transport of powder. For the latter; such as chemical reactors for coal or biomass gasification or combustion or pyrolysis, chlorination processes, catalytic cracking and catalyst regeneration, etc. Most industrial applications of fluidization include gas-solids system (Subramanian 2004) (Halvorsen 2010) (Basu 2006) (J.S.M.Botterill 1975).

2.5.1 Fluidised bed column

As shown in Figure 2.6, most of fluidised bed columns consist of the following components;1) gas plenum (gas inbox), which is a chamber where the gas enters the bed; 2) distributor plate which is used to hold the solid particles and to pass and distribute the gas uniformly through the bed; 3) the bed region with a specific height of solid particles; and 4) the freeboard region to collect the particles which have been escaped from the bed region. In fluidised bed reactors, bed and freeboard regions are reaction regions. More details will be found in next chapters.

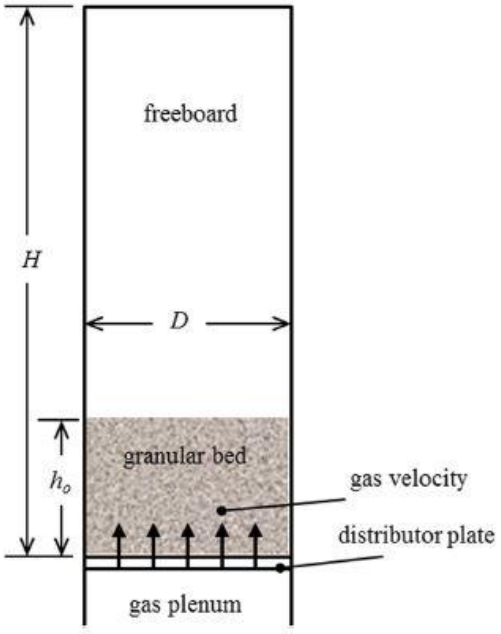

Figure 2. 6 Schematic of fluidised bed column (Teaters et al. 2014)

2.5.2 Solid particles classification:

According to Geldart's classification, there are four solid particle materials, which are classified according to its fluidization properties based on particle density and mean particle size (Geldart 1973) (Daizo and Levenspiel 1991), (Cocco et al. 2014):

- **Type A particles:**

Are describe as aeratable particles. Density is less than about 1400kg/m^3 and mean diameter between 30 and 100 µm. In this type, the bubbles form and appear at velocity larger than the minimum fluidisation velocity, i.e. $U_{mb} > U_{mf}$. **F**luid **C**racking **C**atalysts FCC particles is one material of this type of particles.

- **Type B particles:**

Sometimes these are called sand-like or bubbly particles. Density is in the range between 1400-4000 kg/m^3 and having a mean diameter in the range 40 to 500-600µm. In this type the bubbles appear and form at the fluidisation point at once, $U_{mb} = U_{mf}$. Due to their easy fluidisation, they have wide range of use in industrial applications. Glass beads and coarse silica sand materials are examples of this type particle.

- **Type C Particles:**

These are very fine and cohesive particles. Their mean diameter are less than 30 µm. Due to their high inter-particle force, these very fine solids are difficult to fluidize (Harriott 2003). Materials of this type particle are starch, talc, fly ash, and flour.

- **Type D particles:**

Sometimes they called a spoutable group. This type has very large solid particles greater than 1000 µm and spouted beds may be formed. Some of roasting metal ores, wheat, and coffee beans are classified in this type particle.

Furthermore, a Geldart chart can be used to specify the type of fluidised material depending on three fluidisation parameters: particle density of bed material ρ_p, fluid density ρ_f or ρ_g , and mean particle size of bed material d_p, which can apply only for air at ambient temperature and pressure (Ommen and Ellis 2010).

2.5.3 Types of fluidisations (fluidisation regimes)

Depending on fluid velocity and the type and size of the solid particles as well as bed volume there are various types of fluidization behavior that can be clarified as shown

below. As shown in Figure 2.7-a, a fixed (packed) bed, when a fluid flows upward through a bed of solid particles at very low velocity, the bed is fixed and there is no any movement of particles because the fluid does not have enough velocity (force) to move the particles. In this case, the fluid just percolates through the porous areas between fixed particles. However, this bed is governed by the Ergun equation (2.1) (see Section 2.5.4.1), as superficial fluid velocity increases the pressure drop across the bed increases as well.

2.5.3.1 Incipient fluidization (minimum fluidisation):

As the fluid velocity increases then the bed reaches conditions at which the bed particles start to move and behave as a fluid (or look like possessing liquid properties). At this point, the weight of particles is enough to be supported and counterbalanced by the drag forces, which are exerted by the fluid flow. At this condition the bed is considered to be fluidised as shown in Figure 2.7-b and the fluid velocity is called the minimum fluidisation velocity (U_{mf}) (J.S.M.Botterill 1975)(Harriott 2003)(Sethupathy and E. Natarajan (Institute for Energy Studies, Anna University 2012). More details of gas fluidisation for this point are available in Section 2.5.4.

2.5.3.2 Quiescent state (Particulate fluidisation, or homogeneous):

Quiescent fluidisation is the condition of the bed that lies between the incipient fluidization and bubbles appearance (bubble fluidization). This condition gives a uniform diffusion of particles within the fluid and a uniform expansion of the bed. It only occurs for gas systems over a narrow range of gas velocities between minimum velocity fluidization and minimum velocity of bubbling, when a quiescent state is in the bed (J.S.M.Botterill 1975)(Harriott 2003). This type of fluidization is very clear for type A particles as shown in Figure 2.7- d. Figure 2.7-c shows the smooth fluidisation which is especially related to liquid-solid systems when the liquid velocity is above the minimum fluidisation.

2.5.3.3 Bubbling fluidization (aggregative or heterogeneous fluidisation):

This refers to the condition of the bed, which occurs at the point of bubbles appearing after the quiescent condition. This condition occurs when the gas velocity increases beyond the minimum bubbling velocity, for group A, and directly beyond of the minimum fluidization velocity for group B and group D, respectively. Within this type of fluidization two types of slugging fluidisation conditions can appear when the bed

height to bed diameter ratio is greater than about 2 (narrow column diameter) as shown in Figure 2.7-e and f. However, the bubbles coalesce into larger ones and when their diameter become approximately 2/3 of the bed diameter, the bed introduces slugging conditions. This bubbling fluidisation regime is one of the most applied in gas-solid systems (J.S.M.Botterill 1975)(Harriott 2003) (Yang 2003).

2.5.3.4 Turbulent Fluidization:

When the fluidisation velocity is further increased much larger than minimum fluidisation velocity (U_{mf}) or minimum fluidization bubbling velocity (U_{mb}), a turbulent bed regime will be reached, which is a highly expanded and densely active (Siedlecki et al. 2011). It lies between bubbling and fast fluidisation regimes. In this regime, the bed line surface is hidden, and the different sizes and shapes of solids clusters and gas gaps in turbulent motion can be observed as shown in Figure 2.7g.

2.5.3.5 Fast and Pneumatic Fluidisation:

With a further increase in fluidisation velocity larger than the turbulent fluidisation velocity, the bed material will exhibit to the fast fluidisation and pneumatic transport fluidisation, depending on velocity. Sometimes called a dilute or lean phase fluidisation. It will be spread along the total height of the bed where the solids are in random motion and are held out of the bed with the gas as depicts in Figure 2.7-h. All the above (for all types of fluidisation) can be referred to sources (J.S.M.Botterill 1975) (Daizo and Levenspiel 1991)(Harriott 2003) (Yang 2003)(Cocco et al. 2014).

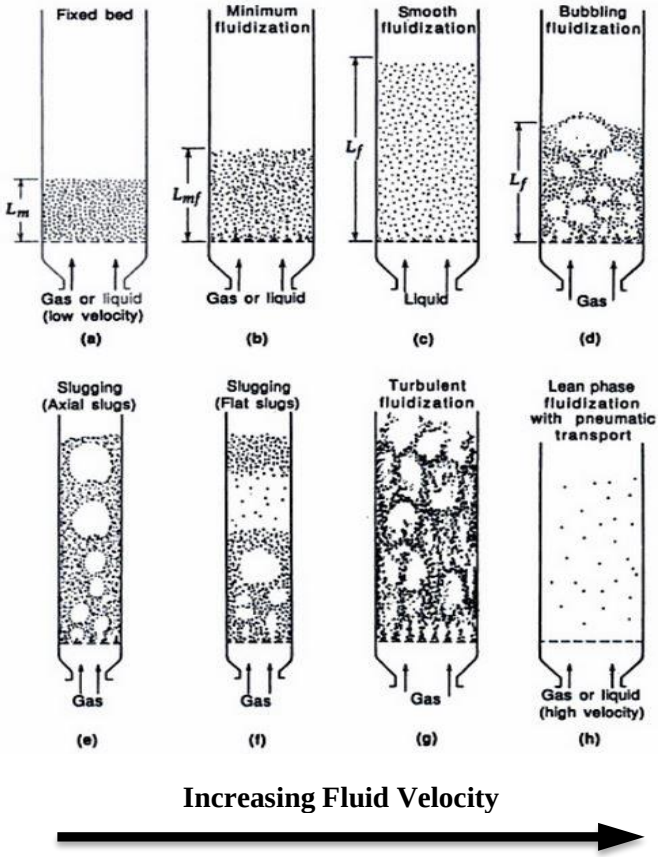

Figure 2. 7 Schematic of various types of fluidisation regimes (Daizo and Levenspiel 1991)

2.5.4 Minimum fluidization velocity and pressure drop

Consider a column of solid particles at any height handled by a porous distributor as shown in Figure 2.6. When any fluid passes and flows through this fixed (packed) bed at low velocity, there is no movement observed and the particles stay in close contact, here the weight of the particles is larger than buoyancy forces and drag forces due to the fluid superficial velocity U_o. Later as the velocity gradually increases the pressure drop across the bed will increase until particles begin to move and this means the pressure drop is equal to the gravity force of the particles and fluid bed per unit cross-sectional area of the bed, as shown in Figures 2.8 and 2.9. Further increase in flow results in unbalanced forces across the bed and the bed becomes fluidize, where the pressure drop reaches to a maximum value ΔP_{max} due to a small drag force, which is needed to overcome the particles frictional forces for rearranging themselves. After this rearrangement, the pressure decreases to its balance forces point. At this point, the pressure drop stays constant for any increase in velocity. The velocity at this fluidization point is called the minimum fluidization velocity (U_{mf}), which represents the transition point between fixed bed and bubbling fluidisation regimes (Daizo and Levenspiel 1991)(Yang 2003)(University of Florida 2015).

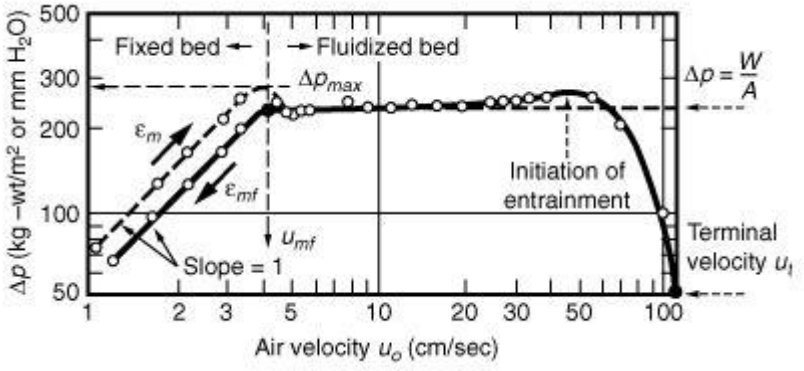

Figure 2. 8 Schematic diagram of pressure drop-gas velocity for solid particles bed (Daizo and Levenspiel 1991)

Overall, the minimum fluidisation velocity U_{mf} is considered an important design parameter in fluidised bed systems, which is very important for characterizing the hydrodynamics of such systems. The value of this parameter can be found by using theoretical or experimental approaches.

2.5.4.1 Theoretical calculations

The theoretical pressure drop-velocity relationship for a height of fixed bed of uniformly sized solid particles, prior the point of fluidisation, is governed by the Ergun Equation which is defined by Equation (2.1) (Daizo and Levenspiel 1991)(Yang 2003).

$$\Delta P/L = \left[\frac{150\mu U_o\ (1-\varepsilon)^2}{(\emptyset_s\, d_p)^2 \varepsilon^3}\right] + \left[1.75\ U_o^2\ \frac{(1-\varepsilon)\rho_f}{(\emptyset_s\, d_p)\varepsilon^3}\right] \quad (2.1)$$

Equation 2.1 can apply for any dimensional consistency units.

To calculate the minimum fluidisation velocity U_{mf}, velocity at which the force of the net weight (net gravitational force) of the bed and the upward force (drag force) exerted by the fluid are balanced. Where:

The drag force of the fluid (upward force) = pressure drop across the bed × cross-sectional area of the bed =

$$= \Delta PA \quad (2.2)$$

The net weight of the particles = net gravitational force of the particles =

$$= AL_{mf} g(1-\varepsilon_{mf})(\rho_p - \rho_f) \quad (2.3)$$

As shown above at the bed fluidisation point (minimum fluidisation), a point of the balancing force, Equation 2.2 equal Equation 2.3, then

$$\Delta PA \ = AL_{mf} g(1-\varepsilon_{mf})(\rho_p - \rho_f) \tag{2.4}$$

Equation 2.4 can be rewritten in the following form to give the pressure drop across the fluidised bed at minimum fluidisation condition:

$$\Delta P/L_{mf} = g\left(1-\varepsilon_{mf}\right)\left(\rho_p - \rho_f\right) \tag{2.5}$$

At the point of minimum fluidisation, Eq. 2.1 becomes

$$\Delta P/L_{mf} = \left[\frac{150\mu U_{mf}(1-\varepsilon_{mf})^2}{(\emptyset_s\, d_p)^2 \varepsilon_{mf}^3}\right] + \left[1.75\, U_{mf}^2 \frac{(1-\varepsilon_{mf})\rho_f}{(\emptyset_s\, d_p)\varepsilon_{mf}^3}\right] \tag{2.6}$$

By equating Eq. 2.5 and 2.6, the result equation is:

$$g\left(1-\varepsilon_{mf}\right)\left(\rho_p - \rho_f\right) = \left[\frac{150\mu U_{mf}(1-\varepsilon_m)^2}{(\emptyset_s\, d_p)^2 \varepsilon_{mf}^3}\right] + \left[1.75\, U_{mf}^2 \frac{\left(1-\varepsilon_{mf}\right)\rho_f}{(\emptyset_s\, d_p)\varepsilon_{mf}^3}\right] \tag{2.10}$$

For very small particles ($d_p \leq 0.1$mm), where the flow conditions $Re_{mf} \leq 10$, only the first term in Equation 2.10 is important (Daizo and Levenspiel 1991)(Harriott 2003)(Subramanian 2004), so

$$U_{mf} = \left[\frac{g\left(\rho_p - \rho_f\right)(\emptyset_s\, d_p)^2}{150\mu}\right]\left[\frac{\varepsilon_{mf}^3}{\left(1-\varepsilon_{mf}\right)}\right] \tag{2.11}$$

For very large sizes dp ≥ 1mm, where the flow conditions $Re_{mf} > 1000$, the laminar flow term in Equation 2.10 can be neglected (Daizo and Levenspiel 1991)(Harriott 2003)(Subramanian 2004), so

$$U_{mf} = \left[\frac{g\left(\rho_p - \rho_f\right)(\emptyset_s\, d_p)\varepsilon_{mf}^3}{1.75\, \rho_f}\right]^{0.5} \tag{2.12}$$

Equation 2.10 was rewritten in the form of Equation 2.13, where

$$\frac{1.75}{\emptyset_s \varepsilon_{mf}^3}\left(\frac{d_p U_{mf}\rho_f}{\mu}\right)^2 + \frac{150(1-\varepsilon_{mf})}{\varepsilon_{mf}^3 \emptyset_s^2}\left(\frac{d_p U_{mf}\rho_f}{\mu}\right) = \frac{d_p^3 \rho_f g\left(\rho_p - \rho_f\right)}{\mu^2}$$

$$\frac{1.75}{\emptyset_s \varepsilon_{mf}^3} Re_{p.mf}^2 + \frac{150(1-\varepsilon_{mf})}{\varepsilon_{mf}^3 \emptyset_s^2} Re_{p.mf} = Ar$$

According to their experimental data, a simple form of Ergun equation was suggested by Wen and Yu in 1966 as shown in Equation 2.13 (Daizo and Levenspiel 1991) (Yang 2003).

$$\boldsymbol{K1}\, Re_{p.mf}^2 + \boldsymbol{K2}\, Re_{p.mf} = Ar \tag{2.13}$$

Where,

- $Re_{p.mf} = \left(\frac{d_p U_{mf} \rho_f}{\mu}\right)$, is defined as the particle Reynold number
- $Ar = \frac{d_p^3 \rho_f g\left(\rho_p - \rho_f\right)}{\mu^2}$, is defined as Archimedes number, a dimensionless group. Sometimes called Galileo number Ga.
- $\boldsymbol{K1} = \frac{1.75}{\emptyset_s \varepsilon_{mf}^3}$, $\boldsymbol{K2} = \frac{150\left(1-\varepsilon_{mf}\right)}{\varepsilon_{mf}^3 \emptyset_s^2}$ are constants, depend on the void of the bed at minimum fluidisation ε_{mf} and sphericity $\emptyset_s$ of the bed particle.

Equation 2.13 is a quadratic equation, which can be solved for $Re_{p.mf}$. Finally, U_{mf} can be obtained. For most practical applications, Equation 2.13 was solved and rearranged in term of Reynold number in the following form.

$$Re_{p.mf} = \left(\frac{d_p U_{mf} \rho_f}{\mu}\right) = [\boldsymbol{C_1^2} + \boldsymbol{C_2}\, Ar]^{0.5} - \boldsymbol{C_1} \qquad (2.14)$$

Where: $\boldsymbol{C_1}$= $\boldsymbol{K2}$/2$\boldsymbol{K1}$ and $\boldsymbol{C_2}$= 1/$\boldsymbol{K2}$ are constants, which can obtained empirically when both parameters ε_{mf} and/or ϕ_s are not available. These constants are available in many published papers for many investigators (Daizo and Levenspiel 1991)(Yang 2003)(Jiliang et al. 2013).

2.5.4.2 Experimental determination

As explained above the transition point between the fixed bed regime and fluidised bed regime has been used practically to determine the minimum fluidisation velocity for gas-solid systems. Experimentally, for any gas-solid particle system the pressure drop-gas superficial velocity diagram can be built. As shown in Figure 2.9 below, for the fixed bed region when the low gas velocity increases the pressure drop across the bed increases linearly until the bed at point A is ready to start to expand and fluidise. A further slight increase of velocity the pressure drop reaches its maximum point (B) and then reduces to point C, a point at which the forces are balanced and pressure drop remains nearly constant for any increase in gas velocity as shown in line CD. The next step is the reversing of process (from fluidisation to defluidisation) by decreasing the gas velocity steadily. The pressure drop in fixed bed region for defluidisation path (EF) is less than fluidisation path due to the particle loosing arrangement. The intersection point E of extended DC line and extended FE line will represent the minimum

fluidisation velocity. In most literature the intersection point A of line DC and increasing velocity line in fixed bed represents the initial fluidisation velocity $U_{mf,i}$ and point C represents the complete fluidisation velocity $U_{mf,c}$ (Subramanian 2004)(University of Florida 2015). Most research used this pressure drop profile method for determining mainly the minimum fluidisation velocity U_{mf} for a specified fluidisation system (Badday et al. 2014) (Chok et al. 2010)(Chok 2009) (Subramani et al. 2007)(Patil et al. 2005)(Hilal et al. 2001)(Gauthier et al. 1999).

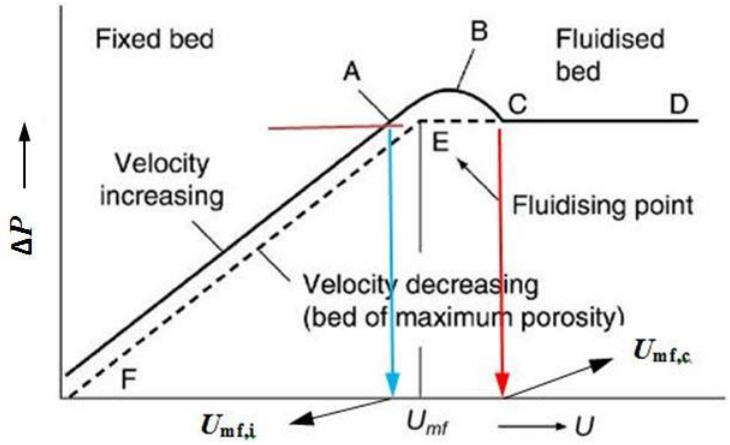

Figure 2. 9 Pressure drop-gas superficial velocity fluidisation diagram (redrawn) (University of Florida 2015)

2.5.5 Biomass fluidisation

Due to their extreme nature, high content of cellulose, hemicellulose and lignin composition and a wide range in physical characterizations (mainly irregular size, shape and density) biomass is considered anisotropic material, which gives it a clear difference in their mechanical property in various directions (Guo et al. 2012). Thereby, these properties have made the characterization of fluidisation of biomass materials, especially agricultural and forest residues (lignocellulosic biomass), is not predictable easily (Cui and Grace 2007)(Escudero and Heindel 2011)(Oliveira et al. 2013)(Shao et al. 2013). The hydrodynamic fluidisation of various types of biomass particles has been investigated by many researchers focusing on; the fluidisation characteristics of biomass particles as a single material, improving their fluidisation characterization by mixing them with a fluidisable second solid (inert) material like sand, alumina, calcite, etc, (Karmakar et al. 2013)(Zhang et al. 2011). Moreover, this parameter also needs to study the effects of related parameters on it such as: biomass particle size, density, biomass weight percent in the bed mixture and the degree of the mixture mixing and

segregation due to the high difference in the densities, particle size and composition of two materials of the mixture.

2.5.5.1 Fluidisation of a single biomass material

For characterising of fluidization of single biomass materials, many studies have been conducted. In their experiments (Aznar et al. 1992) showed that agricultural and forest biomass materials such as sawdust, straw and ground thistle cannot be fluidised unless using a second fluidising solid material.

Fluidisation characteristics such as particle size, bulk density and fluidising velocity for various Malaysian biomass residues (rise husk, sawdust, peanut shell, coconut shell and palm fibre) and coal and bottom ash were experimentally obtained by (Abdullah et al. 2003). These experiments were conducted using an air-cold flow-fluidising column. They classified sawdust, coconut shell, coal and bottom ash were classified in Geldart's B particle size, whereas rice husk and palm fibre type D and A respectively. They concluded that type B group has good fluidising behaviour, while group D and A have a weak behaviour.

(Zhong et al. 2008) carried out their fluidisation experiments on both, single biomass materials and binary mixture with three inert fluidisation medium materials, silica sand, alumina oxide and continental flood basalt (CFB) cinder. Their biomass materials were five, three of them were approximate sphere particles (wood chip ρ_p=564kg/ m^3, millet ρ_p= n.a, and mung beans ρ_p= 1640kg/ m^3), whereas the others were long thin particles (cotton stalk ρ_p = 365 kg/m^3 and corn stalk ρ_p =274 kg/m^3). They measured the minimum fluidisation for each material using a similar procedure that was followed by (Rao and Bheemarasetti 2001). The value of U_{mf} was measured using a descending gas flow curve from the complete fluidised state. For two long thin biomasses, they found that these materials could not be fluidised when the particle aspect ratio was over a certain value. They attributed to their particles nature for bridging and relaxing each other and this affected their fluidisation negatively. While the fluidisation for single biomass for approximate spherical particles was not presented.

In their study, (Chok et al. 2010) considered that palm shell biomass wastes fall in Geldart D group. They reported that this material is difficult to fluidise as a single material. To facilitate fluidisation, it should be mixed with another fluidisable material like sand.

In their experimental study (Zhang et al. 2011) performed a fluidisation experiments for a single biomass (agricultural residues of cotton stalk). Its particle properties: thin long shape with aspect ratio (height/diameter)=5, mean diameter= 5mm, mean height=25mm, ρ_p= 385.3kg/m^3 and ρ_b=147kg/m^3. When they compared the fluidisation behaviour for each single material (biomass and sand) using ΔP-U_o hydrodynamic curve, they found that ΔP slope, which was considered as the characterizing for particle cohesion force in initial fixed bed, for biomass is higher than one for sand. They attributed this to the higher aspect ratio, fibre contents and low density of this biomass type, which caused a higher cohesion and liaison force and this needs an excess force to overcome these forces.

2.5.5.2 Fluidisation of biomass-inert binary mixture

In order to obtain a high performance of fluidised bed reactors, the characterizations of fluidisation of biomass solid fuel materials should be improved. This can be achieved by mixing biomass material with other inert fluidisable solid material such as silica sand, alumina, calcite, etc, to form a binary or multi material system, which can be fluidised easily. This second material will improve, especially in thermo-chemical conversion process, gas-solid reactants contact, heat and mass transfer, temperature uniformity inside the reactor, rate of reactions and fluidisation quality as well (Guevara 2010)(Sharma et al. 2013)((Shao et al. 2013). Due to high differences in the nature and the physical properties of those materials, inert and biomass, like material density, particle size and shape, many fluidisation problems have arisen such as mixing and segregation phenomena, bed channelling, specifying and measuring of the minimum fluidisation velocity of the bed mixture and biomass weight percent effect.

For binary biomass-inert material mixtures, the determination methodology of minimum fluidisation velocity is different compared to a single material as shown above. Experimentally all researchers have used a conventional ΔP-U_o diagram. Most of them have used the defluidising curve for specifying minimum velocity. Also they found that the defluidisation curve was located below the fluidisation curve, except some studies revealed the opposite (Aznar et al. 1992)(Rao and Bheemarasetti 2001)(Karmakar et al. 2013).Three points of fluidisation velocity have been obtained. The first one is called the initial fluidisation velocity U_{if}, which can be obtained at the point of the intersection of the extrapolation of two lines, fixed bed for fluidisation curve (increasing velocity) and constant pressure drop for fluidisation region. The second

velocity is called the minimum fluidisation velocity U_{mf}, which can be specified at the point of the intersection of the extrapolation of two lines, fixed bed for defluidisation curve and constant pressure drop at fluidisation condition. The third velocity is called a complete fluidisation velocity U_{cf}, which was specified when the first conversion of constant pressure drop line for defluidisation curve to fixed bed conditions and vice versa or, by observation, when entire bed materials are moved (Aznar et al. 1992). Figure 2.10 illustrates all these velocities for various studies. Many researchers used these three velocity values to evaluate the fluidisation quality of the system. They said that whenever the interval distance between U_{if} and U_{cf} is small the fluidisation quality is good (Sampaio 2013). This interval sometimes called segregation interval (U_{cf}-U_{if}). In most previous studies, U_{mf} velocity was taken as minimum fluidisation velocity as a design parameter.

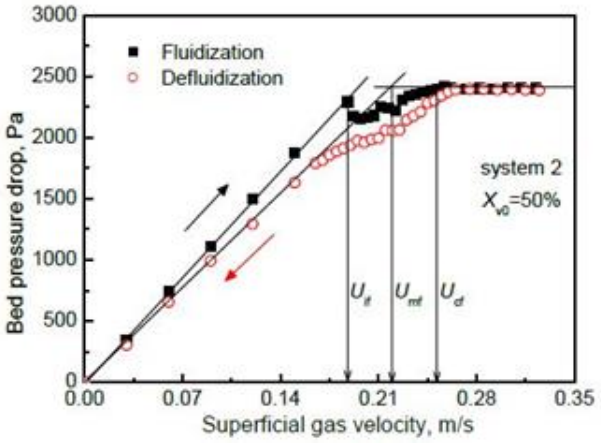

Figure 2. 10 Schematic of pressure-superficial velocity curve for biomass-inert binary mixtures showing three types of minimum fluidisation velocities (Sampaio 2013)

Experimentally, investigators confirmed in their studies the using of the above procedure of the determining of the minimum fluidising velocity (using decreasing velocity) for biomass-inert mixtures. They are, such as (Qiaoqun et al. 2005), (Formisani et al. 2008), (Zhang et al. 2011), (Oliveira et al. 2013), (Sharma et al. 2013), (Sampaio 2013), (Kumoro et al. 2014), etc, whereas (Clarke et al. 2005) used the intersection point of fluidisation (increasing velocity) curve, not the defluidisation curve.

2.5.6 Parameters affect minimum fluidisation velocity

In fluidisation systems, either for single bed or for binary biomass-inert mixtures, many parameters affect the values of the design parameter minimum fluidisation velocity.

2.5.6.1 Particle size of the bed material

For four different particle size ranges between 125 and 500μm of single sand (ρ_s=2700kg/m^3), (Aznar et al. 1992) showed that both velocities U_{mf} and U_{cf} increased as sand particle size increased

(Badday et al. 2014)investigated the effect of particle size on minimum fluidisation velocity U_{mf}. They used three particle sizes of sand bed material 301μm, 454μm, 560μm using 0.1 ID of fluidisation column. They found out that U_{mf} increased as particle size increased. Similar finding was obtained by (Qiaoqun et al. 2005) for sand material only. (Chok 2009) found in their study for compartmented fluidised bed gasifier (gasifier and combustor compartments) that both velocities U_{mf} and U_{cf} for sand material for both compartments increased as mean particle size $\overline{d_p}$ increased (196, 272, 341, 395μm). (Dora et al. 2013) studied the fluidisation characteristics of four ternary mixtures for three different particle sizes of single dolomite solid material in a conical column bed. One aspect of their study, the effect of bed static height H_s (10cm, 12.5cm, 15cm and 17.5cm), cone angle (4.61, 5.13, 7.47 and 11.2), average particle size for each ternary mixture (1.29mm, 1.2mm, 1.125mm and 1.106mm) on pressure drop ΔP_{mf} and superficial velocity U_{mf} at minimum fluidisation conditions were discussed. For average particle size effect they found that for a cone angle of 7.47 and initial static bed height = 10cm, ΔP_{mf} and U_{mf} increased as the particle size increased.

2.5.6.2 Height of static bed

The effect of the static bed height H_s of the sand–sawdust biomass binary mixture on minimum fluidisation velocity was studied by(Aznar et al. 1992). For different ratio of H_s/D (bed height to column diameter), they observed there was no effect of the bed height on U_{mf} or U_{cf}. The minimum fluidisation velocity was conducted by (Marque 2002) for 2*D* rectangular fluidised bed column (1× 0.2 × 0.012 m). For different static bed heights (8, 16, 20, 40, 60 cm) and glass beads particle size range (250-400μm), they showed that static bed height had a significant effect on minimum fluidisation velocity U_{mf}, where U_{mf} increased as H_s increased. For conical tapered fluidised bed (Sau et al. 2007) experimentally showed that the static bed height H_s had no effect on the U_{mf}. For the effect of static height (or biomass bed) on the minimum fluidisation velocity, (Jena et al. 2008) and (Escudero and Heindel 2011) concluded that there was no any change in U_{mf} value when the static bed height was changed. In their experimental study on the flow behaviour of a mixture of four different biomass material, which differed in their

particle shape, size and density, with sand as fluidisation medium, (Shao et al. 2013) showed that for multi composition mixture there was no clear effect of the static bed height H_s on the minimum fluidisation velocity when increased from 100mm to 200mm. As mentioned in previous section for (Dora et al. 2013) study, they showed that for this type of bed column and for a specific cone angle and average particle size of ternary mixture, ΔP_{mf} and U_{mf} increased as the initial static bed height H_s increased. This finding is contrary to the previous study (Sau et al. 2007) above, which used a conical bed, and the conventional bed columns which have been presented above.

2.5.6.3 Percentage of biomass in biomass-solid binary mixture

For different volume percentage of pine sawdust biomass-sand (ρ_s=2700kg/m^3) mixture, for four different sand particle sizes, (Aznar et al. 1992) studied the effect of biomass concentration on both fluidisation velocities U_{mf} and U_{cf}. They found out that a linear increase of both velocities up to nearly 50 % as biomass content increased for four sand sizes. In addition, they showed that the mixture could not be fluidised when the sawdust biomass percentage reached 75-80%. In (Rao and Bheemarasetti 2001) study one aspect of their results shows the effect of the biomass mass percent for three types of agricultural residues, rise husk, sawdust and groundnut shell, for three biomass mass percent, 0%, 2%, 5% and 15%, on the minimum fluidisation velocity of biomass-sand binary mixture. It can be seen that U_{mf} of the mixture increased linearly as biomass percent increased for a range between 0 % and 5 %. Whereas this increased exponentially for a range between 5% and 15%. A similar effect was obtained by (Karmakar et al. 2013) for three biomass types rise husk, bagasse and sawdust for four weight percent 2%, 5%, 10% and 15%.

Also, (Qiaoqun et al. 2005) observed that as mass fraction of rise husk increased (from 0% to approximately 10.5%) the measured U_{mf} increased linearly. (Clarke et al. 2005) showed that for a specific size of glass sphere and sawdust moisture content, as the mass fraction of sawdust increased the U_{mf} of the mixture increased. Also for (Zhong et al. 2008) and (Chok et al. 2010) studies, which have been presented in previous section, a similar finding was found for their biomass materials.

For their fluidisation of biomass material, sweet sorghum bagasse, tobacco residues and soybean hulls, in sand binary mixtures, (Oliveira et al. 2013) found out, for three biomass percent 5%, 10% and 15%, that for biomass material-sand mixture U_{mf}

decreased slightly as biomass percent increased, whereas for the other two materials, U_{mf} increased as the biomass percent increased.

(Sharma et al. 2013) used a cold-flow column to study the effect of the mixture composition of the reactor bed, gasifier solid residues GSR, switchgrass fuel biomass and inert silica sand material, on fluidisation behaviour. Their mixture composition ranged from 0.17 to 5 % (as wt %) of the sand amount for switchgrass, for their binary mixture, and from 5.0 to 35 % of the switchgrass amount for GSR material, for their tertiary mixture. ΔP-U_o graphical method, as described before, was used to determine U_{mf} experimentally. They found that minimum fluidisation velocity for a mixture of sand and GSR was decreased dramatically when GSR increased from 5% to 35 %. In contrast, for a tertiary mixture the minimum velocity was increased as mass fraction of two materials, switchgrass and GSR, increased from 0.17% to 3% and from 5% to 35 %, respectively. Using the effective properties of tertiary mixture the determining of U_{mf} from selected correlations from previous work did not agree well with the experimental values for all mixture composition. Finally, they concluded that bed mixture of 5% weight of switchgrass caused a segregation and bed channelization, whereas up to 3% weight percent the bed fluidisation was sustained.

2.5.6.4 Elevated temperature

As mentioned before, the fluidised bed has been widely used in thermo-chemical conversion processes (combustion, gasification and pyrolysis). These process are working at a high temperature reached to 900-1000^{o}C in fluidised bed gasifiers. This high temperature affects the physical properties of the fluidisation medium, thereby affecting the fluidisation behaviour which is mainly represented by minimum fluidisation velocity design parameter (Lettieri and Macrì 2016). (R. R. Pattipati 1981) experimentally investigated the effect of the temperature on the minimum fluidisation velocity U_{mf}. It was conducted for sand material (for small particle < 2mm and for particles > 2mm) in fluidised bed using hot air as fluidised medium. They found that for small particles (240, 462 and 1310µm) U_{mf} decreased with temperature (from 18 to 900^{o}C), whereas for large particles (3376µm) U_{mf} increased. In their experimental study (Subramani et al. 2007) determined the U_{mf} at a wide range of temperature from 25^{o}C to 700^{o}C for four bed materials type Geldart B (ilmenite, sand, limestone, and quartz magnetite) for various small particle sizes (128, 134, 163, and 200 µm) using air as a fluidising medium. Each value of U_{mf} was determined at steady required temperature.

Their experimental data, which was presented graphically, showed that as the temperature increased U_{mf} decreased for all materials and particle sizes, which agrees with the finding results of (R. R. Pattipati 1981) for small particle sizes. In addition, it was noticed that the trends of U_{mf} took a considerable decrease for temperature ranged approximately from 298^{o}K to 600^{o}K, while this decreasing took place steadily for temperature above 600^{o}K. For particle size, U_{mf} still increased with particle sizes of bed material without any effect of high temperature on particle size. For two bed materials, quartz sand (ρ_s= 2750 kg/m^3) and bottom ash (ρ_s= 2500 kg/m^3) with average particle diameter =0.5mm, and for temperature range from 30^{o}C to 600^{o}C, the experimental results of fluidisation study obtained by (Jiliang et al. 2013) showed similar effect of temperature on U_{mf} that has been presented above. Similar result of temperature effects on U_{mf} was obtained by (Seo et al. 2014). They used a silica sand material with different mean particle size ($\overline{d_p}$ = 135, 210, 270, and 385μm) for temperature ranged from 25 to 800^{o}C. From their results, they confirmed that at high temperature (400-800^{o}C) for small particle sizes ($\overline{d_p}$ = 135, 210, and 270 μm) U_{mf} became constant, whereas a considerable decrease for ($\overline{d_p}$ = 385 μm). Recently, (Lettieri and Macrì 2016) reviewed most experimental and theoretical studies related to the temperature effects on fluidisation parameters, mainly minimum fluidisation velocity.

2.5.6.5 Distributor plate performance

The performance of fluidised bed reactors is strongly affected by the fluidisation quality. Design of the gas distributor plate plays an important role in the fluidisation quality to achieve the aims. There are various types of distributor plate (grates) designs. These plates can be classified into three groups: 1) plate-type distributor, which consists of two types, porous plate and perforated plate, 2) Nozzle (Tuyere) -type or bubble cap-type, 3) Sparge pipe-type. This study focus on the perforated plate design because of its simple manufacturing, cheap, suitable for pilot plant and laboratory researches (Basu 2006), (Yang 2003), (Daizo and Levenspiel 1991).

(Bauer et al. 1981) studied the effect of distributor design on the performance of the fluidised bed reactor by using the fraction of unreacted ozone as a performance parameter. They found that porous plate provided a better conversion than perforated plate distributor.

For studying the effects of distributor plate on the minimum fluidisation velocity U_{mf} (Hilal et al. 2001) used four different type of distributors. Three of them were perforated plates with hole diameter 0.794mm for each, hole pitch were (12, 9, 7mm), and percent of free (open) area (0.34, 0.61, 1.17 %), respectively, whereas the fourth one was a porous plastic with thickness of 1.71cm and permeability of 12.35 Darcy. They found that as the pitch hole decreased, U_{mf} increased. The highest value of U_{mf} value was for porous plate. In the fluidised bed dryer (Jangam et al. 2009) studied experimentally and via modelling the effect of the percentage open area (from 10% to 50%) and orifice diameter of 2mm thick metal perforated distributor plate on the maldistribution function in percent, a criteria which was used for distributor plates comparison. A lower value indicates a better air distribution (uniformity of airflow) across the cross-section of the bed. They found that this maldistribution function decreased when the open area decreased and became near zero when low values of open area were used, approximately 10%-20%. For orifice diameter effect, they showed that the air uniformity reduced when the orifice diameter increased. For their experimental study on fluidisation of bagasse biomass-sand mixtures (Augusta et al. 2011) showed that there were no changes in the value of the minimum fluidisation velocity U_{mf} when the orifice diameter of the tuyere gas distributor changed. (Ghaly et al. 2015) studied the configuration effect (shape and conical angle) of the distributor plate on the pressure drop in a bubbling fluidised bed reactor. They classified the fluidisation quality according to pressure drop fluctuations, which can be observed in gas-fluidised bed. Good fluidisation gives moderate fluctuations, while large fluctuations may denote slugging, and no fluctuations denote strong channelling in the bed. Therefore, a distributor plate should be designed to give moderate pressure fluctuations.

2.6 Summary

The combined effects of the operating and hydrodynamic parameters on the gasification process, generally, and on the bubbling fluidised bed gasifier performance, particularly, have been reviewed. The biomass gasification by the airflow bubbling fluidised bed gasifier has been highlighted. The method of the determination of the minimum fluidisation velocity has been described, analytically using the theoretical equations and experimentally using the ΔP-U_{mf} hydrodynamic curve. The factors, which affect this velocity have been presented.

Overall, from this review it can be concluded and suggested that:

a) Air gas can be utilized as gasifying agent (fluidisation medium) for biomass gasification. Biomass gasification using air-flow bubbling fluidised bed gasifier can be achieved at a range from 350^{o}C to 900^{o}C. Also, between 0.2 and 0.6 the equivalence ratio can be used.

b) According to the literature studies the inert material silica sand, which is belong to Geldart type B, can be used as a high quality fluidised bed material for single material or for biomass binary mixtures at high temperature gasification process. The range of particle size is ranged from 100µm to 600µm.

c) Due to a shortage data in agricultural biomass gasification by air fluidising bed gasifier, and gasifier performance, the operating and hydrodynamic factors that affect the design and performance of the gasifier have been researched.

d) The effect of the number of distributor plate holes on the fluidised bed gasifier performance has not been found in literature. This research is also studied this effect.

Chapter 3

Design and Development of the Rig

3.1 Introduction

In order to study, experimentation, the performance and the conversion rates of the gasification process for solid biomass fuels in bubbling fluidised bed gasifier, a new lab-scale rig for this gasifier was designed and built. The designing and building of the rig specified the main and secondary rig components, which contributed to the study. In this chapter, firstly the whole structure of the rig has been identified by specifying those main and secondary components. Determining the size of the rig depends mainly on determining the size of the reactor itself. It is a gasifier whose is the focus of this study.

The study has required the gasifier to be in a size that is easy to control its operation and at the same time has enough research flexibility. This flexibility will allow for appropriate ranges of design parameters, which are needed to study their effects on the gasifier performance whether for this current or for subsequent studies in this field.

The design method, which is followed in this study, differs from the design methods, which are usually followed in the design of the chemical engineering unit operations. In these methods, the capacity of production or the mass flow rate of any feed material with other given data is firstly specified. Then the calculations of the mass and energy balances will be performed. Finally the needed design parameters and thereby the size of the unit will be obtained. Whereas, in this study the size of the gasifier is firstly specified by selecting a suitable and desire value of the gasifier diameter. Based on the diameter selection the other design parameters have been calculated and their required ranges specified. These ranges can specify the size of the main secondary components of the rig, like biomass screw feeder, air flowrate rotameter, air pre-heater and electrical high temperature heater in addition to the height of the gasifier itself. All these design parameter ranges give enough gasifier flexibility to study the effects of these design parameters.

3.2 Geometry and hydrodynamic design of the bubbling fluidised bed gasifier

3.2.1 Theoretical model of bubbling fluidising bed reactor

In this study, the two-phase model of Kuni-Levenspiel (1969) has been used to represent the behavior of the gas-solid bubbling fluidised bed reactor. It gives a good representation of the experimental data for this system. For this model the two phases are an emulsion phase, often called the dense phase, and a bubble phase, also can be called a lean phase as shown in Figure (3.1) (Daizo and Levenspiel 1991) (Ommen and Ellis 2010).

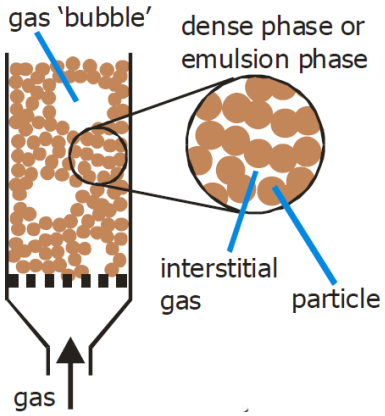

Figure 3. 1 Sketch of the two–phase model in the bubbling fluidised bed (Ommen and Ellis 2010)

The bubble phase consists of a bubble, which contains a very small amount of solid particles. As shown in Figure 3.2 it is not spherical but it has a nearly hemispherical top and a pushed in the bottom. Each bubble has what is called wake that contains a significant amount of solids. This wake, with its solids can be pulled when the bubble is rise. A cloud region which separates the bubble and the emulsion phases is created when a gas from a rising bubble is penetrated for a short distance into the surrounding emulsion phase(Newton 1969) (Daizo and Levenspiel 1991) (Yang 2003).

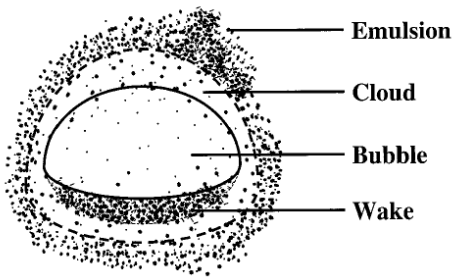

Figure 3. 2 Sketch of the bubble, wake, cloud and emulsion (Newton 1969)

In this model, there are several concepts and definitions, mainly as following (Newton 1969)(Daizo and Levenspiel 1991)(Yang 2003):

The fraction of the total bed occupied by the bubbles without wakes, δ.

The volume of the wake per volume of bubbles, α.

The fraction of the total bed occupied by the wakes, $\alpha\delta$.

The fraction of the total bed that occupied by the emulsion phase including clouds, $(1-\delta-\alpha\delta)$.

3.2.2 Design equations for the reaction bed section

For bubbling fluidised bed reactor a two-phase model, bubble and emulsion phases, will be used for this type of fluidising regime. There are a number of design equations govern this regime and this model.

3.2.2.1 Calculation of the minimum fluidization velocity, U_{mf}:

As mentioned in Chapter 2-Section 2.5.4.1, minimum fluidization velocity U_{mf} is an important parameter in fluidised bed reactor design. It can be calculated using Equation (2.11) or a quadratic Eurgn equation with the form shown in Equation (3.1). For fine particles, the constants C1=33.7 and C2= 0.0408, which were recommended by Wen and Yu (Daizo and Levenspiel 1991).

$$Re_{p.mf} = \left(\frac{d_p U_{mf} \rho_f}{\mu}\right) = [\boldsymbol{C_1^2} + \boldsymbol{C_2}\, Ar]^{0.5} - \boldsymbol{C_1} \tag{3.1}$$

Equation (3.2) was used to calculate the bed void fraction at the minimum fluidization conditions ε_{mf} (Newton 1969) (Daizo and Levenspiel 1991):

$$\varepsilon_{mf} = 0.586\, \emptyset_s^{-0.72} \left[\frac{\mu^2}{\eta\, d_p^3\, \rho_g}\right]^{0.024} \left[\frac{\rho_g}{\rho_s}\right]^{0.021} \tag{3.2}$$

$$\emptyset_s = Particle\ sherecity = \frac{surface\ area\ of\ a\ spherical\ particle}{actually\ surface\ area\ of\ the\ particle} = \frac{A_s}{A_p} \quad (3.3a)$$

$$\emptyset_s = \frac{\pi\left[(6V_{p/\pi})^{1/3}\right]^2}{A_p} = \frac{\pi[6V_p/\pi]^{2/3}}{A_p} \quad (3.3b)$$

Where:

V_p: Volume of a spherical particle

$$Vp = \frac{\pi {d_p}^3}{6} \quad (3.4)$$

$$d_p = \bar{d}_p = \frac{1}{\sum\frac{f_i}{d_{pi}}} = the\ mean\ particle\ size \quad (3.5)$$

f_i is the fraction of particles with diameter d_{pi}.

3.2.2.2 Calculation of the particle terminal velocity, U_t

Terminal velocity is a free fall velocity of the particle. For design purpose, it is considered a maximum superficial velocity (velocity of the agent fluid) in the bubbling fluidised bed. By this limitation superficial velocity must be above U_{mf} and below U_t. Based on Reynold numbers of the particles, two relation- ships of terminal velocity are presented by Kuni-Levenspiel (Newton 1969)(Basu 2006).

$$U_t = \frac{\eta d_p^2}{18\mu} \qquad \text{for } Re_{Ut} < 0.4 \quad (3.6a)$$

$$U_t = \left[\frac{1.78*10^{-2}\eta^2}{\rho_g \mu}\right]^{1/3} d_p \qquad \text{for } 0.4 < Re_{Ut} < 500 \quad (3.6b)$$

3.2.2.3 Calculation of the slugging velocity, *Ums*

Slugging velocity is a fluid velocity at which the slugging regime occurs. It can be expressed by the bubble rise velocity $U_{b,ms}$, where below the value of this velocity slugging shall not take place (Newton 1969) (Daizo and Levenspiel 1991) (Basu 2006). The bubble rise velocity can be expressed by an equation below.

$$U_{b,ms} = U_{mf} + 0.07\ (gD)^{1/2} \quad (3.7)$$

(Daizo and Levenspiel 1991) concluded that when the fluidising velocity (superficial velocity of fluidisation) is more than $\boldsymbol{U_{b,ms}}$ slugging would be the main regime.

3.2.2.4 Calculation of the superficial velocity, U_o

U_o calculation can be suggested according to the conditions

$$U_{mf} < U_o < U_t \qquad \text{and} \qquad U_{mf} < U_o < U_{b,ms}$$

The condition at which the slugs are formed when the maximum stable bubble size d_{bmax}, which is calculated by Equation (3.10), is greater than 0.6 times the diameter of the bed D, the permitted maximum bubble size $d_{bmax,p}$ (Daizo and Levenspiel 1991) (Yang 2003), i.e.

$$d_{bmax,p} = 0.6\,D \tag{3.8}$$

In other reference, $$d_{bmax,p} = \frac{2}{3}\,D \tag{3.9}$$

In other word, d_{bmax} should not exceed 0.6D or 2/3 D; otherwise, the suggested U_o must be changed.

3.2.2.5 Calculation of the maximum bubble-size, d_{bmax}

For the estimation of the bubble size at any superficial velocity it is important and useful to know if the fluidised bed provide the slugging phenomena or not by comparing the estimated value to the bed diameter according to Equation (3.10).

$$d_{bm} = d_{bmax} = 0.652[\,A_c\,(U_o - U_{mf})]^{0.4}, \quad \text{in cm} \tag{3.10}$$

Where A_c = cross-sectional area of the fluidised bed reactor.
U_o - U_{mf} = excess fluidizing velocity

3.2.2.6 Calculation of the bed height, H

According to Baeyens & Geldert analysis (Yang 2003), there are three separate zones in a deep bed operating with an excess velocity U_o - U_{mf} as illustrated in Figure (3.3)

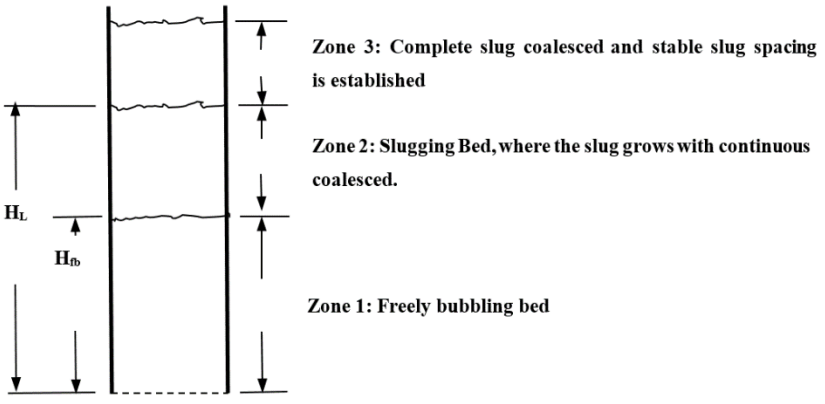

Figure 3. 3 Stages of the slug regime establishment

The minimum bed height for stable slugging can be calculated by equation (3.11).

$$H_{L,min} = 60\ D^{0.175}\ , \qquad D \text{ in cm} \tag{3.11}$$

The maximum bed height below which the bed will be freely bubbling can be calculated from equation (3.12).

$$H_{fb,max} = \frac{(D - 2.51D^{0.2})}{0.13D^{0.47}}\ , \qquad D \text{ in cm} \tag{3.12}$$

The slugging regime can be avoided by operating within zone (1) with freely bubbling bed. Most of the literatures (Daizo and Levenspiel 1991) (Yang 2003) (Basu 2006) stated that to avoid the slugging regime, especially in the lab-scale and pilot plant reactors, the ratio of the bed height to the bed diameter must not exceed 2.

i.e.

$$\frac{H_s}{D} \leq 2 \tag{3.13a}$$

It means that

$$H_{s,max} = 2D \tag{3.13b}$$

H/D ratio sometimes called aspect ratio. For this design study, Equation (3.13b) was recommended to use for H_s specifying.

3.2.2.7 Calculation of the bubble size d_b, at any height h of the bed at any time.

Bubble diameter sometimes called a mean bubble size or an equivalent volume diameter of a bubble. (Daizo and Levenspiel 1991) (Yang 2003) (Basu 2006) mentioned that for Geldart B and D solids, Mori & Wen suggested a correlation for bubble size at any height h in the bed as in equation (3.14).

$$\frac{d_{bm} - d_b}{d_{bm} - d_{bo}} = e^{-0.3h/D}$$

Or

$$d_b = d_{bm} - (d_{bm} - d_{bo}) \times e^{-0.3h/D} \tag{3.14}$$

Where:

$d_{bm} = d_{bmax}$ = The maximum size of bubble, Eq.(3.10).

d_{bo} = The initial bubble size formed near the bottom of the bed at the plate distributor.

Equation (3.14) can be applied within the following conditions

$H/D \leq 1.3$

$60\mu m \leq d_p \leq 450\mu m$

$0.5\, cm/sec \leq U_{mf} \leq 20\ cm/sec$

$U_o - U_{mf} \leq 48\, cm/sec$

For beds with diameter between 7 and 30 cm, Equation (3.14) approximately has good accuracy (Newton 1969).

d_{bo} can be estimated depending on the type of the distributor plate, d_{bo} in cm:

- For porous plates (Newton 1969)(Daizo and Levenspiel 1991) (Yang 2003) (Basu 2006)

$$d_{bo} = 0.00376\ (U_o - U_{mf})^2 \quad (3.15a)$$

- For perforated plate

$$d_{bo} = 0.347[A_c(U_o - U_{mf})/n_d]^{0.4} \quad (3.15b)$$

Where, $\mathbf{n_d}$ is the number of the holes.

3.2.2.8 Calculation of the bubble rise velocity, U_b

It can be calculated from Equation (3.16) (Daizo and Levenspiel 1991) (Basu 2006).

$$U_b = (U_O - U_{mf}) + 0.71\ (gd_b)^{0.5} \quad (3.16)$$

All terms are defined in previous steps.

3.2.2.9 Calculation of the fraction of bed in bubble phase, δ

This represents a volume fraction of the total bed occupied by the bubbles that does not include the wake. It can be calculated from Equation (3.17).

$$\delta = \frac{U_o - U_{mf}}{U_b - (U_{mf} \times (1+\alpha))} \quad (3.17)$$

α is the volume of wake per volume of bubble. It's value vary between 0.25-1, with typical values close to 0.4 (Newton 1969) (Yang 2003) .

Notes 1: The bed material fraction in the wakes is $(\alpha\delta)$.

2: The bed fraction in emulsion phase (not including bubble wakes)

$$=1 - \delta - \alpha\delta. \quad (3.18)$$

3: For fast bubbles or when$U_b > 5\,U_{mf}/\varepsilon_{mf}$, clouds are thin and (Daizo & Levenspiel, 1991).

$$\delta = \frac{U_o - U_{mf}}{U_b - U_{mf}} \tag{3.19}$$

4: In highly bubbling beds where, $U_o \gg U_{mf}$, the approximation of δ is(Daizo and Levenspiel 1991) :

$$\delta = \frac{U_o}{U_b} \tag{3.20}$$

3.2.2.10 Calculation of the mass solid in the bed, W_s

The mass balance for the bed solids gives (Newton 1969),

$$W_s = \rho_s A_c H_s\,(1-\varepsilon_s) \tag{3.21}$$

$$= \rho_s A_c\, H\,(1-\varepsilon)$$

$$= \rho_s A_c H_f\,(1-\varepsilon_f)$$

$$= \rho_s A_c H_{mf}(1-\varepsilon_{mf})$$

Where, ρ_s = a particle density of the solid bed material.

A_c = cross-sectional area of the bed reactor.

H_s = height of the bed settled before particles start to lift (static bed height).

H_f = height of the bed at any time.

ε_s = porosity (void fraction) of the settled (fixed or static) bed.

For Geldert B and D solids bed, (Daizo and Levenspiel 1991) gave an equation represents $\varepsilon_f, \varepsilon_{mf}\ and\ \delta$ relation,

$$\left(1-\varepsilon_f\right) = (1-\delta)(1-\varepsilon_{mf}) \tag{3.22}$$

From equation (3.22) ε_f can be calculated

$$\varepsilon_f = 1 - [(1-\delta)\left(1-\varepsilon_{mf}\right)] \tag{3.23}$$

From equation (3.21) and equation (3.22), the mass of the solid bed can also be calculated:

$$W_s = \rho_s A_c H_f (1-\delta)(1-\varepsilon_{mf}) \tag{3.24}$$

All parameters in equation (3.24) can be given or calculated as shown in previous steps.

3.2.2.11 Calculations of the feed biomass flow rate:

The feed mass rate of biomass can be calculated from the supplied air flowrate and suggested gasification equivalence ratio, ***ER***, where:

$$\boldsymbol{ER} = \frac{[\boldsymbol{mass\ air\ fuel\ ratio,\ \ MAFR}]_{\boldsymbol{actual}}}{[\boldsymbol{mass\ air\ fuel\ ratio,\ \ MAFR}]_{\boldsymbol{stoichiometric}}} \tag{3.25}$$

The actual mass air fuel ratio is a ratio of the actual air mass rate $\dot{m}_{air}$, to the actual biomass mass rate $\dot{m}_{biomass}$. However these actual values can be experimentally specified and calculated and observed from the measurement devices in the rig. Also for design purposes, they can be theoretically calculated from above equation (3.25). Thereafter the feed mass rate of biomass can be calculated by

$$[\ mass\ air\ fuel\ raio\ ]_{actual} = ER\ \times\ [mass\ air\ fuel\ ratio]_{stoichio}$$

$$[MAFR]_{actual} = ER\ \times\ [MAFR]_{stoichio} \tag{3.26}$$

The value of the equivalence ratio ***ER*** can be suggested. For the air gasification system the stoichiometric value of the mass air fuel ratio, depending on the composition of the solid biomass, can be approximately estimated from the Equation (3.27) (PETRO 2007).

$$[MAFR]_{stoichio} = 8.89 \times [\%C + 0.375 \times \%S] + 26.5 \times \%H - 3.3 \times \%O \tag{3.27}$$

Where: %C, %S, %H and %O are the carbon, sulfur, hydrogen, and oxygen composition percent in solid biomass fuel. These percent can be obtained from the ultimate analysis of the fuel.

Finally, the actual (required) feed mass rate of the fuel biomass can be calculated by equation (3.28):

$$\dot{m}_{biomass} = [\dot{m}_{air}]/[\ MAFR]_{actual} \tag{3.28}$$

From the density of the air at a specific temperature and pressure, conditions at which the air volumetric flow rate is specified or measured, which can be calculated from the superficial velocity $\boldsymbol{U_o}$ of the air and bed cross-sectional area $\boldsymbol{A_c}$ as shown in equation (3.30), the air mass flow-rate will be calculated.

$$air\ mass\ flowrate = [volumetric\ flowrate] \times [air\ density\ at\ specific\ temperature\ and\ pressure]$$

$$\therefore \dot{m}_{air} = \dot{V}_{air} * \rho_{air\ at\ \text{ambient cond.}} \tag{3.29}$$

Where

$$\dot{V}_{air} = (U_o)(A_c) \tag{3.30}$$

3.2.3 Freeboard Section

Freeboard is defined as the height of the column section, as a part of the fluidised bed column, between the surface of the bed phase (dense phase) and the outlet of the gas. It is called the freeboard height $\boldsymbol{H_{fb}}$. However, the design of this section is important to give a chance to the solid materials to return to the bed section. In addition, it gives additional time to complete some chemical reactions like tar materials in gasification process. For design consideration, the location of the exit gas should be above the **T**ransport **D**isengaging **H**eight **TDH**, a height at which the flux of the solids material and its size distribution are approximately constant. Figure (3.4) shows these definitions. Note play, when H_{fb} is greater than TDH the carryover of solids will be reduced and vice versa. This will directly affected the duty of the solid separator equipment. In addition, for the thermal conversion the carryover of the unburned solid carbon will be minimized when H_{fb} > TDH. In addition, this height will give additional residence time for the chemical reactions.

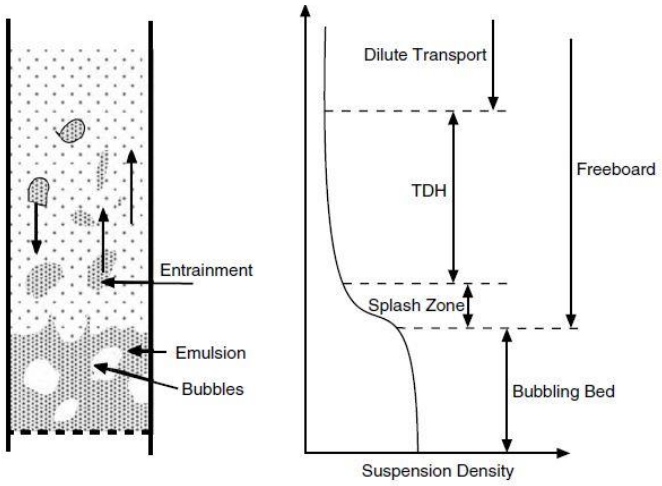

Figure 3. 4 Schematic of freeboard zones in bubbling fluidised bed (Basu 2006)

3.2.3.1 Estimation of TDH and total height of the gasifier

Many empirical correlations can be used to estimate the TDH. Three correlations have been used in this design to calculate TDH.

1. Froud correlation (Yang 2003).

Froud number: $$\frac{U_o^2}{g\ (TDH)} = 10^{-3} \quad (3.31a)$$

$$\therefore \quad TDH = \frac{U_o^2}{g*10^{-3}} \quad \text{in SI unit} \quad (3.31b)$$

2. A correlation related to the bubble size (Basu 2006).

$$TDH = 4.47(d_{eq,s})^{0.5} \quad (3.32)$$

$d_{eq,s}$ is the equivalent volume diameter of a bubble at the bed surface, *TDH*, in meter unit.

In literature, equivalent volume diameter d_V has been calculated as shown in equation, $d_V = \left[\left(\frac{6}{\pi}\right) \times volume\ of\ particle\right]^{\frac{1}{3}}$. Generally, d_V was calculated by equation (3.33):

$$d_V \approx 1.13\ d_p\ , \text{ (Basu 2006)} \quad (3.33a)$$

So, according to Equation (3-33a), $d_{eq,s}$ can be calculated by:

$$d_{eq,s} = 1.13\ d_{b,s} \quad (3.33b)$$

where, $d_{b,s}$ is the bubble diameter at the bed surface. It can be calculated by Equation (3.14).

3. Fung and Hamdullahpur equation (Yang 2003).

$$\text{TDH} = 13.8 \times d_b \quad (3.34)$$

The total freeboard height H_{fb} can be calculated using Equation (3.35). 30 cm was added to its TDH height to calculate H_{fb}, a location of gasifier gas outlet.

$$H_{fb} = 0.3 + TDH \quad (3.35)$$

The total height of the gasifier (above distributor plate) can be calculated using Equation (3.36):

$$H_{Total,g} = H_{fb} + H_{expansion} \quad (3.36)$$

3.2.4 Distributor plate and air box section

3.2.4.1 Pressure drop across distributor plate

Pressure drop is an important factor affected uniformity and stability of fluidization over the entire cross-section and the height of the bed. To overcome these issues most

practical designs of bubbling beds keep the distributor pressure drop within 15%-30% of the bed pressure drop (Yang 2003) (Basu 2006),

For design calculation, pressure drop across distributor plate can be calculated using Equation (3.38) (Yang 2003),

$$\Delta P_{dis} = 0.3 \times \Delta P_{bed} \tag{3.38}$$

ΔP_{bed} Can be calculated from equation (3.39) (Basu 2006),

$$\Delta P_{bed} = \rho_P(1-\varepsilon_f)H_f g = \rho_P(1-\varepsilon_{mf})H_{mf} g \tag{3.39}$$

For superficial velocities up to 5 m/sec and for group (A) particles, ε_f can be approximately calculated,

$$\varepsilon_f = \frac{U_f+1}{U_f+2} \tag{3.40}$$

For a rough estimation of void ε_f, Equation (3.40) can be used for other bubbling beds like B group particles (Basu 2006).

The total pressure drop across distributor plate and bed material can be calculated using Equation (3.41),

$$\Delta P_{Total} = \Delta P_{dis} + \Delta P_{bed} \tag{3.41}$$

3.2.4.2 Gas velocity at orifice, U_{orf}

U_{orf} is related to ΔP_{dis} according to equation (3.42) (Yang 2003)(Basu 2006),

$$U_{orf} = C_d\left[\frac{2\,\Delta P_{dist}}{\rho_{g,orf}}\right]^{0.5} \tag{3.42}$$

C_d, is the discharge coefficient and its value range is 0.5-0.8. For thick plate and $(t/d_{orf}) > 0.09$, C_d can be calculated from equation (3.43) (Basu 2006),

$$C_d = 0.82(t_{distr}/d_{orf})^{0.13} \tag{3.43}$$

3.2.4.3 Number of distributor plate orifices (holes), N_{orf}

For any number of orifices of distributor plate, N_{orf}, which its diameter is d_{orf}, orifice velocity U_{orf} and superficial velocity $U_f = U_o$ may be related by making a gas mass balance,

[Total gas mass inside the orifice] $_{\text{orifice}}$ = [total mass of the gas in the bed above plate]$_{\text{bed}}$

= [total mass of the gas in the air-box under plate] $_{\text{air-box}}$

$$[N_{orf}(\frac{\pi}{4}\, d_{orf}^2)(U_{orf})(\rho_{g,orf})]_{orifice}=[(\frac{\pi}{4}\, D^2)(U_f)(\rho_g)]_{bed} \quad (3.44)$$

$$\therefore\ N_{orf} = (\frac{D}{d_{orf}})^2\ (\frac{\rho_g}{\rho_{g,orf}})\ (\frac{U_f}{U_{orf}}) \quad (3.44a)$$

The number of the holes per unit area can be calculated by equation (3.45)

$$N_{den} = \frac{N_{orf}}{A_c} \quad (3.45)$$

3.2.4.4 Orifices layout

The density of the holes, N_{den}, the number of the orifices per unit area of the distributor plate, depends on the orifices arrangement on the plate and the orifices pitch, the distance between holes center. There are two main orifices arrangement (Yang 2003)(Basu 2006),

1- Equidistance triangular layout

For this arrangement,

$$N_{den} = \frac{2}{\sqrt{3}}\ \frac{1}{P_{pitch}^2} \quad (3.46a)$$

Or

$$P_{pitch} = \sqrt{\frac{2}{\sqrt{3}}\ \frac{1}{N_{den}}} \quad (3.46b)$$

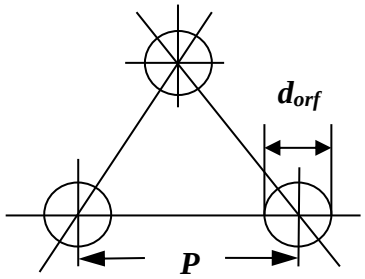

2- Square Pitch Layout

For this arrangement,

$$N_{den} = \frac{1}{P^2} \quad (3.47a)$$

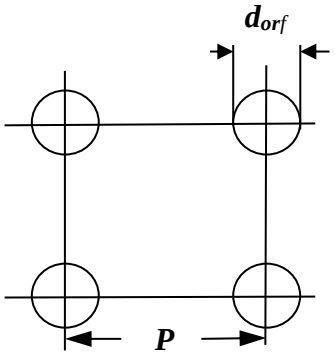

Or

$$P_{pitch} = \frac{1}{\sqrt{N_{den}}} \quad (3.47b)$$

Triangle hole layout was chosen for perforated distributor design for this study because of its more holes per unit area, the equidistance of the pitch for all orifices in the grid and the stagnant zones are less(Yang 2003).

3.2.4.5 Air box (plenum) design

The plenum section is the room that directly located below the distributor plate. Its task is to disperse the gas uniformly under the plate. Through survey research relevant most of the researchers(Yang 2003)(Basu 2006) have not pointed to any design calculations or to the design equations related to air box design through which pushes gas to fluidisation reactor across the distribution plate. (Yang 2003) showed in brief various design configurations and their specifications. (Basu 2006) said that as a result of the air flow there is an additional resistance, i.e. pressure drop. It is called rearrangement resistance ΔP_r.

3.3 Rig and gasifier operating flexibility

The gasifier, which is the focus of this study, is the heart of the rig. This gasifier was needed to design and construct to have flexible design specifications. Thereafter allowing the manipulation and the change of the values of the parameters and factors whose have a direct and indirect impact on the performance and efficiency of the reactor. This will give sufficient flexibility for the researcher to study and search most and a wide range of the variables affecting the gasification process in the bubbling fluidised bed gasifiers.

3.3.1 Design procedure and design steps

According to the hydrodynamic relations, which govern the design of the bubbling fluidised bed reactor, a simple Matlab program was built for this purpose and is presented in Appendix B. According to the required feeding data, presented in Table 3.1, the program was processed. The design procedure and steps are presented in Appendix A. A logarithmic chart for this design procedure is shown in Figure 3.5.

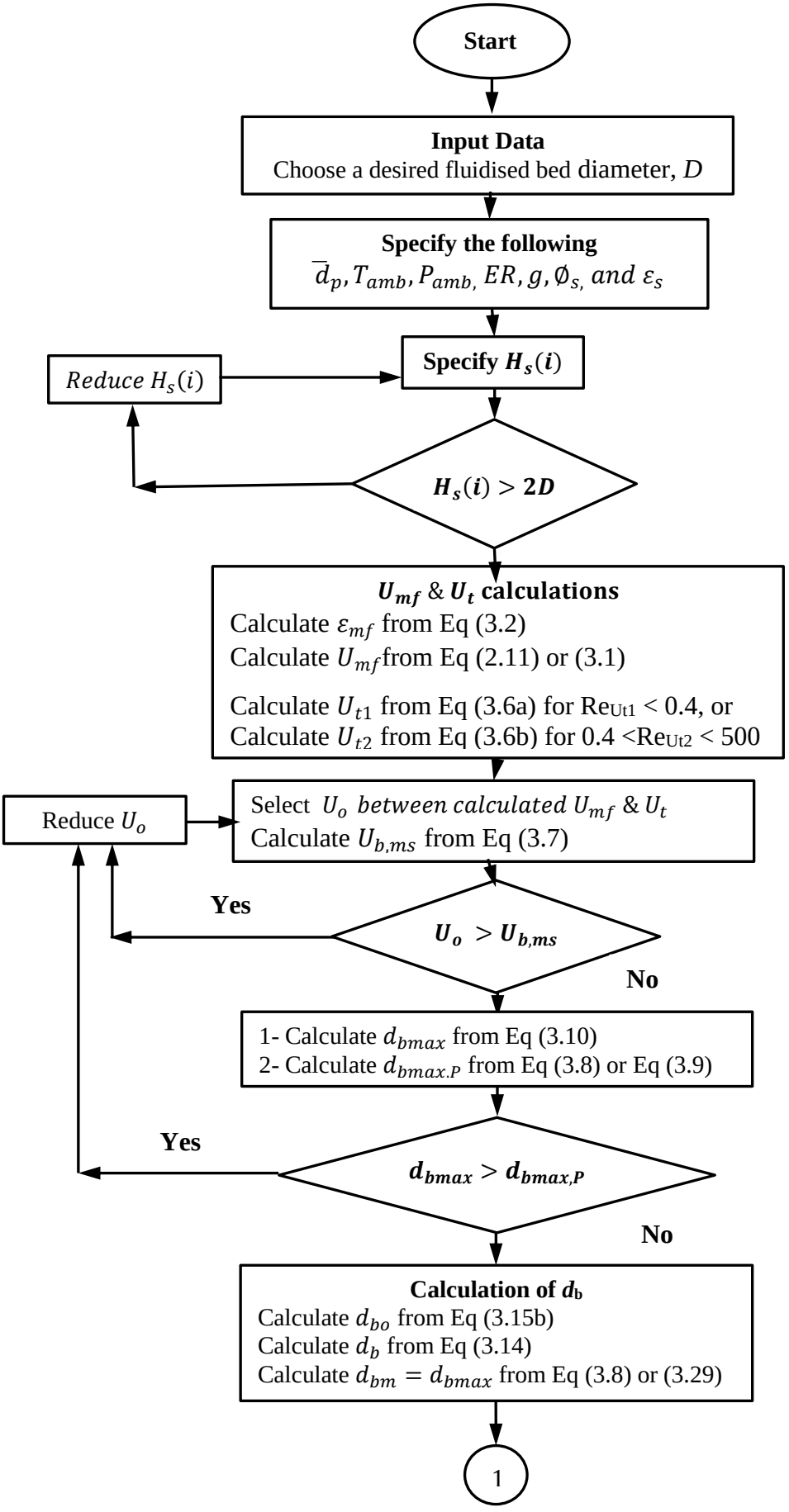
Start
Input Data
Choose a desired fluidised bed diameter, D
Specify the following
$\overline{d}_p, T_{amb}, P_{amb,}\ ER, g, \emptyset_{s,}\ and\ \varepsilon_s$
Specify $H_s(i)$
$Reduce\ H_s(i)$
$H_s(i) > 2D$
U_{mf} & U_t calculations
Calculate ε_{mf} from Eq (3.2)
Calculate $U_{mf}$from Eq (2.11) or (3.1)
Calculate U_{t1} from Eq (3.6a) for Re_{Ut1} < 0.4, or
Calculate U_{t2} from Eq (3.6b) for 0.4 <Re_{Ut2} < 500
Select U_o between calculated U_{mf} & U_t
Calculate $U_{b,ms}$ from Eq (3.7)
Reduce U_o
Yes
$U_o > U_{b,ms}$
No
1- Calculate d_{bmax} from Eq (3.10)
2- Calculate $d_{bmax.P}$ from Eq (3.8) or Eq (3.9)
Yes
$d_{bmax} > d_{bmax,P}$
No
Calculation of d_b
Calculate d_{bo} from Eq (3.15b)
Calculate d_b from Eq (3.14)
Calculate $d_{bm} = d_{bmax}$ from Eq (3.8) or (3.29)
1

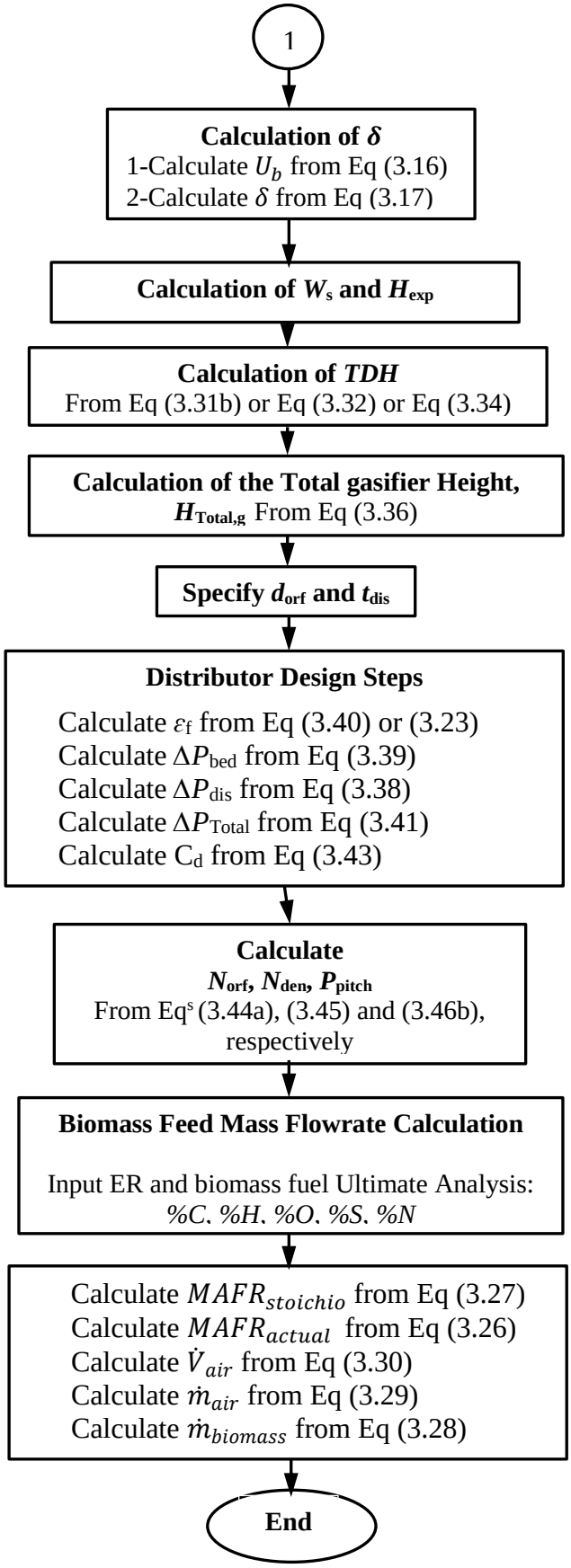

Figure 3. 5 Logarithm layout of the gasifier design

3.3.2 Design Results

Basically, the size of the reactor can be specified by determining the diameter. Also, the size of many accessories of the gasifier rig and material quantities, reactant and bed materials, will be affected by the gasifier size, which should be taken into consideration as well. Therefore, the diameter should be firstly specified. It was needed to be as large lab-scale as possible to study the gasifier performance as if it was a pilot plant size to be closer to the industrial performance. Firstly, 15cm reactor diameter was recommended. A Matlab design calculation program was run out. The first results showed that 15cm diameter gave a large size indication through the biomass feeding quantity, which was considered a control parameter for gasifier sizing. Therefore, three sizes, 15cmm, 11.5cm, 8.3cm were selected to compare their results to choose the suitable one. According to the input feeding data as shown in Table 3.1, the results were obtained as follows:

Table 3. 1 Feeding data for gasifier design program for three-selected diameter

Program Feeding (Input) Data	**Specifications and Values**
1- Bed Material	Solid silica sand particles
2- Gas Agent	Air
2- Solid Fuel	Sawdust Pinewood biomass
3- Bed material Particle Size	1-(300-425)µm dp=0.0396cm, 2-(425-500)µm dp= 0.0478cm, 3-(500-600) dp=0.0546cm
4- Bed Material Static Height Hs, cm	1) 0.5D, 2) 1D, 3) 1.5D, 4) 2D, 5) 3D
5- Operating Temperature, ^{o}C	Ambient Temperature= 20^{o}C
6- Operating Pressure, atm	1 atm
8- Superficial Air Velocity Uo, cm/sec	From U_{mf} (as minimum value) for 5-6 iteration with step =5cm/sec.
9- Sand particle sphericity ϕ_s and sand static porosity ε_s	0.75 and ε_s can be calculated by particle and bulk density.
10- Equivalence Ratio ER	= 0.2 minimum and = 0.6 maximum
11- Ultimate Analysis of sawdust biomass fuel	Provided in Chapter 4

3.3.2.1 Biomass feed mass flowrate:

From the design results, the mass flow rate of biomass feeding fuel, Fedbio in kg/hr, was calculated as a minimum value and maximum value for each selected diameter, 8.3cm, 11.5cm and 15cm as shown in Table 3.2 and Figure 3.6. These minimum and maximum values were calculated according to minimum fluidising air velocity U_{mf}, for the smallest particle size and maximum ER=0.6, and maximum air velocity, for largest particle size, and minimum ER=0.2, respectively.

Table 3. 2 Minimum and maximum values of feeding biomass mass flowrate for three selected values of gasifier diameter.

D, cm	Feedbio (min), kg/hr	Feedbio (max), kg/hr
8.3	0.22	2.46
11.5	0.42	4.72
15	0.72	8.04

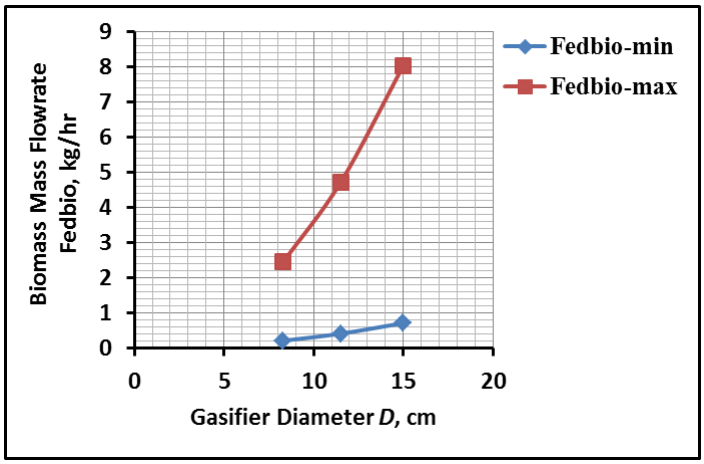

Figure 3. 6 Minimum and maximum values of feeding biomass mass flowrate for three selected values of gasifier diameter.

From the results, it can be seen that the minimum biomass mass flowrates, 0.22kg/hr and 2.46 kg/hr are belong to the diameter 8.3cm. For this diameter, these quantities can be easily provided comparing to other diameters 11.5cm and 15cm.

3.3.2.2 Number of orifices (holes) of distributor plate:

From the results of the design calculations, it can be seen that the minimum and maximum values of the number of holes of the distributor plate N_{orf} was affected by air superficial velocity, static height of the bed and bed material particle size. For the case of D=8.3cm and for bed particle size (500-600), Figure 3.7 shows that number of holes increases when the air velocity increases, whereas it decreases as the bed static height increases. For other particle sizes, the effect shows similar behaviour. The results show that there is no effect of ER. The same behaviour was obtained for other diameters.

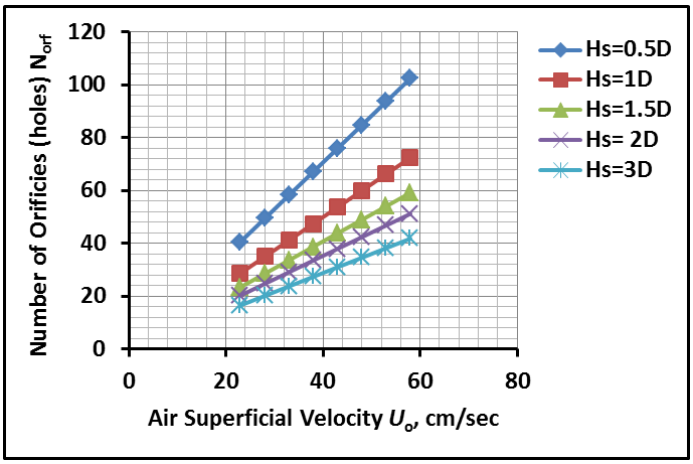

Figure 3. 7 Effect of superficial air velocity and static bed height on the number of holes for gasifier diameter D=8.3cm, for bed particle size (500-600) µm

The summary of the results of minimum and maximum values of number of holes for three diameters, for three particle sizes, for five different static height and for different velocities are presented in Figure 3.8.

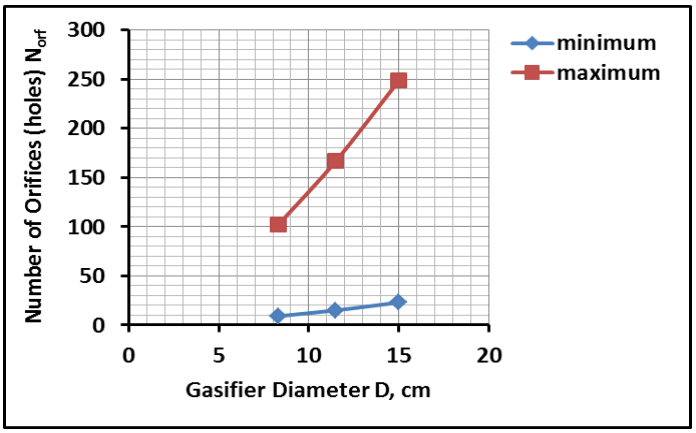

Figure 3. 8 Effect of gasifier diameter on the number of distributor hole. Minimum and maximum values were selected for each diameter.

3.3.2.3 Total height of the gasifier above the distributor plate

The total height of the gasifier $\boldsymbol{H}_{\text{Total}}$ for D= 8.3cm was calculated in meter unit. This height was calculated for three different equations of TDH. As shown in Table 3.3 the minimum value was taken at smallest gasifier diameter, 0.5D and at minimum fluidisation air velocity U_{mf}, whereas the maximum values was taken at 3D and at latest value of air velocity U_{o} with step= 5cm/sec. According to Equation (3.31b), the design calculations showed that H_{Total} varied only as U_{o} varied. Whereas for other two equations H_{Total} varied with superficial velocity and significantly with static height and there is no effect of particle size. From the Table, it can be seen that the values of H_{Total}, whose were calculated by Equations of TDH (3.34) and (3.32) are more satisfied and suitable for the lab-scale gasifier.

Table 3. 3 Minimum and maximum values of total height of gasifier for three different TDH equations for D=8.3cm

Particle Size, µm	**(500-600)**		**(425-500)**		**(300-425)**	
***TDH* Eq.**	$\boldsymbol{H}_{\text{Total}}$**min, m**	$\boldsymbol{H}_{\text{Total}}$ **max, m**	$\boldsymbol{H}_{\text{Total}}$**min, m**	$\boldsymbol{H}_{\text{Total}}$**max, m**	$\boldsymbol{H}_{\text{Total}}$ **min, m**	$\boldsymbol{H}_{\text{Total}}$ **max, m**
(3.34)	0.47	1.54	0.47	1.54	0.47	1.54
(3.31b)	5.9	34.8	3.9	29.4	2.2	23.9
(3.32)	0.47	2	0.47	2	0.47	2

3.3.2.4 Effect of the static bed height and diameter of the gasifier diameter on the minimum fluidisation air velocity

Design calculations showed that the variation of the static bed height H_{s} and gasifier diameter D were not affected the minimum fluidisation air velocity for all three selected particle size of the bed material. From the Figure 3.9a and b, it can be seen that for a specific bed particle size when the gasifier diameter or static bed height increases the design parameter U_{mf} stay constant. This is due to the all-theoretical and empirical equations of U_{mf} calculation have not any effect of H_{s} and D.

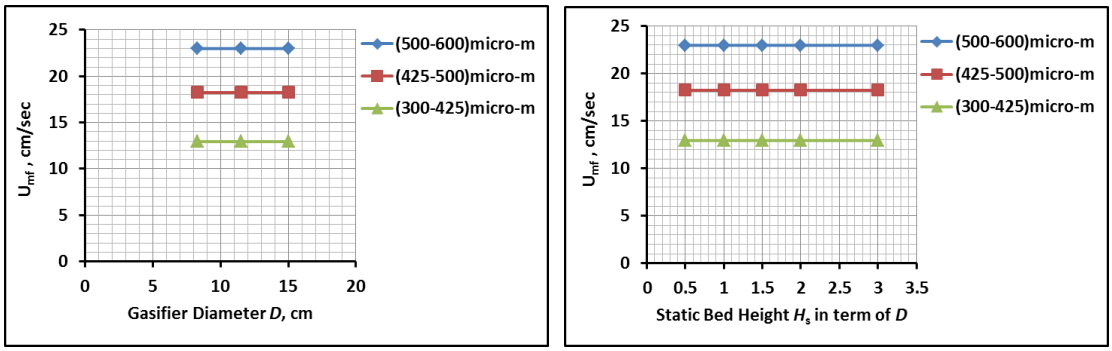

a) **b)**

Figure 3. 9 Effect of a) gasifier diameter *D* and b) static bed height H_s on the minimum fluidisation air velocity U_{mf}

3.3.3 Summary of the flexible design and geometry parameters of the gasifier

3.3.3.1 Summary of the main design parameters

According to the required feeding data, which are shown in Table 3.1, and design results, the range values, minimum and maximum, of the main flexible design parameters are summarized in Table 3.4.

Table 3. 4 Recommended flexible values of design parameters for gasifier diameter D=8.3cm

Parameters	Recommended flexible Range	
	Minimum value	Maximum value
1- Gasifier diameter, D	8.3cm	8.3cm
2- Biomass feed mass rate, Fedbio	0.22 kg/hr	2.46 kg/hr
3- Fluidising agent (Air) flow rate	U_{mf} of (300-425) µm	3-5×U_{mf} of (500-600)µm
4- Gasification Reaction Temp, T2. *	350°C	900°C
5- Reaction Equivalence Ratio, ER *	0.2	0.6
6- Static bed height, H_s **	0.5*D*	2.5*D*
7- Bed Material Particle Size ***	(300-425)µm	(500-600)µm
8- Total height of the gasifier	0.47m	2m
9- No of holes of distributor plate	≈ 10	≈ 100 and more

* Suggested values according to gasification operating conditions.
** Suggested range for design purposes.
*** Suggested ranges according to the supply sand and Geldert B Type.

3.3.3.2 Summary of the geometry and dimension of the gasifier parts

To implement gasifier height and geometry flexibility, a gasifier should be divided into many sections, as columns. According to the sections design, as shown above, the suggested assembled gasifier unit is shown in Figure 3.10 below. Each section should

be had two flanges, upper and lower. These flanges help the researcher to join the required sections as required. These sections are, starting from the bottom of the gasifier as follows:

3.3.3.2.1 Air box (plenum) section

This section has a fixed height 30cm and one upper flange. Its bottom is directly connected to the air supply pipe. This pipe introduce at the center inside the box section for 20cm. There is 10cm between the open top end of the air supply pipe and distributor plate. There is a 2.54cm hole diameter at the center of the air-box bottom to collect the falling materials from the bed through distributor plate. Its geometry drawing and specifications are presented in section A.2.6 in Appendix A.

3.3.3.2.2 Distributor plate (grate) section

This section is a circular thick metal plate. It has the same outside diameter of the flanges. It contains a number of orifices (holes), 1.5mm recommended diameter, with a triangle holes layout. These holes are located within the inside cross-sectional area of the reactor column to distribute the gas into the bed. Also it contains a same number and size of the flange holes, 10 mm diameter, which are located in similar distribution of flange holes. These holes are located outside diameter of the column (pipe) section. Its geometry drawing and specifications are presented in Section A.2.5 in Appendix A.

3.3.3.2.3 Fluidised bed reaction section

The height of this section depends on the results of the design calculations of the expansion height of the bed solid material during fluidisation process. Any excess height for this section can be considered as a part of the freeboard height section. This section has an upper and bottom flanges which can join from the bottom flange to plenum and distributor plate sections. In addition, it includes 2-3 holes. Two of them are used for biomass and bed material feeding point and the third for waste material outlet point. Its geometry drawing and specifications are presented in Section A.2.4 in Appendix A.

3.3.3.2.4 Freeboard section

It is a flexible section. This section may consist of one to three different height pieces depending on the study investigation. Each of them consist two upper and lower flanges. In addition, for design and research consideration the diameter of this freeboard section

can be changed. It includes holes for producer gas outlet, for gas analyzer sample and for measuring instruments. Its geometry drawing and specifications are presented in Sections A.2.2 and A.2.3.

3.3.3.2.5 Gas outlet top section

It is an optional section. Its geometry drawing and specifications are presented in Sections A.2.1.

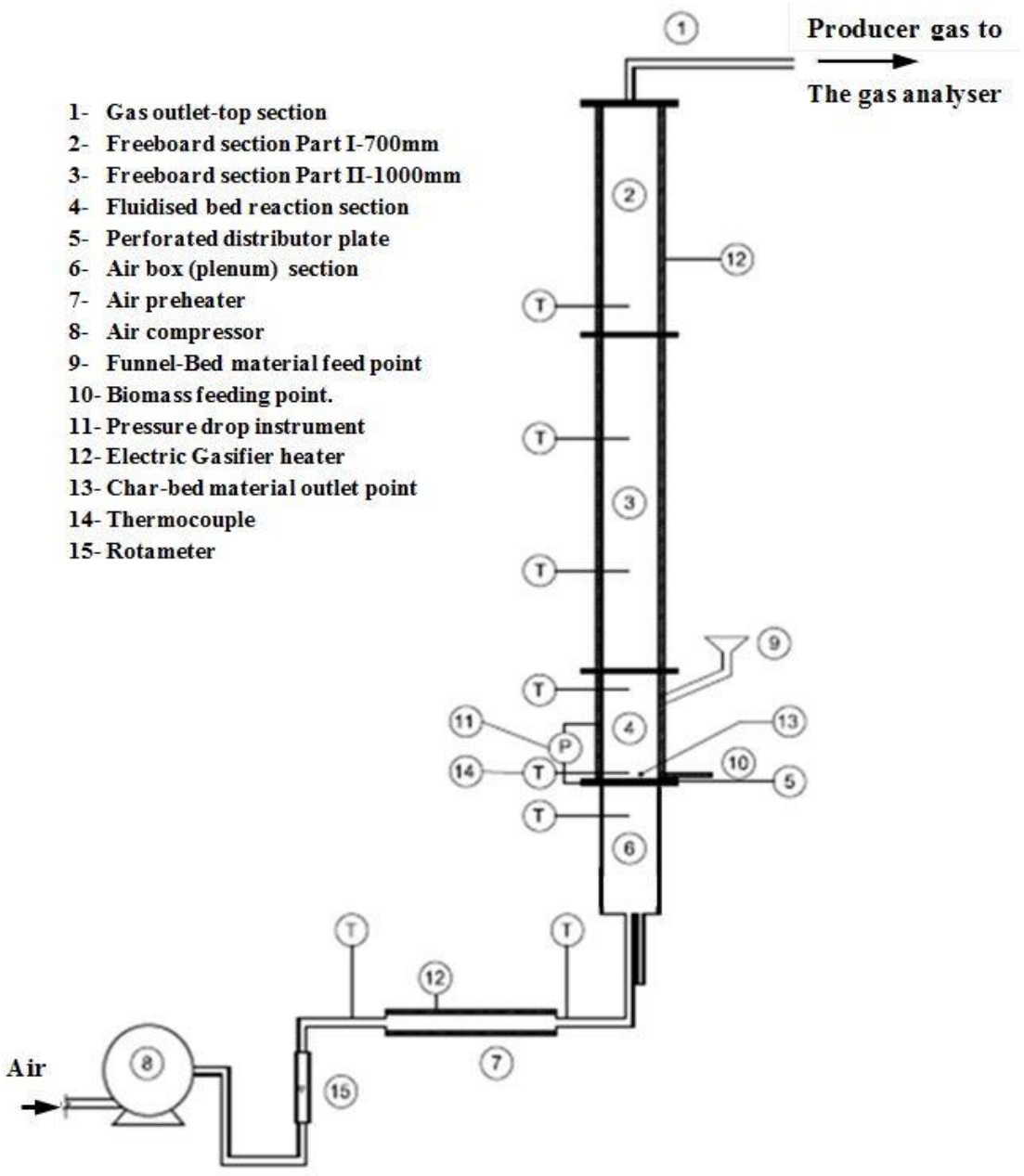

Figure 3. 10 Schematic of the suggested of the assembled air bubbling fluidised bed gasifier

3.4 Summary

In this chapter, a design study and calculations have been conducted for a biomass bubbling fluidised bed gasifier. The size of the gasifier reactor was suggested to be lab and pilot scale and to be more flexible and representative of an industrial process for research purposes.

Hydrodynamic and geometry design equations for a bubbling fluidised bed reactor were outlined. A Matlab code was built for this purpose. Three values of reactor diameters were selected to specify the optimum values for this study. One of the design results was the biomass mass feeding rate, which gives an indication of the size of the reactor and the required quantities of the biomass for each experiment. By using these design results, the reactor diameter was specified.

In addition, the design results have shown the effect of the particle size of the bed material, the static bed height and the number of holes in the distributor plate as a function of minimum fluidisation velocity. These design effects will thus form a preliminary database for the fluidisation hydrodynamics in the cold and hot conditions. Furthermore, according to these results the manufacturing and construction of the parts of the gasifier unit were conducted.

Chapter 4

Materials and Methods for Characterization

4.1 Introduction

This chapter describes the preparation of materials and characterisation methods used in studying the development and performance of the air-blown bubbling fluidised bed gasifier. In Sections 4.2 and 4.3 the procedures for preparing and characterising of quartz sand material and two biomass fuel materials, sawdust pinewood and Iraqi date palm, are presented, respectively. Section 4.2 includes the presentation of grinding, crushing and sieving of sand material, mean particle size determination and some physical properties and their measurement. Similarly, Section 4.3 involves the pre-processing of two biomass materials by grinding, crushing and sieving. Their bulk density measurement and the establishing of their mass-flow rate- screw feeder speed point calibration curve is also shown. In Section 4.3.2, the physical and chemical properties for the two-biomass materials represented by proximate, ultimate, calorific value and thermo-gravimetric analyses are described. The preparation of the cold rig and hot rig materials are highlighted in Section 4.4 and 4.5, respectively.

4.2 Characterization of quartz sand material

4.2.1 Sand material preparation

A commercial quartz sand as shown in Figure (4.1) with a particle size range 0.2mm – 1mm as received was supplied by a Garside company-UK. According to the bubbling fluidised bed theory model and for Geldart B Type material which is used as a fluidised bed material and according to this study aims, an inert quartz sand material was classified to three ranges of particle sizes, (300-425) µm, (425-500) µm and (500-600) µm as a bed material.

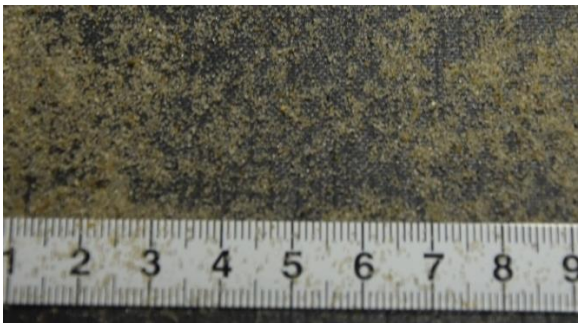

Figure 4. 1 Raw Silica Sand Sample

A sieving method according to the British Standard Institute (BS 1377-9 1990) was used to obtain these three required particle size ranges. Ring mill machine type

Labtech-Essa, (model No 100100-Australia) as shown in Figure (4.2) was used to reduce the sand particle size to get enough quantities of these sand particle size ranges. This sand was mainly used in cold fluidised rig mode for hydrodynamic studying and in hot fluidised rig (gasifier) mode for biomass gasification as an inert bed material.

Figure 4. 2 Sand grinding and crushing machine

4.2.1.1 Mean particle diameter

As shown in Chapter 3 particle size diameter of bed material has been considered an important factor in fluidised bed design calculations. The available standard apparatus of sieving analysis just give a range of particle size measurement such as: (300-425) µm, (425-500) µm, (500-600) µm and etc. They do not give a specific mean value as needed. For this reason each range of above particle size of sand material, a Malvern particle size analysis was done using a Malvern apparatus – Model – Mastersizer-3000. It measures particles from 10nm up to 3.5mm. The principle of the measuring of the particle size distribution in Mastersizer-3000 depends mainly on the laser diffraction technique. In this technique, a laser beam passes through a dispersed particulate sample and the angular variation in intensity of the scattered light is measured. The light is scattered at small angles, relative to the laser beam, by large particles. Whereas it is scattered at large angles by small particles. By using the Mie theory of light scattering, this angular scattering data is then analysed to calculate the size of the particles. This size is then reported as a volume equivalent sphere diameter.

The Mastersizer is comprised of the main following: Optical unit, one or more dispersion units, a measurement cell and computer(Mastersizer application software) (Malvern Instruments n.d.) and (Malvern Instruments 2015).

From the Malvern analysis results, as shown in Appendix (C), a mean particle diameter for each range was calculated using Equation (4.1)(Basu 2006).

$$\bar{d}_p = \frac{1}{\sum_{i=1}^{n} \frac{x_i}{d_{pi}}} \tag{4.1}$$

$\bar{d}_p$ =Mean particle diameter.

x_i = Fraction of particle size (i).

d_{pi} = Diameter of particle size (i).

The calculation procedure was started from the results of the sand Malvern analysis. As shown in Figure (4.3), for example, it is the result of the sand range (500-600) µm, which is available in appendix (C). There are two data columns one for particle size diameter in µm and the second is for its volume percent, which are boarded by a red line box as shown in Figure (4.3) below. These are represented by dp_i and x_i in Eq (4.2), respectively. Then by applying Eq (4.1) the mean particle size for this range of sand, $\overline{d_p}$, will be obtained.

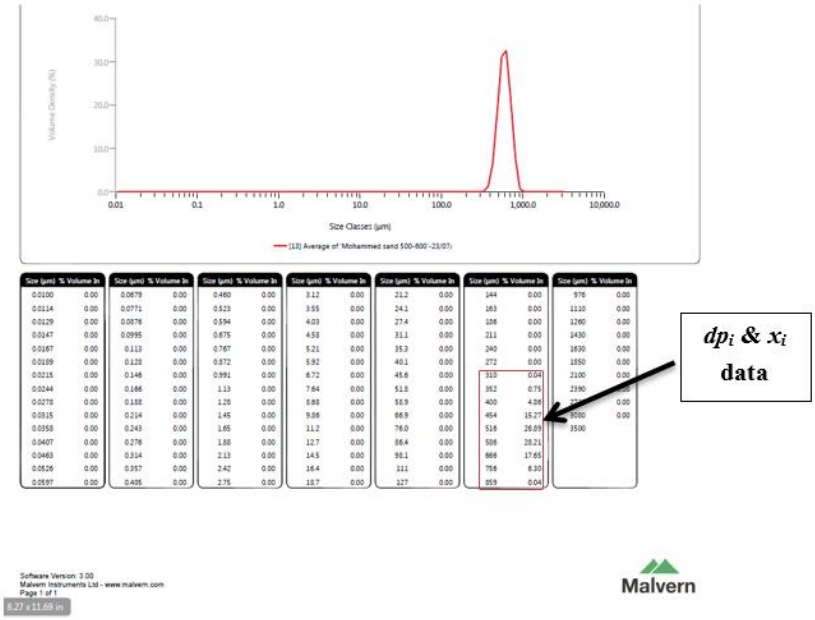

Figure 4. 3 Image of the Malvern analysis results for sand particle size range (500-600) µm

Equation (4-1) is one of a common method that is used in fluidised bed design for mean particle size calculation of bed material. The results of the mean particle size of the three selected ranges are shown in Table (4.1).

Table 4. 1 Mean particle size for three sand particle size ranges

Sand Particle Size Sieving Ranges,	Sand Mean Particle Size $\overline{d_p}$,µm
300-425	395.57
425-500	478.43
500-600	545.92

4.2.1.2 Particle density

Particle density is a physical property of powdered and granular material. It is defined as the mass of particles of material divided to its volume excluding open pores and closed pores. A supplier company gave this density for supplied sand. As shown in the design equations in Chapter 3 this property is considered an important design parameter in hydrodynamic fluidised bed studies.

4.2.1.3 Bulk density

Bulk density is a physical property of powdered and granular material. It is defined as an apparent powder density, which is the mass of a powder divided by its apparent volume. The bulk density of silica sand material was measured by following the British Standard Institute procedure BS EN 1377-9: 1990 (BS 1377-9 1990). As defined, the bulk density can be affected by many factors, such as, particle size, a procedure that follows to measure it and external conditions such as vibration and compaction which should be avoided. Bulk density was used to specify the height of a bed material inside the column with a specific diameter, where the bed height is a design parameter that affected the gasifier performance. Practically, it is difficult to achieve the same bulk density procedure as followed by BSI for material inside the column because of the long height of the pouring distance due to the long height of the column of the rig experiment compared to a required procedure in BSI. Also, bulk density is used to calculate the bed porosity by applying Equation (4.2)

4.2.1.4 Porosity

Porosity is a property of granular and powdered materials. It is defined as a volume fraction of voids between particles of a specific volume of the material. It can be directly related to bulk and particle density as shown in Equation (4.2),

$$porosity = \varepsilon = 1 - \frac{Bulk\ Density, \rho_b}{Particle\ Density, \rho_p} \quad (4.2)$$

4.2.1.5 Sand bulk density measurement

According to BS 1337-9:1990 (BS 1377-9 1990) the sand bulk density (as received) was measured for several ranges of sand particle sizes: (220-300) µm, (300-425) µm, (425-500) µm, (500-600) µm and (600-850) µm by using a sand bulk density apparatus, which is shown in Figure (4.4). The apparatus consists of two pieces: 1) a long cylinder with cone called a pouring cylinder, it is shown in Figure 4.4(a), and 2) a short cylinder with edge at its top, called calibrating container, it is shown in Figure 4.4(b). The internal diameter and height of the calibrating cylinder was measured to calculate its volume (V) in kg/m^3. Its weight (as empty) was measured in kg, (m_1). A quantity of a specific range of particle size of the sand was prepared. The shutter on the pouring cylinder must be closed prior to fill it with the sand. Thereafter it was placed on a flat surface of a wide area of a known weight of a clean glass plate. Then the shutter should be opened to allow sand to run out. When no further flow of sand takes place inside the cylinder the shutter must be closed and the pouring cylinder should be carefully removed. The glass plate and the sand (that had filled the cone of the pouring cylinder) were weighted together. The mass of the sand was calculated. This measurement was repeated three times. Let this mass be (m_2). Finally, after it has been refilled with sand and its shutter has been kept closed the pouring cylinder was directly placed and fitted on the top of the calibrating cylindrical container and all were placed on the glass plate to be sure that all sand was weighed. The shutter was opened to allow the sand run out to fill both, the calibrating cylinder and the cone space until there is no further sound of passing sand throughout takes place in the cylinder. Then the shutter should be closed and subsequently the upper part should be carefully lifted and removed. Afterwards the glass base, calibrating cylinder and sand cone all were together weighed, let their mass be (m_3). Finally the bulk density of the required sand was determined by simple calculations. The net mass of the sand inside the calibrating cylinder m_4, in kg will be,

$$m_4 = m_3 - m_2 - m_1 - mass\ of\ glassed\ plate \quad (4.3)$$

Then the bulk density of the sand will be,

$$Sand\ Bulk\ Dnsity, \frac{kg}{m^3} = \frac{mass\ of\ the\ sand\ inside\ the\ calibrating\ cylinder, kg}{Volume\ of\ calibrating\ cylinder,\ m^3} = \frac{m_4}{V} \quad (4.4)$$

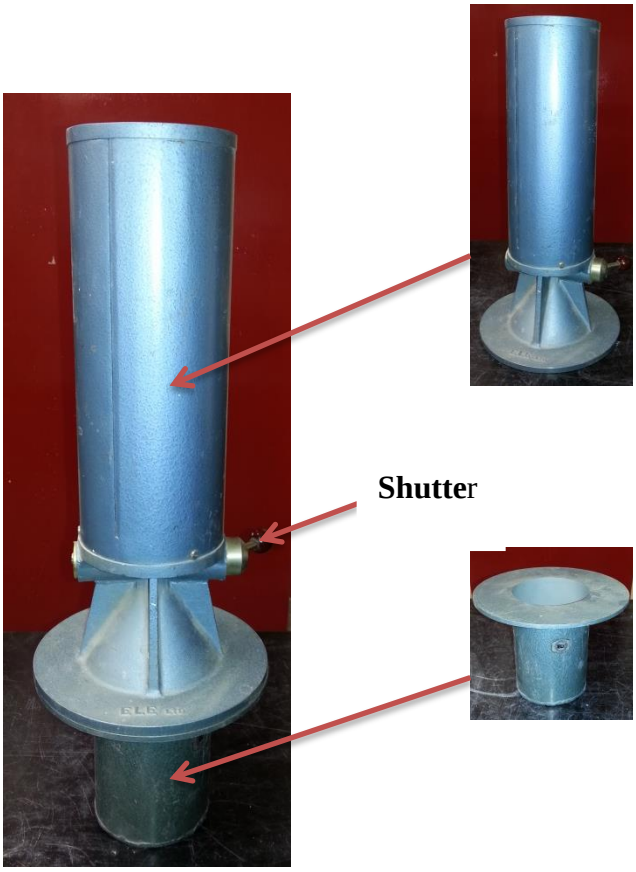

Figure 4. 4 Sand bulk density apparatus: a) Upper piece called pouring cylinder with cone, b) Lower piece called calibrating cylindrical container

The results of sand bulk density for all particle size ranges are shown in Table (4.2).

Table 4. 2 Values of the sand bulk density for each range of sand particle size

Sand Particle Size, µm	Sand Bulk Density, kg/m^3
220-300	1411.7
300-425	1461.8
425-500	1483.0
500-600	1501.1
600-850	1511.3

4.3 Characterisation of biomass materials

4.3.1 Sample preparation

4.3.1.1 Iraqi date palms wastes biomass (IDPWB) material

As shown in Chapter 1 – Section 1.4, it can be concluded that these Iraqi date palm residues can be preliminary considered as one of the varieties of biomass solid fuel which can be used to obtain a clean gaseous fuel and thereafter it will be one of those major biomass renewable energy sources. Therefore, these residues were chosen as one raw material in this study. An Iraqi research centre directory called Project of Organic Fertilizer Preparation and Mushroom Cultivation Directory / Karbala City– Iraq, which belongs to the Iraqi Ministry of Agriculture, supplied this biomass. It was supplied as ground of complete frond with particle size (as length) ranged from 3 to 8cm and from 3 to 6mm (as diameter) as shown in Figure (4.5).

Figure 4. 5A first stage of cutting and grinding of a whole frond of Iraqi date palm (8mm as received)

4.3.1.2 Sawdust pinewood biomass (SPWB) material

For biomass gasification experiments and in order to save enough quantity of Iraqi date palm biomass a second biomass material called pinewood sawdust material was selected as well. This material was used as a main biomass material for all this study experiments either for cold or hot experiments. This commercial pine sawdust was supplied by a commercial supplier (Batleys) with particle size (as received) typically 3 mm size as shown in Figure below (4.6).

Figure 4. 6 Supplied pine wood sawdust samples (3mm as received)

4.3.1.3 Biomass grinding and crushing

Both biomass materials pine wood sawdust and wastes of Iraqi date palm frond were supplied with a particle size larger than desired size as mentioned above, which were called as received material. For this study, three different particle sizes of both biomass materials had been selected (1000 – 1180) µm, (600 – 850) µm, and (300 – 425) µm. These selected sizes give a wide range of biomass particle size for comparing and studying its effects on the gasifier performance. At the grinding and crushing laboratory at Cardiff University, the supplied size of these biomass materials were gradually reduced. A Knife Mill-Type FRITISH model 55743 Idar-Obersten-Germeny, which is shown in Figure 4.7, was used using different sizes of a special curvature mesh trays, which were supplied with the machine 2mm, 1.5 mm, 1 mm, 0.75 mm, and 0.5 mm. After machine activation, a required amount of material was put inside the machine hopper and there is a gate to control the introducing of biomass to the cutting chamber. This consists of several sharp stainless steel knives, which are fixed radially on a stainless steel cylindrical shaft. These knives are rotated with a specific speed by the shaft by an electrical motor. There is a clearance distance between these knives and a curvature mesh tray, which can press the cut biomass to pass through the mesh tray. The passed particles will collect in a stainless steel container, which is positioned at the bottom of the cutting chamber and finally the cut biomass

were packed into a suitable bag to be ready for the sieving step. To get a required particle size as mentioned above four sizes of curved mesh trays 2mm, 1.5mm, 1mm and 0.5mm were used to be a first step of sieving stage for the particle size needed. Following this, the samples were stored in sealed bags.

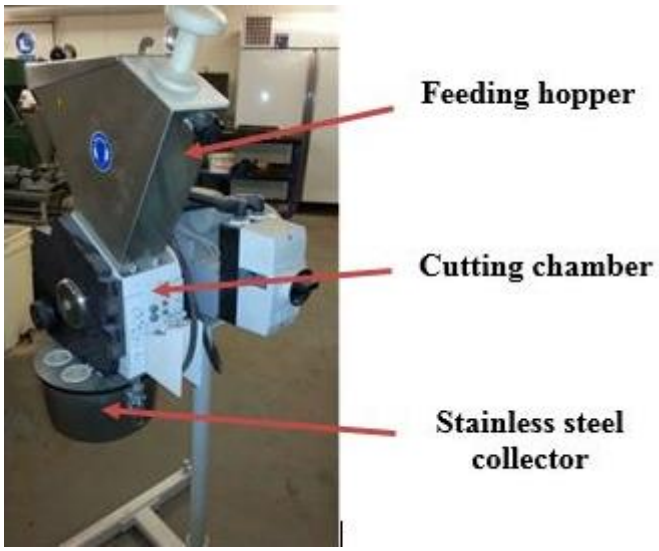

Figure 4. 7 Grinding and crushing machine for biomass materials

4.3.1.4 Sieving of biomass material

According to the required biomass particle size for this study ground biomass materials for a certain mesh size was sieved to a desired size using standard sieving trays available in the soil laboratory. The sieving analysis procedure was followed according to BSI(Anon 2011b) . The sieve apertures 0.300 mm, 425mm, 500mm, 600 mm, 0.85 mm, 1.18 mm, and 1.5mm were employed in this study. However, for this study the required biomass particle size are in the ranges (1000-1180) µm, (600 – 850) µm, (300 -425) µm. As shown in Figures 4.8 and 4.9, the shape of the particles of both two biomass materials takes a longitudinal shape (not spherical) with aspect ratio greater than 1, assuming cylindrical particle shape. Because of the nature of the biomass material and the non-spherical particle shape (needle shape especially for these large particle size ranges), the available Malvern apparatus cannot correctly measures the mean diameter for each selected range of the particles. In addition, because all the selected ranges are the minimum range of the available sieve the mean diameter cannot be calculated by the sieving analysis method.

300-425 µm **(b) 425 – 600 µm** **(c) 1000-1180 µm**

Figure 4. 8 Particle size ranges of Iraqi date palm grinding fronds samples

(a) 300-425 µm (b) 425 – 600 µm (c) 1000-1180 µm

Figure 4. 9 Particle size ranges of sawdust pinewood grinding fronds samples.

4.3.1.5 Biomass bulk density measurement

In this study, biomass bulk density is considered an important parameter for fluidised bed hydrodynamic calculations. It was measured as received according to BS EN 15103:2009 (British Standards Institution (BSI) 2010). A hollow cylindrical measuring container within required measurement specifications and within accepted height-diameter ratio, 1.25 to 1.5, was prepared and weighed. The schematic of the apparatus is shown in Figure 4.10 below.

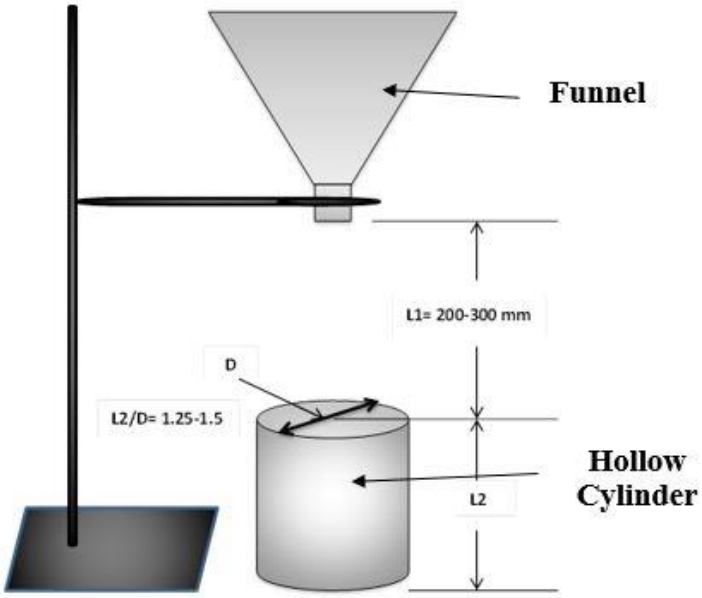

Figure 4. 10 Schematic of the apparatus of the biomass bulk density

For both biomass type, pinewood sawdust and Iraqi date palm, and for three required particle size for both biomass type (300-425) µm, (600-825) µm and (1000-1180) µm, the bulk density (as received) was calculated according to the following equation:

$$BD_{ar}\ (at\ M_{ar}) = \frac{(m_2 - m_1)}{V} \quad (4.5)$$

Where: BD_{ar} Bulk density as received in kg/m^3
BD_d Bulk density of the sample mass on dry basis in kg/m^3
M_{ar} The moisture content, as received, as percentage by mass
m_1 The mass of the empty container in kg
m_2 The mass of the filled container in kg
V The net volume of the measuring container in m^3

The biomass bulk density on dry basis (D_d) can be calculated by Eq. (4.6)

$$D_d = D_{ar} * \frac{(100 - M_{ar})}{100} \quad (4.6)$$

The measuring results of biomass bulk densities, as received, for three particle size ranges for both biomass types are shown in Table (4.3).

Table 4. 3 Bulk density values (as received) for both biomass materials for each particle size range

Biomass Material	Bulk density, as received, ρ_{bulk} in kg/m^3		
	300-425 µm	600-850 µm	1000-1180 µm
Sawdust pine wood	181.81	180.82	156.7
Iraqi date palm residues	260.56	258.65	215.81

4.3.1.6 Biomass screw feeder: calibration of biomass mass flow rate

For DDSR-20 model, where details are shown in Section 4.4.6, a calibration curve of biomass mass flow rate-screw feeder speed setting for two types biomass materials were obtained. These calibration curves can be used to find the speed setting point of the screw feeder apparatus that corresponded to a certain value of required biomass mass flow rate. The biomass mass flow rate value contributes mainly in equivalence ratio calculation, which is an important parameter in the gasification process. The procedure of calibration was conducted as follows: Prior to calibration, some required materials and tools were prepared such as: a medium size of cylindrical metal container to collect the outlet biomass from screw feeder, stop watch to measure the time required for a biomass mass at a certain speed point, accurate balance to weigh the collected biomass and enough quantity of a particular particle size for both types of biomass materials. The calibration procedure is as follows: 1) Suitable quantity of biomass was poured in the screw feeder hopper. It should be a small quantity especially at low speed to avoid stopping of the drive motor due to the biomass quantity. 2) Switch on the screw feeder apparatus to run the motor to allow a biomass to fill the clearance spaces inside the arm, a pipe of the twin- screw rod feeder, which are driven by the electric motor, to ensure a correct measuring of time. 3) An empty cylindrical container, which was previously weighed let it be m_1, was directly placed underneath the outlet of the screw pipe to ensure that all biomass particles were collected inside. 4) For the first starting of the calibration process the speed point setting was firstly set at each 0.5 increment, where the speed setting scale is divided up to 10 increment, starting from 0 to 10. 5). From the screw feeder control panel the screw feeder motor was switched on and at the same time, the stopwatch was immediately run. 6) For 1 minute running time the drive motor was switched off, let this time be t_1 in min. 7) The container with collected biomass were weighted, let it be m_2 in gm. 8) The above procedure was repeated for next speed increment of, 0.5, 1, 1.5, 2, 2.5, 3,……., 9.5, 10. Finally, the mass flow rate for both biomass materials were calculated as following:

$$Biomass\ mass\ flow\ rate\ in\ \ gm/min\ =\ \dot{m_{bio}} = \frac{m_2 - m_1}{t_1} \tag{4.7}$$

These values were drawn to obtain a standard calibration curve for each biomass material as shown in Figure (4.11a & b). From these calibration curves at required biomass mass flow rate the screw feeder speed can be set.

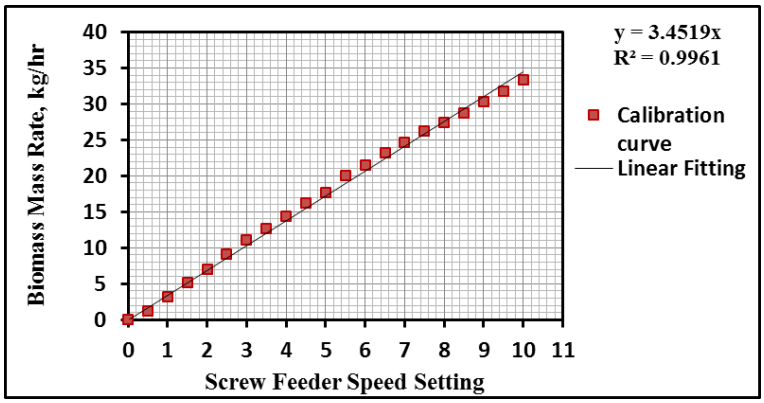

a)

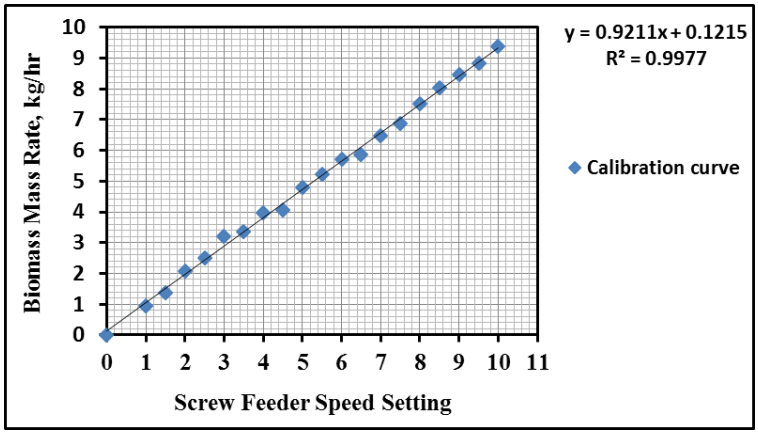

b)

Figure 4. 11 Biomass mass flow rate – screw feeder speed point calibration curve: a) biomass of Iraqi date palm residues, b) Biomass of pine wood sawdust

4.3.2 The composition analysis of biomass solid fuels

For any biomass solid fuels and especially for thermo-chemical conversion process like, combustion, gasification and pyrolysis, four main analyses should be taken into consideration. These analyses are proximate analysis, ultimate analysis, calorific value and Thermo Gravimetric Analysis. Proximate and ultimate analyses provide invaluable information about chemical composition of carbonaceous materials. Proximate analysis parameters include moisture, volatile matter, ash, and fixed carbon, whereas ultimate analysis, which is more comprehensive, depends on quantitative analysis of various elements present in the fuel sample, such as carbon, hydrogen, sulphur, oxygen, and nitrogen.

4.3.2.1 Proximate analysis

In this analysis, contents of moisture, volatile material, ashes and fixed carbon are determined which represent the properties of a specific fuel material. These properties are important to assess the characteristics of any fuel during thermo - chemical conversion processes and thereby their effects on reactor design. The methods used to estimate these contents were explained as shown below:

4.3.2.1.1 Moisture content

The moisture content in the biomass was determined according BSI (En 14774-1 2009). The analysis was conducted in triplicate to monitor the repeatability between the test samples. Three ceramic dishes with lids were pre-conditioned, to remove moisture, by heating at 105^{o}C for 2 hours in a drying oven and then cooled to room temperature in a desiccator. After cooling, the dishes and their lids were weighed to nearest 0.1 mg. After weighing the dishes, a minimum fuel sample of 1 g was weighed to nearest 0.1 mg and spread evenly over the respective dishes and heated in the drying oven at 105^{o}C for 2 hours. Before removing the samples from the oven, the lids were replaced and the assemblies transferred to the desiccator for cooling to room temperature. The moisture content (MC) expressed in percentage was calculated according to Equation (4.8).

$$MC\ \% = \left[\frac{m_2 - m_3}{m_2 - m_1}\right] * 100 \qquad (4.8)$$

Where:

m_1 = The mass of the empty ceramic dish and lid.
m_2 = The mass of the ceramic dish and lid and biomass fuel before heating.
m_3 = The mass of the ceramic dish, lid and residue after heating.

4.3.2.1.2 Ash content

Ash content is the measure of mass of the inorganic matter left after ignition of a fuel under BSI (Technical committee CEN/TC 2005). The analysis was carried out in triplicate to monitor the repeatability between the test samples. Prior to combustion of the fuel samples, three empty ceramic dishes were preconditioned in the muffle furnace to remove volatile matter by heating to 550^{o}C for 2 hours. After conditioning, the dishes were cooled to room temperature in a desiccator and weighed.

Approximately 1 g of dried solid biomass fuel sample weighed to the nearest 0.1 mg was spread over each dish and then heated in the furnace at 550^{o}C for 2 hours to ensure complete combustion. The dishes with residues were then transferred to the desiccator, cooled to room temperature and weighed. The ash content (AC) on dry basis was calculated using Equation (4.9).

$$AC\ \% = \left[\frac{m_2 - m_3}{m_2 - m_1}\right] * 100 * \frac{100}{100 - MC} \quad (4.9)$$

Where:

m_1 = Mass of the empty ceramic dish and lid.

m_2 = Mass of the ceramic dish and lid and biomass fuel before heating.

m_2 = Mass of the ceramic dish and lid and biomass fuel after heating.

MC = Mass fraction of the moisture of the general analysis of the solid biomass sample on wet basis, as percent.

4.3.2.1.3 Volatile matter content

Volatile matter expresses the mass of the material loss, deducting that due to moisture, when a test sample is subjected to heat in the absence of air under specific conditions. Volatile matter normally consists of various hydrocarbons, which affect burning characteristics of the solid carbonaceous fuel such as biomass. In this study, the volatile matter was determined according to BSI (CEN (European Comitte for Standardisation) 2009) standard procedure. Three fused silica crucibles with lids were preconditioned to remove volatiles by heating at 900^{o}C for seven minutes and then were cooled to room temperature in the desiccator. When cool, the crucibles with lids were weighed to the nearest 0.1 mg. Minimum sample of 1 g was spread evenly over the respective crucibles and then heated in a muffle furnace at 900^{o}C for 7 min. After this time, the crucibles with residue were cooled in desiccator to room temperature and then were weighed. The net weight loss of the material was determined by subtracting the loss due to moisture content. The volatile matter (VM) content on dry basis was calculated using Equation (4.10). The analysis was carried out in triplicate to monitor the repeatability between the test samples.

$$VM\ \% = \left[\frac{m_2 - m_3}{m_2 - m_1}\right] * 100 - M_w * \frac{100}{100 - M_{ad}} \quad (4.10)$$

Where:

m_1 = The mass of the empty ceramic dish and lid.

m_2 = The mass of the ceramic dish and lid and biomass fuel before heating.

m_3 = The mass of the ceramic dish, lid and residue after heating.
M_w = The mass fraction of moisture in the solid biomass sample as a percentage.
M_{ad}= The mass fraction of moisture of the general analysis sample on wet basis (*ad* means as analysed) as a percentage = *MC*.

4.3.2.1.4 Fixed carbon content

Fixed carbon (*FC*) is the solid of combustible residue that remains after any heated, gasified or pyrolysed, solid or liquid fuel, where all the volatile matters are released and ash is excluded. The fixed-carbon content of any solid fuel is determined by difference by deducting the percentages of moisture, volatile matters, and ash from a solid biomass sample as shown in Equation (4.11). Since gas-solid combustion reactions are slower than gas-gas reactions, a high fixed-carbon content indicates that the coal will require high temperature and long time to react. So that increased fixed carbon content in the feedstock can reduce the rate of the fuel conversion in the gasifier reactor.

$$FC\ \% = 100 - [Moisture\ content\ \% - Voltile\ matter\ \% - Ash\ content\ \%] \quad (4.11)$$

4.3.2.2 Calorific value

Caloric value is the most important characteristic of any fuel, gas, liquid and solid. It is the amount of energy in MJ generated from combustion of a unit mass in (kg for solid fuel) or volume in (m^3 for liquid and Nm^3 for gas fuel) of fuel by oxygen. Calorific value is expressed as a gross (Higher) calorific value (HHV) or lower calorific value (LHV). The former gives the total energy released when water in the combustion products is in liquid state and the latter, vapour. The principle of the work of the bomb calorimeter basically depends on the heat of the combustion that is created by a sample of a solid fuel which is burned under an oxygen rich atmosphere in a closed pressure vessel called (bomb) under controlled conditions. This vessel is surrounded by water jacket, which absorbs the energy released by the sample combustion and the resulting temperature change within the absorbing medium is observed. Thereby the heat of combustion is then calculated.

In this work, a computerised bomb calorimeter, Parr 6100, Figure (4-12) from Parr Instrument Company was used to determine the gross heating value of the biomass feedstock according to BSI (BS DD CEN/TS 14918 2005) standard procedure. Prior

to analysis, three certified benzoic acid pellets calibrated the bomb calorimeter. After calibration was completed, 1 g of biomass material was analysed in the bomb by following the procedure steps according to the operation manual of 6100 Parr instrument (Parr instrument company n.d.). The test will automatically proceed through the following steps: Pre-period cycle, Fire the sample and Post-period cycle. Once the calorimeter analysing is finished with the post-period cycle the results will print out on the printer or display on the touch screen. This analysis was done in triplicate to monitor the repeatability between the fuel samples. The net calorific value was determined by using Equation (4.12) specified in (Aenor, 2005).

$$q_{wv,net,m} = \{ q_{v,gr,d} - 206W_{H,d} \} * (1 - 0.01M_T) - 23.05M_T \quad (4.12)$$

Where $q_{v,gr,d}$ = Gross calorific value at constant volume in J/g.
$W_{H,d}$ = Hydrogen content (wt %), of the moisture-free (dry) fuel, respectively.
M_T = The total moisture content (wt %).

Figure 4. 12 Bomb calorimeter, Parr 6100

4.3.2.3 Ultimate analysis

Determination of the elemental composition of a fuel is called an ultimate analysis. It depends on quantitative analysis of various elements present in the fuel sample. Most commonly, carbon, hydrogen, nitrogen, sulphur and oxygen (CHNSO) are measured in a particular fuel through complete combustion. These elements are important in calculating the chemical formula of the solid or liquid fuel and determining an appropriate stoichiometric air or O_2-fuel ratio for the combustion or gasification process as well. Additionally, any catalyst activity depends on the concentration of poisoning elements in the feed an example of which is sulphur. In this study, the same type of the sawdust pinewood biomass SPWB, which was used by previous PhD study,

was also used. The ultimate analysis for this biomass was taken from it(Legonda 2012). For checking test, the carbon and sulphur composition for this material were reanalysed in (LECO) analyser model SC-144DR, which is shown in Figure 4.13. It is a software-controlled instrument designed to determine the carbon and sulphur content. This analyser principally works on the flow of the combustion gases through the two infrared detection cells. One cell is carbon IR to measure the concentration of CO2 gas and the second cell is sulphur cell to measure the concentration of SO2 gas. The instrument converts these concentrations to percentage value using an equation pre-set in the software(LECO 2008). For Iraqi date palm biomass IDPWB material, Minton Treharne & Davies LTD Company, UK, did the ultimate analysis.

Figure 4. 13 LECO Carbon-Sulfure analyser, model SC-144DR

The results of proximate, ultimate and calorific analyses of two biomass materials, pinewood biomass and Iraqi date palm wastes biomass materials are presented in Table 4.4. Carbon content of char + sand mixture, a residues solid materials after each biomass gasification experiment, was measured according to BSI – BS EN 15104: 2011 (Anon 2011a) using LECO analyser.

Table 4. 4 Proximate and ultimate analyses for sawdust pinewood and Iraqi date palm wastes biomass materials as received (ar) basis

Analysis	Biomass Material	
	Pine wood sawdust *	Iraqi date palm residues
Proximate Analysis, (% wt.)		
Moisture Content	2.47	8.98
Ash	0.43	7.29
Volatile Matter	82.73	75.59
Fixed Carbon	14.37	8.13
Total	100.00	100.00
Gross calorific value, (MJ/kg)	19.09	18.64
Ultimate Analysis, (% wt.)		
C	49.4	42.6
H	5.9	5.30
S	0.02	0.30
N	0.3	0.89
Cl	N/A	0.62
O by difference	40.68	34.29

* The analysis results data were taken from (Legonda, 2012).

4.3.2.4 Thermo gravimetric analysis (TGA)

Thermogravimetry is a standard method to analyse organic, inorganic and synthetic materials. This analysis includes heating a weighted test sample on a highly sensitive microbalance, which is exposed to a controlled temperature system in a controlled environment according to BS EN ISO 11358:1997 (British Standards Institution (BSI) 2014). The TGA analysis for the two-biomass materials was conducted using a Mettler Toledo TGA Series, model-TGA/DSC 3^{+} as shown in Figure 4.14. In this study, 11mg of each biomass was weighed by a precision balance to the nearest 0.01mg and heated from 35^{o}Cto 900^{o}C. Two test were performed, first by air and the second by N_2 at a flowrate of 50ml/min and heating rate 10^{o}C/min. Mass loss with temperature profiles were recorded for each second using STARe Thermal Analysis software.

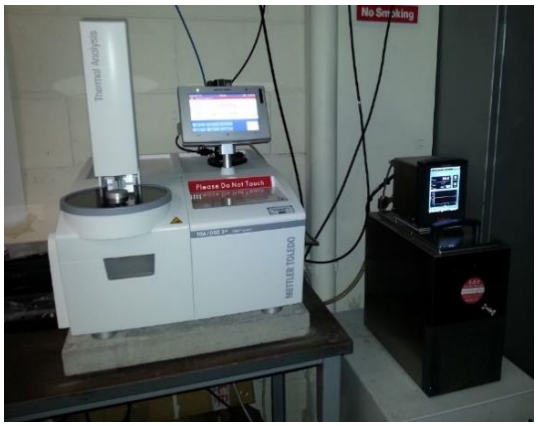

Figure 4. 14 Thermogravimetric analyser (Mettler Toledo TGA Series, TGA/DSC 3+)

A thermogavimetric analysis of two biomass materials, SPWB and IDPWB using air and N_2 were conducted. Their thermal behaviours are presented in Figure 4.15 (a) and (b), respectively. From the two Figures, it can be seen that there are three distinct phases. The first mass loss phase is due to moisture evaporation at a temperature less than 105^{o}C followed by a large mass loss of volatile materials between 200-375^{o}C,. The third phase of mass loss of volatiles takes place between 350^{o}C and 425^{o}C when air was used and between 375^{o}C and 880^{o}C when N_2 was used. Furthermore, for this phase the increase of mass loss was sharply for the former and slightly for the later. In addition, for both biomass the trend of air and N_2 within the first and second phase are identical whereas for the third phase N_2 and air are approximately diverged at 400^{o}C. Also, it can be seen that the mass loss for SPWB is larger than IDPWB for both gases. Overall, it can be concluded that for gasification process, which locates between pyrolysis and combustion, these two biomass can be gasified between 350 and 900^o C

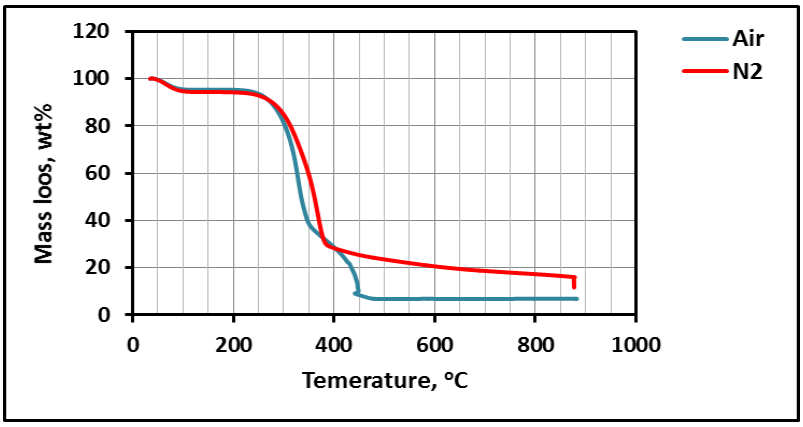

a) SPWB

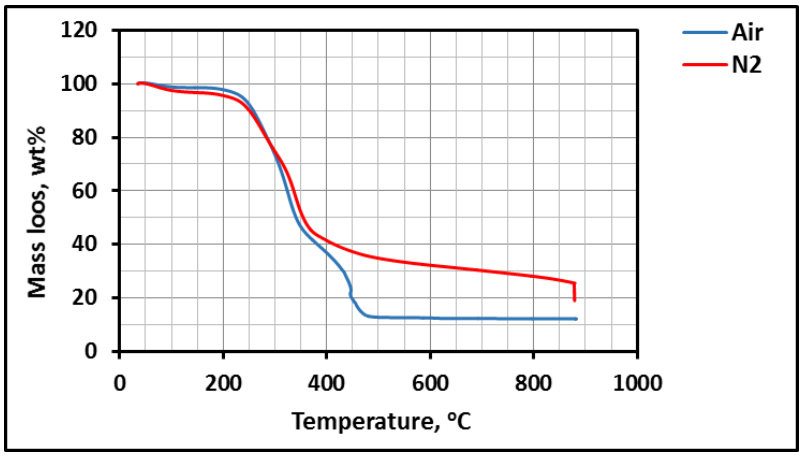

b) IDPWB

Figure 4.15 Thermogravimetric behaviour of the two-biomass materials using air and N_2: a) For SPWB and b) For IDPWB

4.4 Cold rig prepared materials

In order to study the hydrodynamic design parameters of the bubbling fluidised bed reactor experimentally a cold rig fluidised bed was built, constructed and assembled as shown in Figure 4.16 and also presented in Chapter 5.

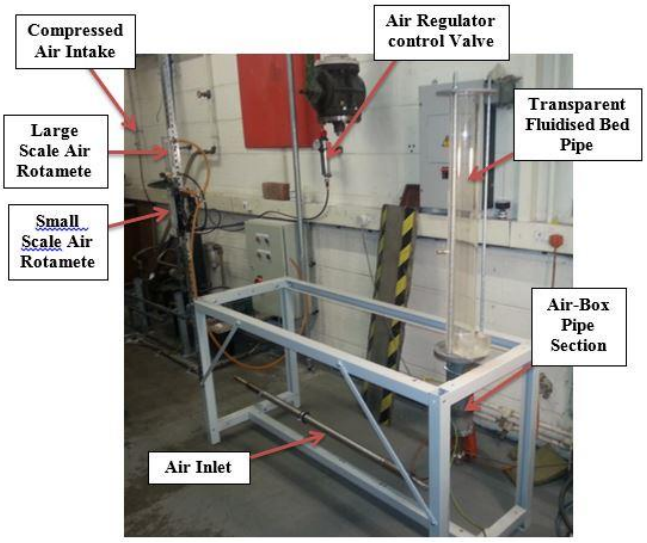

Figure 4.16 Assembled cold rig for fluidised bed column

The prepared materials, which were used in cold rig, are as follow:

4.4.1 Fluidised bed cold column (transparent pipe)

For cold rig experiments, a transparency acrylic pipe was used. As shown in Figure 4.17 (a) and (b), two models of pipe were used as a fluidised bed column to perform

the cold rig hydrodynamic experiments. The first model (a) is a conventional case, which was mainly used for all experiments Whereas the second model (b) was assembled with the intake point hole of the screw feeder by a small unit, which was fixed directly on the outside of the acrylic pipe at a point 4.2cm above the distributer plate. This was to show the movement and dispersion of biomass particles inside bed material when the feeding point is located at the position near the distributer plate or within the bed height area. This model exactly represents the actual case for a hot rig gasification experiments. The former model was drilled with several holes for pressure negative side tube tapping. In addition, one side of this pipe was tightly introduced inside a plastic flange, which has a same specification of metal flange, until both edges pipe and bottom flange surface were levelled. The second end of this pipe was left free. Then this assembled plastic pipe-flange unit was tied with the distributor plate and air-box pipe section by flanges with metal screws to compose the fluidised bed cold rig. For the second model the plastic pipe was joined with a metal flange for both ends by a metal screw rod, thereafter this assembled pipe will be ready to join directly with the distributor plate and air flow-box pipe section. The dimensions of this acrylic pipe: height does not exceed 1m length to give a good using flexibility of bed height and expansion height through fluidisation experiments. Its internal diameter and thickness are the same for metal type, 83mm and 3mm, respectively. Two metric measuring rulers were putted down on the external pipe wall. They were used to measure the bed material height at static bed and during fluidisation conditions for various air flowrates.

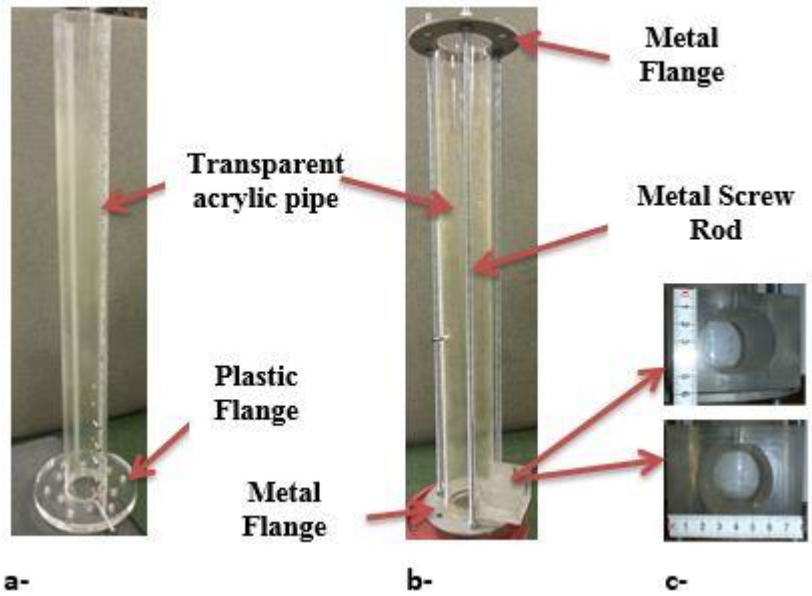

Figure 4. 17 Acrylic transparent column for fluidised bed cold rig, (a) a conventional column, (b) a column assembled with the intake unit of screw feeder, c) screw feeder intake unit.

4.4.2 Air flow-box pipe section

According to the design steps (chapter 3) and dimension, the air box was manufactured with the same specifications of the reactor pipe section. This type of pipe was supplied by CG Rees Supplier Company-UK with the following specification, 316L stainless steel, nominal pipe size 3" for 10S Schedule (outside diameter 88.9 mm, inside diameter 82.8 mm and 3.05 mm thickness). For the section of the air box 300mm of this pipe type was used. Its open upper side was welded with 6 mm thickness of the standard flange and the bottom side was welded with a concave shape of stainless steel material. This bottom side was drilled with two holes. One of them was connected to the 300mm length of 1" diameter of stainless steel pipe to collect and evacuate the bed and residue solid material (char and ash) of gasification process which may drop down through the perforated plate into the air-box. The other end of this pipe is plugged during gasification test. The second hole was used to introduce a 200mm length and 1" diameter stainless steel air flow pipe inside the air box pipe with slight curvature to take a coaxial centre with the air box pipe to allow oxidant gas flow towards the distributor plate. 100 mm length was left free between the top end of the introduced pipe and the upper side of the air box pipe to ensure a good dispersion of air across the distributer plate and subsequently across the fluidised bed material column. This air box section is shown in Figure 4.18 below. For the same purpose, this air box was employed for both cold rig and hot rig experiments. 100mm below the upper open end of air-box pipe a hole was drilled across the pipe wall for positive pressure side taping for gas flow pressure drop measuring across the distributor plate and bed material. 1500 mm length of a stainless steel 1" pipe was used to join the feed source of compressed air supply to the air-box section pipe via inlet gas flow pipe as shown in Figure 4.1. This pipe will give a steady air flow through the air box. For the hot rig this pipe was introduced inside the air preheater furnace for air heating.

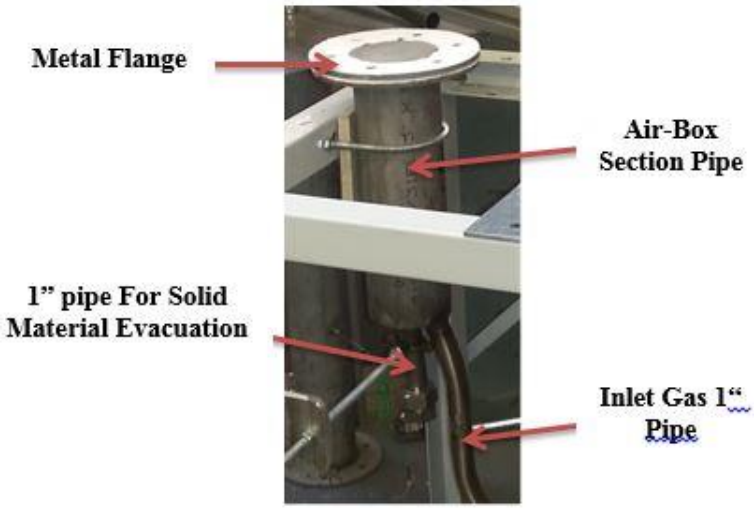

Figure 4. 18 Air-Box section pipe for both cold and hot rig.

4.4.3 Stainless steel flanges

10 open flanges of 6mm thickness, 169 mm external diameter and 89 mm internal diameter (for open side which is equal to the external diameter of the all gasifier pipe-sections) as shown in Figure 4.19 were provided. These flanges were made of 316L stainless steel metal and supplied by Cross Engineering Swansea LTD Company-UK. These flanges were mainly used for gasifier pipe sections connection, where they were welded with the all ends of pipe sections. These welding pipe section-flange can be joined each other throughout the holes of flange by screws to build the completely cold rig fluidised bed column or gasifier column in the hot rig.

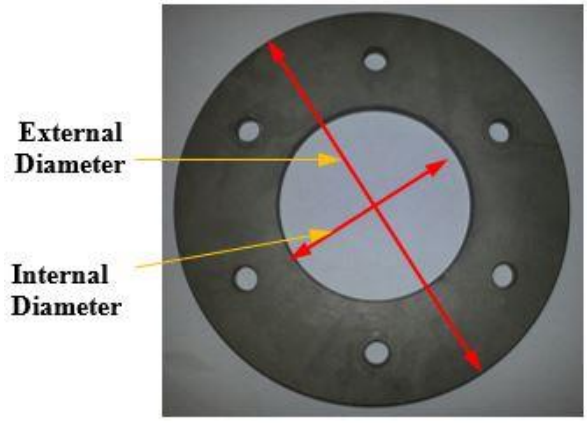

Figure 4.19 Stainless steel type-316L flange

4.4.4 Perforated Distributor Plate

Cross Engineering Swansea LTD Company-UK provided a number of 6mm thickness circular solid 316L stainless steel metal plates. These plates have the same flange

specifications in, metal type, external diameter, number of joining holes and their diameter and position as the rig flanges. These plates were used as a perforated distributor plates to distribute the fluidising gas uniformly through the bed material. According to design calculations and for studying the hydrodynamic effects of the distributor plates open area on the gasifier performance, four plates were prepared by drilling them with 1.5mm diameter holes for different number of holes 19, 55, 85,169, which represent three different open area. As explained in Chapter 3 these holes were arranged with a triangular shape for a specific pitch and located within the inner cross-sectional area of the gasifier pipe, 83mm inside diameter. For each plate, the lengths of pitch, which represents the distance between any two neighbour centre points of the holes are 19, 11.78 9.8 and 5.94mm, respectively. Therefore, the subsequent open area for each distributor plate is, 33.6, 97.1, 150, and 298mm^2, respectively. All distributor plates were signed with a specific formula, which was taken the form, dor1.5mm-N19-P19, dor1.5mm–N55-P11.78, dor1.5mm-N85-P9.8 and dor1.5mm-N169-P5.94, respectively, as shown in Figure 4.20.

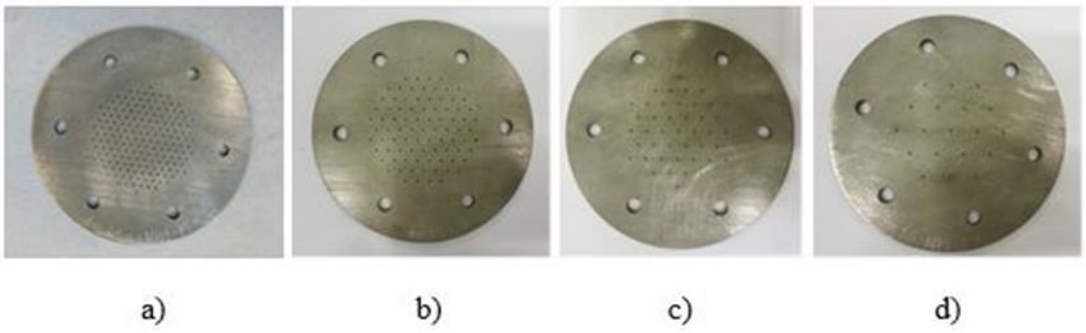

Figure 4. 20 Perfórate distributor plate: a) dor1.5mm-N169-P5.94, b) dor1.5mm-N85-P9.8, c) dor1.5mm-N55-P11.75, d) dor1.5mm-N19-P19. The formula symbols dor-N-P represent dor the hole diameter in mm, N the number of holes and P the pitch distance in mm, respectively.

4.4.5 Air flow measurements

In order to measure a wide range and an accurate gas flow rate inside the fluidised bed column, two measurement apparatus rotameters were used. One of them (small scale) was used for air volumetric flow rates ranging from 0.0 to 50 litre/min whereas the second (medium scale) and was used for air flow rates ranged from 30 litre/min to 300 litre/min. These two flow meters were connected in such a way that can read separately as it was needed.

4.4.6 Air pressure regulator control

For prevention and safety, an air pressure regulator was directly installed after air intake point to maintain and control the pressure inside flowmeters within accepted safety limitations. In addition, this regulator can be used to supply enough pressure to be capable of setting a required airflow rates especially at high-required airflow rates. This regulator is equipped with a control valve, to regulate air pressure thereafter its flow rate, and pressure gauge, in bar and psi units, to read air pressure as shown in Figure (4.16).

4.4.7 Pressure drop device (Manometer)

As shown in Figure (4.21) a digital manometer, model-P200 H, for pressure drop measurement, which Digitron Company made, had been used. This device measured the pressure difference between two points across perforated distributer plate plus fluidised bed column in mbar units and a pressure drop across distributer plate only. The first point (positive point,) is directly located 100mm underneath the perforated distributer plate in the air-box pipe section and this will join to the positive point (red tube) of the manometer. The second point (negative point), represented by multi points, is located in the fluidised bed transparency column above the distributor plate and this will join to the negative point of the manometer. The manometer operates with 3.5-volt battery. The maximum operating temperature is 50^{o}C.

Figure 4. 21 Digital manometer

4.5 Hot rig prepared materials

4.5.1 The pipe of fluidised bed reaction section

1000mm of 316L stainless steel pipe with the same nominal size of air box pipe section, as mentioned in Section 4.4.2 was prepared. Two flanges were welded at the bottom and upper ends of the pipe as shown in Figure 4.22. The former is used to connect together with the assembled air box section pipe and distributer perforated plate via the air box flange. The latter flange is used to connect with any additional required part of free board section. For high temperature conditions a gasket insulated material 5 mm thickness was used between each pair of flanges and between the distributor plate and flanges. This reaction section includes three zones, bed material zone (250-300mm length), splash zone (50-100mm length), and the rest covers the freeboard zone. Four tapping holes for thermocouples starting from the bottom base above distributer plate at 45 mm, 445 mm, 845 mm and 1245 mm to read the temperature at the centre of the inside pipe, T2, T1, T3 and T7, respectively. Additional two holes were used for product gas analyser sample stream at place near thermocouple point of T3 and T4. Another 1"diameter hole is used for pouring a fluidised bed material through a small piece of 1" diameter pipe, which was welded to the main pipe surface. This hole is approximately located at 850 mm from the perforated plate. Two large holes were drilled at the bottom of the pipe. The first one takes the same shape as the front view shape of the arm of the biomass screw feeder. The shape and dimension of front section of this hole is shown in Figure 4.23 (a) and (b). This hole is used as a feeding point for biomass solid fuel material and the centre of this hole is located at 42 mm above the distributer plate. To install and hold a biomass screw feeder arm at this hole, a unit constructed from steel was welded to the outer surface wall of the gasifier pipe reaction section at the position of the biomass feeding hole. This unit was made from steel for the gasifier pipe for the hot rig and from transparent acrylic for the cold rig as explained in section 4.4.1. The last hole, 1" diameter, was made as near as possible the upper surface of the distributor plate. At this hole, one end of a short piece, 50 mm of 1" diameter stainless steel pipe was welded to the reaction section pipe wall of the gasifier, whereas a suitable screw nut can plug the second end. This hole enables the operator to remove and evacuate the

bed material, sand, and all the solid gasification products, ash and char, at the end of each gasification experiment using a vacuum cleaner.

Figure 4.22 Pipe reaction section

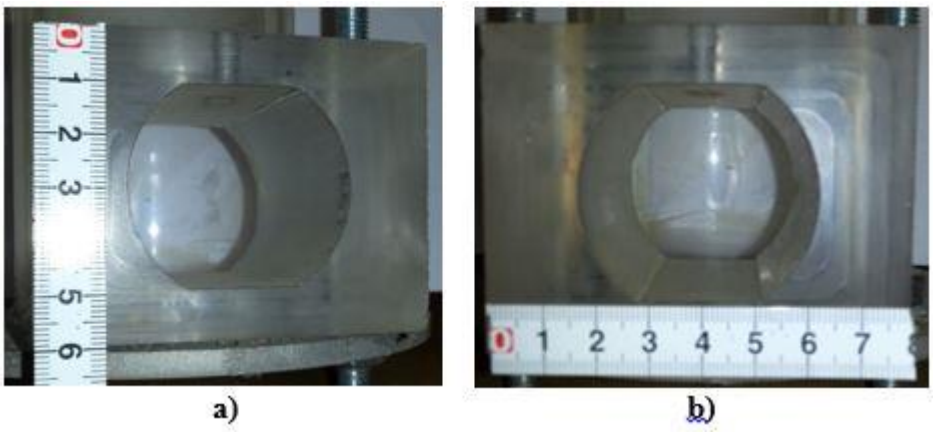

Figure 4. 23 Dimension of the biomass house - hold unit feeding hole: a) For longitudinal measure and b) For width measure

4.5.2 Freeboard pipe section- second part

A 300 and 700 mm length of the same pipe specifications of previous sections was prepared to construct the second part of freeboard reactions section. This pipe is a complementary section to the first part free board, which was included in the pipe of the bed reaction section. Similarly, these freeboard pipe sections were also welded with two flanges at the upper and bottom pipe ends as shown in Figure 4.22. The former end was opened to the atmosphere to the extraction ventilation system and the latter end was connected to the upper flange end of the bed reactions pipe section. Two holes were drilled in this section first one for product gas analysing, 100mm below the upper pipe end and the second hole for thermocouple installing at a position 1245 mm above distributor plate to measure T7.

4.6 Summary

This chapter has shown the materials and methods used in characterising the bed material sand and two solid fuel biomasses, sawdust pinewood SPWB and Iraqi date palm IDPWB. According to a range of standard methods, these materials were characterised. Grinding machines were used for sand and biomass size reduction. In addition, their bulk densities were also measured. To calculate the mean particle size of the sand material for each range, a Malvern analyser was used.

Characterization of two biomass fuels involved proximate and ultimate analysis as well as thermogavimetric analysis. Ultimate analysis was useful for the fuels to quantify the combusting elements and then determine MAFR at stoichiometric conditions and thereby the equivalence ratio. Proximate analysis was used to quantify the reaction characteristics of the biomasses. In addition, thermogravimetric analysis was used to show the weight loss of the fuel material at specific working conditions as a function of temperature and time. Finally, a total carbon analyser was used to measure the carbon content of biomass fuel and char + sand mixture, i.e. the residue of biomass gasification fluidised bed.

To construct the cold and hot rigs the materials and components of each rig were prepared such as the air-box section, distributor plates, flanges, transparent pipe for the cold fluidising column and stainless steel pipe for the reactor and freeboard sections of the hot rig.

Chapter 5

Cold and Hot Rig: Construction, Hydrodynamic and Gasification Experiment Set-Up

5.1 Introduction

This chapter describes the building and construction of the experimental-rig for both, cold and hot operation. In Sections 5.2 and 5.6, all equipment and instruments used during cold and hot (gasification experiments) rigs are presented and described. In Sections 5.3 and 5.7 the procedures for preparation and operation for two rigs, cold and hot are outlined in details, respectively. Moreover, safety steps are highlighted, especially for gasification trials because of its hazardous products. Commissioning trials to test the temperature distribution limitations along the gasifier and commissioning trials for biomass gasification by bubbling fluidised bed are detailed in Sections 5.7.1 and 5.7.3, respectively. For gasification trials, testing parameters and experiments plan design in tables and flow chart form are presented in Section 5.5. Sections 5.4 and 5.8 highlight the experimental data measurements for specific parameters in cold and hot rigs, respectively. Procedures in measuring and determining the design parameters and gasifier performance are included in these sections.

5.2 Cold experiment rig hardware

A schematic layout and the experimental test of the cold rig fluidised bed used in this study are shown in Figure 5.1 and Figure 5.2, respectively. The rig mainly consists of an air pressure regulator, two rotameters, to feed a required air flow rate to the fluidised bed column. The digital manometer was used to measure the pressure drop across the fluidised bed column. The cold rig also included standard fittings to give connection between components using either 316 stainless steel pipes or PVC tubes.

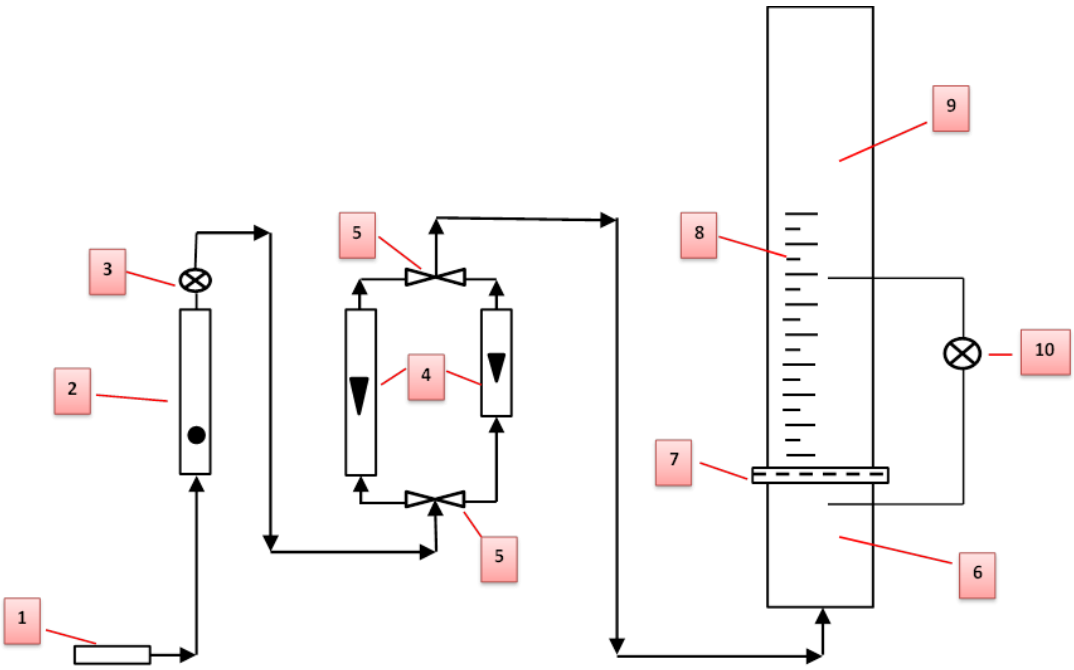

1- Compresed air intake, 2- air pressure regulator, 3- pressure gauge, 4- Air rotameter, 5- Flow divider, 6- Air-box section, 7- Perforated distributor plate, 8- Metric ruler, 9- Transparency fluidisation column, 10- Manometer.

Figure 5. 1 Schematic layout of cold rig fluidised bed column

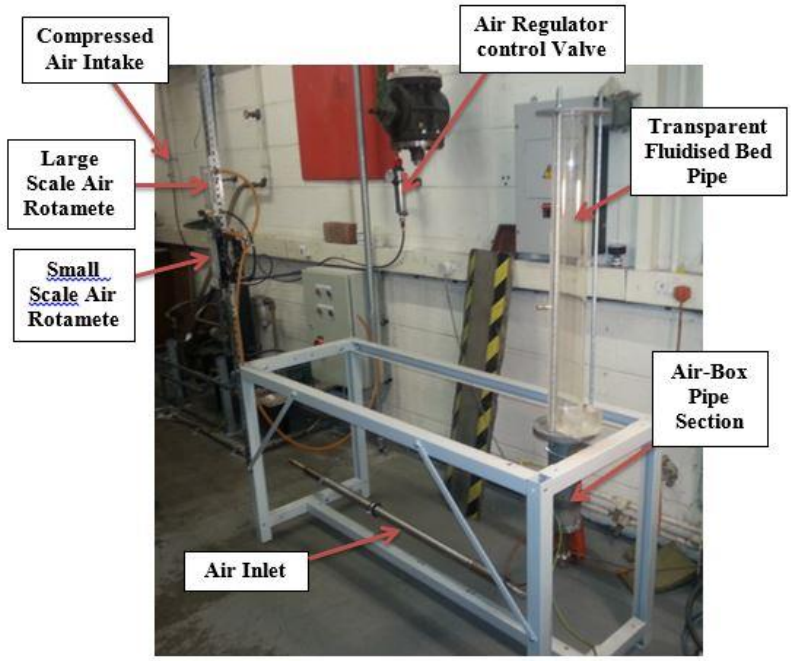

Figure 5. 2 Experimental test cold-rig for hydrodynamic bubbling fluidisation studies

5.2.1 Feed air pressure regulator

Compressed air was supplied by a pipeline to the laboratory where the cold rig was installed. This air was used as a gas phase for the hydrodynamic experiments in the cold rig and as a gasifying agent for hot rig air gasification experiments. To avoid

rotameter damage due to high pressure of air supply and to control air flowrate within the required limitation, an air pressure regulator was used. This regulator also provided a wide range for air velocity measurement by decreasing or increasing the air pressure.

5.2.2 Rotameters

To cover a wide range of a required air flow rate to obtain a hydrodynamic curve of the bubbling fluidised bed system of this study, two rotameters were used to control and measure a specific air flow rate which was supplied to the fluidised column. One rotameter is a large scale, Platon Glass Flowmeter NGX series, model GTF 3ASS and was supplied by RM&C company UK. Its flow rate-operating limit ranged between 30 and 300 l/min at ± 1.25 accuracy of full scale with scale length 100mm nominal. For flow, controlling a fine needle valve was provided on the flowmeter inlet. The other rotameter was a small scale and its operating limit ranges from 0 to 50 l/min at ± 1.25 accuracy of full scale with 2 l/min of its sub-graduated scale.

5.2.3 Bubbling fluidised bed column

The fluidised bed column is the main part in cold-rig set-up. It consisted of air-flow box pipe section, distributor plate and transparent pipe. These components were described in detail in Chapter 4 Section 4.4. The assembly layout of the column is shown in Figure 5.3.

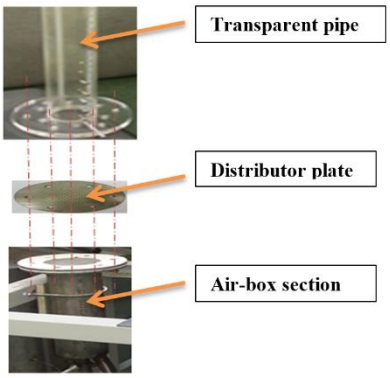

Figure 5. 3 Cold-rig: fluidised bed column assembly

5.2.4 Cold rig sundry equipment

In cold rig setting-up, various accessories and materials were used involving:

- **Pipes and fitting:** A 1 inch diameter stainless steel pipe type 316 with fittings were used to transfer the supplied air to the air-box section, for connecting between the rotameters group and fluidised column unit.
- **PVC tubes:** Various diameters (6mm & 9mm) of un-reinforced PVC tube was used for rig components connections. They were a connection from air pressure regulator to rotameters group, from rotameters to stainless steel pipe to transfer air to the air-box section via stainless steel pipe and for manometer connections to fluidised bed unit to measure the pressure difference between any required two points across the column unit.
- **Metric scale ruler:** This ruler was attached to the external surface of the transparent pipe, for two sides of the pipe, taking the upper surface of the distributor plate as a zero level. These rulers were used as a mean to measure the bed height in centimetres for static H_s, minimum fluidisation H_{mf} and expansion H_{exp} conditions.
- **Standard measuring container:** From the same specification of the transparent pipe, which was used for fluidised column, a short piece, 30cm height, was formed as a cylindrical measuring unit scale. A metric scale ruler ranged between 0 and 30 cm was attached to the wall and the cylinder base was considered as zero level. This measuring container was used to measure a required static height H_s and its corresponding weight and a bulk density for any required experiment. Due to the difficulty of the obtaining a direct accurate measurement for the static height of a bed material inside fluidised bed column due to inability to obtain a uniform bed surface level, this container was initially used to measure the static height of any bed material and thereafter to calculate its bulk density or porosity.
- **Video camera:** A Canon type video camera was used to film each cold fluidised bed experiment as movie files and images. These movie files help to study visually, as required, the hydrodynamic behaviour of the bed for one bed material such as sand and a mixture of two different materials such as sand and biomass materials for different biomass weight percent before and after fluidisation limits as shown in this study. These movies can be directly used or converted to images. They can be used to estimate the bubble size at different static bed height at different air superficial velocities at different bed particle size, bubble velocity, and to measure the expansion height of the bed H_{exp}.

- **Digital manometer:** This was used to measure the pressure drop between any two points in the bubbling fluidized bed column. Its specification was mentioned in section 4.4.7.

5.3 Cold rig process procedure

According to the cold rig set-up described in Section 5.2, the hydrodynamic behaviour experiments of the bubbling fluidised bed for bed materials, sand and biomass, were performed. The obtained data were employed as a baseline data in the biomass bubbling fluidised bed gasification experiments. The preparation and operating procedure for these hydrodynamic experiments are presented in the two next sections, respectively.

5.3.1 Preparation procedure

For the cold-rig set up the preparation procedures were as follows:

(a) It should be ensured that all rig components and measuring instruments were securely installed and fixed. According to the risk assessment all required safety tools were prepared and supplied as well. Also the lab extraction system was checked for sufficient ventilation.

(b) It should be ensured that compressed air was supplied to the laboratory, and the manometer and its batteries worked correctly.

(c) Prior to starting any experiment, it should be ensured that the control valves of compressed air and rotameters were closed.

(d) For a required range of particle size for a selected static bed height, a bed material, sand or biomass or their mixture, was prepared.

(e) Prior to its using, the empty measuring cylinder container was weighed. A bed material for a selected static bed height filled it. After levelling the bed surface inside the container the height was read. Then the filled measuring container was weighed.

(f) The net weight of the bed material was calculated by difference. Usually, the bed static height was taken in term of bed static height to bed column inside diameter ratio, H_s/D, such as: 0.5D, D, 1.5D, 2D, 2.5D.

5.3.2 Operation procedures

The experimental procedures for the operation of the cold-rig for the hydrodynamic studying of the bubbling fluidised bed were as follows:

5.3.2.1 Measuring of pressure drop across distributor plate only

The following steps were conducted to measure the pressure drop across the distributor plate only for each specific air flowrate. This pressure drop was symbolized by ΔP_{dist}.

(a) The positive and negative points of the manometer were connected to tapping points underneath the distributer plate and above it, respectively. The manometer was switched on, where its reading was zero at zero air flowrate.
(b) Prior to opening the rotameter valve, the main intake valve of compressed air was opened. For small air flowrate, from 0-30 l/min, a small rotameter was used.
(c) Starting from 10 l/min a rotameter control valve was opened. At the same time the air pressure at 1 bar or more, not exceeding than 3 bars, was regulated.
(d) At this flow rate and after air flow steadying, the manometer was read.
(e) For a new flow rate, usually the flow rate step is 10 l/min, the above steps, from (c) to (e) were repeated. The pressure drop values across the distributor plate for each air flow rates from (0)- to (140) l/min were taken.
(f) For four required perforated distributor plates, the steps from (a) to (e) were repeated to measure their pressure drop at a specific flow rate.

5.3.2.2 Procedure of establishing of the hydrodynamic curve of the bubbling fluidised bed for a specific bed material

Experimentally, to measure, estimate and calculate the main hydrodynamic design parameters, mainly air-agent velocity at minimum fluidisation conditions for any fluidised bed material system, an experimental hydrodynamic curve was built and developed. For each perforated distributor plate, the procedure steps are as follows:

I. Measuring a pressure drop across distributor plate plus bed material together $\Delta P_{dist+bed}$.

a) According to steps (a-f) in Section 5.3.1, a prepared bed material was poured from the open top end of fluidised bed column. The bed was levelled to permit measurement the static height H_s of the bed in correct way.

b) For increasing air flowrate the same procedure steps (a – e) in Section 5.3.2.1 was followed. Note that the measuring values of pressure drop in this step represented the pressure drop value across distributor plate plus bed material together at a specific air-agent flow rate. It was symbolized by, $\Delta P_{dist+bed}$.

c) In this step, the value of pressure drop across distributor plate plus bed material was re-measured for each specific air flowrate in the decreasing direction. It means that the starting flow rate for decreasing direction was the last flow rate in increasing direction. At each step of specific air flowrate value the total pressure drop was measured.

d) At zero value of air flowrate the bed height inside column was read. This represents the bed height at minimum fluidisation conditions, H_{mf}.

e) Each experiment, for each air flowrate was recorded by a video camera especially for all increasing values of air flowrates to show and watch the hydrodynamic behaviour of the fluidised bed. The top view of cross-sectional area, for each increasing value of flow rate, and the height bed H_{mf} were also recorded.

II. Establishing of the hydrodynamic curve

a) A net value of pressure drop across the bed material for the increasing air flow rate case and the decreasing case were calculated by subtracting the pressure drop across distributor plate ΔP_{dist} from the total pressure drop across distributer plate plus bed material, $\Delta P_{dist+bed}$, i.e.

$$(\Delta P_{bed})_{inc} = (\Delta P_{dist+bed})_{inc} - \Delta P_{dist} \quad (5.1)$$

$$(\Delta P_{bed})_{dec} = (\Delta P_{dist+bed})_{dec} - \Delta P_{dist} \quad (5.2)$$

b) For measuring values of bed pressure drop at a specific air-agent flow rate, for both increasing flow rate case and decreasing case, hydrodynamic curves for a specific bed material for both cases were established. The details will be shown in Section 5.4.3.

III. A required experiment repetition

a) To study the effect of static bed height on the minimum fluidisation velocity for one particle size range and bed material and on the fluidisation regime nature, the experiment steps in Section 5.3.2.2, I a-e and II a-b, were repeated for different static bed height, 0.5D, D, 1.5D, 2D and 2.5D.

b) The experiment steps in Section 5.3.2.2, I a-e and II a-b, were repeated for a mixture of sand bed material and pine wood sawdust material as follows, 2.1cm biomass/ 8.3cmsand, 4.15cm biomass/ 8.3cm sand and 8.3cm biomass/ 8.3cm sand, respectively. These height ratios were converted to the biomass weight percent, 2.68 %, 5.22 %, and 9.93%, respectively.

c) The experiment steps in Section 5.3.2.2, I a-e and II a-b, were separately repeated for pine wood and Iraqi date palm biomass materials to show the fluidisation hydrodynamic behaviour of each.

5.4 Cold-rig experimental data measurements

5.4.1 Pressure drop across distributer plate and bed column

As illustrated in Section 5.3.2.1 the pressure drop across distributer plate only and the combined pressure drop across the distributer plate and bed material column were measured. Then the net pressure drop across bed material column was calculated for increasing and decreasing cases as shown in Equations (5.1) and (5.2) in Section 5.3.2.2-II-a.

These pressure drop measurements are essential for hydrodynamic curve establishing where pressure drop across the bed column ΔP_{bed} represents the Y-axis of the curve. This pressure drop parameter was calculated for sand material alone for three ranges of sand particle sizes, for different static bed height for each range of sand particle size, for biomass material alone and for different biomass and sand mixtures. The measurements of all these pressure drops were conducted for increasing and decreasing air flowrate cases, separately. All these measurements were conducted using a digital manometer in mbar pressure units.

5.4.2 Measuring of superficial velocity of air flow through bed column

The second important coordinate, X-axis, for hydrodynamic curve development is the superficial air velocity or flow rate for a specific column diameter. As mentioned in Section (5.2.2), this parameter was measured using an air rotameter instrument and for velocity measurement. To create this curve, the pressure drop for each flowrate was measured for two flowrate paths. The first path was an ascending flowrate, which started from zero to any flowrate above 100l/min. whereas the second path was a descending flowrate starting from the last flowrate, where the ascending path ended,

to the zero flowrate. These two paths formed a hysteresis curve as shown in Figure 5.4 in next Section.

5.4.3 Minimum fluidisation conditions finding from measuring parameters

The two parameters, pressure drop of the bed column and superficial air velocity or flow rate represent the axes-coordinates for the hydrodynamic curve, Y-axis for the former and X-axis for the latter. From the measured data of the two axes, the hydrodynamic curve was developed as shown in Figure (5.4).

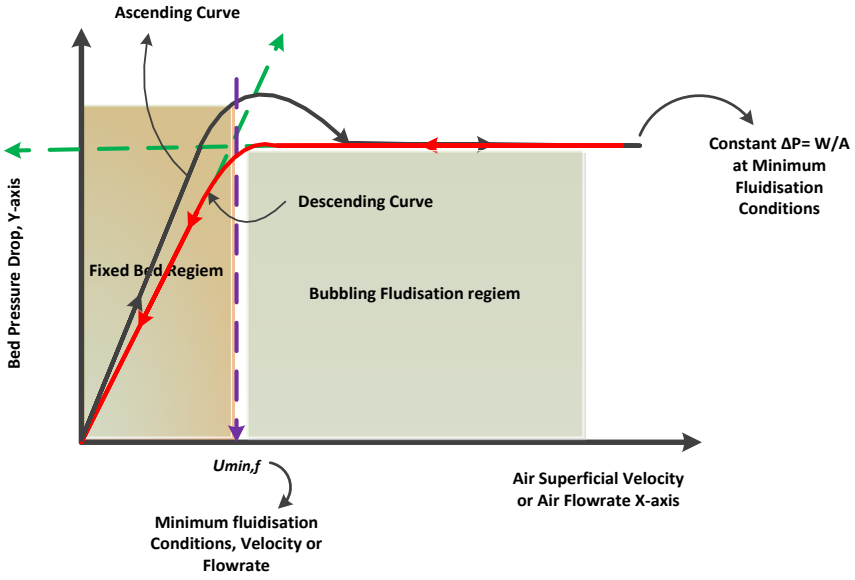

Figure 5. 4 Hydrodynamic curve of bubbling fluidised bed system

In this study, a hydrodynamic curve was used to find minimum fluidisation air velocity or flow rate. The pressure drop at minimum fluidisation conditions can also be found. As displayed in Figure 5.4, the pressure drop was directly increased with increasing gas flow rate in fixed bed regime area. When the bed reached the fluidisation conditions, this pressure drop was constant with any further increasing gas flow rate.

To specify the value of the minimum air velocity or flowrate the following steps were followed:

a) For the bubbling fluidised system, the hydrodynamic curves for ascending and descending cases were drawn as presented in the Figure above. The former case is represented by a solid black curve whereas the latter is represented by a solid red curve.

b) In the fluidisation region, the straight line of constant pressure drop was extended toward Y-axis to intersect this axis. The green dashed line represented this extended line.
c) Similarly, the descending line (red line) in the fixed bed region was extended toward the top. This extended line was also represented by green dashed line.
d) From the intersection point of those extension lines, which were generated in above steps (b) and (c), a new dashed line was extended toward the X-axis. From this new intersection point (at X-axis), the air velocity or flow rate was read, which was represented the minimum fluidisation of air velocity $U_{min,f}$ or flow rate.

This procedure was used to find a minimum fluidisation conditions for a bed materials, sand and sand-biomass mixture with a specific biomass weight percent.

5.4.4 Measuring of bed height at minimum fluidisation conditions

After the completing the fluidisation experiment for ascending and descending gas flow measurements, i.e. mean at zero gas flow rate, the new static height of bed material was measured in using the two rulers, which were fixed on the external wall of the transparent fluidised bed column. The average of two rules reading was taken. This bed height is a result of bed expansion at minimum fluidisation conditions due to fluidisation phenomena and is called a minimum fluidisation bed height $H_{min,f}$. This parameter was used to calculate hydrodynamic design parameters by using theoretical or empirical equations as shown for, example, in Chapter 3- Section 3.2.2.10.

5.5 Hot-Rig testing parameters and experimental plan design

According to the aim and objectives of this study, the experimental plan for the biomass gasification by the bubbling fluidised bed gasifier was designed. This design was achieved depending on the main design parameters, hydrodynamic and operating parameters of the process, which affected the gasifier performance. According to the literature review in Chapter 2, these parameters were specified and selected. To study each parameter effects experimentally, three values for each parameter were specified a minimum number to satisfy the comparison of parameter effects. The selected parameters and their values are presented in Table 5.1. This table shows seven parameters and their corresponding values.

Table 5. 1 Fluidised bed gasification parameters and their selected values

Parameters	Unit	Parameter selected values			
1- Sand Material Particle Size:	µm	300– 425	425 – 500	500 – 600	
2- Biomass Material Particle Siz	µm	300 – 425	600 – 850	1000-1180	
3- Equivalence Ratio ER:	_	ER = 0.2	ER = 0.277-031	ER = 0.381-0.5	ER=0.43-0.55
4- Superficial Gas Velocity U_o:	m/sec or l/min	U_o=1.25U_m	U_o = 2.U_m	U_o = 2.5U_m	
5- Gasification Temperature at bed section T_2:	°C	360	460	560	
6- Static Bed Height H_s:	cm	4.15=0.5D	6.225=0.75D	8.3=1D	16.6=2D
7- No of Distributer Plate Hole N_{orf}:	_	19	43	85	169

According to the number of the parameters and number of their values, the experiment plan was designed. The experiments were classified into seven groups and each group represented the values of one parameter related to the other parameters to form one experiment for each value of specified parameter. These groups and the experiment parameter relationships were explained by each group flow chart as shown in Figures 5.5 and 5.6. For example, to study the effect of the sand bed material particle size, three experiments were conducted for three particle size values at the same operating conditions and values of the other six parameters as shown in Group I flow chart in Figure 5.5.

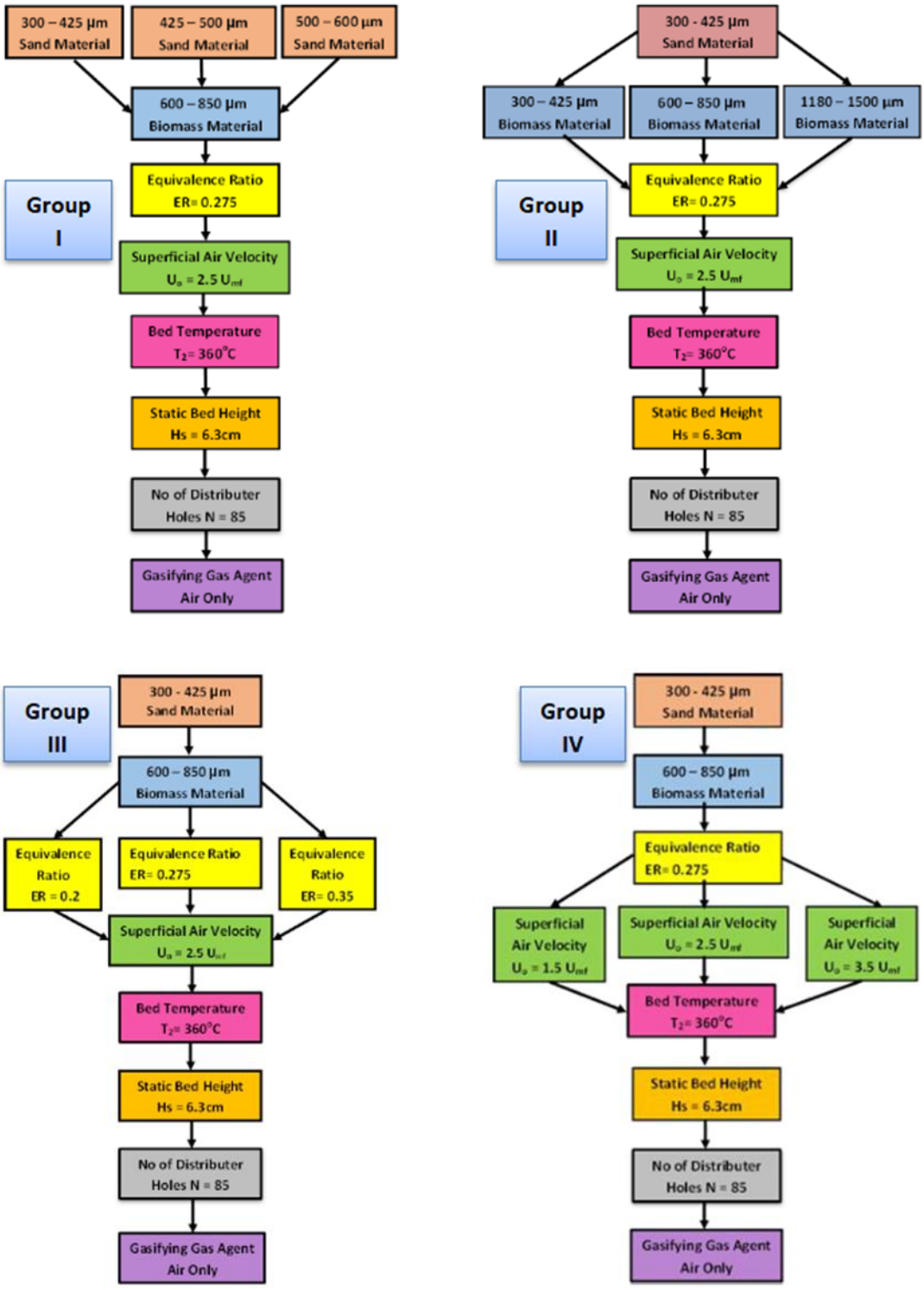

Figure 5. 5 Experiment flow chart for Groups I, II, III and IV

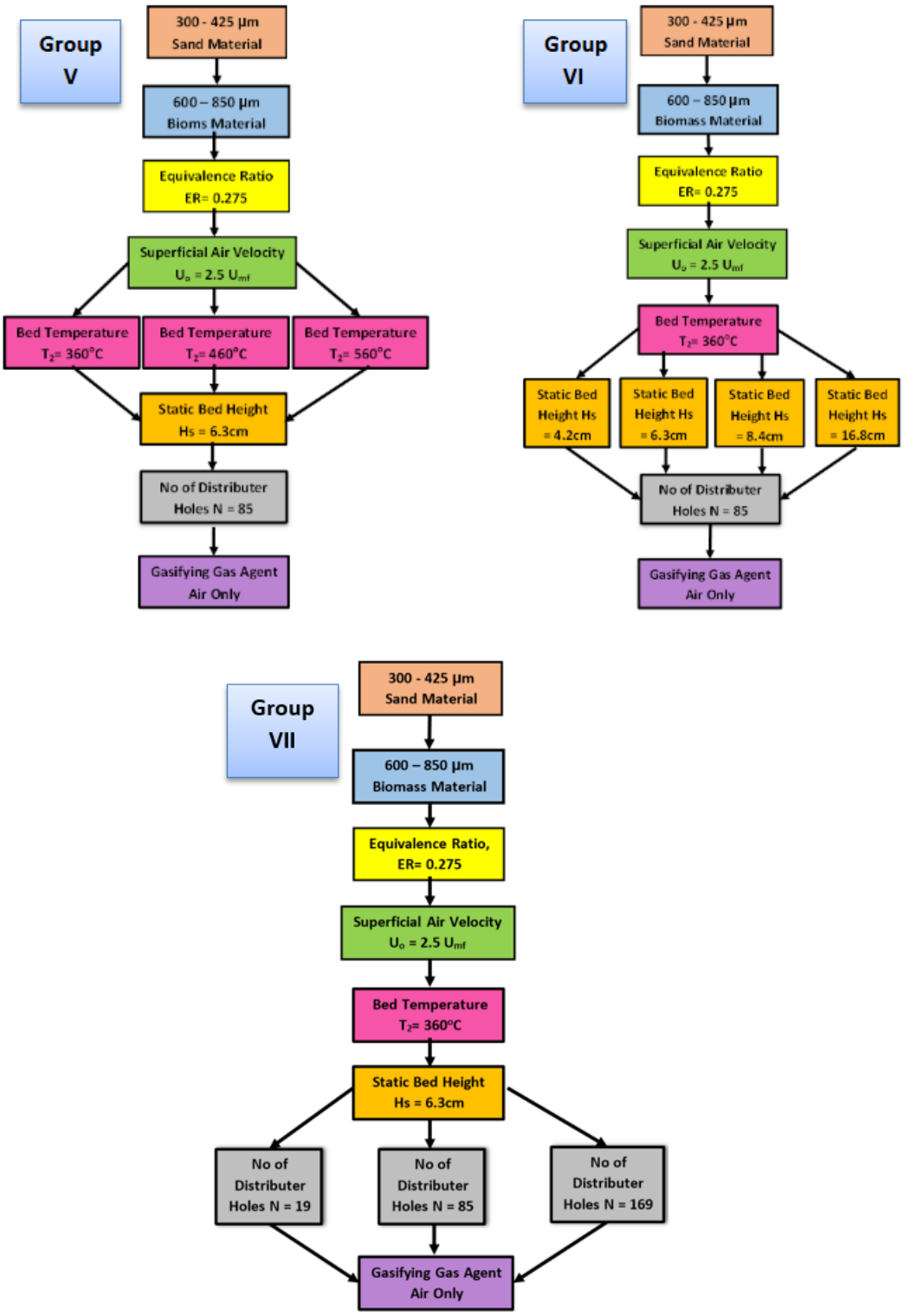

Figure 5. 6 Experiment flow chart for Groups V, VI, and VII

5.6 Equipment of hot (gasification) experiment-test rig

The schematic layout and the experimental test rig of bubbling fluidised bed gasifier used in this study are shown in Figure 5.7 and Figure 5.8, respectively. The rig consisted of an air regulator, two-air feeding rotameters group, an air preheater furnace, a bubbling fluidised bed gasifier, (which in turn consists of an air box section and perforated distributor plate. Also, it consisted a reaction bed and freeboard sections), an electrical gasifier heater and its control panel, a biomass screw feeder system and its water cooling system and nitrogen gas supply system. In addition, a producer gas filter, a tar capturing system, a vacuum pump and a gas analyser system, These rig components comprised of standard 316 stainless steel pipes, PVC pipes and their fittings to give connection between components using 316 stainless steel pipes. The digital manometer was used to measure the pressure drop across the fluidised bed column. High temperature theromocouples, Type-K, were used to measure temperature where they were needed.

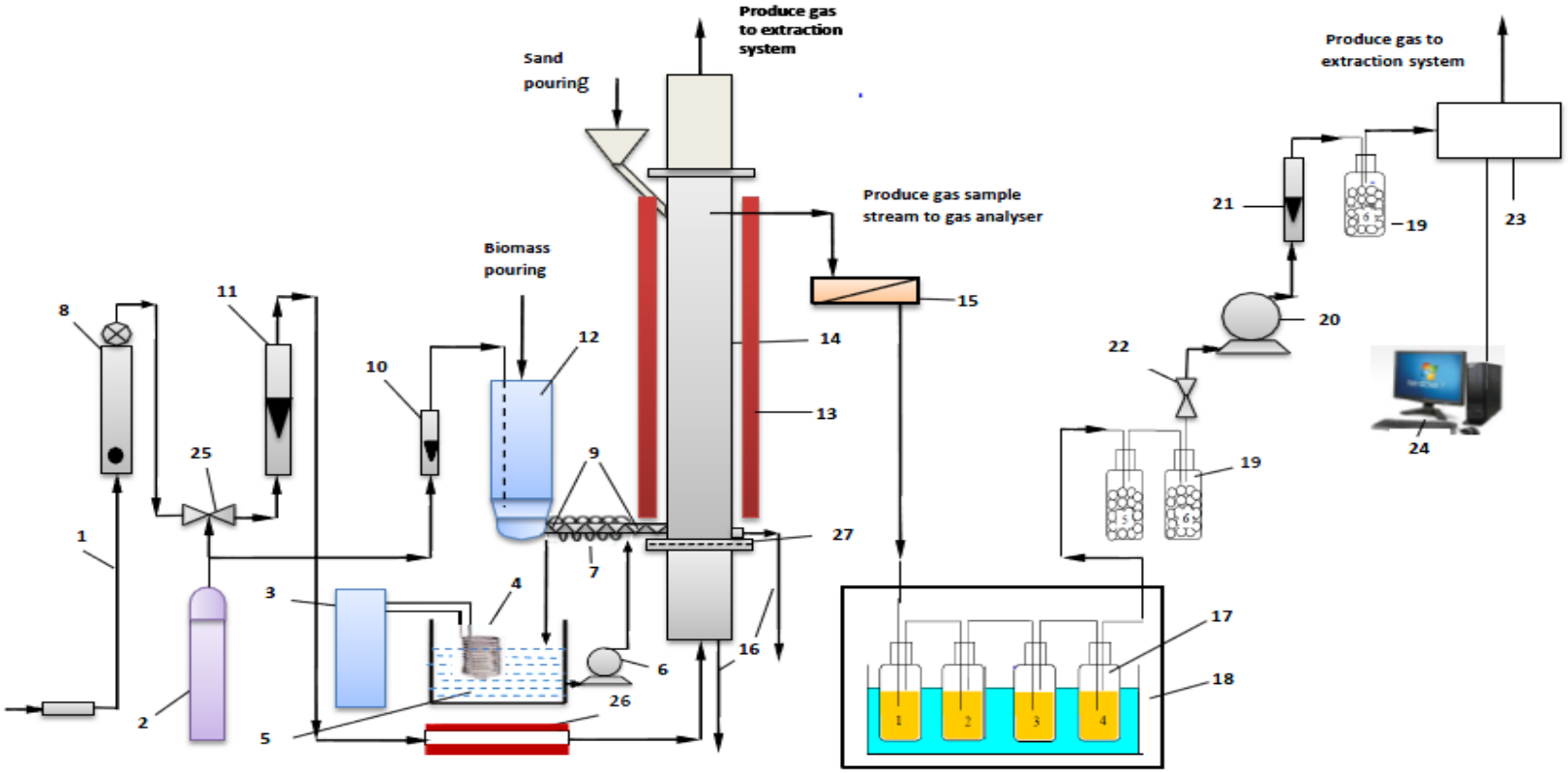

Figure 5. 7 Schematic layout of the biomass bubbling fluidised bed gasification trials set-up

1-Compressed air stream, 2- N_2 gas bottle, 3- Water chiller, 4- Chiller coil heat exchanger, 5- Water pan, 6- Water pump, 7- Cupper water coil heat exchanger, 8- Air pressure regulator, 9- Screw feeder arm, 10- N_2 gas rotameter, 11- Air rotameter, 12- Biomass screw feeder, 13- Furnace heater, 14- Bubbling fluidised bed gasifier, 15-Produce gas filter, 16- Sand-char discharge stream, 17- Impinger bottles set with isopropanol solvent, 18- Freezer room, 19- Silica gel bottles set, 20-Vacuume pump, 21- Produce gas rotameter, 22- Control valve, 23- Gas analyser device, 24- Computer unit, 25- Change valve, 26- Air preheater furnace, 27- Distributor plate.

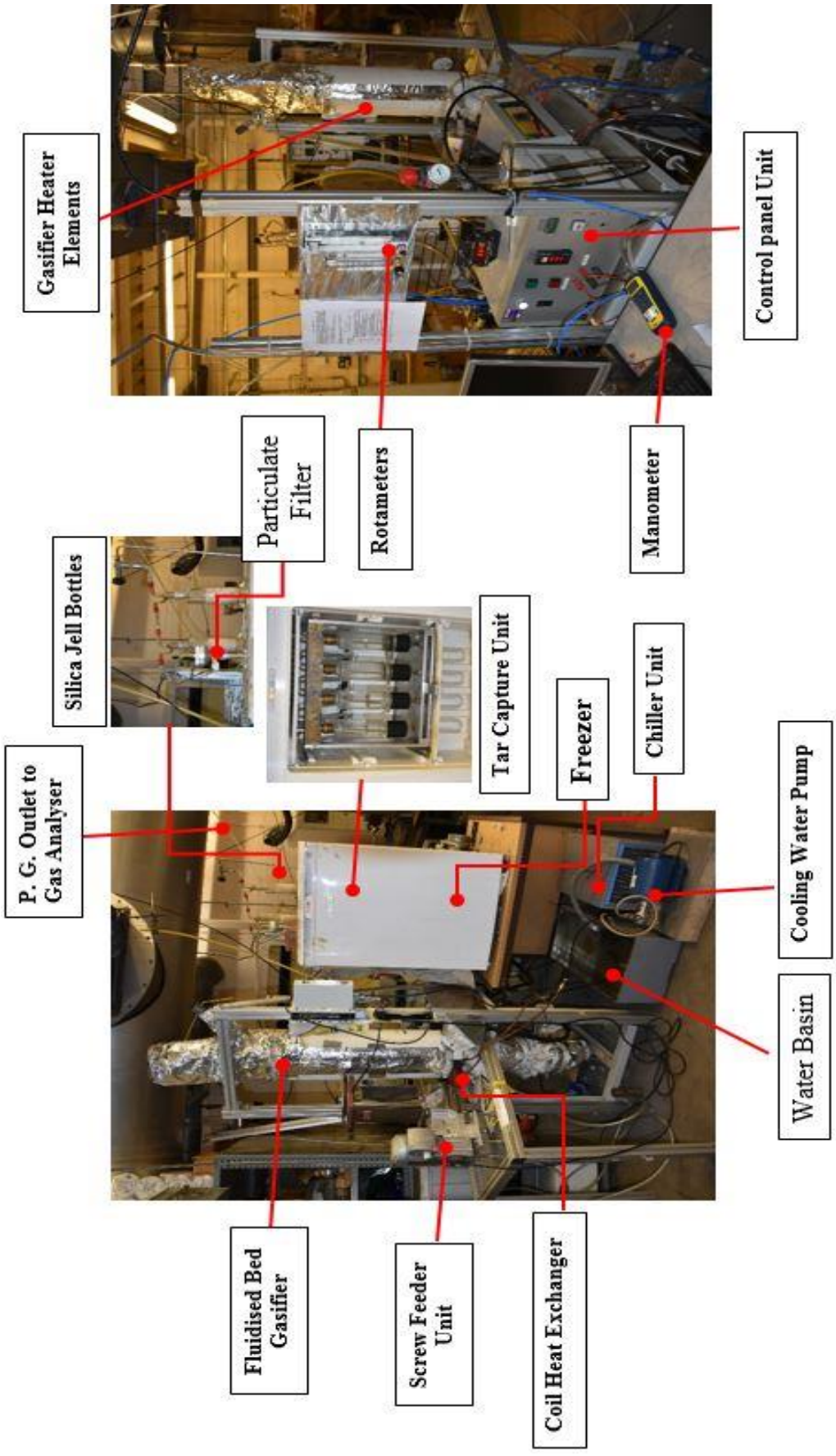

Figure 5. 8 Experimental test hot rig for biomass bubbling fluidised bed gasification studies.

A tubular furnace Type MTF 12/38B as shown in Figure (5.9) was used to heat the supply air from the ambient temperature to a required reaction temperature to enhance the gasification reactions. Carbolite Company-UK manufactured this furnace. Its specifications are, 220-240 Volts, 50-60 Hz, 1500 Watts, 6.3 Amps maximum, and 1200^{o}C maximum allowed temperature. An in-built control panel was provided to set and control the temperature inside the furnace.

Figure 5. 9 Air Preheater Tubular Furnace, Type-MTF 12/38B

5.6.1 Bubbling fluidised bed reactor BFBR (gasifier)

In the same way as mentioned in Section 5.2, this hot test rig consists of a main part of the gasification process called gasifier. It composed of the following main components: air flow-box section, perforated distributor plate, fluidised bed section and freeboard section. The design details of each section are available in Chapter 3-Section (3.3.3.2) and Appendix A. The manufacturing of each section is available in Chapter 4 Section 4.4.2, 4.4.4, 4.5.1 and 4.5.2, respectively. These four sections were all assembled by joining their flanges together using stainless steel bolts to form the intended gasifier. The schematic layout of the assembled gasifier is shown in Figure 5.10. Thermal gasket material, 5mm thickness, was used between each two sections as a thermal insulator to avoid any air or/and gas leakage along the gasifier flanges and to avoid any thermal adhesion that may take place between two metal surfaces due to high surface temperature exposure. For heat saving and for thermal safety, the whole gasifier and the connecting stainless steel pipe between the air preheater outlet and air-box inlet were wrapped with 50 mm thickness of a high quality glass wool insulator blanket material and aluminium foil.

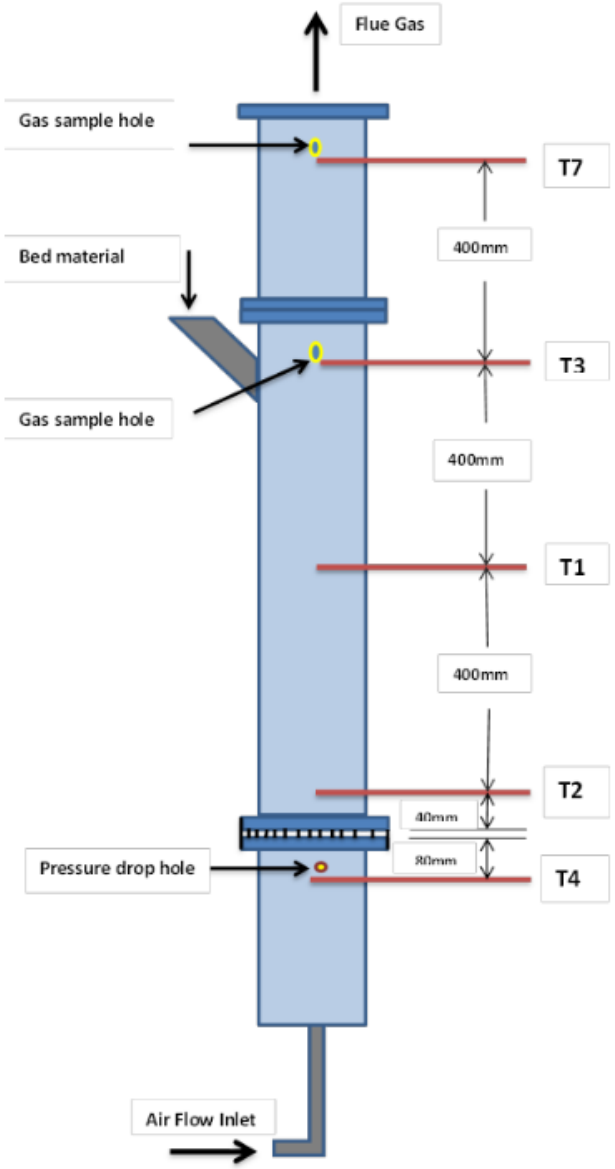

Figure 5. 10 Schematic layout of biomass bubbling fluidised bed gasifier illustrating thermocouples distribution along it and produce gas analysing streams

5.6.2 High temperature gasifier electric heater

Ceramic fibre electric-heater was used to heat the main rig section of the gasifier, mainly the fluidised bed and freeboard reactions section, which included part of the freeboard section, to gain the appropriate and required temperature for gasification reactions. Watlow Company-UK supplied this product. A semi-cylindrical unit – Type 1 with full vestibule was selected for this purpose as shown in Figure 5.11 (a) and (b). Two halves of this heater were needed to enfold the full external surface area of the reaction section pipe with dimensions of, D= 89mm, L= 737mm, E=64mm. The

electrical rating for each half are, Volts= 240, Power= 2500 watts, and surface loading= 2.1 W/cm^2. These ceramic heaters operate at a maximum temperature up to 1204^{o}C and exclusively use radiant heat transfer mode providing a high temperature performance. The supplied heater is suitable for use up to 1093^{o}C (WATLOW 2013). These two heaters were controlled using a PID temperature controller panel.

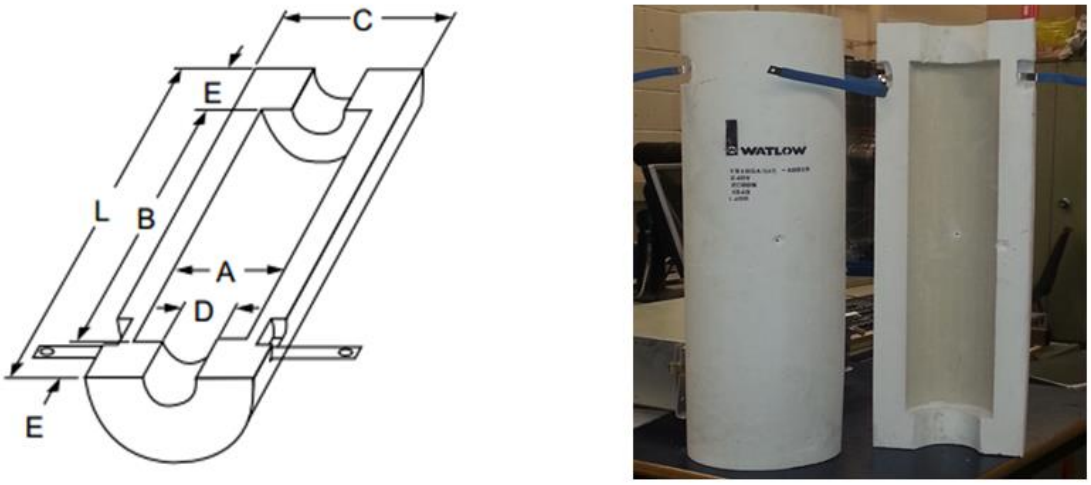

a) b)

Figure 5. 11 Type1- full vestibule ceramic fibre electric heater: a) schematic of a half with its dimensions, b) Image of two halves

5.6.3 Biomass screw feeder

DDSR-20 model of stainless steel biomass screw feeder was used as a biomass feeding driver. This biomass feeder was manufactured by Braender Technology and supplied by Genesis Process Solution Ltd-UK. This model was designed for feeding biomass bulk solids. It composes of the components shown in Figure (5.12). The biomass material can be poured in the hopper of the device and driven into the twin-screw feeder by an electric drive motor. The filling of the screw trough was improved by a trough agitator, which is rotated in combination above the twin-screw feeder, and all were driven via a spur gear unit by the motor. A separate drive controller unit FC-B1 was provided with the feeder. This controller was used to control: the main power supply by a main switch, the speed of screw feeder by speed potentiometer regulator to set a desired speed from 0.0 -100% and finally to control the starting and stopping of the operation by using an operating switch. This feeder can give a maximum design mass flow rate 24 kg/hr.

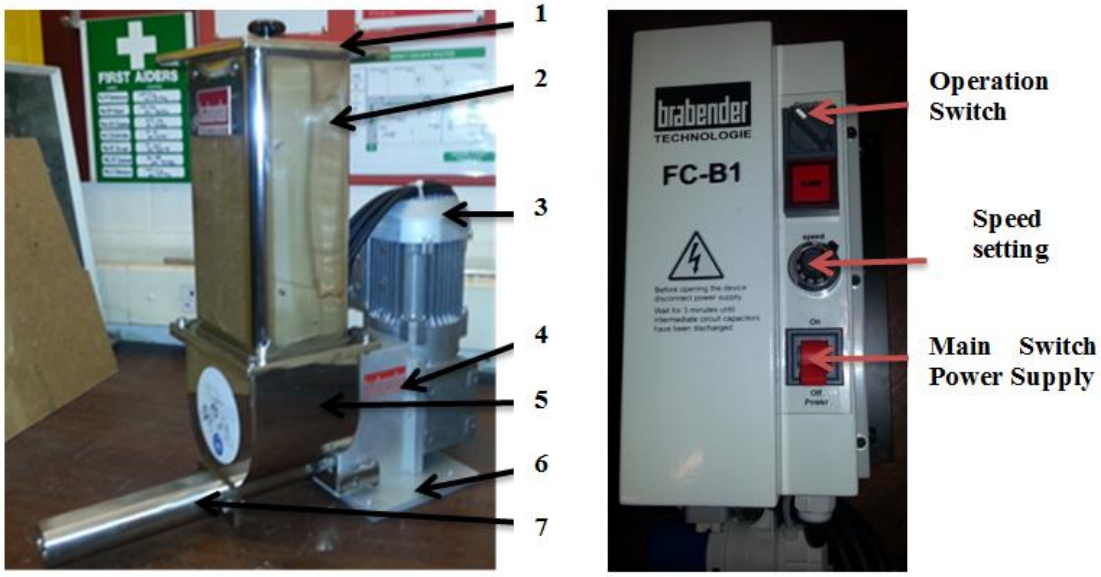

a) b)

Figure 5. 12 DDSR –20 biomass screw feeder: (a) Complete screw feeder unit: 1-Hopper lid 2-Hopper 3- Drive motor 4- Spur gear unit 5- Agitator trough 6- Screw feeder base 7- Twin-screw arm, (b) Power supply and drive controller unit

For this feeder, a calibration curve for a specific biomass mass flow rate can be obtained. It was shown in Section 4.3.1.6.

5.6.4 Screw feeder-cooling system

To prevent biomass pyrolysis inside the arm of the screw feeder at the gasifier fuel feeding point due to higher temperature during gasification experiments, a water cooling system was installed. The cooling system consisted of a basin filled with water, a water chiller, which has an external cooling coil submerged in water basin for water cooling, a copper coil which was wrapped along the screw feeder arm to cool the biomass fuel, and a water pump to circulate a cool water from the water basin to copper coil then again to a water basin. The cooling temperature provided by this system depends mainly on the temperature of the fluidised bed section T2, shown in Figure 5.10. The temperature of biomass at the gasifier feeding point was measured by a K-type thermocouple. The thermocouple was installed on the external surface of screw arm, which was away 50mm from gasifier feeding point. An-inert environment was provided, to prevent biomass combustion inside screw feeder, using N_2 gas. 0.3-0.4

l/min of N_2 gas was fed inside the hopper of biomass screw feeder through a small-scale N_2 gas rotameter.

5.6.5 Producer gas particulate filtration

The producer gas from the rig holds many impurities such as fine particles of sand, char, unreacted biomass and traces of condensed tar vapours. These contaminants have a detrimental effects on the downstream equipment and instruments causing deposition in this rig, i.e. the vacuum pump and the GC gas analyser, which is highly sensitive to these contaminants. In order to obtain a high purity producer gas for GC gas analyser purposes these impurities must be removed as a first step for purification. Therefore, a filter paper medium was used for this purpose. A GA55 grade, circular, 47mm diameter and 0.6 µm pore Whatman glass fibre filter paper type was used for this purpose. After each experiment, the filter was cleaned from the tar and other impurities using an isopropanol solvent. A new filter paper was replaced.

5.6.6 Tar capturing system

A schematic diagram of the tar capturing system is shown in Figure 5.13. It was designed with the same principle design as used in the tar sampling, which was designed according to the standard method for biomass gasification–Tar and particles in product gases - sampling and analysing tar from gasification processes by BSI-CEN/TS 15439:2006 (Energy research Centre of the Netherlands 2004). The main purpose of using a tar capturing system was to remove all condensable compounds from producer gas to avoid any damage in downstream devices due to tar compounds condensation and deposits. The system consisted mainly of an assembly frame of four positions for fixing standard dreschel bottles MF 29/3/250 as shown in Figure 5.8(real image of assembly from lab). These four bottles were connected in series and were filled with 100 ml of isopropanol solvent (99.8 %) from Fisher Scientific. This solvent was used for tar compounds screening. Each bottle position has inner tubes, which were made from 316 stainless steel pipe ϕ 6 x 145 x 1mm. A freezer (BEKO, ZA630W) rated 50 W and minimum temperature of -15^{o}C was used to accommodate the impinger bottles assembly to achieve solvent cooling. The inlet pipe from the outlet filter from the gasifier was connected to the first bottle inner tube through a hole on a top side of the freezer. The outlet of the fourth bottle train was connected to silica gel bottle train.

Silica gel was used to ensure that water vapour in the gas stream was completely removed and any other impurities may available in the gas stream as well.

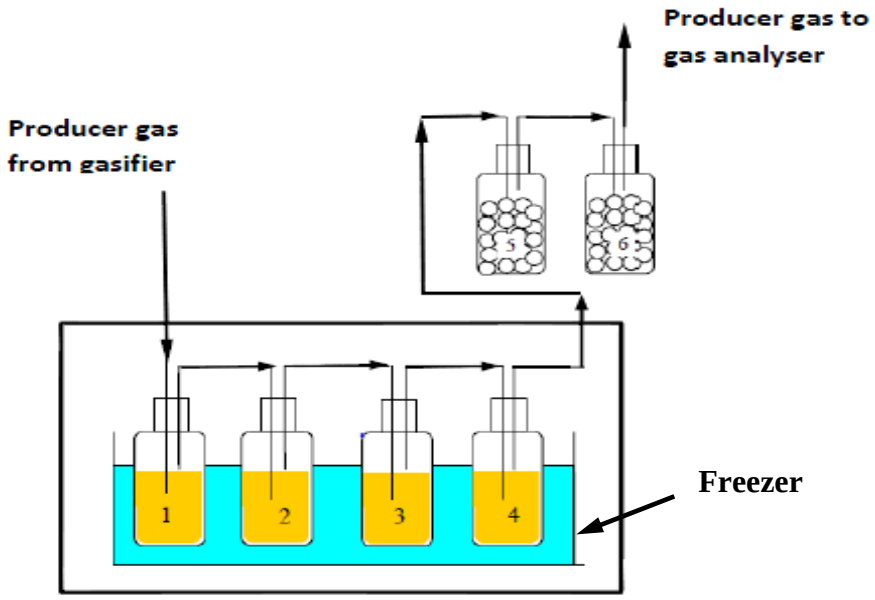

Figure 5. 13 Schematic diagram of the tar capturing system: 1-4 are impinger bottles, each 100 ml of isopropanol, in the freezer at (-15ºC). Silica gel bottles 5 and 6 were kept at 20-25ºC

5.6.7 Producer gas analyser unit

After cleaning and tar capturing, producer gas was sent to gas analyser unit. This unit consisted of, a vacuum pump, a small-scale rotameter, one bottle of silica gel and gas analyser. The vacuum pump was necessary to supply enough flow of producer gas to overcome the pressure drop from the filtration and tar capturing system. A small-scale rotameter, ml/min scale, was used to control the producer gas flow rate within flow rate limitations of the gas analyser, not more than 1 ml/min. A silica gel bottle was installed directly before the analyser to ensure a high purity of producer gas. Finally, the gas analyser type (X-STREAM X2GP - EMERSON) as shown in Figure (5.14) was used to analysis a biomass gasification producer gas. The new X-STREAM gas analysers can measure up to five different gas components using any combination of the following analysing techniques: IR = non-dispersive infrared analysis, UV = ultraviolet analysis, pO_2 = paramagnetic oxygen analysis, eO_2 = electrochemical oxygen analysis, TC = thermal conductivity analysis (Emerson Process Management 2012).

Due to the high sensitivity of gas analyser against any impurities, the producer gas must be free from them. This analyser was capable of analysing into CO, CO_2, CH_4,

H_2 and O_2. It has five channels, one for each above-mentioned gases. These channels must be firstly purged by N_2 gas and calibrated by a standard mixture of gases: 15% CO, 15%CO_2, 15% H_2, and 5.0 % CH_4 where the difference was N_2. This analyser has inlet and outlet streams for producer gas. The output gas stream was directly exhausted to the extraction system. These data provided a volume percent composition for each gas mentioned above as a function of time in seconds.

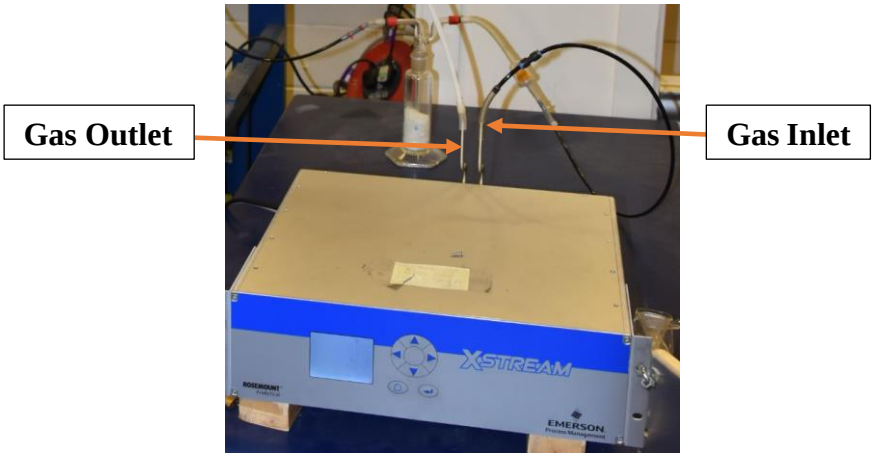

Figure 5. 14 X-STREAM X2GP-EMERSON gas analyser

5.7 Hot-rig bubbling fluidised bed gasification process procedures

5.7.1 Commissioning and preparation procedures

After completing the first stage (without insulation, tar capturing unit, biomass feeding screw feeder and its cooling system) of the gasifier structure, gasifier commissioning temperature setting tests were needed. This was for testing and understanding the performance of the gasifier electric heater and the temperature distribution along gasifier sections at equilibrium conditions for cases of with and without air preheater, airflow, bed material. The temperature distributions were specified according to the thermocouples points that were distributed and fixed along gasifier as shown in Figure 5.10. These tests helped to specify the minimum and maximum limits of the temperatures of the gasification reaction section at fluidised bed reactions zone and freeboard gas reactions zone as well at thermally steady state conditions. Firstly, the top section (reaction section) of the gasifier was tested. It was operated with electrical heaters only without pipe reactor insulation and without bed material silica sand and without airflow. This was performed for several electrical heater setting temperatures Tset=T1, 500^{o}C, 700^{o}C, 800^{o}C, 900^{o}C and 1000^{o}C. Unfortunately, the results show

that the required range of temperature at the gasifier reaction section cannot be obtained. To improve these results all active exposed surfaces of the gasifire were well insulated. Also a quantity of 8.3 cm height of a 300-425 μm particle size of bed material silica sand was used and poured inside the reactor. The tests were repeated for several heater-setting temperatures T1 between 500^{o}C and 1000^{o}C. All tests were let to achieve equilibrium conditions. The results are displayed in Figure 7.1, which shows the values of the temperature T2, the temperature at bed reaction zone, 4.15 cm above distributor plate at biomass feeding point as a function of time. The final equilibrium values of T2 corresponding to setting temperatures T1: 500^{o}C, 700^{o}C, 800^{o}C, 900^{o}C and 1000^{o}C are shown in Table 7.1

Additional sets of electrical heater setting temperatures, 400^{o}C, 600^{o}C, 750^{o}C and 825^{o}C were selected to obtain the equilibrium temperature value T2 (when T2 in gasifier reaches steady state). These temperatures are shown in Table 7.1

Tests were conducted to see the possibility of making T_2 to be a setting temperature Tset instead of Tset=T1. This was because; theoretically it was best to put T2, a required bed reaction temperature, as a Tset. However, particularly it was found that the point of the heater at T1 still behaved as supply temperature, by the electrical heater, and this led to rise the temperature T1 more rapidly than new setting temperature T2 and was expected to go to overload conditions of the upper limit of the heater temperature supply (1200^{o}C).

5.7.2 Vertical temperature distribution a long fluidised bed gasifier

Experiments at specific conditions, for various particle sizes of silica sand bed material, 300-425μm, 425-500μm and 500-600μm , for a range of gasifier setting temperature (gasifier electrical heater setting temperature) without preheater and with preheater and for different air flow rate were conducted. There are two main aims for these experiments: first to gain a database for axial temperature distributions along the gasifier and its limits. This enables the researcher to observe and specify a desired gasification reaction temperature according to the setting conditions. The second aim is to study the hydrodynamic behaviour of the fluidised bed reactor mainly the minimum fluidisation velocity, an important design parameter, at high temperature conditions. However, 600^{o}C, 750^{o}C and 900^{o}C of gasifier setting temperatures Tset=T1 without air preheating were chosen as a first set experiments for gasifier

operating with air flow rate ranged from 10 l/min to 100-140 l/min. The results are presented and discussed in Chapter 7-Section 7.2.2 and shown in Figure 7.3 (a-a^{-}), (b-b^{-}) and (c-c^{-}).

The second set of experiments for setting temperature Tset=T1=950^{o}C, 900^{o}C and 825^{o}C with air preheating, using tubular furnace setting temperature at T_{preset}= 750^{o}C, were also conducted. They are shown in Figure 7.4 (a-a^{-}), (b-b^{-}), (c-c^{-}), respectively.

The third set of experiments for setting temperature Tset=T1=825^{o}C and 900^{o}C with air preheating, using tubular furnace setting temperature at T_{preset}= 900^{o}C, were also conducted as shown in Figure 7.5 a-a^{-} and b-b^{-}. For temperature points, their positions are shown in Figure (5.10) T4, T2, T1, T3 and T7 at gasifier temperature measuring points, -10cm, 4cm, 44cm, 84cm and 124cm, respectively, their equilibrium temperature results were obtained for two groups where mentioned above. The results presented and discussed in Chapter 7, Figure 7.5

The last comparison of the bed temperature T2 levelling, a temperature at 4.15cm point above distributor plate, for three experiments is shown in Chapter 7-Figure 7.6. Each of them had a setting temperature Tset=T1=900^{o}C and T_{preset}= 900^{o}C, 750^{o}C, 0.0^{o}C as well.

5.7.3 Commissioning of biomass gasification experiments

These experiments were conducted according to hydrodynamic and gasifier temperature distribution results, and considered as a preliminary test for preparing the gasifier for next study of complete rig experiments. Pine wood sawdust as biomass solid fuel, quartz sand as bed material and air as gasifying gas agent were used for these tests. For a specific range of the particle size of the sand material a superficial velocity of airflow, expressed as volumetric flow rate in l/min, according to its minimum fluidisation velocity, was specified. Then at a specific gasification equivalence ratio and air flowrate, a mass flow rate of biomass was calculated. Subsequently, from the sawdust biomass screw feeder calibration curve the mass flow rate of biomass was specified.

5.7.4 Preparation procedures of gasification hot-rig

After completing gasifier temperature setting and commissioning and after joining all gasification hot-rig secondary units and accessories, at this step the rig was considered

ready to conduct the required gasification experiments. Prior to any experimental operation, a number of preparation steps should be followed.

I. Safety preparation

Prior to start any gasification experiments the following safety and security steps were performed:

- The lab extraction system for gasification product gas ventilating was checked to ensure its operation readiness.
- Lab gas detector alarm and personal gas monitor was tested to be ready at any time.
- Trip hazard, hot equipment signs and required protective equipment (PPE) were prepared to avoid any harm.
- Electrical circuits for all electrical component of the rig were checked to be ready in operation.
- Any flammable material such as biomass fuel and isopropanol liquid solvent were deported outside the rig area.

II. Experiment preparation procedures

The preparation procedures for the experiment set-up were as follows:

a) According to fluidised bed biomass gasification process and plan of experiments, specific required materials were prepared such as: A specified particle size range of the sand bed material for a specific static bed height was weighted. This sand particle size let to know the value of the cold minimum air fluidization flow rate, which was obtained from the cold-rig experiments. Also a specific particle size range of the biomass solid fuel was weighed. This weight of biomass was calculated according to the required biomass mass flow rate for a required time of gasification process for each experiment. The biomass mass flow rate was calculated according to a selected value of each air flowrate and equivalence ratio (by mass). Prior to use this experiment, it was dried up to 105-110^{o}C for 2 hours using a dryer oven.

b) Availability of N_2 gas and supplying compressed air were checked and prepared.

c) The biomass screw feeder was tested for driving a consistent flow of the biomass particles especially at low biomass flow rates, which correspond to low values of screw feeder speed point. These speed points need a low quantity of biomass in the hopper to reduce the weight load limits of biomass during low screw speeds.

This will ensure the driving of screw feeder motor and then the smooth flow of biomass inside gasifier.

d) The function of the water cooling system for screw feeder cooling was checked. The water pump was checked for supplying a suitable water flow rate. The function of chiller and its coil were also checked. This was operated after gasifier heating up. A K-Type thermocouple was used to monitor the temperature near biomass feeding point.

e) Due to tar compounds precipitation and blockage, especially between gasifier outlet point of producer gas for analysing and a vacuum pump suction point, a connection gas pipe lines, type PVC, were replaced by a new pipes, whereas the stainless steel pipes were cleaned. Then for gas pipelines leakage checking, a purging with air at 15 l/min for 30 minutes was used, which was appropriate to produce sufficient pressure to detect any leaks.

f) The tar capturing system was preconditioned by cleaning the 250 ml dreschel bottles using, firstly an isopropanol solvent and secondly a laboratory liquid detergent and then dried at 115^{o}C for 2-3 hours to remove any impurities.

g) To confirm that the tar-capturing unit was properly functioning, the fridge was turned on for 24 hours to achieve an effective cooling environment, approximately -10^{o}C. This was monitored using a K type thermocouple.

h) The function of the vacuum pump was verified by using the producer gas rotameter, which was placed before the gas analyser.

i) The electrical heater of the gasifier was tested for the setting temperature at point T1 inside gasifier column. This temperature was set at 900^{o}C and the temperature rise observed through the controller. All temperature measurement points T4, T3 and T7 distributed along gasifier were observed. External K-Type thermocouples for these points were connected to the thermometer, whilst T1 and T2 points were connected to the electrical heater controller panel. The air preheater tubular furnace was tested for the required temperature of the inlet air to the gasifier T4. Its controller monitored the temperature inside the preheater furnace, whereas the air outlet temperature at the preheater furnace end was monitored by a K-Type thermocouple. The setting temperature of the preheater was 900^{o}C or 750^{o}C.

j) Prior to producer gas analysis, the five channels of the gas analyser were purged using N_2 gas. Then a standard gas mixture calibrated these channels.

5.7.5 Operating procedure of gasification hot-rig

The thorough experimental procedures conducted for the running of the gasification hot-rig were as follows:

1) Prior to any test, the gasifier furnace was switched on and the temperature along the gasifier was observed. Similarly, if it was operating, the air preheater tubular furnace was also switched on.
2) A specified weighed amount of the sand bed material (for a specified particle size range and static bed height) was poured inside the gasifier through a hole located at the top of the gasifier.
3) During the gasifier furnace activation, the preheating period took 3-4 hours, the first and second dreschel bottles in the tar-capturing unit were each filled by 100 ml of isopropanol measured at room temperature. The third and fourth bottles were left empty. Finally, the whole unit was assembled.
4) While the setting temperature inside the gasifier at point T1 reached (250^{o}C), the extraction system in the laboratory was run to take out undesirable gases (combustible and toxic gases) which may be present.
5) During gasifier furnace activation, the gas analyser was purged by N_2 gas and calibrated by a standard gas. This purging and calibration procedure was undertaken once per day for all experiments.
6) When the bed temperature at point T2 in the gasifier reached a required reaction temperature, the control valve of the air rotameter was opened to supply a required air flowrate in l/min (within fluidisation conditions). This air flowrate depends mainly on the minimum fluidisation flow rate value for sand material which in turn depends on a selected sand particle size range. At this step, adjustable balancing between a required air flowrate and a required gasification temperature T2 was needed to keep the operating parameters at their required specified values for each experiment.
7) During step (6) the required dried biomass (for a specific particle size range) was poured inside the screw feeder hopper. At this time the N_2 gas rotameter control valve was opened up to 0.3-0.4l/min to prevent biomass pyrolysis inside the screw feeder. This required biomass was specified according to its mass flow rate calculations. The biomass mass flow rate was calculated at a specific gasification equivalence ratio and at a selected air gasifying agent flow rate. From this mass

flow rate and for a specified experiment time, the required biomass mass for any experiment was allocated. The procedure of the biomass mass flow rate calculations will be shown in Section 5.8.4.

8) For a calculated biomass mass flow rate value, the corresponding speed point value of the biomass screw feeder was determined using biomass-speed point calibration curve, which was prepared as shown in Chapter 4. This speed point was adjusted using a speed point regulator in the screw feeder controller.
9) The vacuum pump in the gas analyser system was switched on to supply enough producer gas flow rate (not exceed 1 ml/min) to the gas analyser. A rotameter control valve was opened to supply this flow rate.
10) A compatible gas analysis online software was prepared using a personal computer. This software was used to record the gases analysing data at time=0.0 i.e. the moment of the gasification reaction experiment starting.
11) When the gasifier reached the required operating temperature, the biomass screw feeder was switched on. The required experiment time (in minutes) was specified according to the weight of the prepared biomass, as explained in step 7. From the commissioning tests, it was seen that the biomass feeding time, which was required to achieve equilibrium conditions was less than 2 min. So most of the experiments were conducted for 5min.
12) After the experiment reached its specified time, the gasification reaction was stopped by switching off the biomass screw feeder and electrical heater. The airflow was also closed. Finally, the vacuum pump in gas analyser system was switched off, the producer gas rotameter was closed and the data analysing software were stopped after 15 min from the experiment starting.
13) At this step, the air flow was replaced by inert N_2 gas to prevent char reactions as much as possible for accurate calculation of carbon conversion with respect to its reaction time period. N_2 gas flow rate was maintained at a minimum flow rate for fluidisation conditions to ensure a perfect inert environment for all the bed (sand + char) and to cool a gasifier as quickly as possible.

5.8 Hot-Rig experimental data measurements and calculations

5.8.1 Temperatures

As shown in Chapter 2-Section 2.5.1.3 operating temperature is an important factor in the biomass gasification process. Gasifier performance and gasification process efficiency are highly affected by the operating temperature where the temperature inside the gasifier affects the producer gas composition. At bed section, the bed measurement temperature T2 controls the biomass gasification reaction rates, whilst in the gasifier freeboard section the temperatures T1, T3 and T7 control the tar cracking reaction rates. Also, in case of the using the preheater furnace, the inlet air temperature to the gasifier affected the temperature distribution along the gasifier. Moreover, the tar capturing process needs low temperatures to prevent isopropanol solvent evaporation and to improve the tar solution in the solvent. As a result of gasification exothermic and endothermic reactions, the fluctuation of bed temperature T2 throughout the gasification experiment as a function of time was also recorded. Finally, at the inlet biomass feeding point a low temperature environment below 150^{o}C was needed to prevent biomass pyrolysis, which affects the gasifier performance. Therefore, measuring these temperatures was significant in controlling the overall gasification process.

As mentioned in Sections 5.5.1 and 5.5.2, these temperatures were measured using K-Type thermocouple and were observed using a multichannel digital thermometer and a built-in thermometer for both: gasifier furnace control panel and air preheater furnace.

5.8.2 Minimum fluidisation conditions at high temperature

Due to the variation of air density with temperature, tests were conducted to measure the minimum fluidisation conditions (especially minimum fluidisation air flowrate) at elevated temperature conditions. In the same manner, which was followed to find the minimum fluidisation conditions for air - sand material system at cold conditions, the airflow rate at minimum fluidisation conditions at elevated temperature was found. Firstly, the tests were conducted for sand particle size range (300-425) µm for three gasifier furnace setting temperature T1, 600^{o}C, 750^{o}C and 900^{o}C, where these temperatures gave a corresponding bed temperature T2, 70^{o}C, 95^{o}C and 400^{o}C,

respectively. The obtained values of minimum fluidisation air flowrate are displayed and discussed Chapter 7 in Table 7.2 and Figure 7.7.

5.8.3 Required time for gasification experiment

For continuous of biomass gasification process experiments, the required time was considered an important parameter because it indicated that the point at which the gasification reactions reached equilibrium (steady state) conditions. The steady conditions mean that the composition of the gasification producer gas does not change with time. For three times, 2.5 min, 5 min and 10 min, biomass gasification experiments were conducted at the same conditions: air flowrate, equivalence ratio, bed temperature T2, biomass mass flow rate and sand material particle size. The testing results were indicated that the required time to reach the equilibrium conditions was 2.5min. According to these results and depending on biomass amount availability, most of the continuous gasification experiments were performed for a 5 min period time. For biomass gasification experiments, a stopwatch was used to measure a required time of the process. At the same time, the online gas analyser results provided the change of the compositions of a producer gas with time (in seconds) during gasification experiments interval. This time-gas composition data was helpful to measure and specify the following: 1) starting point of reaction equilibrium conditions, 2) the starting point of the decline of the gas composition at the end time of the experiment and 3) the time that was required to reach the equilibrium point.

5.8.4 Biomass mass flow rate settings

As discussed in Chapter 2, for gas-solid reactions the gasification process depends mainly on two essential reactants, gasifying agent gas and solid fuel material. The reaction quantities of these two reactants are related by equivalence ratio. The gasification process operates within incomplete combustion conditions, which means that the required quantity of oxygen is always less than its stoichiometric quantity (partial oxidation). To achieve these conditions the actual air-fuel ratio must be less than the stoichiometric air-fuel ratio. As mentioned above these two ratios are related by ER where the value of this ratio depends on the process type. For gasification process, the fuel was definitely considered as excess reactant whilst the oxidant was the limiting reactant.

5.8.4.1 Equivalence ratio, biomass feeding rate and air mass flow rate setting

As shown in Equation (3.25), ER relates the mass flow rate of both reactant materials, air and biomass fuel, in actual and stoichiometric conditions. The main objective is the specifying and setting the required biomass feeding mass flowrate for a specific air flowrate and required equivalence ratio. This biomass air mass flowrate can be calculated as shown in Chapter 3 Equation (3- 25) to Equation (3.30)

Usually, the stoichiometric quantities of air and biomass can be calculated from the chemical reaction equation for complete combustion for all quantity of each combustible element in the fuel as illustrated in Table 5.2. The formal quantity was calculated by summing the required O_2 for each element, using the ultimate analysis of biomass fuel, subtracting the latent oxygen in the biomass fuel.

Table 5. 2 Quantities of O_2 required for stoichiometric calculation for biomass fuel

Component	Reaction	Atomic mass	Atomic moles	Required O_2 (mole)	Req.O_2 (mass)
C	$C+O_2= CO_2$	W_C as C	$W_C/12.01$	$[1\times (W_C/12.01)]/1$	$[[1\times (W_C/12.01)]/1]\times 32$
H	$H_2 + 0.5O_2= H_2O$	W_H as H_2	$W_H/2.016$	$[0.5 \times (W_H/2.016)]/1$	$[[0.5 \times (W_H/2.016)]/1]\times 32$
O	----------	W_O as O_2	$W_O/32$	$[W_O/32]$	$- [W_O/32] \times 32$
N	----------	----------	----------	----------	----------
S	$S + O_2= SO_2$	W_S as S	$W_S/32.07$	$[1\times (W_S/32.07)]/1$	$[[1\times (W_S/32.07)]/1]\times 32$

From the net O_2 required mass, the required air mass can be calculated using O_2 weight percent in air, 0.232, whereas N_2 weight percent=0.7547)(Basu 2010). For this purpose a general equation for any biomass fuel was developed, by this study, to determine the stoichiometric mass air fuel ratio $(MAFR)_{stoichio}$ as shown in Equation (5.4).

$$(MAFR)_{stoichio} = \frac{[2.664\times C\ wt\% + 7.937\times H\ wt\% - O\ wt\% + 0.998\times S\ w\%]}{0.232\times[C\ wt\%+H\ wt\%+O\ wt\%+S\ w\%+N\ wt\%]} \quad (5.4)$$

Where: *C wt%, H wt%, O wt%, S w%, N wt%,* represent the weight percent of the elements C, H, O, S, and N, respectively, in the ultimate analysis of the biomass fuel.

By applying Equation (5.4) and from ultimate analysis for each biomass, the stoichiometric mass air fuel ratio $(MAFR)_{stoichio}$ for each biomass, SPWB and IDPWB are 6.2 and 6.352, respectively.

Equation 3.25 was considered a first step for biomass mass rate determination and this led to determining the corresponding screw feeder speed point. The steps of the biomass fuel mass flow rate calculations have been detailed in Chapter 3. These steps were arranged and summarized as a flow chart as shown in Figure 5.15.

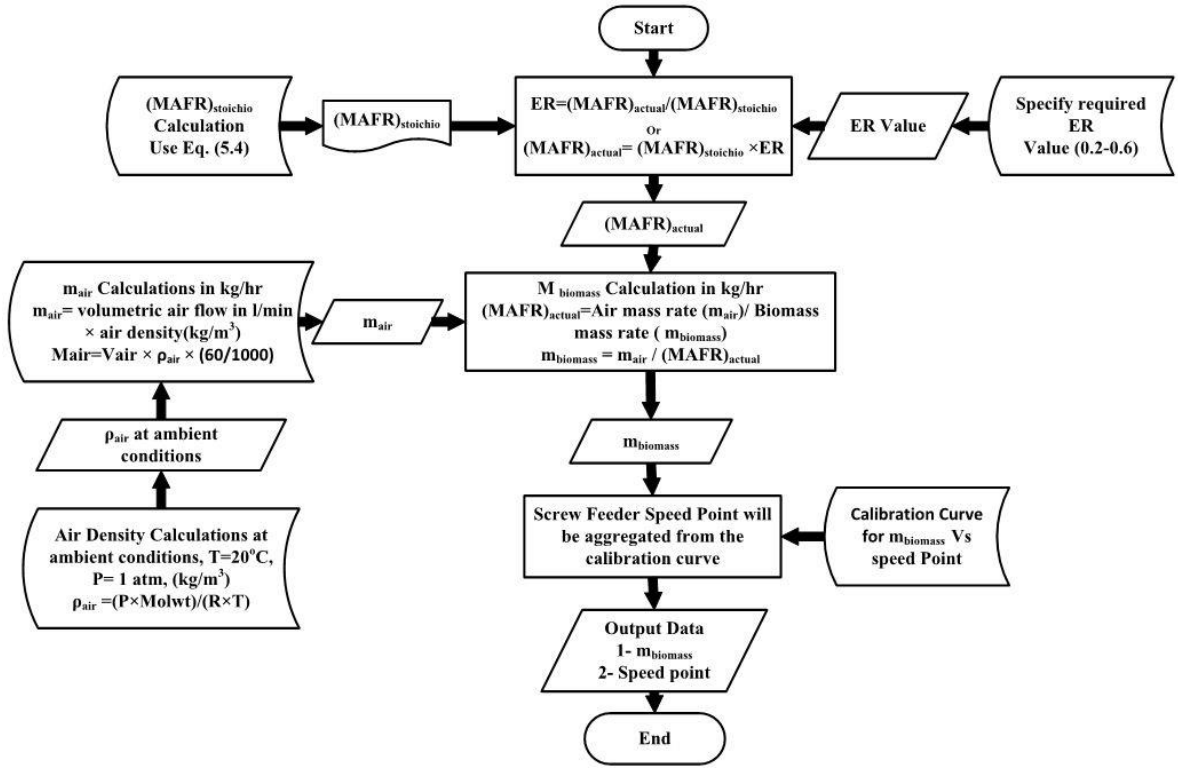

Figure 5. 15 Flow chart of the biomass mass flow rate and the speed point determination of the screw feeder

5.8.5 Measuring of producer gas composition

In this study, a biomass gasification producer gas composition was analysed using a gas analyser type (X STREAM - EMERSON). This analyser was capable of analysing into CO, CO_2, CH_4, H_2 and O_2. The flow rate of the inlet of any gas to the analyser does not exceed 1 l/min.

For any new experiment and prior to any producer gas analysis, the analyser was firstly purged by N_2 gas (zero calibration) for all five-gas channels. Secondly, a standard producer gas mixture (span calibration) directly calibrated the analyser. By volume percentage, this standard gas was composed of 15% CO, 15%CO_2, 15% H_2, 5% CH_4 and the difference was N_2. This analyser has input and output streams. These streams were for gas inlet and outlet, respectively. The output gas stream was exhausted to the extraction system. Once the calibration was completed, the analyser was ready to receive any gas. For this analyser it was not needed to repeat the purging and calibration process for a new experiment on the same day. The accuracy of the analyser for the calibration gas was found to be less than ± 1%. This analyser was on line connected to a personal computer. These data provided a volume percent composition

for five producer gas components, which have been mentioned above as a function of time in seconds.

5.8.6 Gasification Performance Parameters Calculations

5.8.6.1 Producer gas Yield (GY)

Due to the inactivity of N_2 at gasification conditions, Producer Gas (P.G.) yield in Nm^3/hr can be estimated making use N_2 mass balance for gasifier system as shown in Chapter 7 Figure 7.37. For total N_2 mass balance,

$$Mass\ rate\ of\ total\ input\ N_2 = Mass\ rate\ of\ total\ output\ N_2$$

$$Mass\ rate\ of\ total\ input\ N_2 = Mass\ rate\ of\ N_2\ in\ air + Mass\ rate\ of\ N_2\ in\ biomass\ fuel$$

$$Mass\ rate\ of\ N_2\ in\ air = wt\%\ of\ N_2\ in\ air \times mass\ rate\ of\ feeding\ air\ \dot{m}_{air}$$

$$Mass\ rate\ of\ N_2\ in\ fuel = wt\%\ of\ N_2\ in\ fuel \times mass\ rate\ of\ feeding\ fuel\ \dot{m}_{biomass}$$

The total moles of N_2 in producer gas P.G. can be calculated using its molecular weight, 28 using Equation (5.5)

$$Total\ moles\ of\ N_2\ in\ P.G. = Total\ output\ mass\ rate\ of\ N_2/28 \quad (5.5)$$

Then, the total moles rate of P.G. can be calculated, making use total moles of N_2 in P.G. using Equation (5.6).

$$Moles\ rate\ of\ P.G. = \frac{Total\ mole\ rate\ of\ N_2\ in\ P.G}{vol\%\ of\ N_2\ in\ P.G./100} \quad (5.6)$$

Volume parentage of N_2 in P.G. was estimated using Equation (5.7) by the difference of the producer gases, which were analysed. These gases are CO, CO_2, CH_4, H_2, and O_2 in volume percentage.

$$Vol\%\ of\ N_2\ in\ P.G. = 100 - vol\%\ of(\ CO + CO_2 + CH_4 + H_2 + O_2) \quad (5.7)$$

It can be noticed that for ideal gas, the volume percent and mole percent are equal. The volumetric flowrate of producer gas in Nm^3/hr can be calculated making use that for ideal gas at standard conditions, 273.15°K and 101.325 kPa, each 1 kgmol of the gas occupied 22.4 Nm^3. Therefore, the producer gas in volumetric flowrate, for example Nm^3/hr, at ambient conditions can be calculated using Equation (5.8).

$$P.G.volumetric\ flowrate = moles\ rate\ of\ P.G.\ \times 22.4 \quad (5.8)$$

Finally, the gas yield GY of producer gas per unit mass of biomass feeding fuel, for example in Nm^3/kg of feed biomass can be calculated using Equation (5.9).

$$GY\ in, (Nm^3/kg\ feed\ fuel) = \frac{volumetric\ flowrate\ of\ P.G\ in\ (Nm^3/hr)}{mass\ rate\ of\ feed\ fuel\ in(\dot{m}_{biomass}/hr)} \quad (5.9)$$

5.8.6.2 Carbon conversion efficiency (CCE)

This Efficiency can be estimated making use the yield of producer gas in (kgmol/kg biomass feed) and the composition of three gases in producer gas, which are hold carbon atom C mainly, CO, CO_2 and CH_4 as follows (Basu 2006).

$$Total\ moles\ of\ output\ C\ in\ P.G.per\ unit\ mass\ of\ feed\ biomass = \left[\frac{CO\%+CO_2\%+CH_4\%}{100}\right] \times \left[\frac{Total\ mole\ rates\ of\ P.G}{Mass\ rate\ of\ biomass\ feed}\right] \quad (5.10)$$

$$Total\ mass\ of\ C\ in\ P.G.per\ unit\ mass\ of\ feed\ biomass = [Total\ moles\ of\ C\ in\ P.G.per\ unit\ mass\ of\ feed\ biomass] \times 12 \quad (5.11)$$

The mass rate of input carbon to the gasifier can be calculated from the weight percent of carbon C in the biomass fuel, Ultimate analysis, and the mass rate of the biomass feeding, using Equation (5.12).

$$Total\ input\ mass\ rate\ of\ C\ = \left[\frac{wt\%\ of\ C\ in\ feed\ biomass}{100}\right] \times [Biomass\ feed\ mass\ rate] \quad (5.12)$$

Finally, CCE can be calculated using Equation (5.13).

$$CCE\% = \left[\frac{Total\ output\ of\ C\ mass\ rate\ in\ P.G}{Total\ input\ of\ C\ mass\ rate\ in\ feed}\right] = \left[\frac{Total\ output\ of\ C\ mass\ per\ mass\ of feed\ biomass}{Total\ Input\ of\ C\ mass\ per\ massof\ feed\ biomass}\right] \quad (5.13)$$

5.8.6.3 LHV of producer gas

The LHV of producer gas in MJ/Nm^3 can be calculated as follows (Basu 2006).

$$P.G.LHV = \left[CO\ heat\ of\ comb \times \frac{CO\%}{100}\right] + \left[CH_4\ heat\ of\ comb \times \frac{CH_4\%}{100}\right] + \left[H_2\ heat\ of\ comb \times \frac{H_2\ \%}{100}\right] \quad (5.14)$$

The heat of combustion of the gases CO, CH_4 and H_2 are 11.97, 33.95, and 10.22 MJ/Nm^3, respectively (Legonda 2012), (Basu 2006).

From producer gas yield in, Nm^3/kg fuel feed, the output LHV of producer gas in MJ/kg fuel feed can be calculated using Equation (5.15).

$$P.G.LHV\ in\ \left(\frac{MJ}{Nm^3}\right) = \left[P.G.LHV\ in\ \left(\frac{MJ}{kg\ fuel\ feed}\right)\right] / \left[P.G.Yield\ in \left(\frac{Nm^3}{kg\ fuel\ feed}\right)\right] \quad (5.15)$$

5.8.6.4 Cold-Gas Efficiency CGE

Cold –gas efficiency can be calculated using Equation (5.16) (Basu 2006).

$$CGE\% = \left[\frac{LHV\ of\ P.G.(output)}{LHV\ of\ fuel\ feed\ (Input)}\right] \times 100 \quad (5.16)$$

5.9 Summary

In this chapter, the experimental approach used and data measured during biomass cold fluidisation and gasification trials is presented. .For each rig the components and procedure of preparation and operation are described. In addition, the experimental data measured for both rigs are presented.

For the cold rig, the visual observation of the fluidisation phenomenon for sand, biomass and their mixtures was recorded. Also, the procedure of the establishing of the hydrodynamic curve, ΔP-U_o curve, was derived. This curve has been used to determine the minimum fluidisation velocity for each set of conditions such as particle size for sand bed material, static bed height and mass percent for biomass - sand mixtures.

For the hot rig, the design of the biomass gasification experimental tests was prepared. This was useful to study the effect of the hydrodynamic and operating parameters on the performance of the bubbling fluidised bed gasifier. Seven groups of experimental tests were established and each group had three or four experiments. Finally, the experimental data measurements such as temperatures, air flowrates, producer gas composition and the weight of the char + sand mixture residue are presented. Furthermore, the procedure of the calculation of the performance parameters such as, ER, CCE, LHV and CGE are presented.

Chapter 6

Results and Discussion for Cold Hydrodynamic Fluidisation Experiments

6.1 Introduction

This chapter presents and discusses the research results of the experimental study for a hydrodynamic bubbling fluidised bed for cold conditions. In the cold experiments, the profile of pressure drop vs air velocity for the perforated distributor plate is presented. The images of specific experiments for single bed material; sand, SPWB, IDPWB, and mixture of biomass-sand bed material for various conditions are presented to show and analyse the fluidisation hydrodynamic behaviour of these bed materials. These various conditions mainly include the changing of; type of bed material, biomass weight percent in biomass-sand mixture, particle size of biomass, number of holes of distributor plate and static bed height. In addition, the hydrodynamic curves, ΔP-U_o curve, for four groups of experiments for pure sand, pure biomass and their mixtures for different weight percent, 2.68%, 5.22% and 9.93% are exhibited. These curves were firstly used to determine the critical design parameter, minimum fluidisation velocity for each case and secondly to show the effects of the bed material particle size, static height of the bed and biomass weight percent in the bed mixture on the value of the minimum fluidisation velocity. The empirical equation for minimum fluidisation velocity U_{mf} vs weight percent of the biomass bed for (500-600)μm range of sand particle size was realized.

6.2 Hydrodynamic results for cold experiments

In this section, most of the experimental cold results are presented as the following:

6.2.1 Distributor plate pressure drop-air velocity profile

Air pressure drop across the perforated distributor plate for two hole diameters 1.5mm and 2mm versus air velocity for a range of number of holes 19, 43, 55, 85 and 169 is shown in Figure 6.1-(a), (b) and (c). Air pressure drop versus distributor open area for two hole diameters for a wide range of air velocity are shown in Figure 6.1- (a*) and (b*) as well. For ΔP- air velocity graph (Figure 6.1-(a), (b) and (c)), it is noticed that the relationship takes an exponential trend especially for low number of holes, small hole diameters and for high air velocities (more than 10cm/sec for N_{orf}=19 and more than 30cm/sec for N_{orf}=43). However, for N_{orf} more than 43 the relation shows linear. For a specific value of air velocity, pressure drop increased inversely with the number of holes and diameter of hole. A possible explanation for this might be that according to Equations 3.42 and 3.43 the velocity of the air inside the orifice U_{orf} decreases as d_{orf}

increases. As shown in Equation 3.42, the effect of U_{orf} on ΔP_{dist} is more effective compared to d_{orf} effect. In addition, from Equation 3.44-a, it can be seen that as the number of holes increase the velocity U_{orf} increases and thereby ΔP_{dist} decreases.

From the Figure 6.1-(a*) and (b*), it can be shown that at specific air velocity ΔP_{dist} decreases as the distributor open area increases. For d_{orf}=1.5mm, Figure 6.1-(a*) shows a sharp decrease of pressure drop from 0.36 to 0.76cm^2, whereas for d_{orf}=2mm, as shown in Figure 6.1-(b*) the decrease was gradual. In addition, the Figure shows for specific open area the pressure drop decreased as air velocity decreased. High air velocities more than 18.1cm/sec shows show sharp increase in pressure drop for d_{orf}=1.5mm and a gradual increase for d_{orf}=2mm. In addition, it can be seen that for both hole diameter and for all velocities the pressure drop across distributor plate is than 10 mbar for N_{orf} more than 43 holes. A possible explanation for this might be, first as has explained in above paragraph and second that the large open area has a low resistance against the air and subsequently low-pressure drop across the plate.

For this finding, it can be concluded that at specific air velocity the pressure drop across the perforated plate decreases as the available cross sectional area of the holes increases. In addition, for a specific open area (number of holes N_{orf}) the pressure drop increases as air velocity increases.

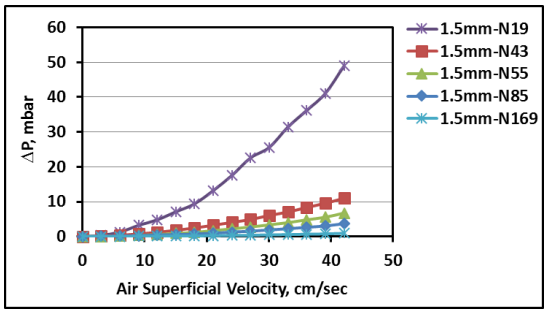

a)

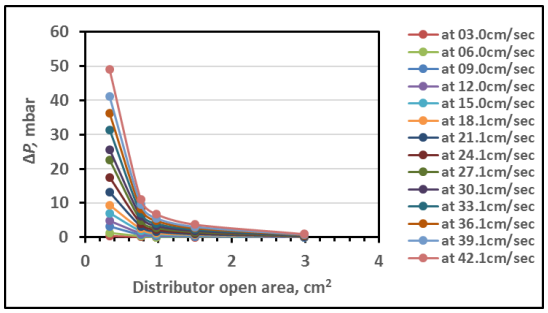

a*)

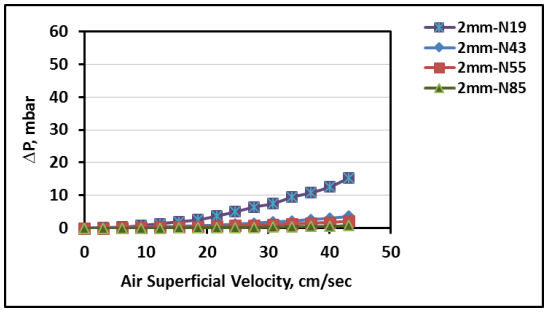

b)

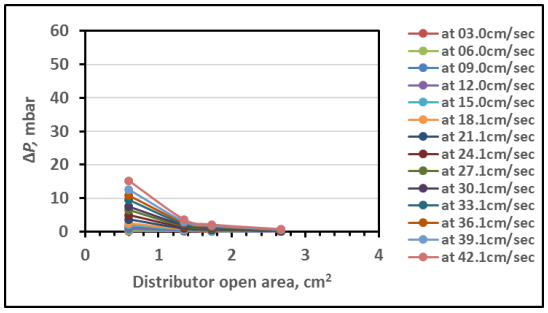

b*)

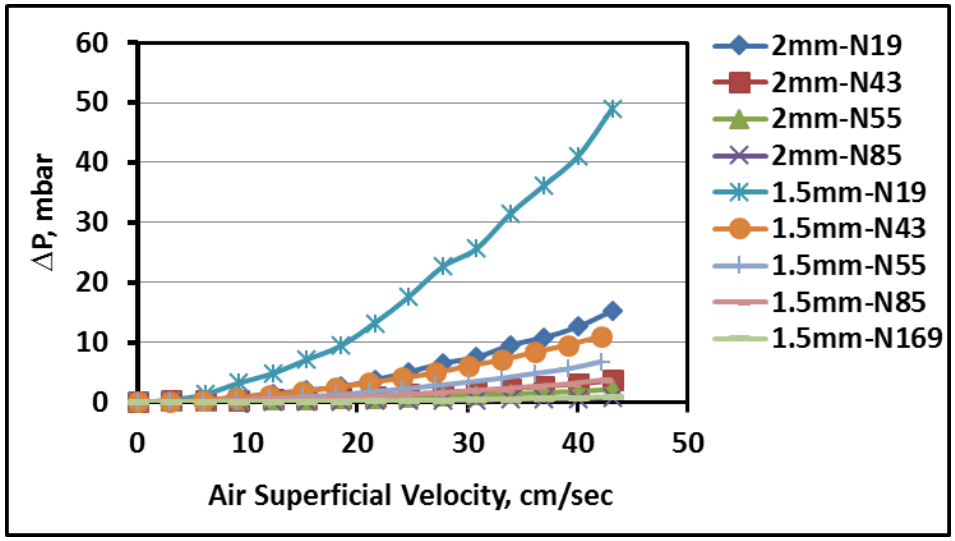

c)

Figure 6. 1 Pressure drop-air velocity profile and distributor open area across distributor plate: a) 1.5mm-hole diameter, a*) 1.5mm-open area, b) 2mm-hole diameter, b*) 2mm-open area, c) two holes diameter, 1.5mm and 2mm.

6.2.2 Air fluidisation behaviour for a single bed material

6.2.2.1 Air-sand fluidisation system (300-425) µm

An experimental fluidisation behaviour of an air-sand system as a single bed mateial is shown in Figure 6.2. In this experiment, a sand of particle size (300-425) µm, static

height of the sand bed column H_s =8.3cm and distributor type 1.5mm-N85-P9 is taken an example to show the sand fluidisation behaviour. Figure 6.2 displays the sequnce of images of the experiment for a sequence of air velocity increase, from 0.0 l/min= 0.0 cm/sec to air flowrate 110 l/min = 33.9 cm/sec. According to the sequence, the images show that the bed remained fixed and stagnant for air flowrates from 0.0 l/min to 30 l/min. Any appearance of air bubbles was not observed. For this range of velocity the bed can be described as a fixed bed. At 40 l/min the image shows the bubbles appearance. Small bubbles revealed at the bottom and became larger during their transit upwards through the sand bed and finally they burst at the top of the bed surface. At this low velocity the motion of the bubbles were comparatively slow. The practical experience told that fluidisation started between 30 l/min and 35 l/min. This was confirmed by the hydrodynamic curve, ΔP-U_o curve, which was established and used for minimum fluidisation velocity determination as shown in Figure 6.5-c. From this curve, the value of this velocity for this range of particle size was approximetly 35 l/min (10.875cm/sec) as shown in the Figure 6.2 and Figure 6.5-c and this value is compatible with the observed value. As velocity increased the following bed changes were observed: the fluidisation of the bed became more clear, the bubble rising velocity and their size were increased, due to their coalesance, also the expansion of bed height became greater. Also at high velocities the bed became more violent, the bubbles burst strongly at the top of the bed surface causing greater mixing, increasing the bursting region above the bed and the bed pressure drop became more variable. Overall, it can be concluded and confirmed that this sand material, as a single material for 300-425 μm particle size range, was fluidised naturally and smoothly and can be classified as a Gldert B group (Yang 2003),(Daizo and Levenspiel 1991)**.** The similar behaviour was also experimentally observed for other two sand particle sizes of this study, 425-500 μm and 500-600 μm for all conditions which were used in all experiments.

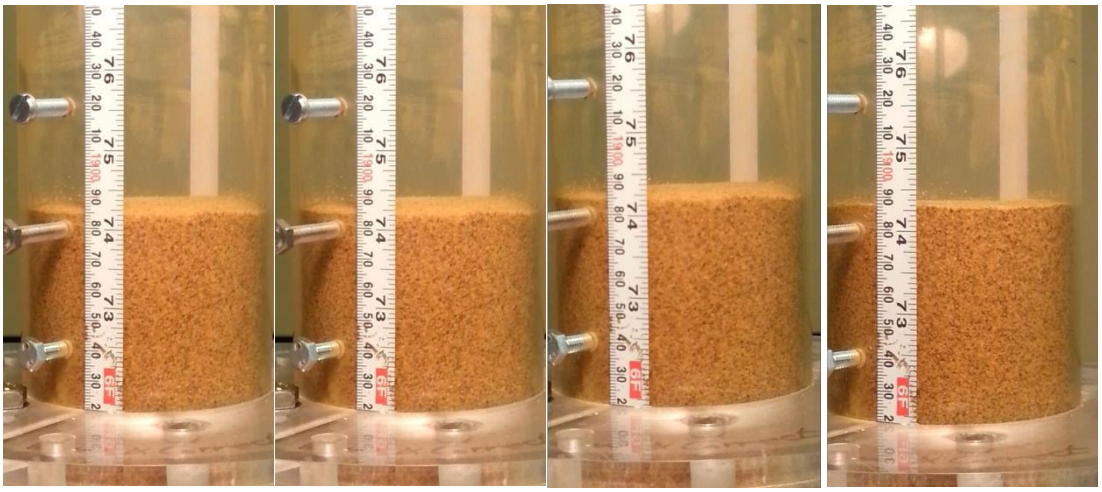

Uo= 0.0 l/min Uo= 10 l/min Uo= 20 l/min Uo= 30 l/min

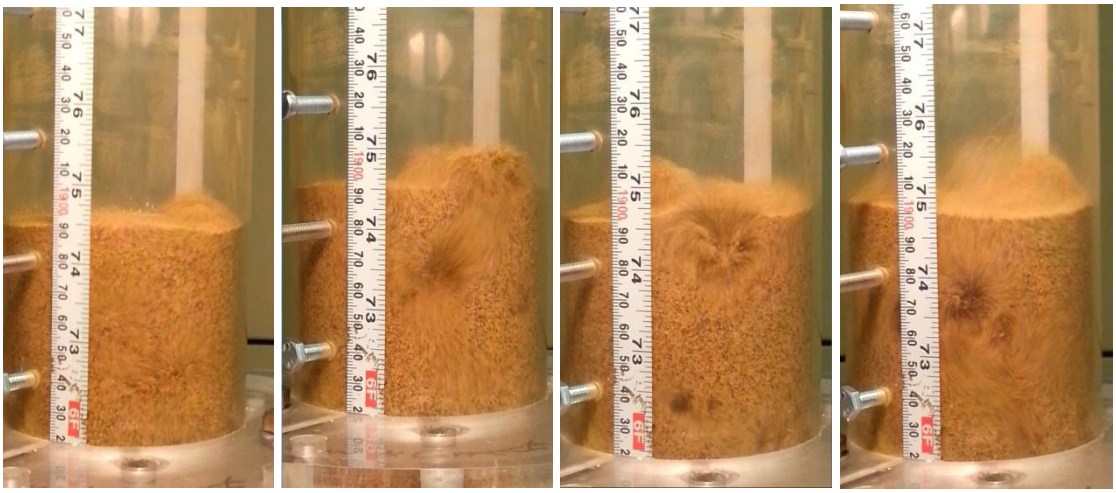

Uo= 40 l/min Uo= 50 l/min Uo= 60 l/min Uo= 70 l/min

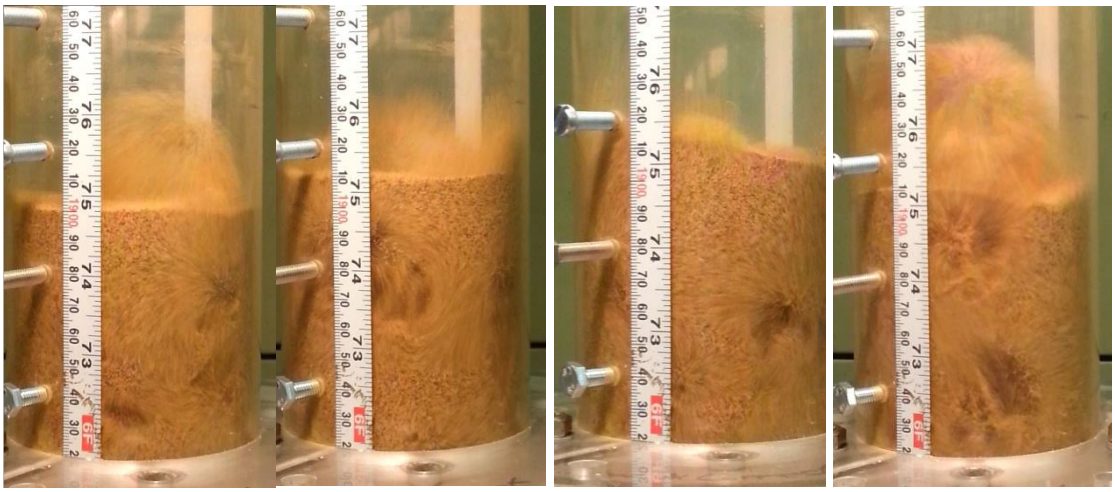

Uo= 80 l/min Uo= 90 l/min Uo= 100 l/min Uo= 110 l/min

Figure 6. 2 Images of fluidisation behavior for air-sand system, (300-425)µm, for air flowrates from 0.0 to 110 l/min

6.2.2.2 Air- biomass fluidisation system

I. Sawdust pinewood biomass SPWB

The results of the experiment of fluidization for air-(300-425) µm pure sawdust pinewood biomass system for a wide range of air flowrate, from 0 l/min to 120 l/min was observed to show its fluidization behavior as a single material. observed hydrodynamic behavior are presented as images, for each air flowrate, in Figure 6.3. For each flowrate, a number of images for different sides of the bed column were taken to show the bed behavior clearly and in detail. At air flowrates from 0.0 l/min to 30 l/min, the images show that the top bed surface is not level, is irregular and rough. At these velocities there were no effects of air velocity on the bed fluidization, e.g. air bubbles, bed expansion and bed shape. From the image at 40-50 l/min velocities and from experimental observation, clear changes in bed strength and shape along the bed column were seen. Cracks, bridges (arching) and caves creation, bed expansion, air channeling along the bed which led to form holes at the top of the bed surface are the evidence of these changes. From the images of the sawdust bed at air velocities 60 to 120 l/min it can be seen as air velocity increases the number and size of the cracks, bridges, cavities and air channel diameter inside the bed were increased, causing bed expansion at some regions of the bed, bed attritions at the top surface edges in other regions. This also, creates a number of different sized holes at the top of the bed surface and projects biomass particles from the top surface above the bed as shown in Figure 6.3. These effects continuously changed the shape of the bed irregularly and randomly. These phenomena can be attributed to the structure and physical properties of this type of biomass materials especially wood and agricultural residues. The low particle density, irregular shape, high particle aspect ratio, moisture content, high cohesion, friction, inter-particle forces between biomass particles themselves and high electrostatic actions represent main characteristics of this type of material. All these characteristics contribute directly to bridging, arching, cluster formation, and particle interlocking during the fluidization process, causing material defluidisation. According to experimental observation, to prevent such bridging, clustering and channeling in biomass fluidization, a high drag force is needed to overcome these forces. Thereafter a high gas flowrate is needed. Due to high flowrate and low biomass particle density, the particles will project easily and conveyed outside the fluidized column resulting in significant mass loss. However, it can be concluded that these types of biomass material,

which hold these properties cannot obey fluidization laws, thereafter they cannot be fluidized easily as a single material.

Uo= 0.0 – 30 l/min

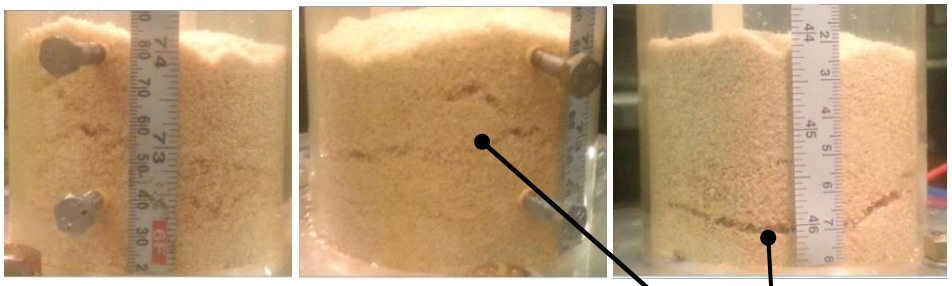

Uo= 40 - 50 l/min

Bed Arching and Bridging

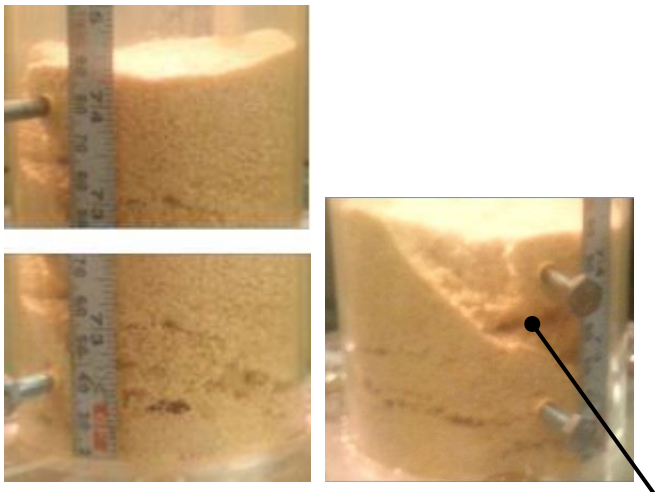

Uo= 60 l/min

Channelling and Collapse

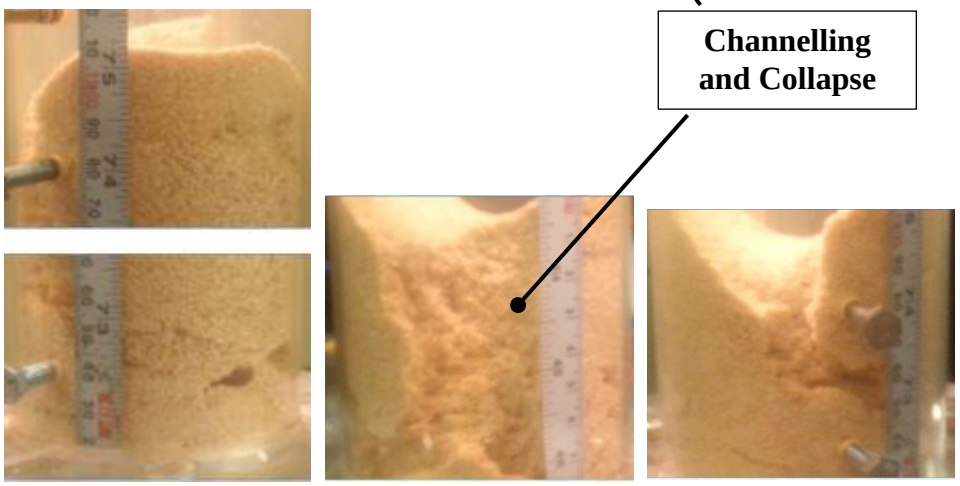

Uo= 70 l/min

Channelling and Collapse

Uo= 80 l/min

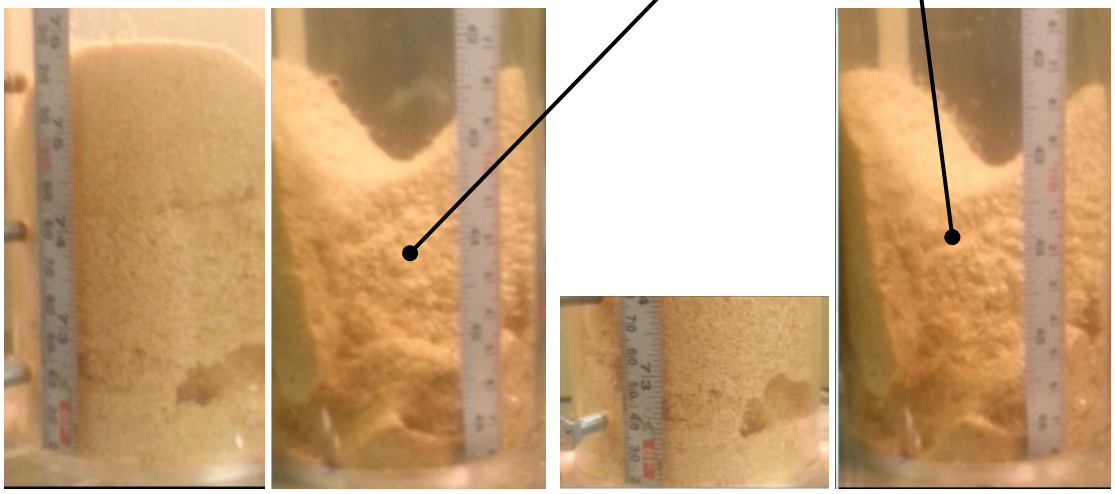

Uo= 90 l/min

Uo= 100 l/min

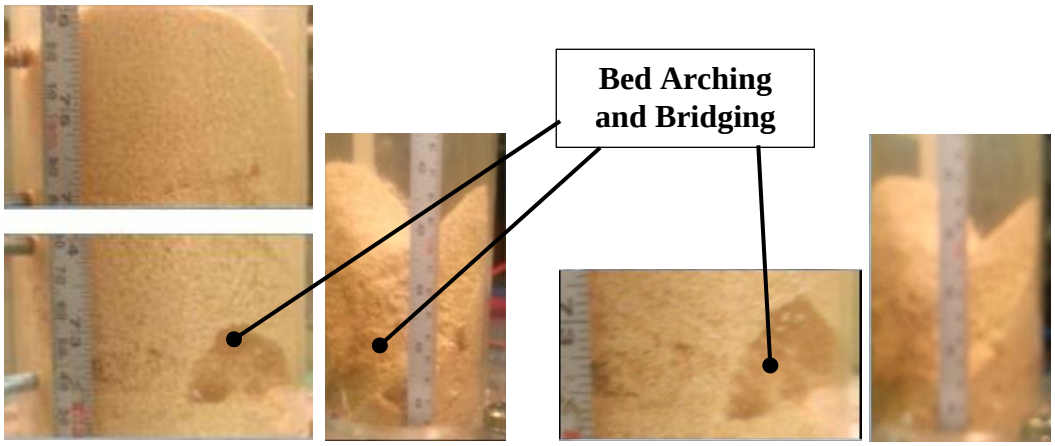

Bed Arching and Bridging

Uo= 110 l/min

Uo= 120 l/min

Uo=0.0 l/min at descending velocity, for H_{mf} measurement

Figure 6. 3 Images of fluidisation behavior for air- SPWB system for air flowrates from 0.0 to 120 l/min.

II. Iraqi date palm waste biomass, IDPWB (300-425)µm

An experiment for the fluidization of air - (300-425) µm pure Iraqi date palm biomass (IDPWB) for a wide range of air flowrates, from 0.0 l/min to 90 l/min was conducted to show its fluidization behavior as a single material. The results of the observed hydrodynamic behavior are presented as images for each air flowrate in Figure 6.4. From experimental observations and as shown in the images, it was noticed that IDPWB particles, as a single material, behave similarly to air-fluidization behavior of sawdust material for all velocities. The first appearance of air bubbles was observed between 40 l/min and 50 l/min. All un-fluidization phenomenon, which were shown in sawdust fluidization experiments, such as: particles agglomeration, bridging or arching, caves, air channels and holes, and biomass projection occurred with IDPWB as well. However, this un-fluidisation ability of this material can also be attributed to the material physical characteristics, which are similar to sawdust biomass properties. Finally, it can be concluded that this biomass material, IDPWB, with such properties cannot obey the fluidization laws thereafter they cannot be fluidized easily as a single material. Therefore, IDPWB and SPWB materials, which were used in this study, were considered as a one type of biomass material for the hydrodynamic fluidization study. The other observed results are presented and discussed in Appendix D.

Uo= 0.0 l/min

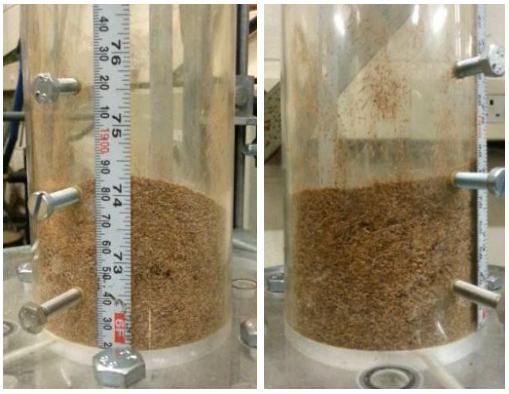

Uo= 10 l/min

Uo= 20 l/min

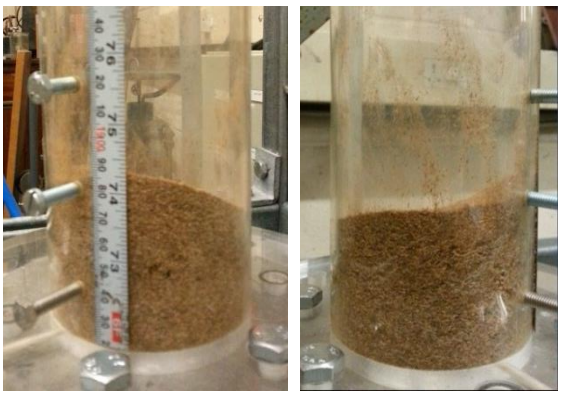

Uo= 30 l/min

Uo=40 l/min

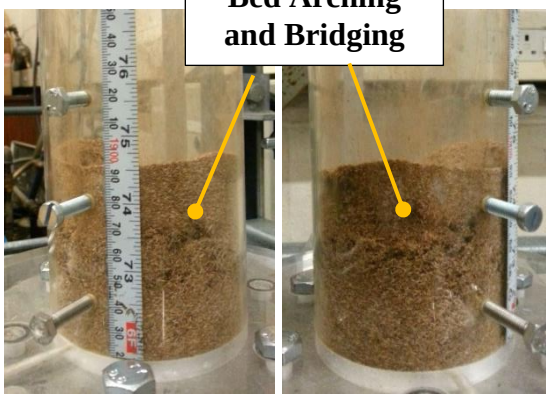

Uo=50 l/min

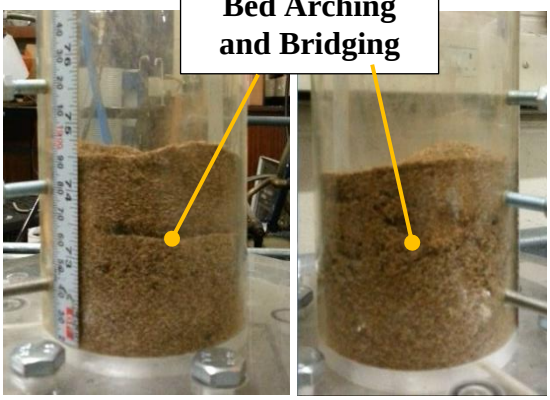

Uo= 60 l/min

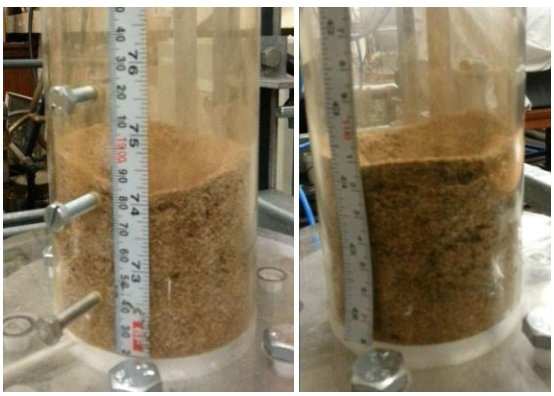

Uo=70 l/min

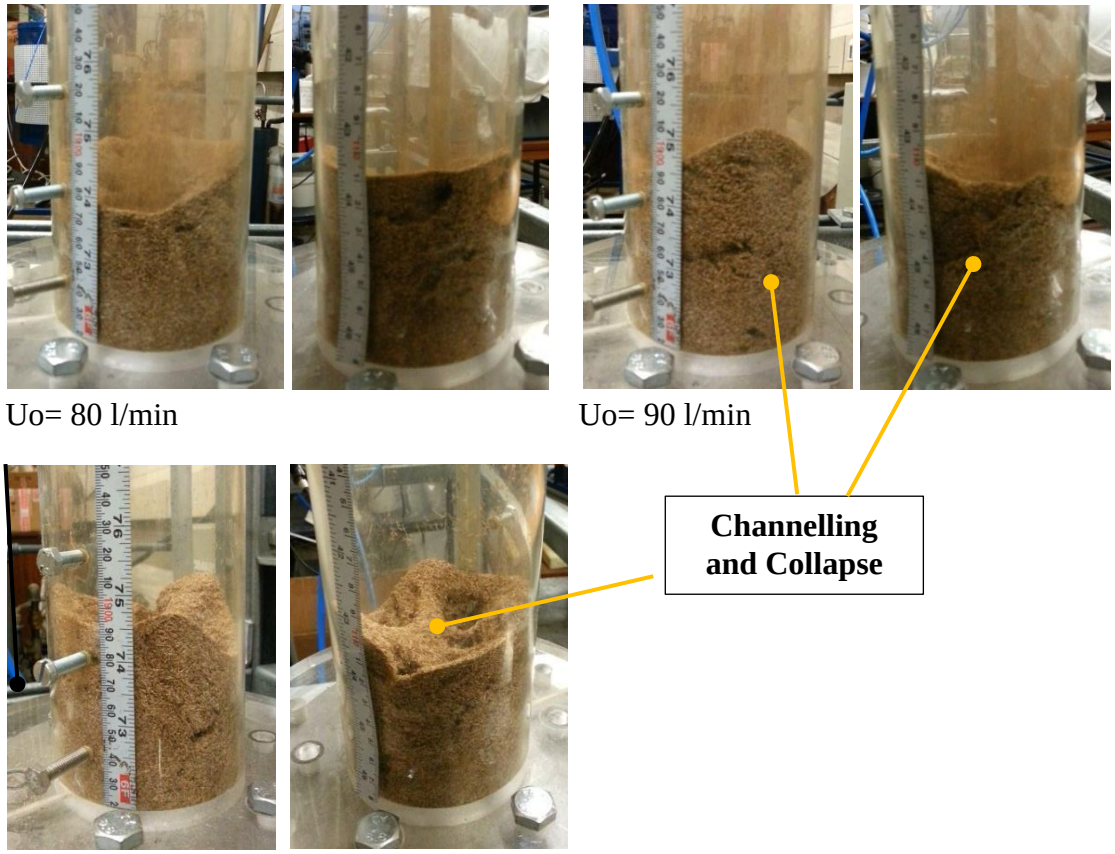

Figure 6. 4 Images of fluidisation behavior for air- IDPWB system for air flowrates from 0.0 to 90 l/min.

6.2.3 Pressure drop-air velocity for air-sand system at minimum fluidisation conditions

In order to determine the governing phenomenon, minimum fluidisation air velocity U_{mf} , for the air-sand fluidised bed system, the hydrodynamic curves were established for each range of particle size of sand material (500-600)µm, (425-500)µm and (300-425)µm for two cases, ascending (fluidising) and descending (defluidising) air velocity U_o, as shown in Figure 6.5 a, b and c, respectively. The procedure of this curve establishment has been presented in Chapter 5-section 5.4.3. For each particle size range the experiment was repeated for three static heights of bed material H_s: 8.3cm, 16.6cm and 20.75cm, which was represented in terms of internal column (pipe) diameter D, 2D and 2.5D, respectively, to show the effect of the static bed height on the bed fluidisation behaviour as displayed in Figure 6.6 a, b and c, respectively. The hydrodynamic curve represents the relationship between the pressure drop of the airflow across the fluidised bed material and the air superficial velocity flowing through a bed. This curve can be drawn for ascending (fluidisation) and descending (defluidisation) air flowrate. As

shown in the Figure 6.5, the trend of the relation is approximately similar for all cases. For a specific static bed, height at a fixed bed region and for ascending case the pressure drop is linearly proportional to airflow, where it rises considerably, until reaching a point at which the pressure drop across the bed stays evenly constant for any additional flow increase. This condition can also include forces required to overcome wall friction, bed compaction and adhesive forces between bed and distributor (Rhodes 2008)(Yang 2003)(Daizo and Levenspiel 1991). At the constant pressure drop point the forces which are exerted on the bed material are balanced and all bed particles are upheld and supported by the upwards air flow stream. The air drag force and the gravitational force on the mass of the bed represent these forces. Thereby the pressure drop is approximately equal to the weight of the bed material divided by cross sectional area of the bed W/A (Yang 2003)(Daizo and Levenspiel 1991). For a descending case (decreasing air flowrate), it can be seen that the pressure drop is constant until it reaches a fixed bed region (below fluidisation point). After that, the pressure drop decreases significantly as airflow decreases. For the same flow rate, the pressure drop for the descending case is mostly less than for the ascending case. This is due to the formation of a loose fixed bed due to the particles settling**.** A typical sketch of this curve has been shown in Figure 5.4, Chapter 5 – Section 5.4.3. For this reason the minimum fluidisation velocity is taken as the intersection of the constant pressure drop horizontal line with the straight line of fixed bed ΔP- U_o line for defluidisation case (Daizo and Levenspiel 1991). In addition, From Figures 6.5 (a) and (b) and (c) and 6.6 (a), (b) and c, it can be shown that the bed pressure drop increased with increasing static bed height H_s for three particle size ranges, respectively. This is because, that for constant diameter more drag force is required to fluidise more bed mass, (to overcome the resistance forces). The pressure drop values are around (32-33)mbar, (25-26)mbar and (12-13)mbar for the static bed height H_s 2.5D=20.75cm, 2D=16.6cm and 1D=8.3cm, respectively, for all three particle size ranges as shown in clear in Figure 6.6 as well. In addition, it can be noticed that for a specific height the pressure drop at fluidisation conditions is not affected by sand particle size.

a)

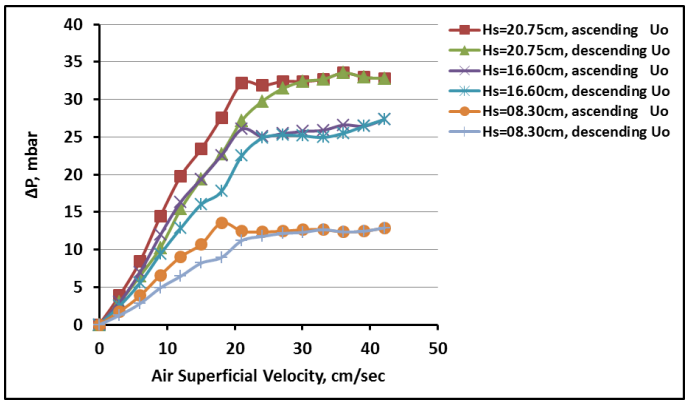

b)

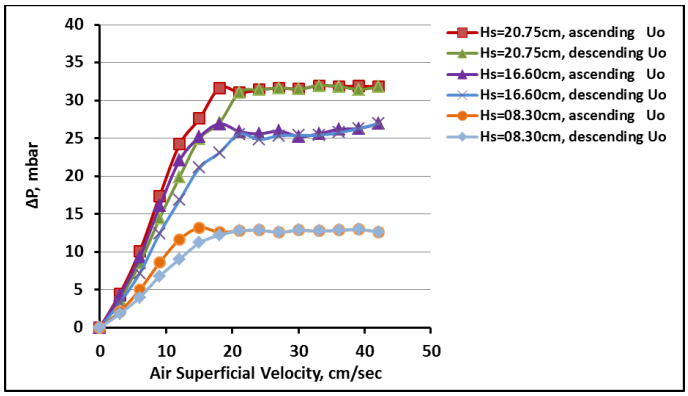

c)

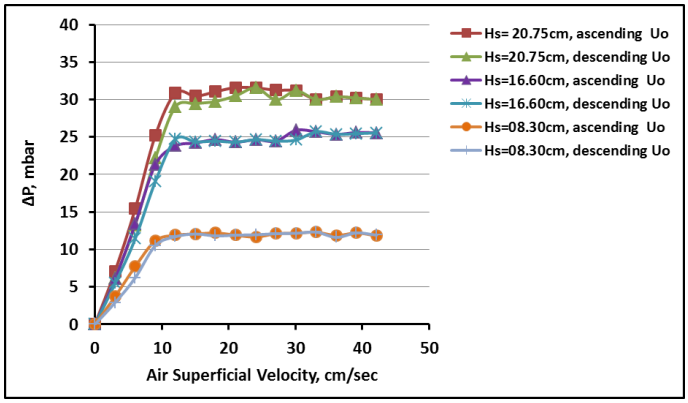

Figure 6. 5 Hydrodynamic curve for air-quartz sand system for bubbling fluidised bed: a) for 500-600µm, b) for 425-500µm, c) for 300-425µm of quartz sand

a)

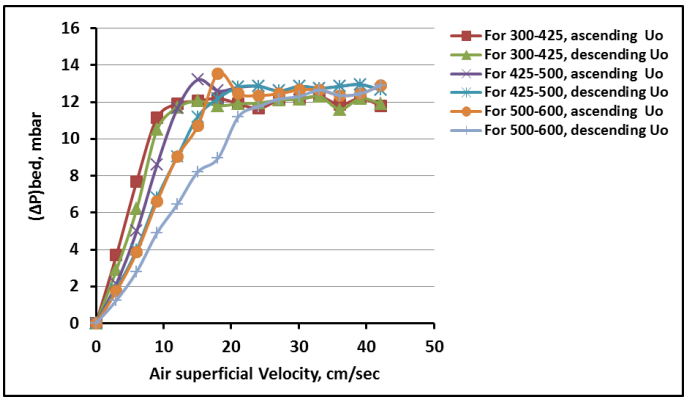

b)

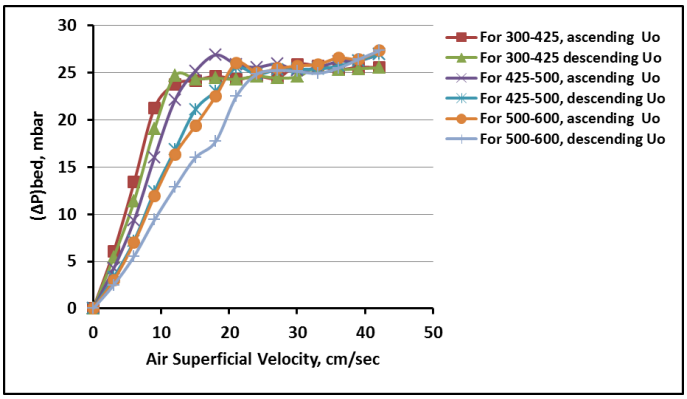

c)

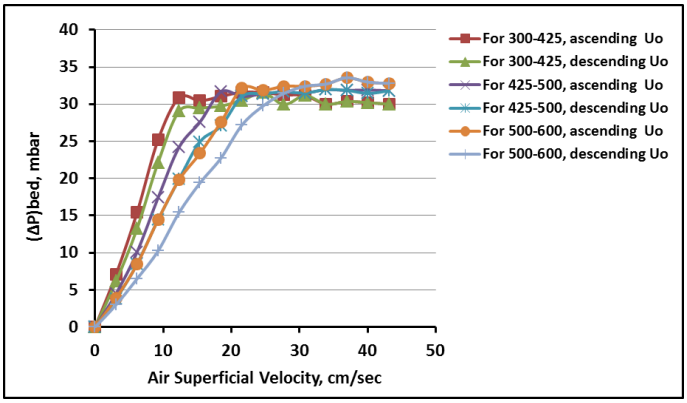

Figure 6. 6 Hydrodynamic curve for air-quartz sand system for bubbling fluidised bed: a) for H_s= 8.3cm, b) for H_s= 16.6cm, c) for H_s= 20.75cm of sand bed

As mentioned before the main purpose of the ΔP-U_o plot is to determine the governing parameter in a gas-solid fluidised bed system, the velocity of the air at minimum fluidisation conditions. Because of the difficulty of specifying and determining this parameter by experimentation, the plotting of this curve is considered a successful method for determining the minimum velocity. A common procedure for determining this velocity has been included in Chapter 5-section 5.4.2. The values of the minimum fluidisation air velocity for air-sand cold system for three particle size ranges, 300-425, 425-500 and 500-600 µm are: 10.875cm/sec, 18.665cm/sec and 23cm/sec as shown in

Figure 6.7. In this study for fluidised column inside diameter (gasifier inside diameter) ID=8.3cm, the corresponding values in (litre/min) units are 35.29, 60.56, 74.63, respectively. From Figures 6.5, 6.6 and 6.7, it can be seen that the velocity at minimum fluidisation conditions are increased gradually as the particle size of the bed material increases. This can be explained by the Eurgan equation, where the gas velocity equation at the minimum fluidisation conditions shows a proportional relationship with particle size, either for Reynold number Re < 20 or for Re >1000. However, the particle diameter has a significant effect on the minimum velocity for the former relationship comparing to the later relationship (Daizo and Levenspiel 1991)(Yang 2003). Physically, at the point of the minimum fluidisation the frictional force between particle and fluid just counterbalances the weight of particles. These forces will increase when the particle diameter increases. This means that it needs more force, and then it needs high air (gas) flowrate to overcome the particles weight to achieve the minimum fluidisation point.

On the other hand, it can be noticed that for a specific bed material particle size and for a specific column diameter this velocity is approximately constant as the height of the static bed H_s increases. This finding corroborates with the literatures (Karnik et al. 2013) (Escudero and Heindel 2011),(Gunn and Hilal 1997)(Shao et al. 2013). Also in all theoretical and empirical equations of minimum velocity in the literature review, the bed static height effects have not included. Additionally this can be attributed to frictional forces, as stated above; there is no change in these forces between the particle and the fluid, which could be a result of the bed compacting due to the static height increasing. U_{mf} is therefore constant for the selected static bed height, although the pressure drop will increase as the static bed increases because of the bed mass increasing.

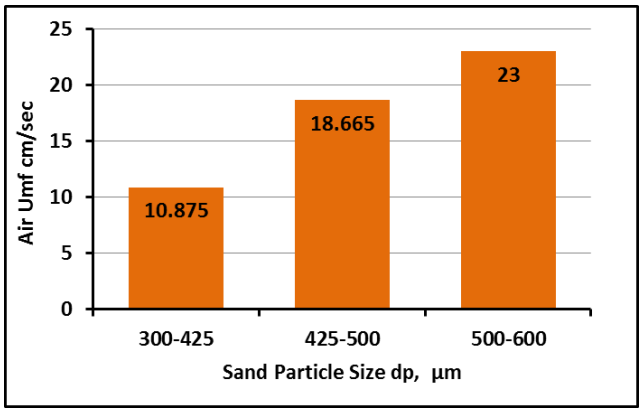

Figure 6. 7 Values of the minimum air fluidisation velocity for air-sand system for three particle size ranges of sand (300-425) µm, (425-500) µm and (500-600) µm

6.2.4 Pressure drop and air velocity for air-(biomass-sand mixture) system at minimum fluidisation conditions

6.2.4.1 For single biomass material system

For a single biomass material (in this study was SPWB) for particle size ranges (300-425) µm and (1180-1500)µm for static bed height H_s= 8.3 cm, efforts were conducted to fluidise this material as shown in Figure 6.8 (a) and (b), respectively. It can be noticed that in the fixed bed region both system behave sand material, where the bed pressure drop increases as the air superficial velocity increases until reaching the maximum point of ΔP. Normally this point gives an indication that the system will fluidise and then the pressure drop will take a constant trend. However, it can be seen that this biomass deviates from normal fluidised bed behaviour. As shown in Figure 6.8-a, the pressure drop for the ascending case after the fluidisation point fluctuates widely and the trend is downward while in Figure 6.8-b the pressure drop after a peak point takes the opposite behaviour. In addition, it was observed that for the same biomass, the hydrodynamic curve, especially after peak point, took a different trend for ascending and descending cases. This abnormal fluidisation behaviour can be attributed to the biomass material physical properties; cohesion and mechanical forces between their particles (Miccio et al. 2013) and (Miccio et al. 2011). In addition, low particle density which cannot be classified as Geldart B material, it's irregular particle shape with high aspect ratio (length/width) and high electrostatic charges between particles and the plastic wall. Therefore, from these results it can be inferred that a single biomass material cannot be easily fluidised. This infer is supported by (Rao and Bheemarasetti 2001), (Qiaoqun et al. 2005), (Zhong et al., 2008), (Karmakar, et al., 2013) and (Kumoro

et al., 2014). This finding is in good agreement with previous works (Zhang et al., 2011).

a)

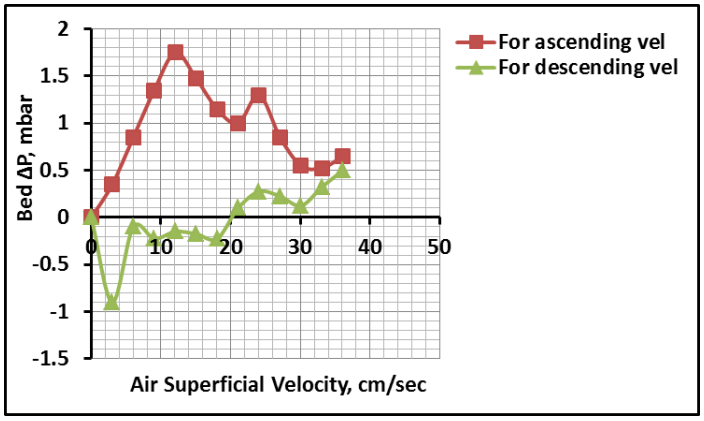

b)

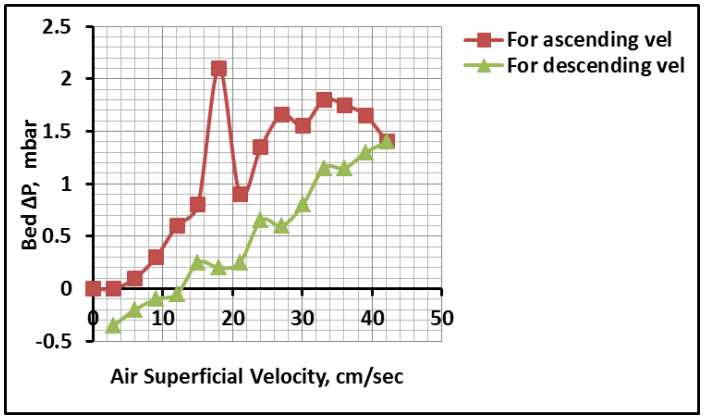

Figure 6. 8 Hydrodynamic curve for air - sawdust pinewood biomass SPWB system for bubbling fluidised bed: a) for H_s= 8.3cm and d_p between 300 and 425µm and b) for H_s= 8.3cm and d_p between 1180µm and 1500µm

6.2.4.2 For sand-biomass mixture materials system

According to the results in the previous section and as stated in the literature review (Chapter 2), the fluidisation characteristics of the agricultural and forest residues of the biomass solid fuels can be improved. In this study, the fuel biomass materials are SPWB and IDPWB. This improvement can be achieved by mixing with an inert fluidised material, Geldert B group, such as sand to obtain the required fluidisation hydrodynamic characteristics of the bed. For biomass (SPWB)-sand fluidisation experiments, their condition data and results are presented as groups as shown in Table 6.1: group I, group II, group III and group IV. In addition, their hydrodynamic curves, for each group, are presented in Figure 6.9.

Table 6. 1 Cold fluidisation experiments for group of pinewood sawdust biomass-sand mixture: information and results.

Experiments, Group I (continue Table 6.1)

Distributor Plate Type	**No of holes**	**Open Area cm^2**	**Biomass P.S. (µm)**	**Sand P.S.[mean] (µm)**	**Height Ratio Bio, cm/ Sand, cm**	**Biomass wt %**	**H_s as observed in column, cm**	**U_{mf} cm/sec**	**H_{mf} cm**	**ΔP- U_o Curve In Figure**
dor-1.5mm-N85-P9	85	1.501	1180-1500	500-600 [545.92]	2.07/8.3	2.68		28	9.5	Fig 6.9, G I-a
dor-1.5mm-N55-P10.5	55	0.971	1180-1500	500-600 [545.92]	2.07/8.3	2.68	8.95	27.5	9.5	Fig 6.9, G I-b
dor-1.5mm-N19-P19.19	19	0.336	1180-1500	500-600 [545.92]	2.07/8.3	2.68	-	-	-	Fig 6.9, G I-c

Experiments, Group II (continue Table 6.1)

Distributor Plate Type	**No of holes**	**Open Area cm^2**	**Biomass P.S. (µm)**	**Sand P.S.[mean] (µm)**	**Height Ratio Bio, cm/ Sand, cm**	**Biomass wt %**	**H_s as observed in column, cm**	**U_{mf} cm/sec**	**H_{mf} cm**	**Δ P- U_o curve In Figure**
dor-1.5mm-N85-P9	85	1.501	1180-1500	500-600 [545.92]	4.15/8.3	5.22	10.25	32	9.5	Fig 6.9, G II-a
dor-1.5mm-N55-P10.5	55	0.971	1180-1500	500-600 [545.92]	4.15/8.3	5.22	11.65	31.5	9.5	Fig 6.9, G II-b
dor-1.5mm-N19-P19.19	19	0.336	1180-1500	500-600 [545.92]	4.15/8.3	5.22	10.3	-	-	Fig 6.9, G II-c

Experiments, Group III (continue Table 6.1)

Distributor **Plate Type**	**No of** **holes**	**Open Area** **cm^2**	**Biomass** **P.S. (µm)**	**Sand P.S.[mean] (µm)**	**Height Ratio Bio, cm/ Sand, cm**	**Biomass** **wt %**	**H_s as observed in column, cm**	**U_{mf}** **cm/sec**	**H_{mf}** **cm**	**∆ P- U_o curve** **In Figure**
dor-1.5mm-N85-P9	85	1.501	1180-1500	500-600 [545.92]	8.3/8.3	9.93	12.9	43	15.5	Fig 6.9, G III-a
dor-1.5mm-N55-P10.5	55	0.971	1180-1500	500-600 [545.92]	8.3/8.3	9.93	13.4	43.5	16	Fig 6.9, G III-b
dor-1.5mm-N19-P19.19	19	0.336	1180-1500	500-600 [545.92]	8.3/8.3	9.93	13.3	-	16.1	Fig 6.9, G III-c

Experiments, Group IV (continue Table 6.1)

Distributor **Plate Type**	**No of** **holes**	**Open Area** **cm^2**	**Biomass** **P.S.(µm)**	**Sand P.S.[mean] (µm)**	**Height Ratio Bio, cm/ Sand, cm**	**Biomass** **wt %**	**H_s as observed in column cm**	**U_{mf}** **cm/sec**	**H_{mf}** **cm**	**∆ P- U_o curve** **In Figure**
dor-1.5mm-N85-P9	85	1.501	500-600	500-600 [545.92]	10/12.45	8.85	18.4	37	22	Fig 6.9, G IV-a
dor-1.5mm-N55-P10.5	55	0.971	500-600	500-600 [545.92]	10/12.45	8.85	18.4	36	17.5	Fig 6.9, G IV-b
dor-1.5mm-N19-P19.19	19	0.336	500-600	500-600 [545.92]	10/12.45	8.85	19	-	17.7	Fig 6.9, G IV-c

Group I

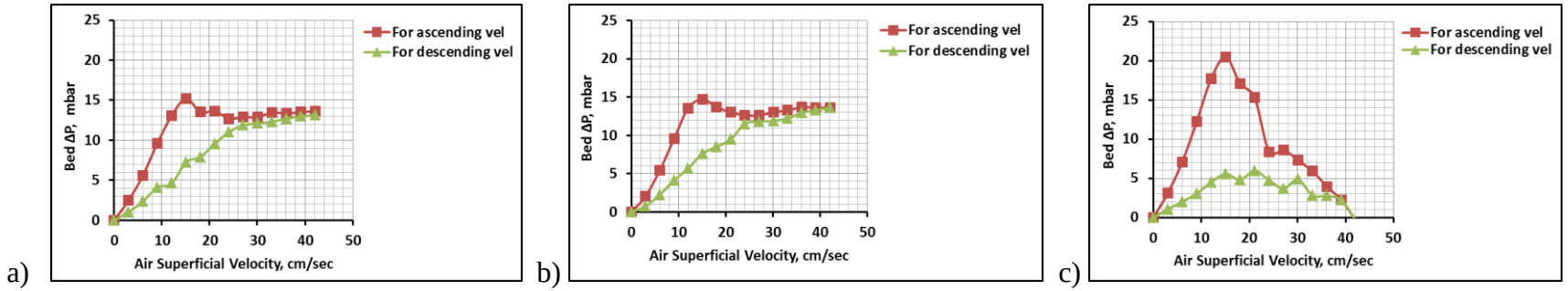

Group II

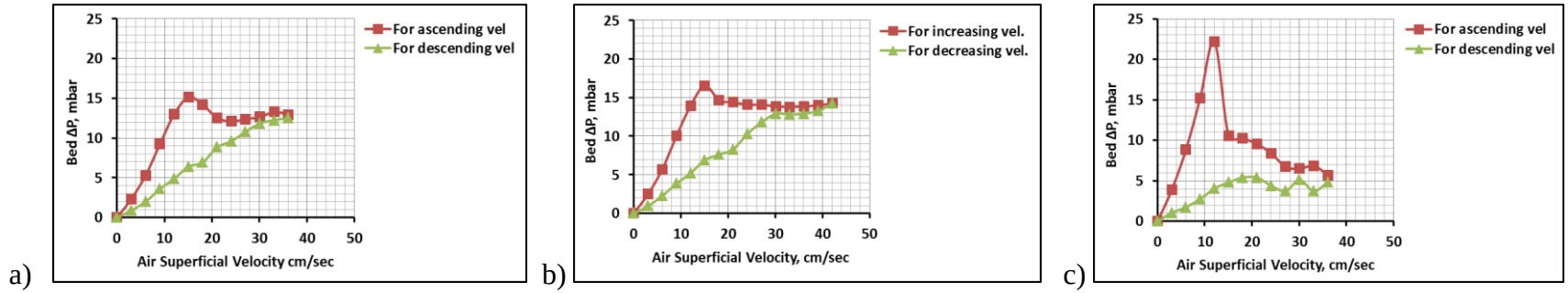

Figure 6. 9 Hydrodynamic curve for sawdust pinewood biomass SPWB - sand mixture fluidisation system for experiments Group I, Group II, Group III, Group IV

Group III

a) 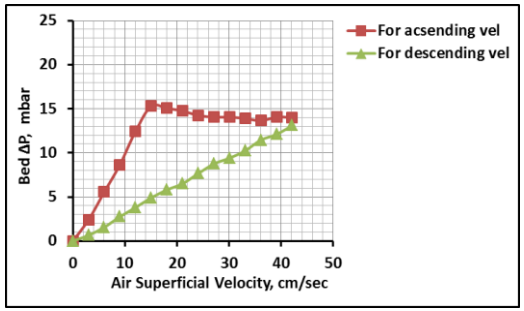

b) 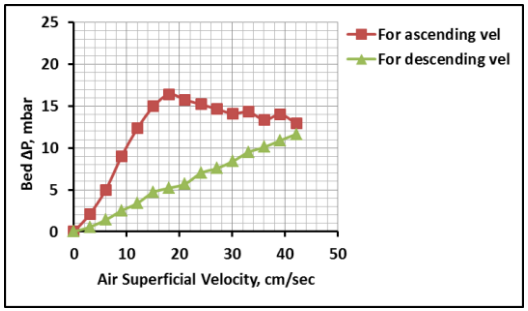

c) 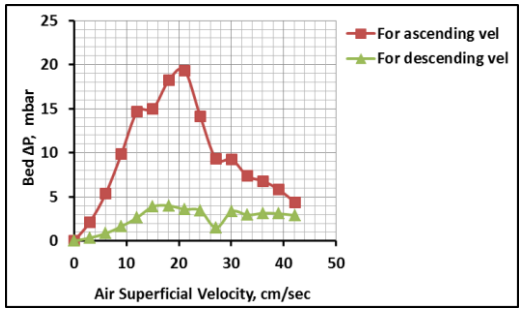

Group IV

a) 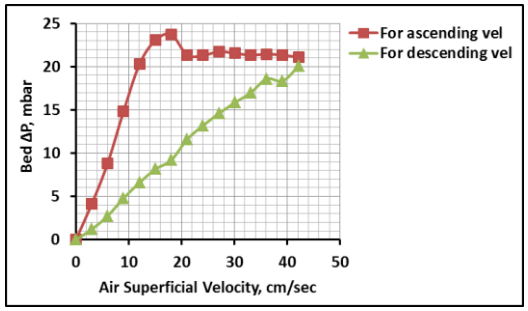

b) 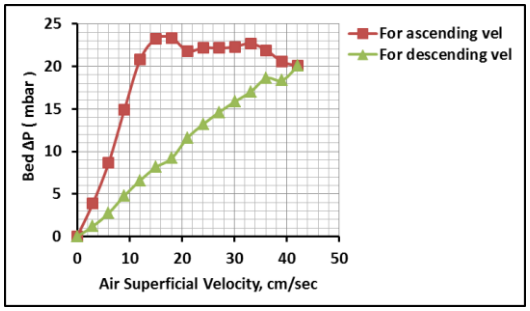

c) 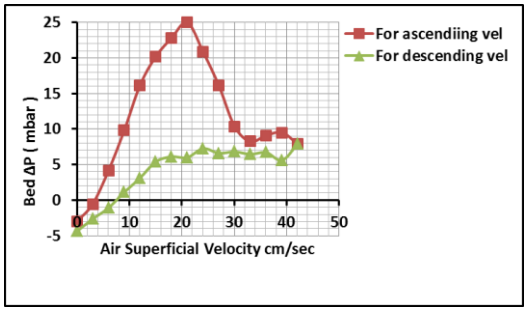

Figure 6.9 (continue)

Table 6.1 shows the selected experiments, which were conducted with specific conditions to test the fluidisation behaviour of the biomass-sand mixture. Parameters that may affect this behaviour were taken into consideration. These parameters are: number of holes of a distributor plate (distributor plate open area), biomass-sand mixtures represented by a ratio of biomass height to sand height and biomass weight %. All these parameters and their values are represented in the columns in Table 6.1. In addition, the other columns are the static height of the bed H_s, minimum fluidisation velocity, bed height at minimum fluidisation H_{mf} and the last column gives the figure number for ΔP- U_o, hydrodynamic curve, for each experiment.

From the values above the value of the minimum fluidisation velocity for each weight percent of the biomass in the mixture for each group, as shown in-group tables in Table 6.1, was obtained. The same procedure steps for obtaining the minimum velocity from hydrodynamic curve for a single material, which presented in Chapter 5, Section 5.4.2 were followed. The values of the static and minimum fluidisation heights for each experiment were obtained from the transparent column by direct observation. From Figure 6.9 the hydrodynamic curve for air velocity of ascending and descending cases for all groups are shown. These figures can be discussed throughout the following points:

- ΔP-U_o curves for ascending air velocity

  In general, for all experiment conditions, which are shown in Table 6.1, the trend of the curve for ascending case at fixed bed region is similar. ΔP across the bed column is increased linearly as air velocity increases, until reaching a point at which the bed pressure drop becomes constant as the velocity increases. At this point, the bed introduces its fluidisation region. For most experiments it can be seen that a peak point of pressure drop appears and after that the bed pressure drop fall linearly and then level off reaching the balance of the forces exerted on the bed, at which the bed pressure drop start to be constant as velocity increases (refer to the discussion presented in section 6.2.4). Except for experiments which used a distributor plate of N=19, there was not a clear constant pressure drop line. This means that it is difficult to reach the forces balance point for all increases in velocity as shown in Figure 6.9 in Group I-c, Group II-c, Group III-c and Group IV-c. These phenomena can be attributed to two reasons. The first is due to the existence of some cohesion and

friction forces between bed particles, mainly in bed mixture of significantly different particle densities. The second reason is due to the distributor plate hole number. It can be seen that the bed, which used a low open area plate type, low number of hole, follows this behaviour clearly. However, these plates have also a high-pressure drop, as shown in section 6.2.1, so it need a high-pressure drop to overcome this resistance compared to the high open area plates. The figures of the experiments of the distributor plate type dor-1.5mm-N19-P19.9 show these effects compare to the other plate types dor-1.5mm-N55-P11.75 and dor-1.5mm-N85-P9. In addition, from the figures of this plate, it can be seen that the pressure drop after the peak point drops sharply and fluctuate at high velocities. Therefore, these plate types could not give accepted bed fluidisation behaviour and it was difficult to estimate the minimum fluidisation velocity from their hydrodynamic curves. In contrast, the figures for all experiments, which used distributor plate type dor-1.5mm-N55-P11.75 and dor-1.5mm-N85-P9 show a normal behaviour.

- ΔP-U_o curves for descending air velocity

  For descending airflow cases, generally when air velocity decreased the bed pressure drop stayed constant until it reached the fixed bed region and then decreased linearly until zero velocity. From Figure 6.9, for all Groups, it can be seen that the separation distance between the ascending curve and descending curve increases as the biomass weight percent in the bed mixture increased and the curves tend to a single linear trend, at high biomass concentrations, 9.93%. This can be attributed to the inter-particle forces between bed particles. These forces increase as the biomass weight percent is increased (Karmakar et al. 2013). During fluidisation and because of its low density compared to sand material, most of the biomass segregated from the sand and escaped to the top bed surface. At this point, the bed behaved as if it was sand only, then the bed will lose most of the inter-particle forces caused by biomass particles and behave as a different cycle. Consequently, according to the estimation procedure of the minimum fluidisation velocity, U_{mf} will be high for this high biomass weight percent. Tables 6.1 and Figure 6.10 show U_{mf} increases as biomass weight percent is increased. The U_{mf} values for 0 %, 2.68 %, 5.22 % and 9.93 % biomass –sand mixture are 23, 28, 32 and 43cm/sec, respectively.

The values of the minimum fluidisation velocity, which were obtained for the experiments that used a distributor plate type dor-1.5mm-N85-P9 were adopted. This is

due to their smoothing hydrodynamic curves compared to the other plate types. Their experimental values are summarised and presented in Figure 6.10.

The Figure shows that the design parameter, minimum fluidisation velocity increased gradually as biomass weight percent increase. For sawdust biomass weight percent from 0% to 10%, this trend agrees with that obtained by (Rao and Bheemarasetti 2001) and (Karmakar et al. 2013).

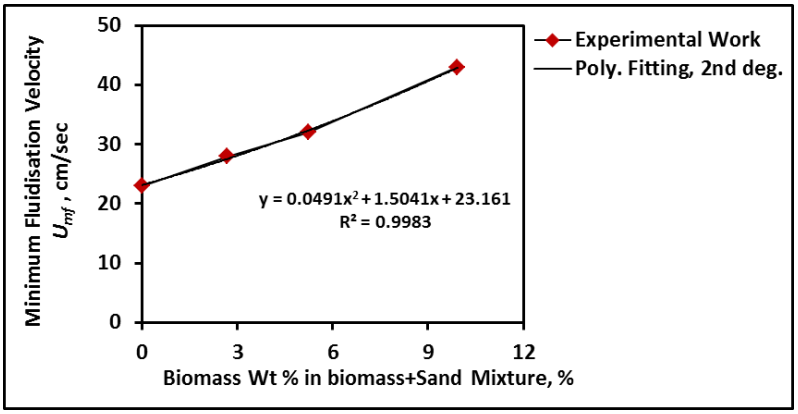

Figure 6. 10 Pinewood sawdust biomass wt % -air minimum fluidisation velocity relationship

Theoretically, for the same conditions, which have been used in biomass-(500-600) µm sand mixtures, it was assumed that the other ranges of sand particle size (425-500 and (300-425µm) behave the same behaviour and take the same trend line. Figure (6.11) shows their trend lines.

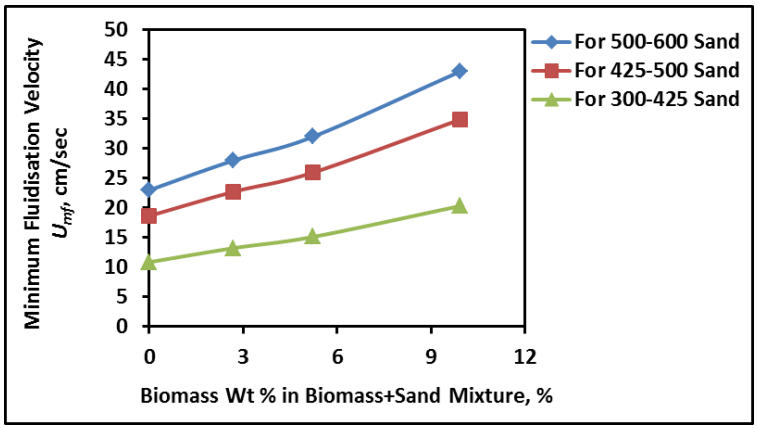

Figure 6. 11 Pinewood sawdust biomass wt % -air minimum fluidisation velocity relationship for three ranges of sand particle size

6.3 Summary

This chapter has shown the results of the hydrodynamic fluidisation experiments for cold rig. The image results of the fluidisation behaviour for three materials, sand, SPWB, IDPWB and sand has discussed. These results has explained that the sand has a good fluidisation behaviour whereas the two biomass have shown a weakened behaviour. The results have shown that the fluidisation of the biomass can improved by mixing it with the inert material sand with a small mass percent. Furthermore, for sand material the hydrodynamic curve has established, while for biomass has not achieved.

For pure sand material and for sand-biomass mixtures, the measurement of the minimum fluidisation velocity has observed and estimated from the hydrodynamic curve. The results have shown that minimum velocity affected by the sand particle size. It has increased as particle size increased, but it has not affected by the static bed height. In addition, the minimum fluidisation velocity has affected considerably by biomass mass percent. It increased as the mass percent increased.

The obtained results of the values of this design parameter will use as a preliminary design data for biomass gasification experiments.

Chapter 7

Results and Discussion of Biomass Gasification

7.1 Introduction

In this chapter the results of the experimental study of the two biomass, SPWB and IDPWB, under air gasification in the bubbling fluidised bed reactor are presented and discussed. The results of the setting and bed temperature relationship and the temperature distribution for the experiment conditions along the empty gasifier are also presented and discussed. The gas analysis results of the two biomasses feedstocks are provided to evaluate the performance of the bubbling fluidised bed gasifier. Seven operating and design parameters that affect the gasifier performance are researched and discussed. These seven parameters are: air flowrate, particle size of the sand bed material, particle size of the biomass fuel feedstock material, static bed height, air Equivalence Ratio, bed temperature and number of holes (orifice) in the distributor plate. The effects of these parameters are discussed through the performance parameters: producer gas composition (PGC), carbon conversion efficiency (CCE), cold gas efficiency (CGE), lower heating value (LHV) of the producer gas, producer gas yield (GY) and producer gases ratios.

7.2 Hot rig experiments -biomass air gasification results

7.2.1 Gasifier temperature distribution for gasifier preparation

As shown in Chapter 5- Section 5.7.1 (commissioning and preparation procedures) for temperature distribution along the gasifier, especially for bed temperature T2, Figure 7.1 shows the results of temperature T2 based on each set point temperature Tset=T1. The operating conditions were for 8.3 cm static bed height and 300-425µm particle size of sand bed material. There was no air flowing through the bed and no preheating. It can be seen that for a specific set point temperature Tset=T1, T2 increased with time. At the first, T2 increases dramatically, then after 300min the trend will approximately be levelled off which considered a thermal equilibrium state for a specific set point temperature.

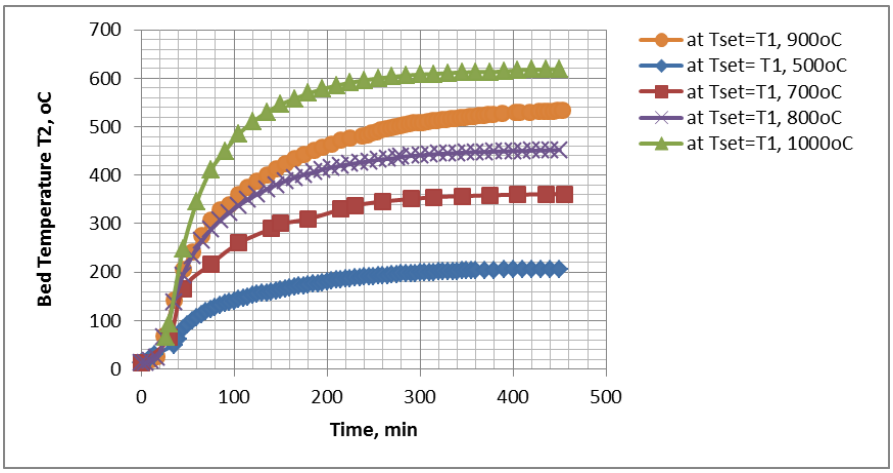

Figure 7. 1 Experimental results of a gasifier temperature at bed section at T=T2, 4.15cm above the distributor plate, for different setting temperature Tset=T1 of the electric heater using 8.3cm static bed height of 300-425 µm of sand bed material and no air flow (no preheated air)

Also, a group of experiments for various setting temperature were conducted. The corresponding T2 was taken directly at steady state (thermal equilibrium) conditions. All set point temperature Tset=T1 and their corresponding T2 are listed in Table 7.1.

Table 7. 1 Experimental values of bed temperature, T2 for each set point temperature, Tset=T1 for present fluidised bed gasifier study at specific conditions

T_{sett}=T1 ºC	T_{bed}= T2 ºC	Comments
400	151	*
500	215	**
600	293	*
700	361	**
750	410	*
800	452	**
825	485	*
900	551	**
1000	640	**

* T2 was directly recorded from experiment test at steady state (thermal equilibrium) conditions
** T2 was extracted from Figure 7.1 at steady state (thermal equilibrium) conditions

As shown in Chapter 5- Section 5.7.1 the data in Table 7.1 were plotted and fitted as shown in Figure 7.2. A power fitting empirical equation was obtained with R^2 =0.9994.

$$T2 = 0.0114 * (T_{set})^{1.5845} \quad (7.1)$$

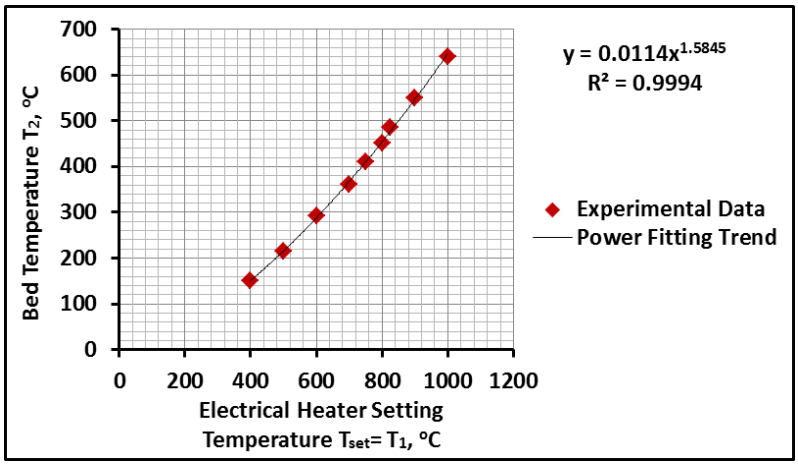

Figure 7. 2 Empirical correlation for bed temperature, T_{bed}=T2 and setting temperature, Tset =T1 for fluidised bed gasifier (for gasifier of this study) for zero air flowrate

Equation 7.1 can be used to predict the temperature at the bed zone T2 in gasifier for any specific setting temperature Tset. From the Figure, it can be inferred that the highest bed temperatures T2, which can be obtained for a maximum allowable stetting temperature 1000^{o}C and 900^{o}C, are approximately 640^{o}C and 551^{o}C, respectively for zero air flowrate. For safety purposes and to avoid the electrical heater damage, it was recommended to operate at 900-950^{o}C as a maximum setting temperature for the gasifier electrical heater.

7.2.2 Vertical temperature distribution along the fluidised bed gasifier

The details of the temperature distribution along the fluidised bed gasifier during fluidisation process of (300-425) µm, H_s=8.3cm of sand bed material for several air flowrates and their results have been presented in Chapter 5-Section 5.7.2. This section highlights the optimum conditions of the gasifier setting temperature that should be followed for subsequent biomass gasification experiments. The Figures below 7.3, 7.4 and 7.5 consist of three sets of Figures. Each set displays two Figures, the (left hand side), shows the measured temperature variation, at each position along gasifier T4, T2, T1, T3 and T7 with air flowrates, while (right hand side) shows the temperature distribution along specific gasifire positions, -10cm, 4cm, 44cm, 84cm and 124cm, respectively for each air flow rate. For the left hand side figure of each set conditions a, b and c as shown in Figures 7.3, 7.4 and 7.5, it can be observed that the temperature T1=Tset stayed constant as air flowrate increased. This because it was a temperature controlling at 600^{o}C, 750^{o}C and 900^{o}C, respectively and all temperatures below it (T4 and T2) and above it (T3 and T7) are less than T1. T3 and T7 increase dramatically with air flowrate increase initially time then temperatures gradually decrease especially

at high velocities. On the contrary T4 and T2 decrease at initially and then levelled off at approximately 40 l/min. For T2, its trend draws attention where it reaches to a minimum temperature at 30 l/min for T1= 600^{o}C and 750^{o}C and at 10 l/min for T1=900^{o}C and then it increases steadily and then levelled off at 40 l/min. This phenomenon can be attributed to the fluidisation of bed material, which led to increase the bed void and consequently cause a reduction in temperature for a short time. This phenomenon was also repeated for all setting conditions as shown in Figures 7.3, 7.4 and 7.5. Figures 7.3, 7.4 and 7.5 show the temperature distribution along a specific gasifier position for each air flowrate for each setting conditions. It can be seen that the maximum temperature inside the gasifier represents a set point temperature T1=Tset at position= 44cm, from distributor plate level, for any value of air flowrate. The heat transfers from the point T1 to the top and bottom gasifier regions because of temperature gradient. By comparing the three Figures 7.3, 7.4 and 7.5, it can be noticed, in general, that conditions with the air preheater give a best temperature distribution results, especially for T2, a temperature at bed region at biomass fuel feeding point. Unfortunately, the set point temperature conditions with air preheater were excluded because of the repetition damages of the air preheater. For the temperature setting conditions without air preheater, as shown in Figure 7.3 and summary Figure 7.6, it can be seen that the highest temperature at T2 point =340-350^{o}C can be gained at Tset=T1= 900^{o}C compared to T2 temperature =100-120^{o}C and 180-200^{o}C at Tset=T1 600^{o}C and 750^{o}C, respectively. For these reasons Tset=T1=900^{o}C was adopted for all biomass gasification experiments. The temperature values T2, which can be obtained by any set point temperature of the gasifier heater, were directly affected according to selected parameters: air flowrates, gasification equivalence ratio, particle size and static height of bed material.

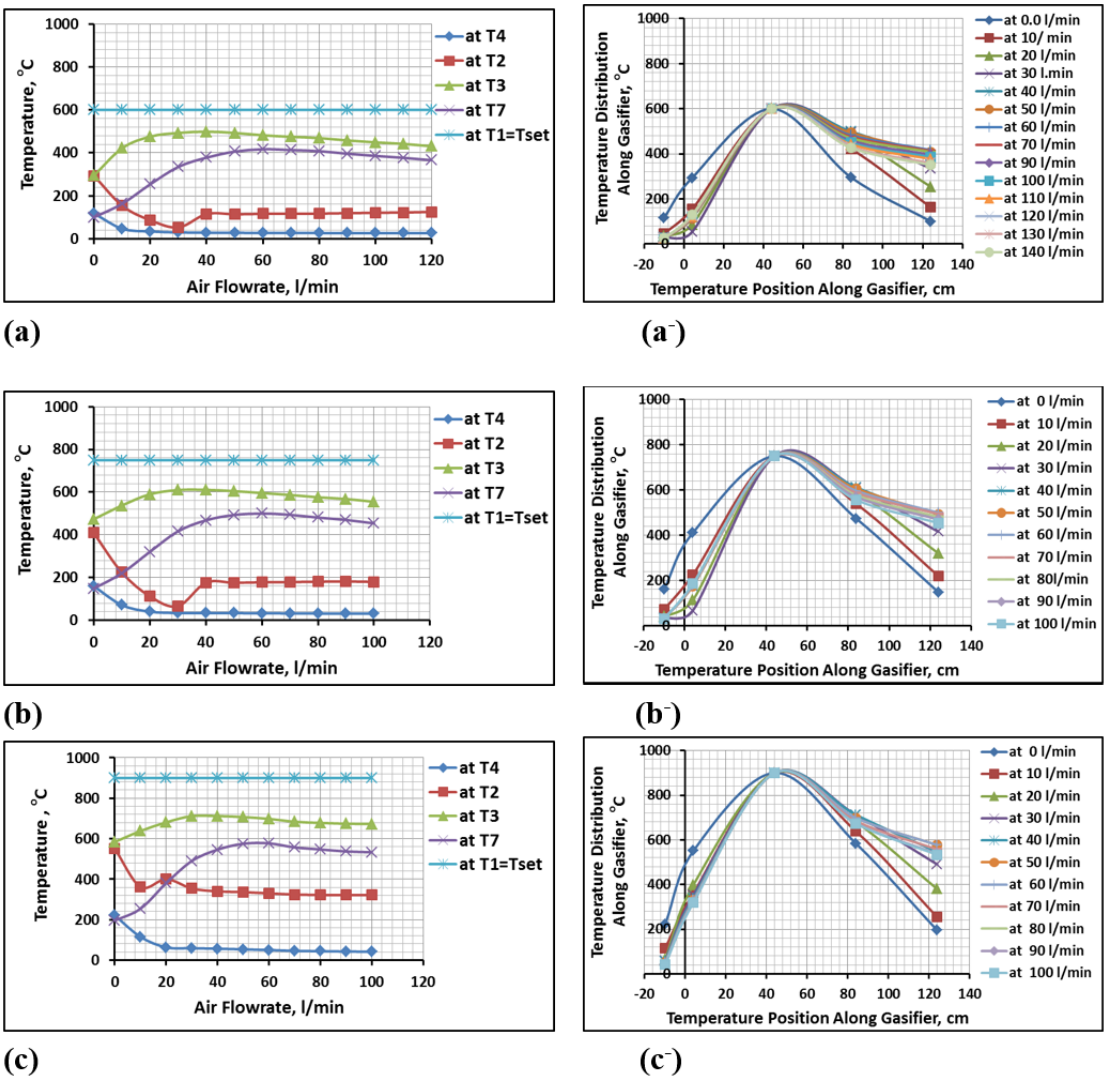

Figure 7. 3 Temperature distribution along gasifier, T4, T2, T1=Tset, T3, T7, without preheater: (a) and (a^-) at Tset=T1=600ºC, (b) and (b^-) at Tset=T1=750ºC, (c) and (c^-) at Tset=T1=900ºC

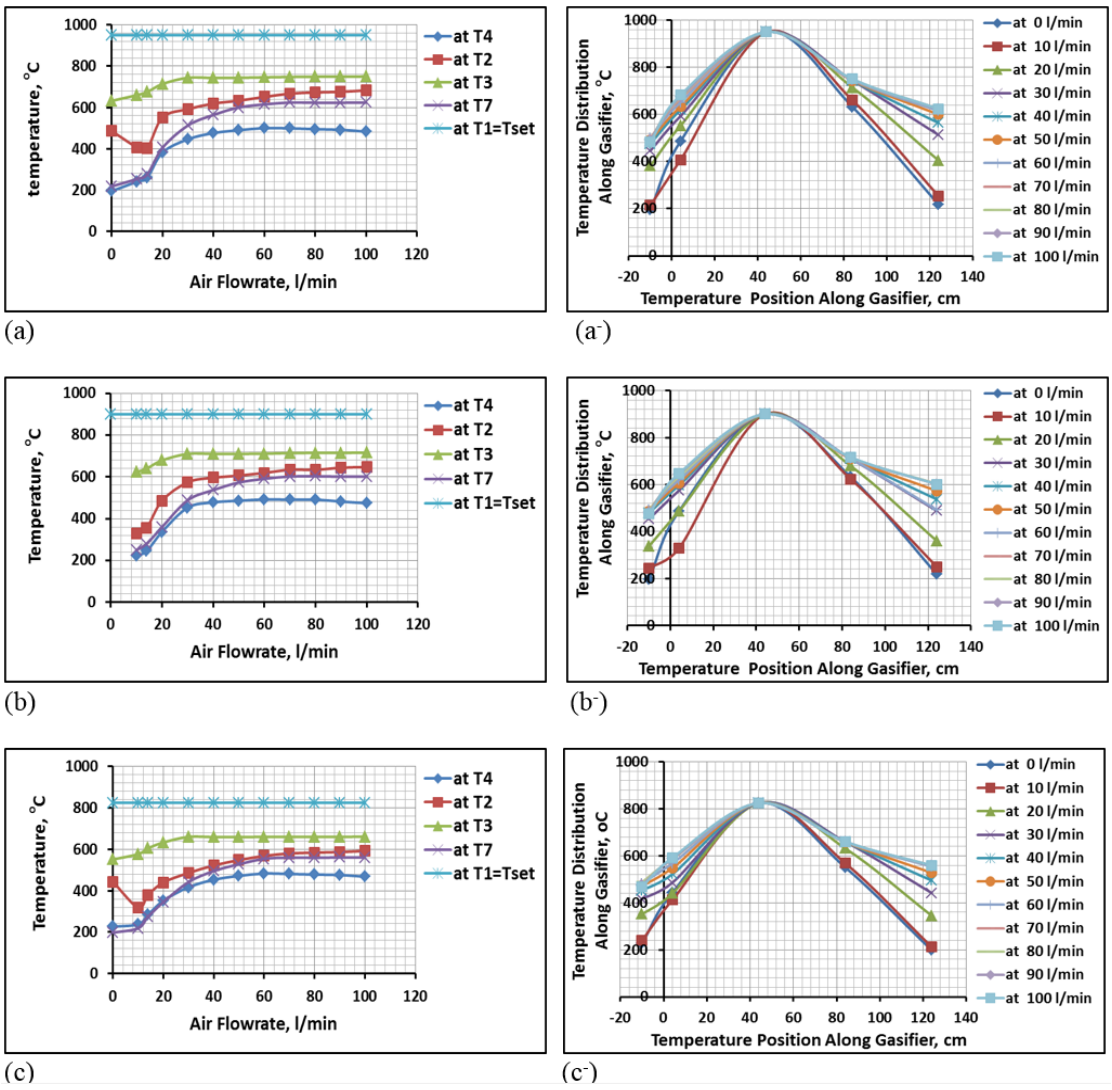

Figure 7. 4 Temperatures distribution along gasifier, T4, T2, T1=Tset, T3, T7, with air preheater: (a) and (a-) at Tset=T1=950ºC, Tpreset=750ºC, (b) and (b-) at Tset=T1=900ºC, Tpreset=750ºC, (c) and (c-) at Tset=T1=825ºC and Tpreset=750ºC

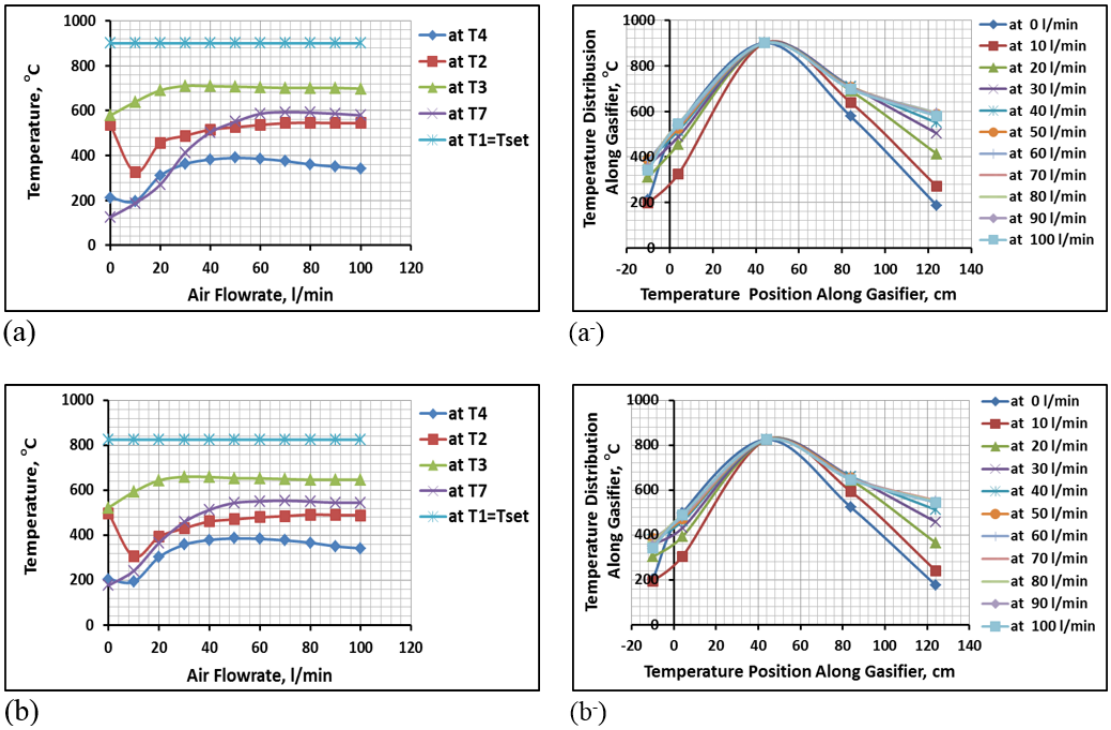

Figure 7. 5 Temperatures distribution along gasifier T4, T2, T1=Tset, T3, T7, with air preheater: (a) and (a-) at Tset=T1=900ºC, Tpreset=900ºC, (b) and (b-) at Tset =T1=825ºC and Tpreset=900ºC

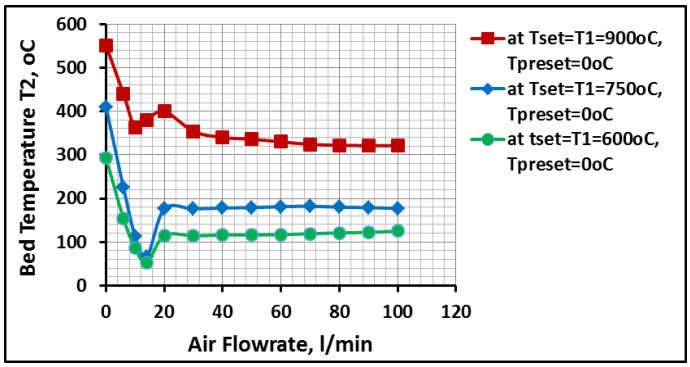

Figure 7. 6 Temperature trends for T2 for Tset=T1=900ºC, 750ºC and 600ºC without preheater

7.2.3 Results of minimum fluidisation conditions at high temperature

In Chapter 5-Section 5.8.2, an experimental procedure of the determination of the minimum fluidisation velocity for sand-air system at elevated temperature has been presented. The results obtained from the experiments, for air-sand system, sand particle size (300-425) µm, Hs=8.3cm and gasifier diameter ID=8.3cm, are presented in Table 7.2 and Figure 7.7. The results show that air flowrate at minimum fluidisation conditions decreased significantly as temperature increase. This decrease is less significant at (20-100)^{o}C, whereas at 400^{o}C the decrease is more significant. This phenomena could be attributed to the fact that as temperature increases the fixed bed

voidage increases due to increase of the bed inter-particle forces (Van der Waals forces) with temperature (Formisani et al. 1998). These results broadly agree with the findings of other studies with a slight difference in trend at the low temperatures (20-100)ºC (Formisani et al. 1998), (Subramani et al. 2007) and (Jiliang et al. 2013).

Table 7. 2 Experimental data of minimum fluidisation air flow at elevated temperature for air-sand system, sand particle size (300-425) µm, Hs=8.3cm and gasifier diameter ID=8.3cm

Temperature Conditions	T_{bed}=T2, ºC	$(Air\ Flow)_{mf}$, l/min	$(Air\ Velocity)_{mf}$, cm/sec
at cold conditions	20	35.286	10.875
at Tset= T1= 600ºC	70	34.5	10.633
at Tset= T1= 750ºC	95	33.5	10.324
at Tset= T1= 900ºC	400	21.0	06.472

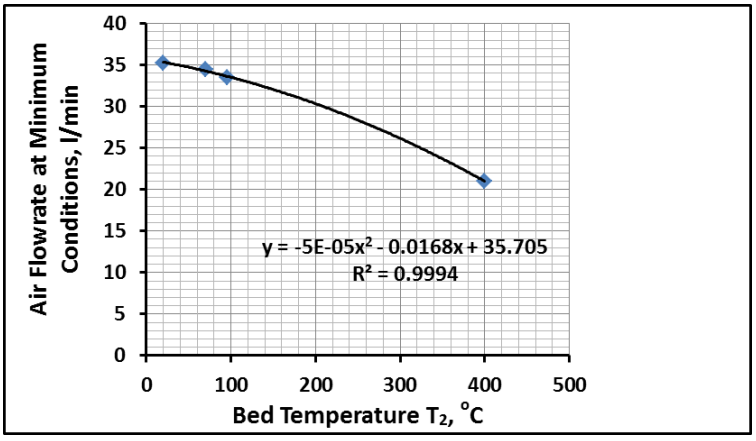

Figure 7. 7 Effect of bed temperature on the minimum fluidisation air flow rate for air-sand system, sand particle size (300-425)µm, H_s=8.3cm and gasifier diameter ID=8.3cm

An empirical equation was obtained for these experiment data conditions as shown in Equation 7.2. These data were fitted for temperature range (20-400) ºC by polynomial 2nd degree function with regression value R^2= 0.9994.

$$Y = 35.705 - 0.0168\,X - 5 * 10^{-5} * X^2 \qquad (7.2)$$

Where Y represents air flowrate at minimum fluidisation conditions and X represents a bed temperature T2 in ºC.

7.2.4 Performance of the biomass bubbling fluidised bed gasifier

This study set out with the aim of assessing experimentally the effects of the gasification operating and hydrodynamic parameters on the performance of the biomass bubbling fluidised bed gasifier within a low gasification temperature conditions. These

gasification parameters are the gasifying agent (medium) flowrate, the sand bed material particle size, the biomass fuel particle size, the static height of bed material, the gasification equivalence ratio the bed temperature and the number of holes of the distributor plate. Whereas gasifier performance is mainly understood through the following concepts: The Producer Gas Composition (PGC), the Fuel Carbon Conversion Efficiency (CCE), the Gas yield (GY), the Cold Gas Efficiency (CGE) and the producer gas Lower Heating Value (LHV).

7.2.4.1 Gasification test for steady state producer gas composition

A few tests were conducted to evaluate and determine the steady state producer gas composition, also to determine the minimum required time for the continuous biomass feeding for gasification experiments to achieve the steady state objective. Continuous gasification experiments for 5 and 10 minutes were conducted for this purpose. Prior to start the experiment, for each test the gasifier was prepared at a specific temperature and the air was fed through the bed at a required flow rate. At starting time t=0, the gas analyzer was turned on to analyze initially the air composition for 30 sec. At this time the screw feeder was turned on to feed a quantity of biomass (according to a specific ER) for 5 minutes (300 sec for first test) and 10 minutes (600 sec for second test). For both tests, the same conditions of biomass gasification were used. For two tests, the screw feeder was turned off and air flow was closed at the end of the 330 sec and 630 sec period, respectively.

Their results are shown in Figures 7.8a and b, respectively. It is apparent from the figures that no appearance for all producer gases, except O_2 gas, in the period time between 30 sec and approximately 100-110sec. As a result of the gasification reactions, at this time (100-110 sec) O_2 gas composition declined suddenly whereas CO, CO_2, H_2 and CH_4 were released and rose gradually (for a few seconds) then they rose sharply. For most experiments, at any specific time the composition of producer gases took a descending trend, $CO > CO_2 > H_2 > CH_4$. Also from the Figures, a and b, it can be shown that at the end of 330 sec and 630 sec when the gasification process (reaction) was stopped, all producer gases were reduced significantly. In addition, for both tests it can be seen that gases took their composition steady approximately around180-220 sec. Due to the location of the gas analyzer, it was seen that there was a delay time , giving a delay in the analysis time of around (100-120) sec. This case was confirmed by conducting a test for a standard gas mixture where its composition (in volume %) was

CO=0.1 %, CO_2= 1 % and O_2= 1 % and the rest is N_2. The results are shown in Figure E.1 (a) and (b) in Appendix E-Section E.1. It can be seen that analyzing results revealed a similar behaviour comparing to the results of previous tests for all aspects: feeding starting time, analyzing delay time, time of gases appearance, steady state time of gas composition, etc.

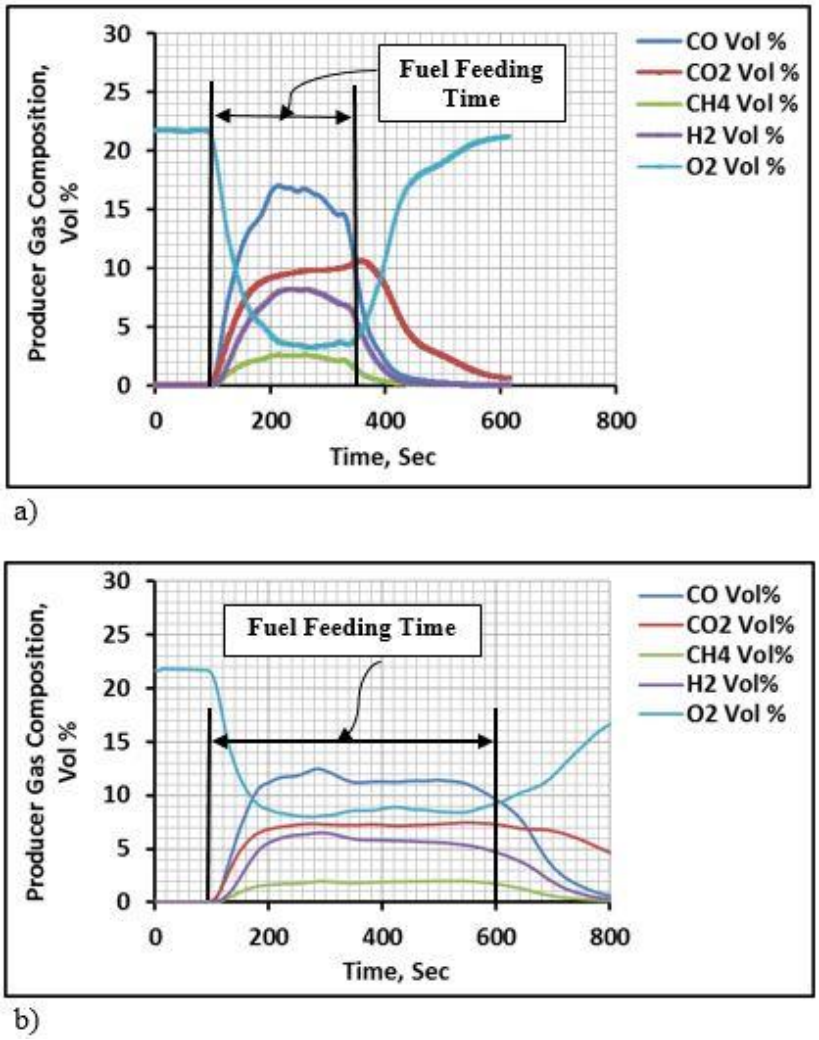

Figure 7. 8 A tested experiments for biomass producer gas composition: a) For 5 minutes biomass feeding time and b) For 10 minutes biomass feeding time

Finally, it can be concluded as follows that: there was an analyzing delay time of 70-90 sec starting from the commencement of biomass feeding. This is due to the distance there was a period time to reach a steady state gas composition, the real reading of producer gas composition was taken at the period time between steady state starting time and biomass feeding stop time taking into account the analyzing delay time. At

this steady state period time, the average composition for each producer gas was taken and realized in the performance calculations.

7.2.4.2 Effect of gasifying agent (Air) flowrate

Table 7. 3 Operating conditions for air flowrate parameter experimental tests

a) For SPWB

Operating Parameters	Air Flowrate, l/min (kg/hr) at 20°C		
	44 (3.18)	**66 (4.77)**	**88 (6.36)**
1- Equivalence Ratio ER	0.42	0.42	0.42
2- Reaction Bed Temperature T2, °C	360	360	360
3- Bed Material (Sand) Particle Size, µm	300-425	300-425	300-425
4- Biomass solid Fuel Particle Size, µm	600-850	600-850	600-850
5- Static Bed Height H_s, cm	6.225	6.225	6.225
6- Mass Rate of biomass Feeding, kg/hr	1.21	1.82	2.42
7- $(MAFR)_{stoichiometric}$ For SPWB	6.2	6.2	6.2
8- Air superficial velocity U_o, cm/sec	13.56	20.34	27.12

b) For IDPWB

Operating Parameters	Air Flowrate, l/min (kg/hr) at 20°C		
	44 (3.18)	**66 (4.77)**	**88 (6.36)**
1- Equivalence Ratio ER	0.381	0.381	0.381
2- Reaction Bed Temperature T2, °C	360	360	360
3- Bed Material (Sand) Particle Size, µm	300-425	300-425	300-425
4- Biomass solid Fuel Particle Size, µm	600-850	600-850	600-850
5- Static Bed Height Hs, cm	6.225	6.225	6.225
6- Mass Rate of biomass Feeding, kg/hr	1.32	1.97	2.63
7- $(MAFR)_{stoichiometric}$ For IDPWB	6.352	6.352	6.352
8- Air superficial velocity U_o, cm/sec	13.56	20.34	27.12

(a) Producer gas composition (PGC) for two biomass materials

According to the operating conditions which have been shown in Table 7.3(a) and (b), Figure 7.9 (a) and (b) presents the effect of air flowrate on the producer gas composition for two biomass feedstock materials, SPWB and IDPWB, respectively. The effect of this parameter was taken under constant ER, where the air flow increased to achieve a constant value of equivalence ratio. For both biomass it can be seen that as flowrate increased the CO composition increased gradually whereas CO_2, H_2 and CH_4 composition decreased gradually, except CH_4 which stayed constant for the former biomass. These CO and CO_2 findings disagreed with the findings published by Almeida et al. (2016) for olive bagasse gasification, Muazu et al. (2015) and Xiao et al. (2007) for polypropylene gasification, where CO decreased and CO_2 increased. . But, for CO_2 the finding agreed with the results published by Ramin Radmanesh, Jamal Chaouki (2006) for both ER 0.25 and 0.35. For this study, the increase in CO composition can

be attributed to the increase of O_2 gas as air flowrate increased and consequently the exothermic partial oxidation reactions of carbon R2.3 and high hydrocarbon (CnHm) R2.6 will occur under low bed temperature and high freeboard temperature and partial oxidation atmosphere. These reactions can be considered as dominant reactions for CO production compared to the complete combustion reaction for CO_2 production. Also according to the R2.6 the partial oxidation of the hydrocarbon compounds including light hydrocarbon such as CH_4 leading to consume them and produce CO and H_2 gases, especially in the freeboard section due to the high temperature at 900^{o}C. In contrast, the exothermic reaction R2.5 (hydrogen oxidation) maybe enhanced by the air increase at partial oxidation conditions consuming H_2 gas. Furthermore, the shorter residence time, due to increasing air flowrate, leads to a smaller release of volatile matter(Sadaka et al. 2002) ,(Xiao et al. 2007), and (Almeida et al. 2016). The above analysis explains why CO increased while H_2 and CH_4 decreased as air flowrate increased. At the same time the slight reduction of CO_2 can be attributed to its consumption in the freeboard section by the endothermic dry reforming reaction of high hydrocarbon compound R2.14 and the Boudouard reaction R2.13 due to escaping char in the freeboard due to higher velocity(Maglinao et al. 2015).

Furthermore, variations in the air flowrate have an effect on the bed hydrodynamics, which take place mainly by affecting bubble size and velocity thereby the bubble area fraction, residence time of the gas phase and biomass particles. When the air flowrate is increased the bed will expand, thus making the emulsion phase of the bed more porous, providing more O_2 and increasing the bubble size and velocity. This gives more mixing and higher heat and mass transfer rates leading to higher rate of partial oxidation reactions in bed section (Das and Datta 2014) (Ramin Radmanesh, Jamal Chaouki 2006) . On the other hand, for constant ER the flowrate increase will require more biomass causing an increase in minimum fluidisation velocity and thereby decrease the gas flow in the bubble creating a smaller bubble size and velocity and hence a uniform bubble distribution improving fluidisation quality (as explained in Chapter 6) (Fotovat et al. 2015). These fluidisation conditions will keep the bed in partial oxidation environments (because of the constant ER) and a quiet fluidisation behaviour (due to the rise of the biomass mass fraction in the bed) compared to the low air flowrates (which need low biomass mass fraction). The partial oxidation environment does not sufficiently increase the bed temperature to enhance the exothermic, endothermic and cracking reactions in the bed. On the other hand, the residence time at low air flowrates is higher

than high air flowrates, which gives greater chemical contact time. Thereby these hydrodynamic conditions resulted in reduction in composition of H_2, CO_2 and CH_4 in producer gas as air flowrate increased. As shown in Figure 7.9 (a) and (b) it can be also observed that the combustible gases produced from IDPWB were lower than SPWB whereas CO_2 was higher, which affect the LHV of the producer gas. In addition, the observed high percent of CH_4 and H_2 might be related to the tar cracking in the initial region of the gasifier freeboard section promoted by high temperature at 900°C.

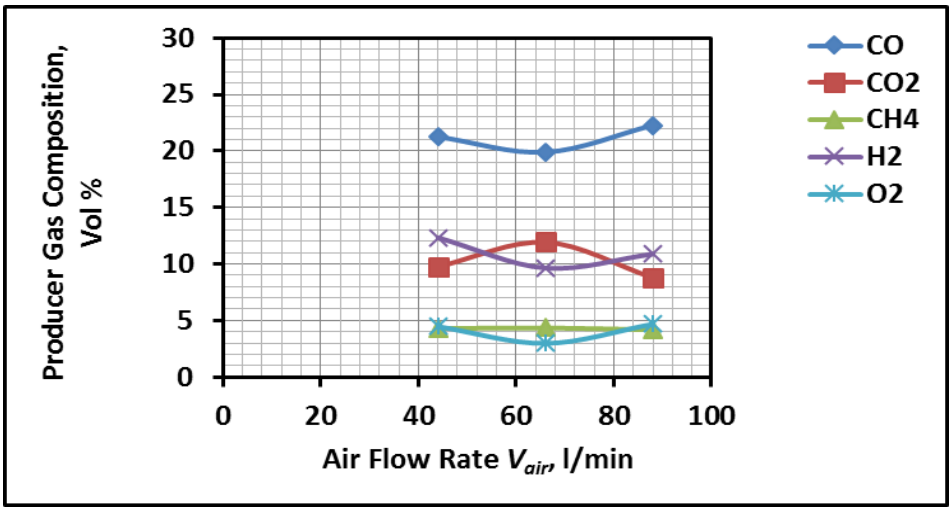

a) SPWB

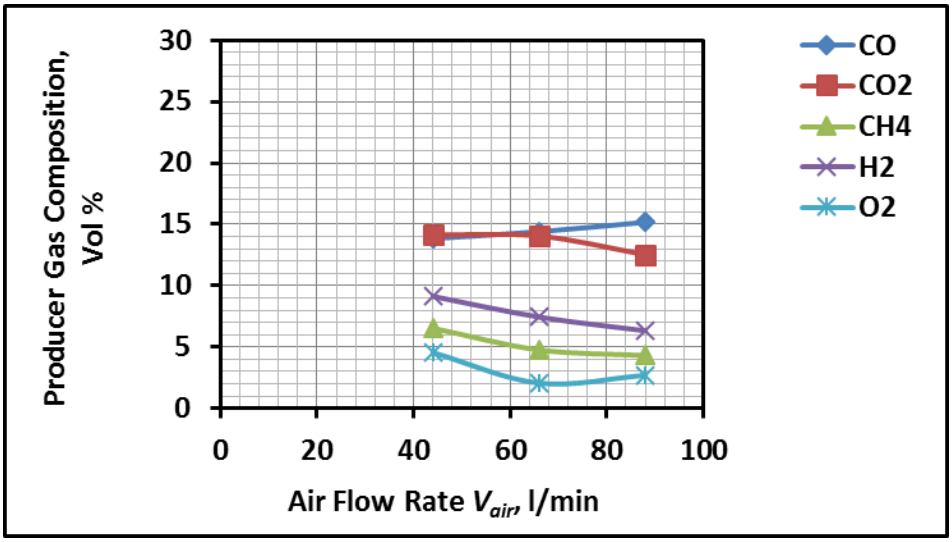

b) IDPWB

Figure 7. 9 Effect of air flowrate on producer gas composition (PGC): a) For SPWB biomass material, b) For IDPWB biomass material

(b) Carbon conversion efficiency (CCE), producer gas heating value (LHV) and cold gas efficiency (CGE)

Carbon conversion efficiency, producer gas heating value and cold gas efficiency are principal parameters for gasifier performance verification. From the Figure 7.10 for the range of the air flowrate (44l/min to 88 l/min) it can be seen that as the air flowrate increases the CCE increases from (105% to 122%) for SPWB biomass while it decreases from 122% to 98% for IDPWB biomass. This is due to the composition of the carbonaceous producer gas CO, CH_4, CO_2 For further performance verification a producer gas LHV was determined. The Figure shows generally as air flow rate increases a slight reduction for (LHV) of SPWB biomass from 5.3 MJ/Nm^3 to 5.2 MJ/Nm^3 whereas for IDPWB reduces gradually from 4.81 MJ/nm^3 to 4.43MJ/nm^3 . A possible attribute to this LHV reduction could be due to the reduction in combustible gases composition CH_4 and H_2 and a slight increase in CO for both biomass materials as shown in Figure 7.9 Xiao et al. (2007), and Almeida et al. (2016). These gases have a heating value 33.95, 10.22 and 11.97 MJ/Nm^3, respectively. Also at the same time as air flow rate increases the producer gas becomes more diluted by non-combustible gases N_2 and unreacted O_2 lowering the producer gas heating value. Figure 7.10 shows that as air flowrate increases the CGE decreases slightly approximately from 90% to 84% for SPWB and from 70% to 55% for IDPWB. For these operating conditions, these results infer that the biomass gasification in a fluidised bed should be worked at low air flowrates (more than minimum fluidisation velocity) for producing higher (LHV) producer gas. Also, it can be inferred that SPWB is more efficient than IDPWB due to its higher performance parameters.

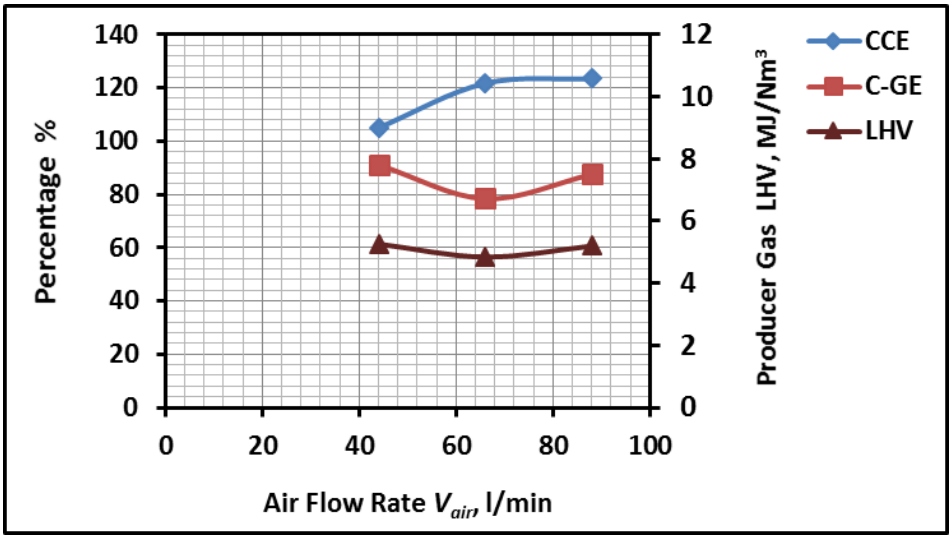

a) SPWB

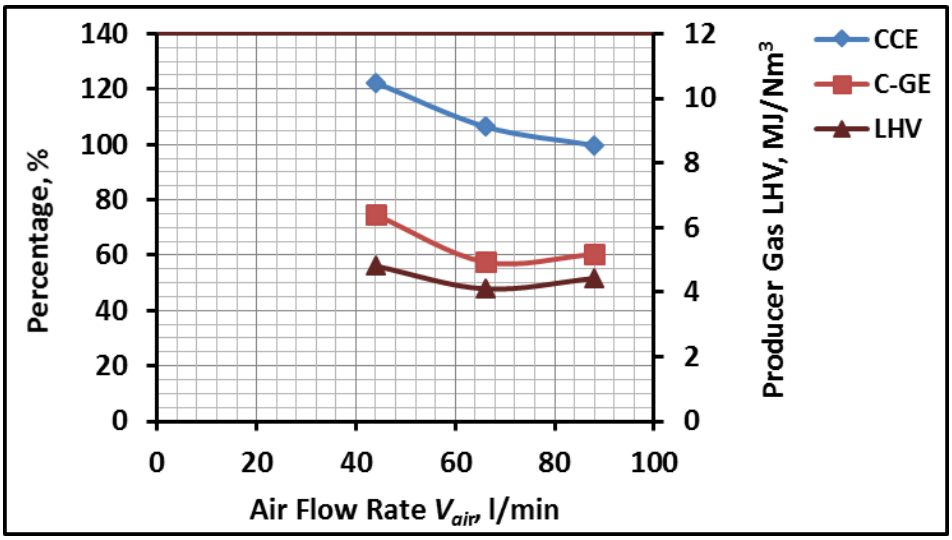

b) IDPWB

Figure 7. 10 Effect of air flowrate on performance parameters: a) for SPWB biomass material and b) For IDPWB biomass material

(c) Producer gases yield (GY)

Figure 7.11 (a) and (b) highlights the effect of the air flowrate (air velocity) bed material on the gases yield for two biomass materials. It can be seen that for SPWB, the total gas yield was slightly decreased from 3.32 to 3.2Nm^3/kg feed db, while for IDPWB as shown in Figure (b) the total gas yield was slightly decreased from 2.82 to 2.48Nm^3/kg feed db. For SPWB, the gas yield for each individual gas: N_2 stayed constant at 1.59Nm^3/kg feed db, CO_2 was slightly increased from 0.32 to 0.37 and then decreased to 0.28nm^3/kg feed db, CO increased a little from 0.71 to 0.72, CH_4 approximately stayed constant at 0.14Nm^3/kg feed db, H_2 decreased slightly 0.41 to o.35 Nm^3/kg feed db and O_2 decreased from 0.15 to 0.09 and then increased to 0.15Nm^3/kg feed db. For IDPWB the gas yield of the individual gases: N_2 stays constant at 1.46 nm^3/kg feed db, CO an CO_2 CH_4, H_2, and O_2 decreased slightly from 0.39 to 0.38, from 0.4 to 0.31, from 0.15 to 0.1, from 0.26 to 0.6 and from 0.12 to 0.06 Nm^3/kg feed db, respectively. It can be concluded that a higher gas yield can be obtained at low air flowrate 44l/min. In comparison with, SPWB produced higher gas yield than IDPWB. This finding is agreed with the finding published by (Xiao et al. 2007) for polypropylene air gasification. The yield of the producer gas in (wt/wt pp) was slightly decreased as fluidisation velocity increased. At ER=0.3 and U_o/U_{mf}=3.0, the gas yield was between 2.79 and 2.88 Nm^3/kg feed db.

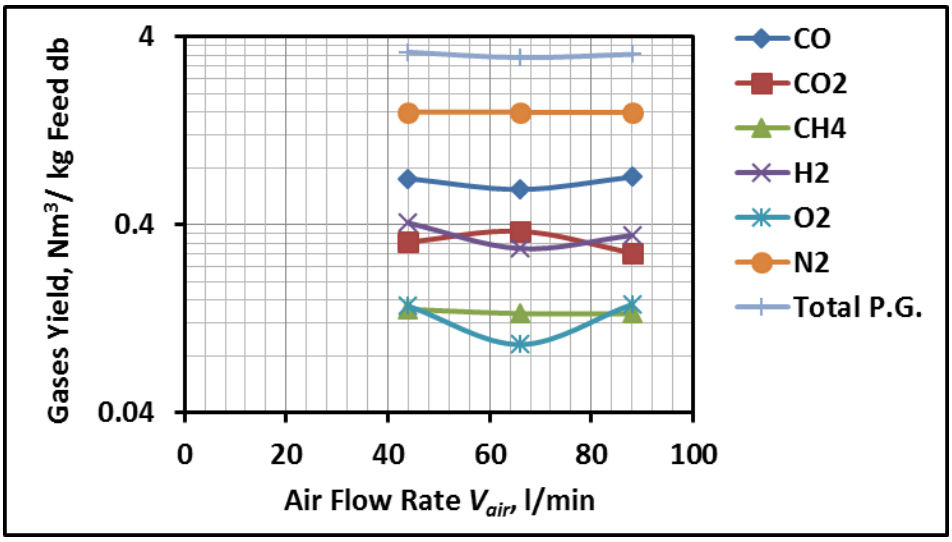

a) SPWB

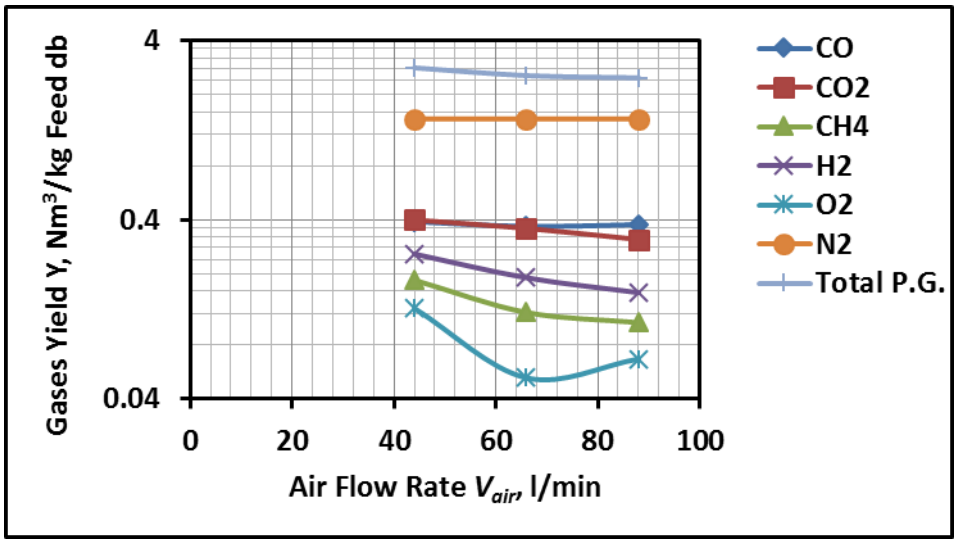

b) IDPWB

Figure 7. 11 Effect of air flowrate on gas yield: a) For SPWB biomass material and b) For IDPWB biomass material

(d) Gases ratios

Figure 7.12 (a) and (b) presents the effect of air flowrate on the gases ratios in producer gas for both biomass feedstock materials. These ratios can consider as a mean for expressing and assessing the producer gas quality. From the Figure 7.12, it can be seen that the general trends of ratios for both biomass are similar. CO/CO_2 ratio increased from 2.18 to 2.54 for SPWB and from 0.98 to 1.2 for IDPWB as air flowrate increased. The ratios 2.54 and 1.2 were maximum ratio that were achieved by both biomass at the highest air flowrate. These high ratios confirm the gasification reactions due to partial

oxidation and low CO_2 producing compared to CO. The high difference in this ratio between two biomass refers to the occurrence of combustion reactions for IDPWB (which was also confirmed by H_2/CO_2, 0.64 to 0.51 along the flow rate interval) compared to SPWB (which has H_2/CO_2, 1.26 to 1.24). For IDPWB, H_2/CO_2 and CH_4/CO_2 ratios indicate to less amount of H_2 and CH_4 compared to CO_2. The H_2/CO ratio is an important ratio to specify the syngas quality. From the Figure 7.12 it can be seen that this ratio is less than 1.0 and decreases (from 0.58 to 0.49 for SPWB and from 0.66 to 0.42 for IDPWB) as air flowrate increases for both biomass. From these results, it is possible to conclude that the water-gas shift reaction was not active due to insufficient quantities of H_2O. Thus, for increasing H_2 gas in producer gas a specific amount of steam or a moist biomass or moist air should be introduced. It can be concluded that according to syngas utilization a low air flowrate is preferred to produce high H_2.

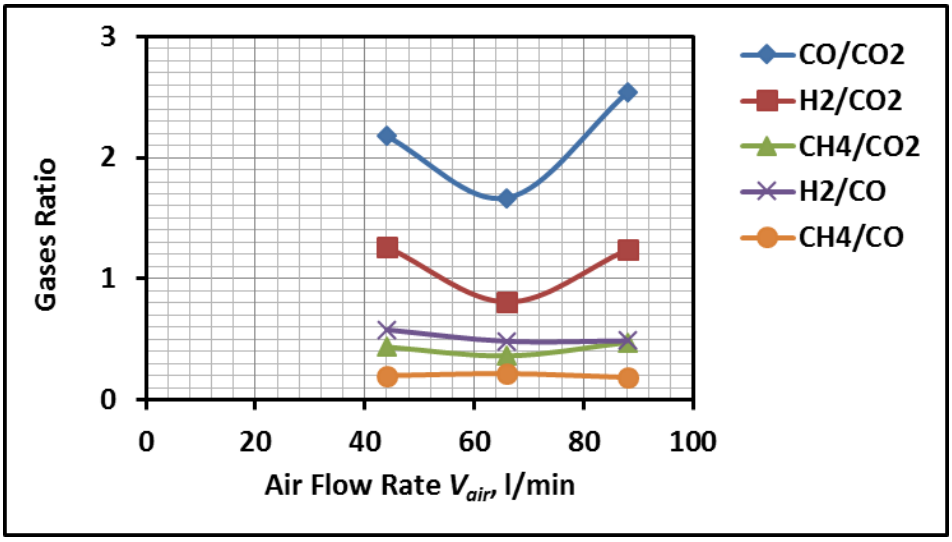

a) SPWB

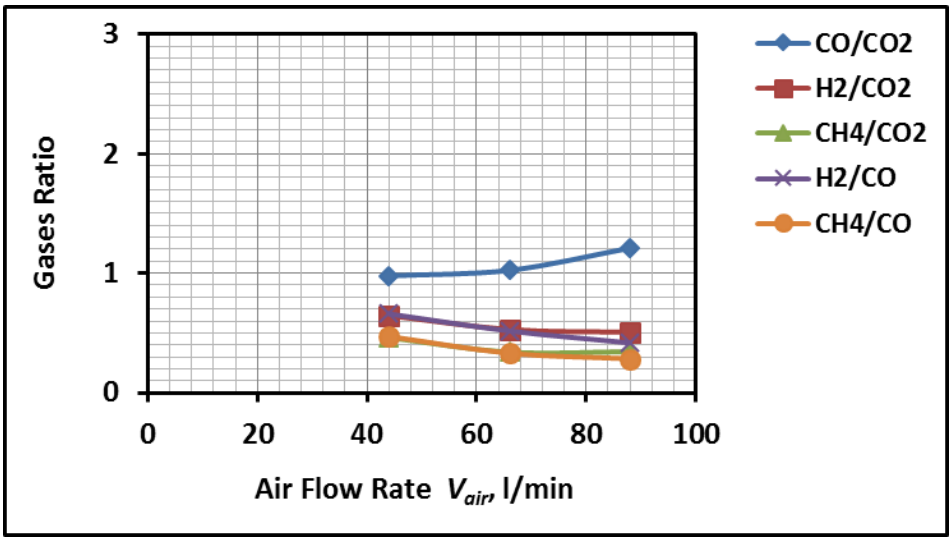

b) IDPWB

Figure 7. 12 Effect of air flowrate on producer gases ratios: a) For SPWB biomass material and b) For IDPWB biomass material

7.2.4.3 Effect of particle size of sand bed material

Table 7. 4 Operating conditions for sand bed material particle size parameter experimental tests:

a) For SPWB

Operating Parameters	Bed Material (Sand) Particle Size, µm		
	300-425	**425-500**	**500-600**
1- Air Flowrate l/min (kg/hr)	44 (3.18)	75 (5.45)	95 (6.72)
2- Reaction Bed Temperature T2, °C	360	360	360
3- Equivalence Ratio ER	0.43	0.43	0.43
4- Biomass solid Fuel Particle Size, µm	600-850	600-850	600-850
5- Static Bed Height Hs, cm	6.225	6.225	6.225
6- Mass Rate of biomass Feeding, kg/hr	1.2	2.05	2.6
7- $(MAFR)_{stoichiometric}$ For SPWB	6.2	6.2	6.2
8- Air superficial velocity U_o, cm/sec	13.56	23.11	29.28

b) For IDPWB

Operating Parameters	Bed Material (Sand) Particle Size, µm		
	300-425	**425-500**	**500-600**
1- Air Flowrate l/min (kg/hr)	44 (3.18)	75 (5.45)	95 (6.72)
2- Reaction Bed Temperature T2, °C	360	360	360
3- Equivalence Ratio ER	0.381	0.381	0.381
4- Biomass solid Fuel Particle Size, µm	600-850	600-850	600-850
5- Static Bed Height Hs, cm	6.225	6.225	6.225
6- Mass Rate of biomass Feeding, kg/hr	1.32	2.26	2.78
7- $(MAFR)_{stoichiometric}$ For IDPWB	6.352	6.352	6.352
8- Air superficial velocity U_o, cm/sec	13.56	23.11	29.28

(a) Producer gas composition (PGC) for two biomass materials

According to the operating conditions which have been shown in Table 7.4(a) and (b), Figure 7.13 (a) and (b) presents the effect of the particle size of the sand bed material on the producer gas composition for two biomass materials for constant operating conditions. It can be seen, in general, that the trend of the effect of sand particle size for both biomass for all gases are similar. As particle size increases from 300-425µm to (500-600) µm CO composition increases slightly from 21.3% to 23.2% for SPWB and from 11% to 12.5% for IDPWB. Whereas, for CO_2, CH_4 and H_2 their composition decrease slightly from (9.8% to 8.8%), (4.4%to 4%) and (12.3% to 11.9%), respectively, for SPWB and from (6.5% to 5%), (10.2% to 10 %) and (5% to 3%), respectively for IDPWB. In addition, it can be shown that SPWB provided higher producer gas quality than IDPWB and the latter was more affected by bed particle size than former. This can be due to the high difference in chemical and physical properties between two biomass materials as shown in Table 4.4. The slight effect of the sand bed particle size on the producer gas quality can be attributed to firstly, the sand is un-catalytically active (inert) material which does not play any chemical conversion role in enhancement for tar conversion and producer gas quality so for this case there is no clear effect of particle size. Secondly, from the hydrodynamic aspect when the particle size increases the minimum fluidisation velocity U_{mf} of the air increases as explained in (Chapter 6). For a specific air superficial velocity U_o, U_o=1.25U_{mf} was taken for each experiment. As shown in Chapter 6-Section 6.2.3, for 300-425µm sand particle size U_{mf}= 10.875cm/sec= 35.3l/min and for U_o=1.25U_{mf}, U_o = 44l/min. Therefore, for the particle size 425-500µm and 500-600µm, which has U_{mf} =18.665cm/sec= 60.6l/min and U_{mf}-=23cm/sec = 74.6l/min and their U_o will be 75.75l/min and 93.25l/min, respectively. This means that for the last two particle size more air is required than for 300-425µm, 1.72 U_o = 75.75l/min and 2.12U_o = 93,25l/min, respectively. This will give the same effect of the increasing air flowrate as shown in previous section. However, at the same time this air increase needs an increase in the biomass feeding mass flowrate to keep ER constant. This biomass increase (41.9%) for 425-500µm and 52.8% for 500-600µm will lead to an increase in the mass fraction of biomass in the bed and thereby increases the minimum fluidisation velocity of the bed mixture. These hydrodynamic changes will weaken the bed fluidisation behaviour as particle size increases and finally, will weaken gasifier performance.

The function of the bed material is to hold heat between fuel particles and provide a high transfer capacity. This high transfer capacity ensures sufficiently high heating rates and homogeneous temperature distribution and therefore good control of flue gas or producer gas composition (Folkeson 2014). Due to their high surface area, small bed particles size can give a high heat and mass transfer and high contact between bed and biomass particles leading to high rate of reactions. (Kern et al. 2013) attributed the highest H_2 content in producer gas, in addition to the steam effect, to the increase of the catalytic activity of the fine olivine particles 370µm due to their increased specific surface area compared to the coarse particles of 510µm diameter. In addition, they concluded that the significant effect of the particle size on the tar content could not be found.

Koppatz et al. (2012) reported in their research that there was no common agreement in the literature where the principal properties, which control the bubbling fluidised bed characterization such as bubble size, bubble rise velocity and bed expansion, are to be considered independent of the mean particle size or not. They concluded that general gas composition (main gaseous components) was found to be broadly independent of the bed particle size. This agrees with the results for SPWB but disagrees for IDPWB. This disagreement might be due to their irregular needle shape, which has a higher aspect ratio than SPWB particles.

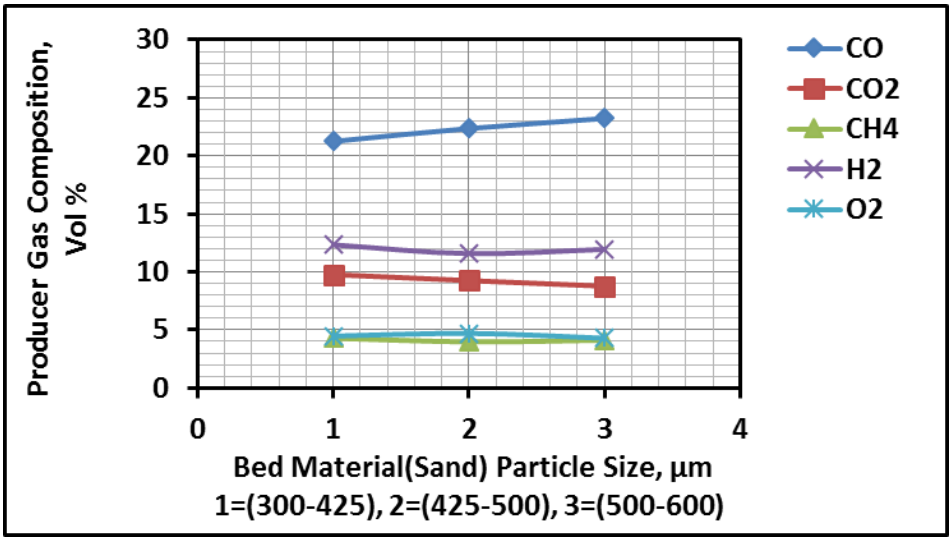

a) SPWB

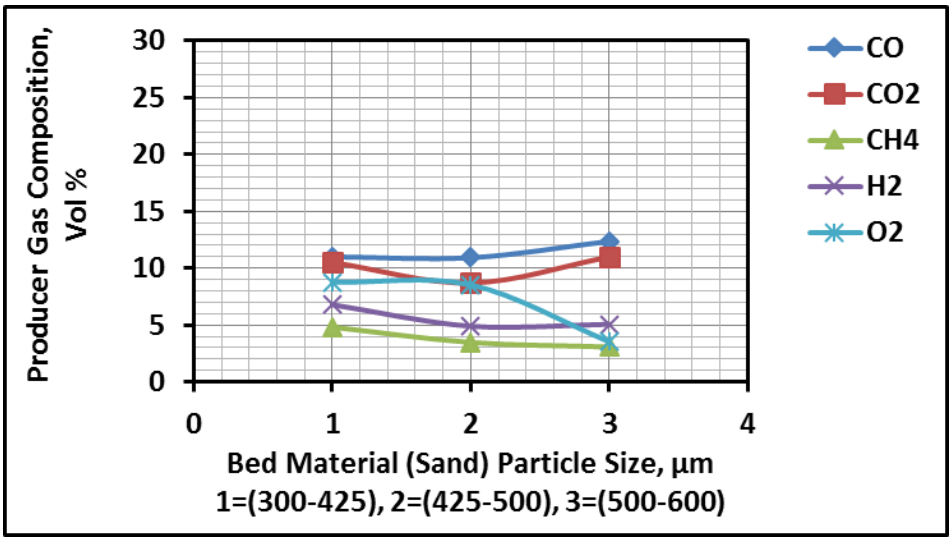

b) IDPWB

Figure 7. 13 Effect of particle size of sand bed on producer gas composition (PGC): a) For SPWB biomass material and b) For IDPWB biomass material

(b) Carbon conversion efficiency (CCE), cold-gas efficiency (CGE), and producer gas heating value (LHV)

Figure 7.14 (a) and (b) shows the effect of the particle size of sand bed material on the performance parameters CCE, CGE and LHV for two biomass materials. It can be seen that for SPWB there is no effect of particle size, whereas for IDPWB the parameters decline moderately as particle size increases. For SPWB the performance parameters CGE and LHV were approximately levelled off at 109% and 6.2MJ/Nm^{3}db, respectively, whereas CCE was slightly increased from128 to 131%. For IDPWB the relation is different where CCE, CGE and LHV are declined, approximately from (83% to 75%), (48% to 36%) and (3.65 to 3.04 MJ/Nm^3 db), respectively as the sand particle size increases. Comparatively, gasification with SPWB gives high performance than IDPWB. Using small particle size of the bed is preferable for producing high LHV gas, high CGE and CCE for IDPWB. However, it is a little different for SPWB.

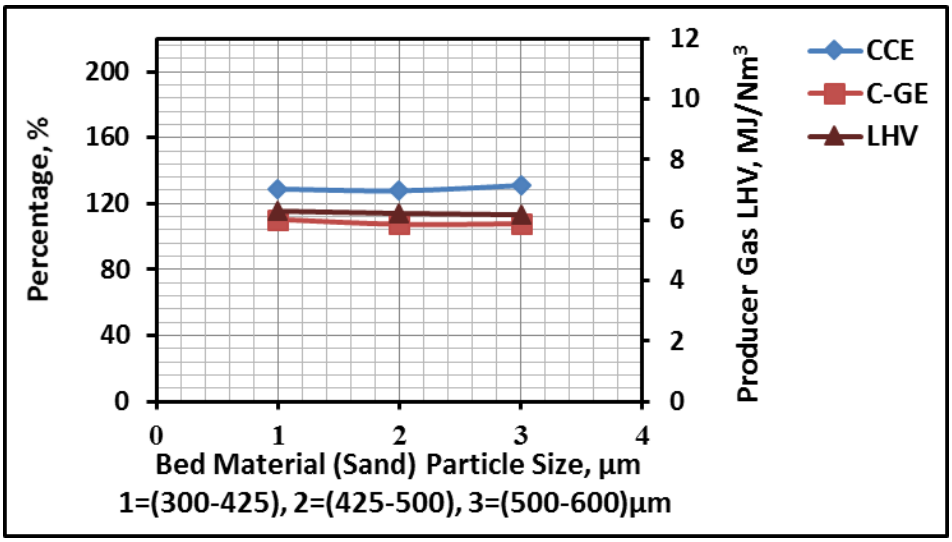

a) SPWB

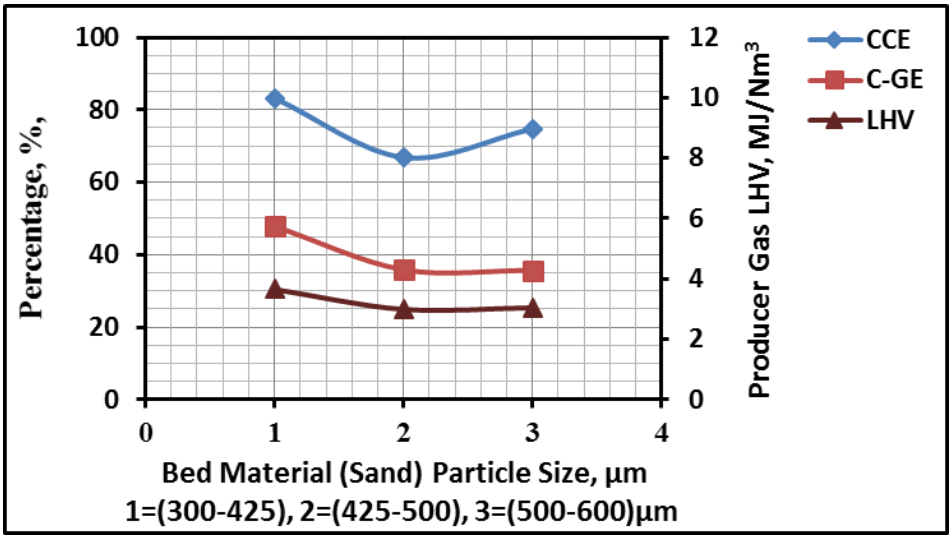

b) IDPWB

Figure 7. 14 Effect of particle size of sand bed on CCE, CGE and LHV performance parameters: a) For SPWB biomass material and b) For IDPWB biomass material

(c) Producer gas yield (GY)

Figure 7.15 (a) and (b) highlights the effect of the particle size of the sand bed material on the gases yield for two biomass materials. It can be seen that for SPWB, the total gas yield was stayed constant on 3.3 Nm^3/kg feed db as sand particle size was increased; while for IDPWB, the total gas yield was decreased moderately from 2.5 to 2.25Nm^3/kg feed db. For SPWB the gas yield for most individual gas stay constant. CO showed highest gas yield compared to H_2, CO_2, CH_4 and O_2. For IDPWB, the individual gases, except N_2, CO_2 and CO, slightly increased along the range of the sand particle size. In comparison with, SPWB produced higher CO and H_2 gas yield than IDPWB. The small

effect of particle size on gasifier performance and gas yield especially for SWPB can be attributed to the constancy of the ER for the three ranges of sand particle size. Although the larger particle size needs more air flowrate for fluidisation, but due to the constant ER, its effect is decreased**.** Hydro-dynamically, it was thought that these particle sizes were approximately convergent. Consequently, this was resulted in a similar hydrodynamic behaviour.

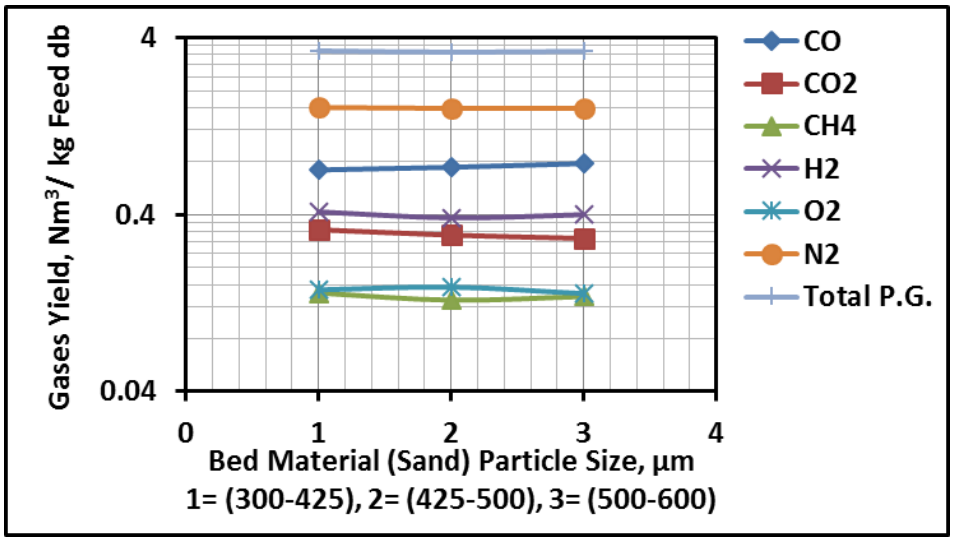

a) SPWB

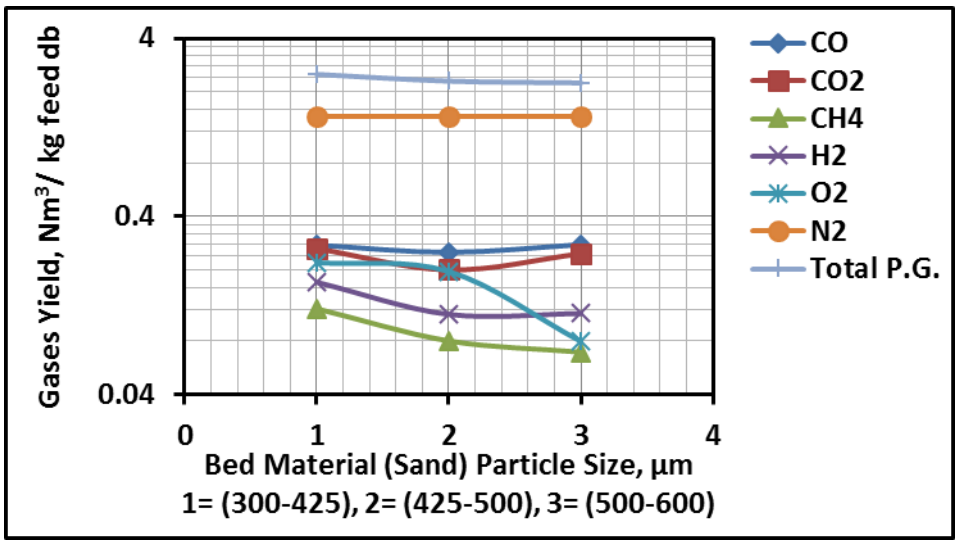

b) IDPWB

Figure 7. 15 Effect of particle size of sand bed on gases yield (GY): a) For SPWB biomass material and b) For IDPWB biomass material.

(d) Gases Ratios

Figure 7.16 (a) and (b) highlights the effect of the particle size of the sand bed material on the gases ratio for two biomass materials. It can be shown that SPWB implemented

high CO/CO_2 and H_2/CO_2 ratios in comparing with IDPWB, whereas the other ratios are less than 0.6 for both biomass. For both biomass, the general trend of the CO/CO_2 ratio increases gradually from 2.3 to 2.65 for SPWB and slightly increases from 1.05 to 1.15 for IDPWB as particle size increases. This ratio gives an indication that CO amount is more than CO_2 especially for large particle size. Due to the partial oxidation environment and low residence time, due to the air flowrate increase due to the particle size increase, these resulted in producing high CO and reducing H_2 and CO_2. For SPWB, the H_2/CO ratio decreased slightly from 0.65 to 0.5, CH_4/CO_2 increased slightly from 0.4 to 0.45 and CH_4/CO stays constant at 0.2. For IDPWB. H_2/CO decreased from 0.6 to 0.5, CH_4/CO_2 and CH_4/CO decreased a little from 4.5 to 3.0. The result confirms that IDPWB produced low CO and H_2 gas in comparing with SPWB. The bed particle size, (300-425)µm revealed a best H_2/CO_2 and H_2/CO ratios for SPWB and IDPWB producer gas.

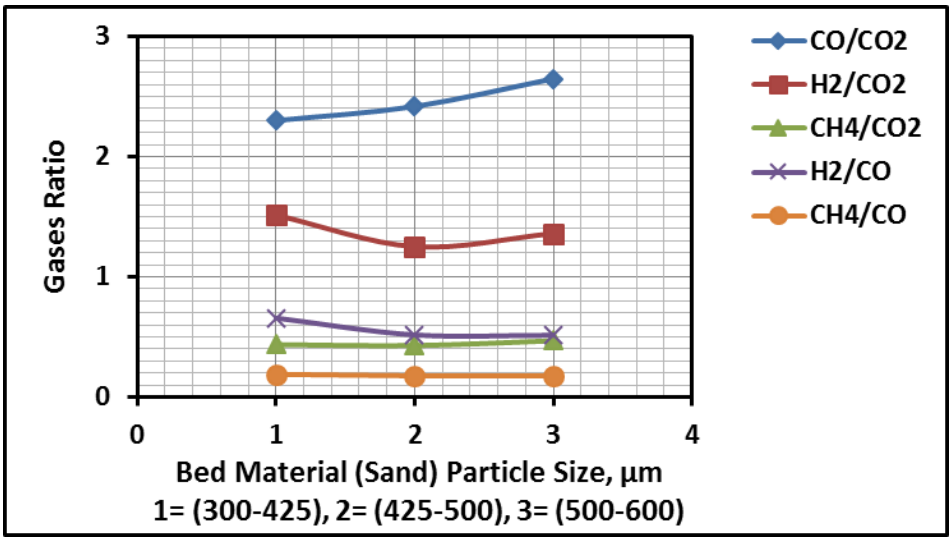

a) SPWB

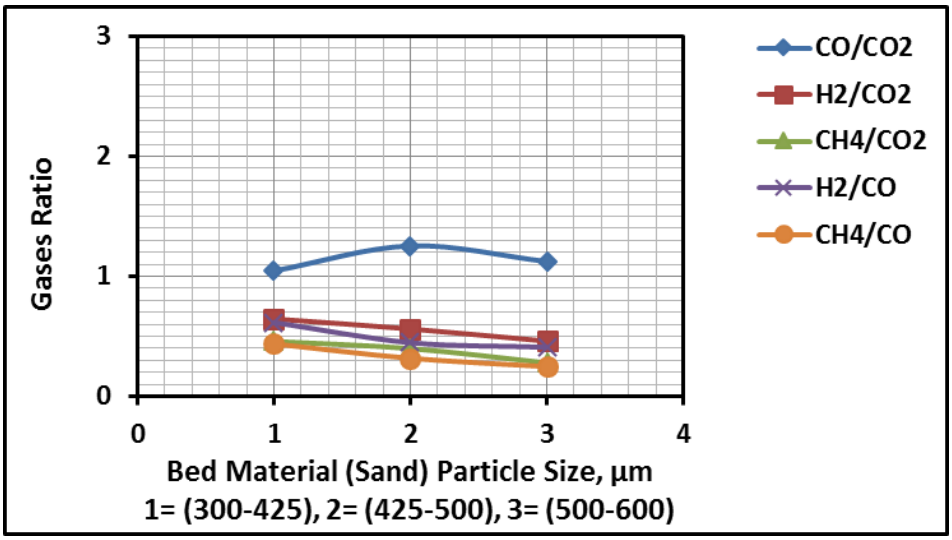

b) IDPWB

Figure 7. 16 Effect of particle size of the sand bed on gases ratio: a) For SPWB biomass material and b) For IDPWB biomass material

7.2.4.4 Effect of the biomass fuel particle size

Table 7. 5 Operating conditions for biomass fuel particle size parameter experimental tests

a) For SPWB

Operating Parameters	Biomass Solid Fuel Particle Size, µm		
	300-425	**600-850**	**1000-1180**
1- Air Flowrate l/min (kg/hr)	30 (2.17)	30 (2.17)	30 (2.17)
2- Reaction Bed Temperature T2, ºC	360	360	360
3- Bed Material (Sand) Particle Size, µm	300-425	300-425	300-425
4- Equivalence Ratio ER	0.55	0.55	0.55
5- Static Bed Height Hs, cm	6.225	6.225	6.225
6- Mass Rate of biomass Feeding, kg/hr	0.641	0.641	0.641
7- $(MAFR)_{stoichiometric}$ For SPWB	6.2	6.2	6.2
8- Air superficial velocity U_o, cm/sec	9.25	9.25	9.25

b) For IDPWB

Operating Parameters	Biomass solid Fuel Particle Size, µm		
	300-425	**600-850**	**1000-1180**
1- Air Flowrate l/min (kg/hr)	44 (3.18)	44 (3.18)	44 (3.18)
2- Reaction Bed Temperature T2, ºC	360	360	360
3- Bed Material (Sand) Particle Size, µm	300-425	300-425	300-425
4- Equivalence Ratio ER	0.381	0.381	0.381
5- Static Bed Height Hs, cm	6.225	6.225	6.225
6- Mass Rate of biomass Feeding, kg/hr	1.315	1.315	1.315
7- $(MAFR)_{stoichiometric}$ For IDPWB	6.352	6.352	6.352
8- Air superficial velocity U_o, cm/sec	13.56	13.56	13.56

(a) Producer gas composition (PGC) for two biomass materials

According to the operating conditions, which have been shown in Table 7.5 (a) and (b), the results of the effect of the biomass particle size on the producer gas composition for two biomass materials SPWB and IDPWB are presented in Figure 7.17 (a) and (b), respectively. Three particle size ranges were used 300-425µm, 600-850µm and 1000-1180µm. Generally, it can be seen that the average trend of the effect of the biomass particle size for both biomass for most gases (CO, H_2, CH_4 and O_2) are similar except CO_2 for SPWB, which has an opposite trend. The average trend of the composition of the gases decreased as particle size increased: For SPWB, the gases CO from 16.5% to 14%, H_2 from 13% to 9%, CH_4 from 3% to 2.5% decreased, whereas CO_2 increased from 6% to 10%. For IDPWB the gases decreased gradually: for CO from 14.5% to 7.7%, H_2 from 9% to 5% CO_2 from 12.5% to 9.8%, CH_4 from 5% to 3.5%. For the both biomass materials, the Figure shows that the smaller particle size produced more CO, H_2, and CH_4 and, less CO_2 for SPWB and more for IDPWB, than the larger particles. Three explanations may possible to interpret this particle size effect. **1)** The smaller particles have faster heating rate due to their larger surface area than large size. **2)** For smaller particle size the main control step in the pyrolysis process is reaction kinetics, while for larger particle size the gas diffusion step is controlled because of the product gas generated inside the particle is not easy to diffuse out (Lv et al. 2004) (Dr. Sami Sadaka, P.E. n.d.) and (Feng et al. 2011). **3).** Depending on fluidisation conditions, it might be due to the low weight of small particles, most of them were segregated quickly to the bed surface and entrained to the freeboard section, which was kept at high temperature 900^{o}C at gasifier position 44cm. In addition, the pyrolysis process is dominated by a heat transfer process, so both particle size and shape affect the conversion time significantly, especially for large size particles (Lu et al. 2010). These conditions lead to high pyrolysis and gasification reactions producing high quality gases. (Mohammed et al. 2011) attributed this effect to the greater temperature gradient inside the particle for large particles than small particles at a given time leading to an increase in the char and decrease in gases. It can be concluded that SPWB produced higher CO, and H_2 gases than IDPWB for this study range of biomass particle size, whereas for CH_4, the latter produced higher. Also According to this gasifier design study and for this range of particle size the result reveals that the smaller size is more favorable for high quality producer gas production.

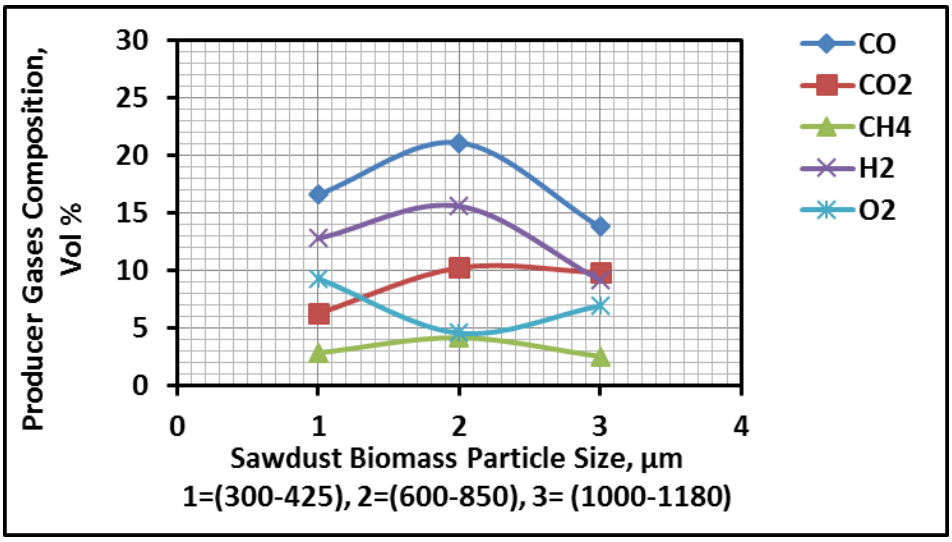

a) SPWB

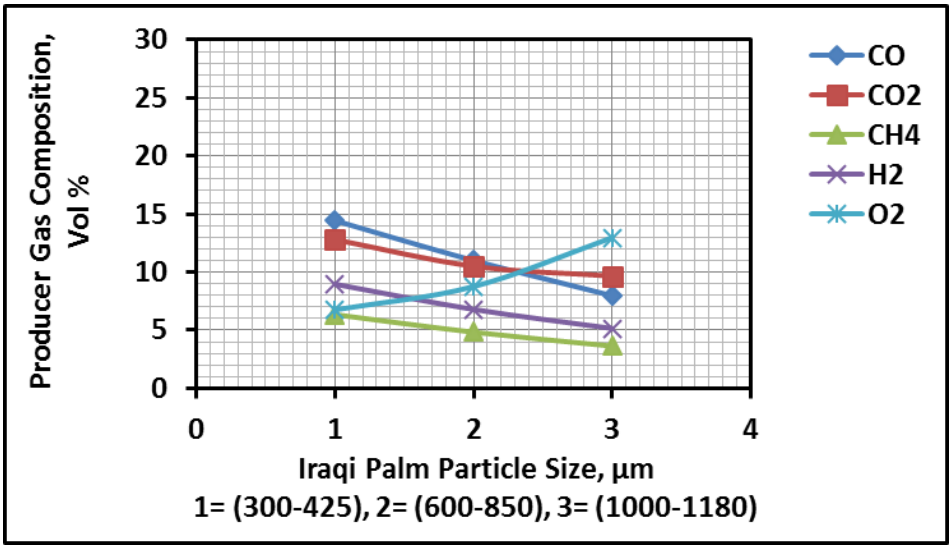

b) IDPWB

Figure 7. 17 Effect of particle size of biomass fuel on producer gas composition (PGC): a) For SPWB biomass material and b) For IDPWB biomass material

(b) Carbon conversion efficiency (CCE), cold-gas efficiency (CGE), and producer gas heating value (LHV)

Figure 7.18(a) and (b) shows the effect of the biomass particle size on the performance parameters CCE, CGE and LHV for two biomass materials. According to the composition results in previous section for SPWB, it can be said that those performance parameters increased significantly to the maximum value and decreased to the minimum value as biomass particle size increased. They increased: CCE from 109% to 177%, CGE from 89.48% to 136% and LHV from 4.26 to 5.53MJ/Nm^3 db as particle size increased from No 1 to No 2, respectively. Then they decreased to 100%, 65% and 3.44MJ/Nm^3 as particle size increased to No 3, respectively. For IDPWB the parameters declined significantly as particle size increased: CCE from 116% to 62%, CGE from

80% to 43% and LHV from 4.8 to 3.07MJ/Nm^{3}db. This is due to that the improving gas quality, as the particle size decreased will improve those performance parameters. These results are in agreement with the published papers (Lv et al. 2004) (Mohammed et al. 2011). It can be concluded that the optimum biomass particle size for SPWB is No 2 and for IDPWB is No 1 because they achieved a high LHV which are acceptable values for air as a gasifying agent (Cirad (2009). Furthermore, the optimum results confirmed that SPWB is more suitable and efficient than IDPWB for gasification by air fluidisation due to their higher LHV.

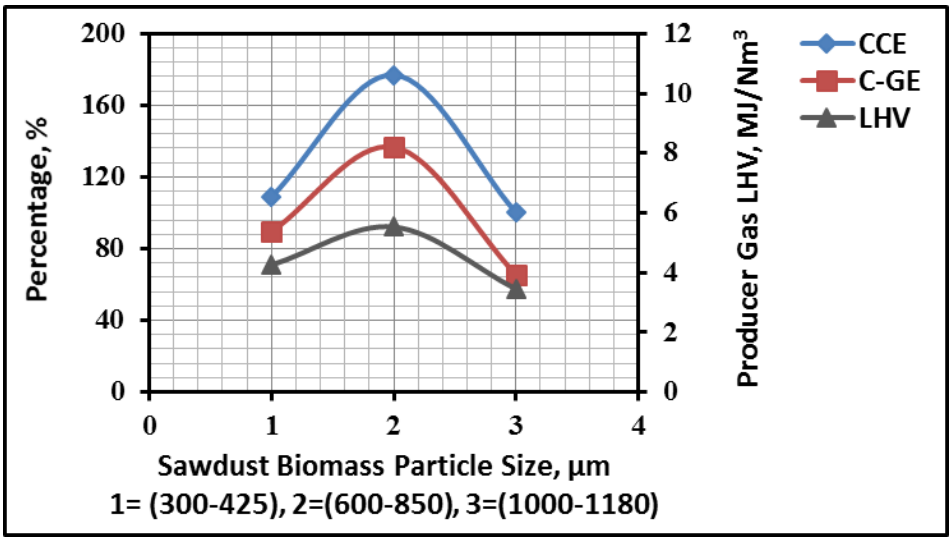

a) SPWB

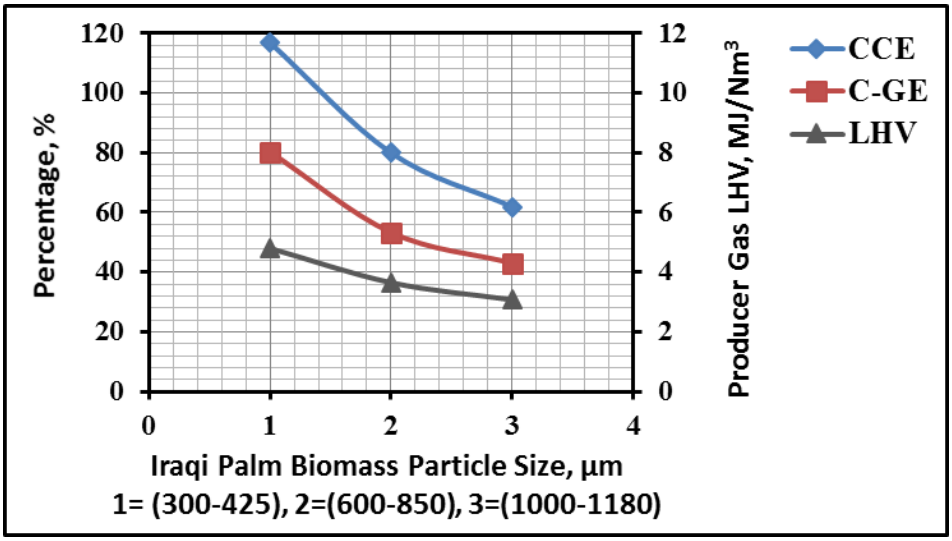

b) IDPWB

Figure 7. 18 Effect of biomass particle on CCE, C-GE and LHV performance parameters: a) For SPWB biomass material and b) For IDPWB biomass material

c) Producer gas yield (GY)

Figure 7.19 (a) and (b) highlights the effect of the particle size of the biomass fuel on the gas yield for two biomass materials. Similarly, to gas composition it can be seen that for SPWB, the general average trend of the gas yield decrease as biomass particle increase, except for CO_2 yield there is a slight increase from 0.1 to 0.2 Nm^3/kg feed db and N_2 stayed constant on 2.0 Nm^3/kg feed db. For total gas yield, the decrease was from 3.9 to 3.6Nm^3/kg feed, while for the rest gases the decrease was CO from 0.65 to 0.49, CH_4 from 0.11 to 0.09, H_2 from 0.5 to 0.32 and O_2 from 0.36 to 0.25Nm^3/kg feed db. For IDPWB the general trend for all gases is moderately decreased except N_2, which stayed constant at 1.63Nm^3/kg feed db and O_2 from 0.22 to 0.35Nm^3/kg feed db. The total gas yield decreased moderately from 3.2 to 2.7Nm^3/kg feed, whereas the rest gases decreased slightly: CO from 0.46 to 0.21, CO_2 from 0.41 to 0.26, CH_4 from 0.2 to 0.1, H_2 from 0.29 to 0.14. Again, the gas yield gives a good indication for gasifier performance. It can be confirmed that the smaller biomass particles produce higher gas yield than larger particles per each kg of biomass. In addition, the SPWB biomass fuel is more efficient than IDPWB due to its higher elemental composition.

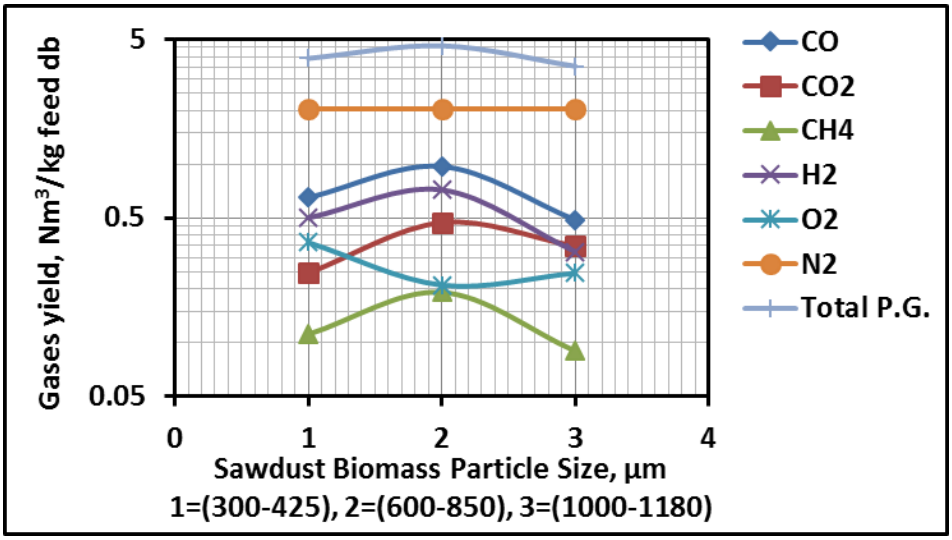

a) SPWB

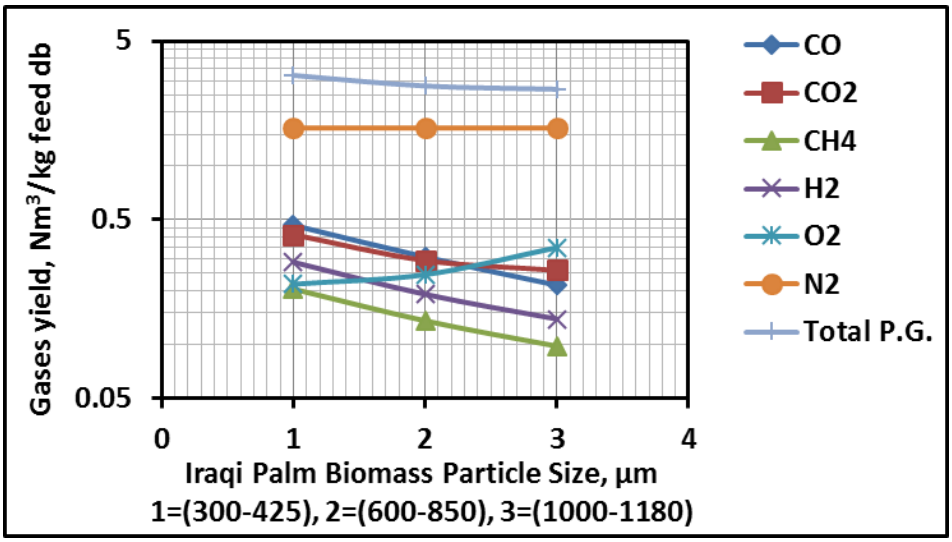

b) IDPWB

Figure 7. 19 Effect of particle size of biomass feedstock on gases yield: a) for SPWB biomass material and b) for IDPWB biomass material

(d) Gases Ratios

Figure 7.20 (a) and (b) highlights the effect of the particle size of the biomass feedstock on the gas ratio for two biomass materials. It can be shown that as particle size increased CO/CO_2 and H_2/CO_2 ratios decreased dramatically from 2.6 to 1.4 and from 2 to 0.9, respectively for SPWB and from 1.13 to 0.83 and from 0.7 to 0.53, respectively for IDPWB. H_2/CO and CH_4/CO_2 ratios decreased slightly from 0.75 to 0.68 and from 0.45 to 0.27, respectively for SPWB whereas, CH_4/CO ratio remained constant on 0.15. For IDPWB H_2/CO and CH_4/CO increased a little from 0.62 to 0.66 and from 0.44 to 0.46, respectively, while CH_4/CO_2 decreased a little from 0.48 to 0.38. These ratios give an indication of the heterogeneous and homogenous reactions that may occur inside the bed and freeboard sections. From the values of CO/CO_2, H_2/CO_2 for both biomass at smaller particle size indicates that the exothermic partial oxidation reactions, R2-R6, are dominant because these reactions are related to the particle itself and thereby the rate of devolatilisation rate, for higher hydrocarbon yield. Furthermore, H_2/CO and CH_4/CO ratios indicate the contributions of the exothermic reactions, water gas shift R8 and Methanation R12. The shortage of the H_2 gas may be due to the Methanation reaction because it consumes three times the amount of H_2 compared to CO. It can be inferred that SPWB produced more CO rich syngas than IDPWB, especially at smaller particle size. In addition, the observed high CO/CO_2, H_2/CO_2 and CH_4/CO_2 ratios

emphasizes the partial oxidation existence for both biomass, especially for smaller particle size.

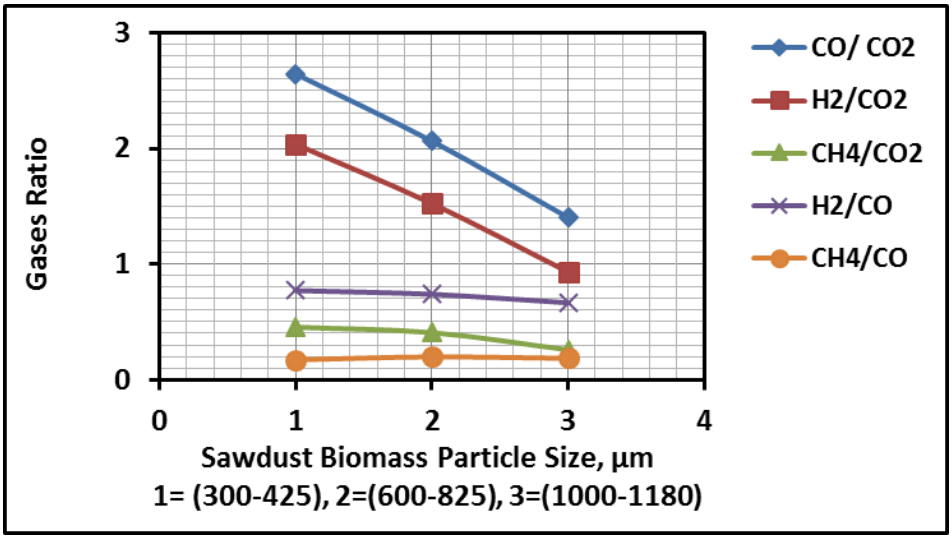

a) SPWB

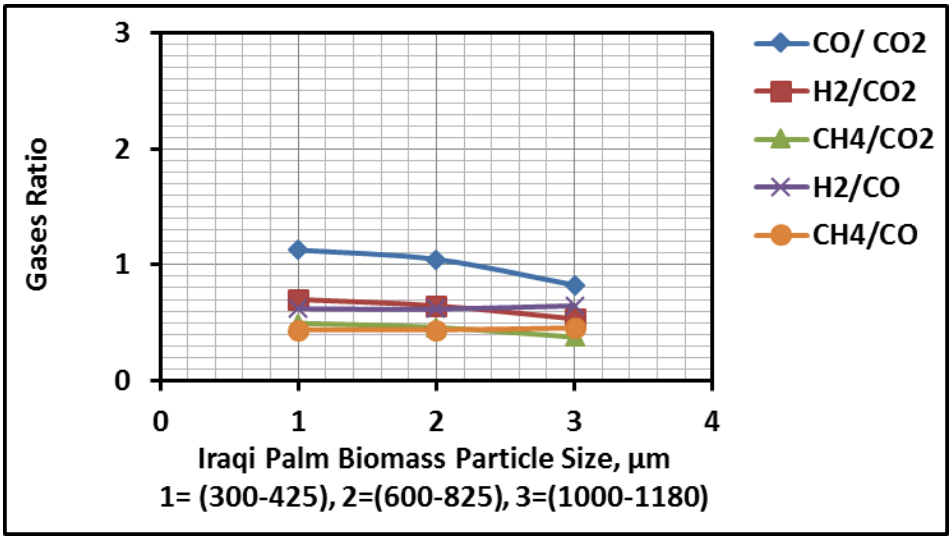

b) IDPWB

Figure 7. 20 Effect of particle size of the biomass feedstock on gases ratio: a) for SPWB biomass material and b) for IDPWB biomass material.

7.2.4.5 Effect of the bed static height *H*s

Table 7. 6 Operating conditions for static bed height parameter experimental tests:

a) For SPWB

Operating Parameters	Static Bed Height H_s, cm		
	4.15=0.5D	**6.225=0.75D**	**8.3=1D**
1- Air Flowrate l/min (kg/hr)	44 (3.18)	44 (3.18)	44 (3.18)
2- Reaction Bed Temperature T2, ºC	360	360	360
3- Bed Material (Sand) Particle Size, µm	300-425	300-425	300-425
4- Biomass solid Fuel Particle Size, µm	600-850	600-850	600-850
5- Equivalence Ratio ER	0.42	0.42	0.42
6- Mass Rate of biomass Feeding, kg/hr	1.192	1.192	1.192
7- $(MAFR)_{stoichiometric}$ For SPWB	6.2	6.2	6.2
8- Air superficial velocity U_o, cm/sec	13.56	13.56	13.56

b) For IDPWB

Operating Parameters	Static Bed Height H_s, cm		
	4.15=0.5D	**6.225=0.75D**	**8.3=1D**
1- Air Flowrate l/min (kg/hr)	44 (3.18)	44 (3.18)	44 (3.18)
2- Reaction Bed Temperature T2, ºC	360	360	360
3- Bed Material (Sand) Particle Size, µm	300-425	300-425	300-425
4- Biomass solid Fuel Particle Size, µm	600-850	600-850	600-850
5- Equivalence Ratio ER	0.381	0.381	0.381
6- Mass Rate of biomass Feeding, kg/hr	1.315	1.315	1.315
7- $(MAFR)_{stoichiometric}$ For IDPWB	6.352	6.352	6.352
8- Air superficial velocity U_o, cm/sec	13.56	13.56	13.56

(a) Producer gas composition (PGC) for two biomass materials

According to the operating conditions, which have been shown in Table 7.6 (a) and (b), Figure 7.21 (a) and (b) presents the influence of the static bed height on the producer gas composition for two biomass SPWB and IDPWB, respectively. Three static bed height *Hs* were used: 4.15cm, 6.225cm and 8.3cm, which correspond to *Hs/D* ratio: 0.5, 0.75 and 1, respectively, where *D* is the bed diameter=8.3cm. From Figure 7.21 (a) and (b) for SPWB, it can be seen that the effect on producer gas composition was as follows: the trends of production CO, H_2 and CH_4 are similar. Their lowest composition was at H_s = 4.15cm, whereas the highest was at H_s = 6.225cm. CO_2 stayed constant along H_s range. In addition, the sequence of the gas composition is CO> H_2> CO_2> CH_4 for all H_s range. For IDPWB the trend of the gases is different, CO decreased steadily while H_2 increased steadily along *H*s range. Whereas CO_2 and CH_4 stayed constant. The sequence of the gases at H_s = 4.15cm is CO> CO_2> H_2 >CH_4, whereas at H_s = 8.3cm the sequence is CO_2> CO> H_2 > CH_4.

There are several possible explanation for these results. The observed low value of the gas composition of CO, H_2, CH_4 and O_2 at the bed height 4.15cm for both biomass materials compared to other heights, except CO for IDPWB was higher, might be attributed to the biomass feeding position. For this bed height, 0.5D= 4.15cm, the biomass feeding was on-bed, the biomass was fed directly on the bed surface, unlike other two heights where the feeding was in-bed, 2.075cm under the bed surface for the bed height 0.75D=6.225cm and under 4.15cm for the bed height 1D=8.3cm. In both cases, the feeding position was at 0.5D= 4.15cm above distributor plate. In-bed feeding gives an actual fluidisation and thereby results in robust mixing and sufficient contact of the biomass with bed particles enhancing the devolatization, gasification tar cracking and reforming reactions and therefore increasing the conversion efficiency (Wilk et al. 2013) (Rapagnà et al. 2008).

For CO_2 gas this constant concentration for both biomass materials might be attributed to the abundant availability of O_2 at the bottom of the bed height due to a small size and low rise velocity of bubbles (Ross et al. 2007). In addition, the diffusion of the oxygen from the bubbles , especially at the higher bed position is low (Basu 2006), so it might be the same amount of CO_2 was produced due to the combustion reactions R2.3 and R2,4. The bed height also affects the residence time of the produced gases in the dense bed, where for a specific fluidisation flowrate a longer residence time could be achieved by increasing the bed height, which subsequently enhances the cracking reactions of tar and hydrocarbons (Xiao et al. 2007).

For H_2 gas, the bed length 0.75D and 1D improved H_2 production comparing to 0.5D bed length. This might be due to the feeding position, where for the later length there was no residence time for reactions inside the bed due to direct biomass feeding to the bed surface. At the same time the thermal cracking of the tar was not effective at this bed height to produce enough hydrogen (Sudipta 2013). For the 1D bed height, although it has longer residence time than 0.75D length, there is no high difference in composition of H_2. This is might be due to the negative bubble effects at higher bed heights. In addition, it could be said that there was no high difference in the residence time of the two lengths, 0.75D and 1D. For CH_4 gas for both biomass, there was a small effect of the bed height, especially at 0.75D and 1D heights. The low value of CH_4 at 0.5D height it might be attributed to the position of the feeding point position, as has been explained above, where there was a poor hydrogen gasification reaction R11 due to a lower amount of H_2 and carbon. In addition, it can be observed that production of

CH_4 from IDPWB was higher than SPWB. This it might be due to the difference in their physical and chemical properties. For O_2 gas it can be seen a high consuming at 0.5D height for IDPWB. This might be due to high partial oxidation of exothermic reactions as shown in high CO production.

In overall, for this range of bed height the results show that the effect of the bed height on producer gas composition is not highly significant.

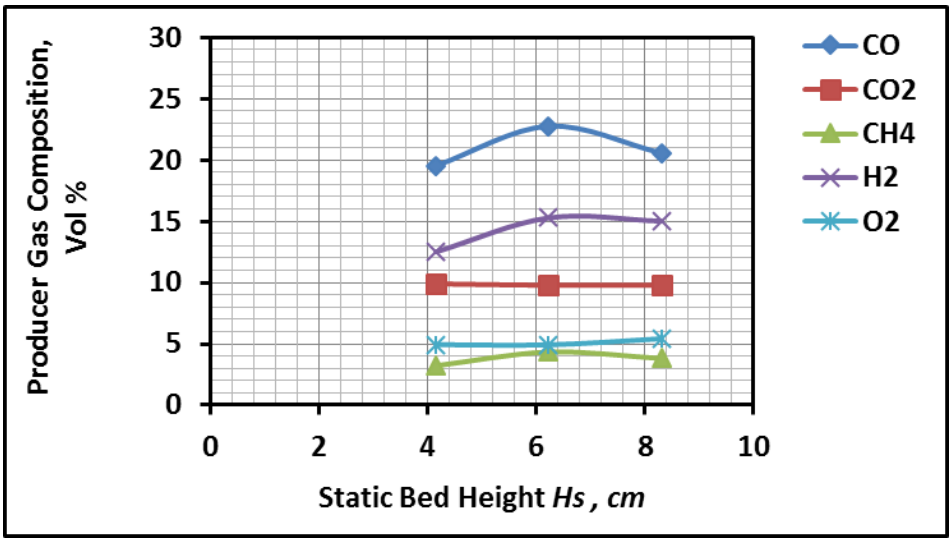

a) SPWB

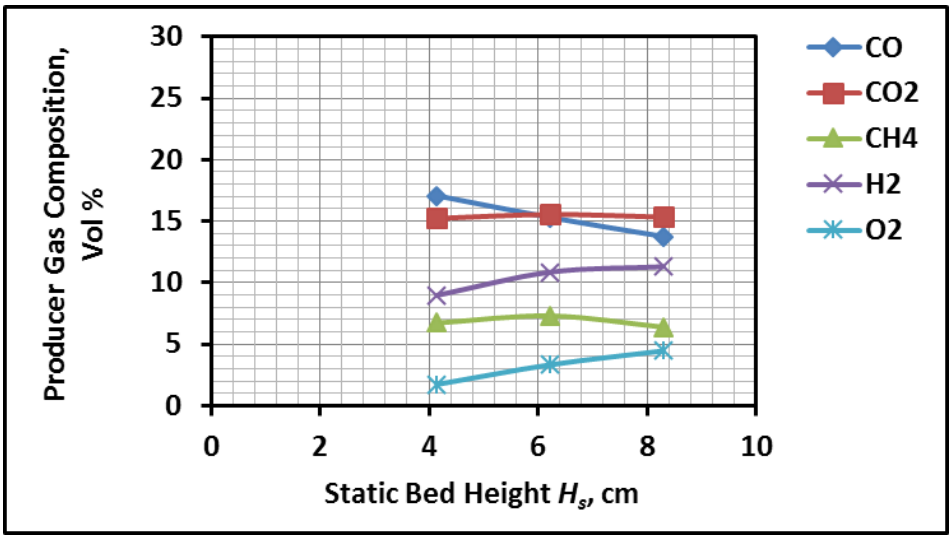

b) IDPWB

Figure 7. 21 Effect of the bed static height *Hs* on the producer gas composition (PGC): a) for SPWB biomass material and b) for IDPWB biomass material

(b) Carbon conversion efficiency, cold-gas efficiency, and producer gas heating value

Figure 7.22 (a) and (b) provides the effect of the static bed height Hs on the performance parameters for two biomass SPWB and IDPWB, respectively. It can be observed that the performance parameters CCE, LHV and CGE increased from 112% to 148%, 4.71

to 5.76 MJ/Nm^3 db and 81% to 114% for SPWB, while from 142% to 147%, 5.24 to 5.42MJ/Nm^3 db and 84% to 91% for IDPWB as bed height increased from 0.5D to 0.75D, respectively. For bed height increasing from 0.75D to 1D the results show decreasing in CCE, LHV and CGE to 130%, 5.29MJ/Nm^3 db, respectively and 100% for SPWB, while to 134%, 4.97MJ/Nm^3 db and 82% for IDPWB, respectively.

These results might be possibly explained that the observed increasing and decreasing of these performance parameters along the three bed heights can be linked to the increasing and decreasing of CO, CO_2, H_2 and CH_4 concentration in producer gas, as revealed in Figure 7.21-(a) and (b), as discussed in previous section. As has been shown in the calculation procedure for CCE, LHV and CGE in Chapter 5-Section 5.8.6, the gases CO, CO_2, and CH_4 represent the carbon conversion in producer gas, whereas the gases CO, H_2 and CH_4 represent the chemical energy conversion, LHV and CGE, where each of them has a specific heating value. Therefore, from the Figure, it can be found that for SPWP, in all cases, the performance parameters for two bed heights 0.75D and 1D were higher than for 0.5D. This might be due to the position of the feeding point, which for 0.5D the feeding was on–bed, whereas for the others was in-bed. This difference mainly affected the residence time and bed hydrodynamic behaviour. However, for the other bed heights the difference may be mainly affected by the bed hydrodynamic conditions due to the creation of larger volume bubbles in the higher bed height. The larger bubble size produce a faster bubble velocity and a less gas-solid contact time (Van Den Enden and Lora 2004) and (Xiao et al. 2007). At the same time the maximum values of those three performance parameters was obtained at 0.75D. The same finding was also obtained for IDPWB, 0.75D height has a maximum values, but the two heights, 0.5D and 1D, were in competition.

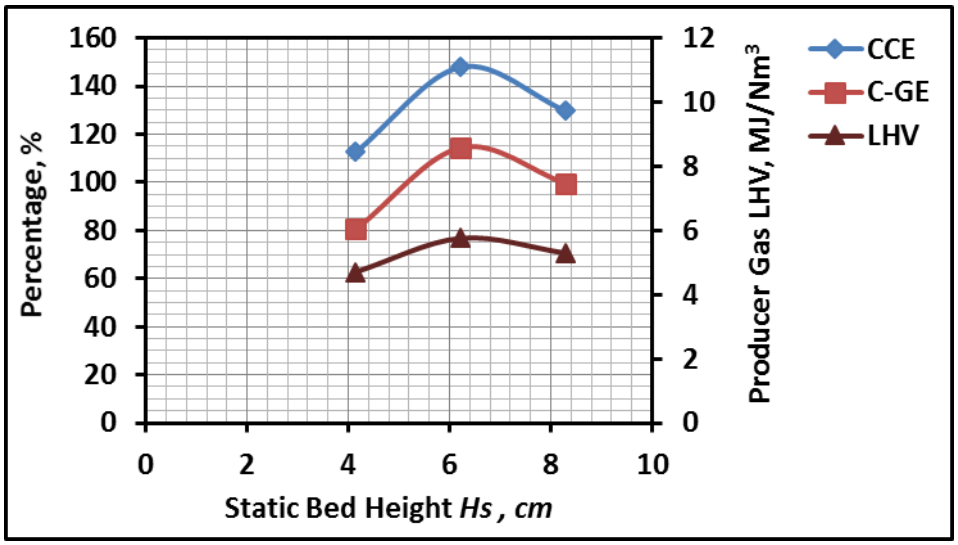

a) SPWB

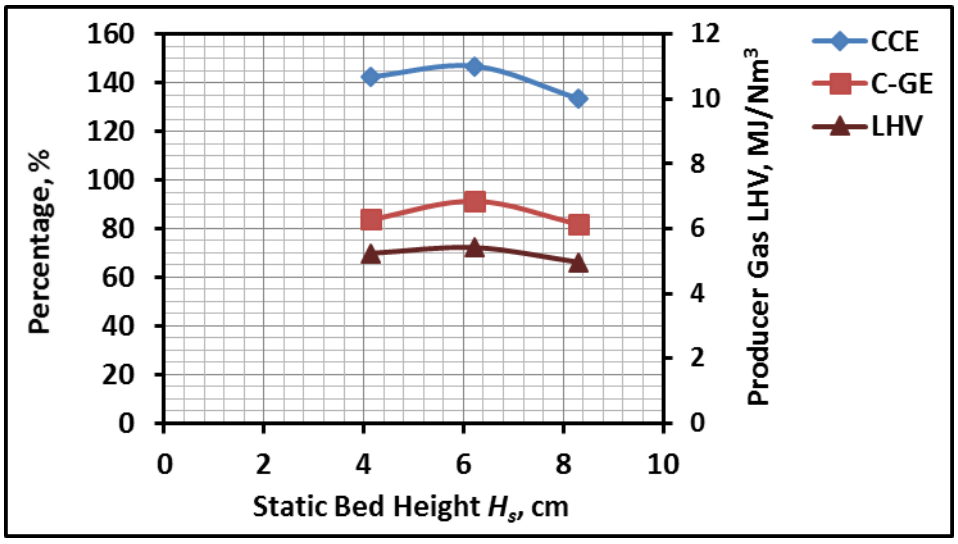

b) IDPWB

Figure 7. 22 Effect of the bed static height *Hs* on CCE, CGE and LHV performance parameters: a) for SPWB biomass material and b) for IDPWB biomass material

(c) Gases Ratios

Figure 7.23 (a) and (b) provides the effect of the bed height on the gases ratio for two biomass materials. It can be shown that SPWB implemented maximum CO/CO_2, 2.3, at 0.75D bed height and decreased to 2.1 at 1D. H_2/CO_2 was increased from 1.25 at 0.5D and approximately levelled off at ratio=1.5 at 0.75D and 1D. H_2/CO increased slightly along the bed height from 0.62 to 0.7. A slight increase for CH_4/CO_2 ratio from 0.3 to 0.4 at 0.75D and then a little decrease to 0.35 at 1D was observed. CH_4/CO remained constant at 0.18 along the bed height. For IDPWB Figure (b) shows mostly low gas ratio, less than one. CO/CO_2 ratio decreased gradually along the range of bed

height from 1.7 to 0.9, H_2/CO increased gradually from 0.5 to 0.8, H_2/CO_2 increased slightly from 0.55 at 0.5D and then levelled off at 0.7 and CH_4/CO and CH_4/CO_2 ratios show approximately identical and constant trend along the bed height range at 0.2. The possible explanation for these results can be linked to the composition distribution for the gases CO, CO_2, H_2 and CH_4, which has been explained in Section 7.2.4.5-(a)**.** A further observation that can be obtained from the Figure is higher CO/CO_2 and H_2/CO_2 ratios for SPWB than IDPWB, whereas for H_2/CO ratio was approximately the same. Overall, for this range of bed height it can be concluded that there is no high significant effect, especially at 0.75D and 1D due to their position feeding point under bed surface. The ratio of H_2/CO is differently affected by the operating parameters in the gasification processes. In order to this, the ratio of H_2/CO has been selected as a benchmark of efficiency to evaluate the purpose of applying produced syngas in methanol synthesis process. In addition, the ratio of CO/CO_2 is selected as a scale to measure the efficiency of the process and to contemplate the competition of the gasification/combustion, (Ravaghi-ardebili et al. 2014).

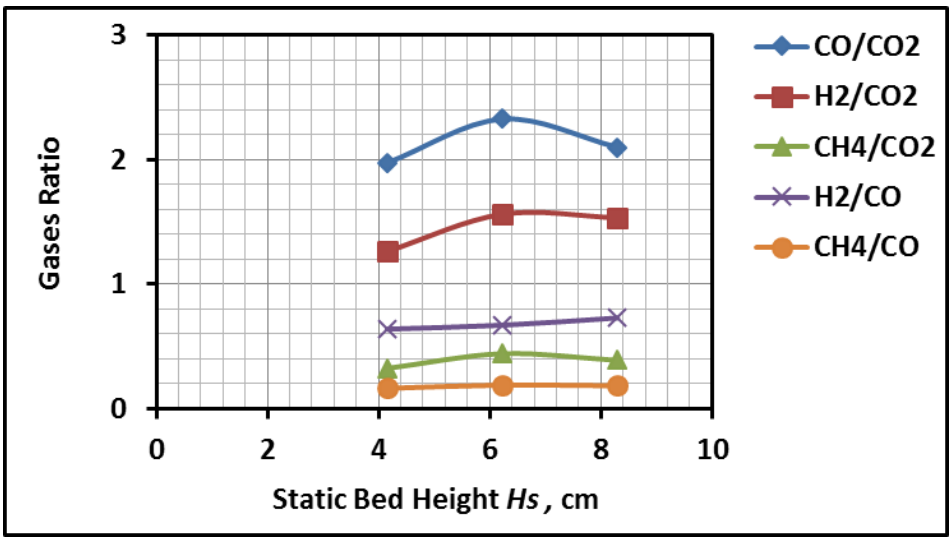

a) SPWB

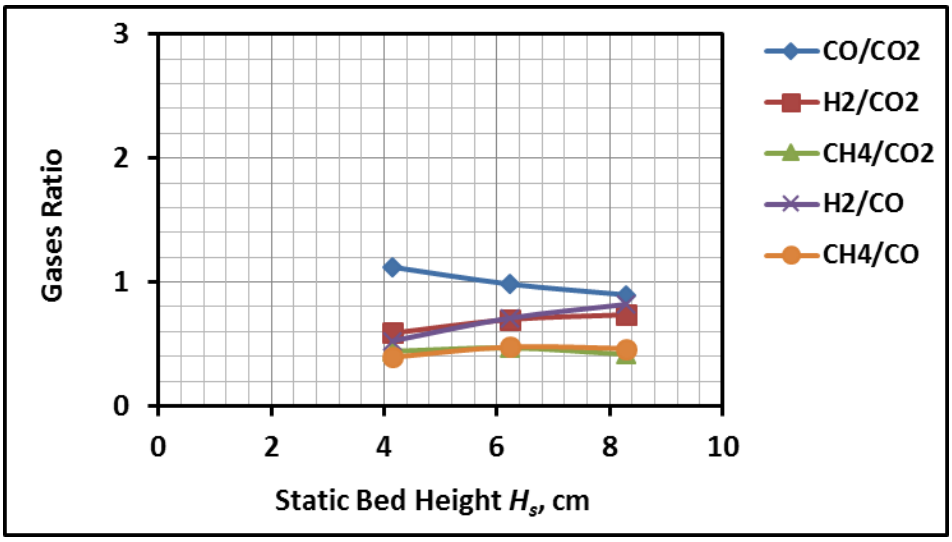

b) IDPWB

Figure 7. 23 Effect of the bed static height *Hs* on the gas ratio: a) for SPWB biomass material and b) for IDPWB biomass material.

(d) Producer gas yield (GY)

Figure 7.24 (a) and (b) highlights the effect of the static bed height on the gases yield for two biomass materials. It can be observed that for SPWB, the total gas yield was increased significantly from 3.18 to 3.8Nm^3/kg feed db as bed height increased from 0.5D to 0.75D and then decreased moderately to 3.7Nm^3/kg feed db at 1D bed height. For IDPWB the total gas yield was increased slightly from 2.9 to 3.1Nm^3/kg feed db as bed height increased from 0.5D to 0.75D and then approximately levelled off at 3Nm^3/kg feed db at 1D bed height. Furthermore, the gas yield observation for each gas along the three bed heights was as follows: For SPWB, the maximum yield was for CO= 0.84 at 0.75D, H_2= 0.6 at 0.75D, CH_4=0.16, CO_2 and N_2 approximately stayed constant on 0.35 and 1.59Nm^3/kg feed db along bed height interval, respectively. For IDPWB the gas yield for each gas was; CO and CO_2 approximately stayed constant at=0.47, H_2 and O_2 increased slightly from 0.26 to 0.34 and from 0.05 to 0.13, respectively, CH_4 approximately stayed constant at 0.2 Nm^3/kg feed db and N_2 stayed constant on 1.46Nm^3/kg feed db.

As discussed before the yield results completely depend on the producer gas composition. In general, from the Figures (a) and (b) it can be seen that SPWB achieved gases yield higher than IDPWB. This can be linked to the higher gas composition as has shown in Figure 7.21 (a) and (b) and discussed in Section 7.2.4.5-(a).

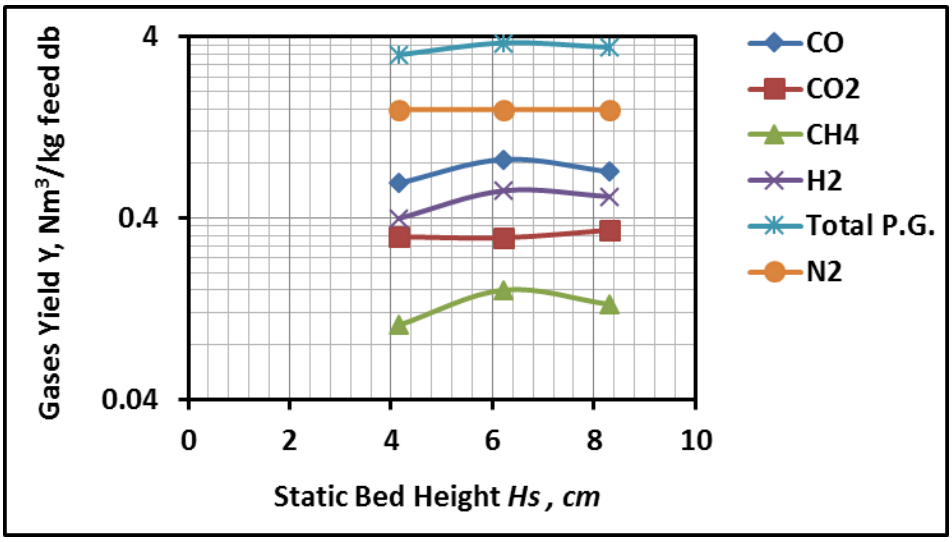

a) SPWB

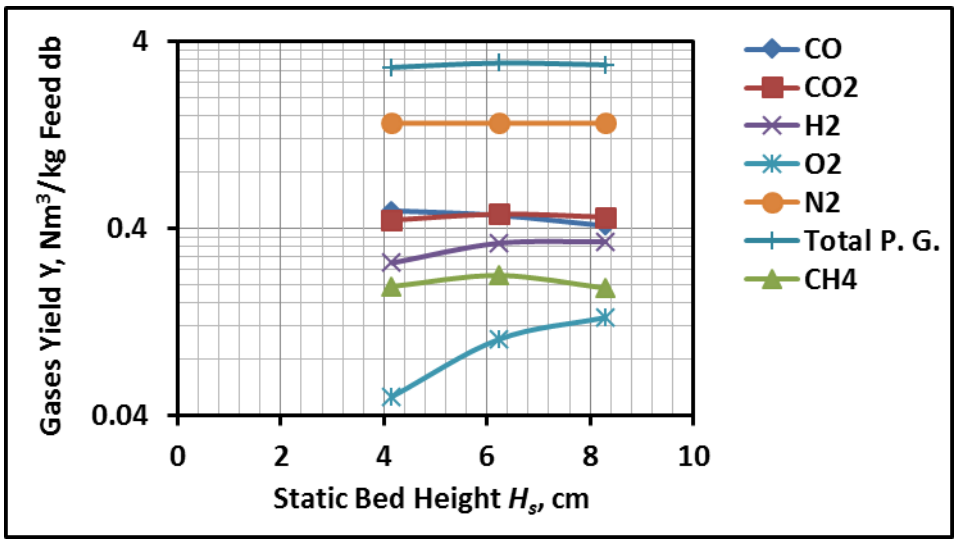

b) IDPWB

Figure 7. 24 Effect of static bed height Hs on gases yield (GY): a) for SPWB biomass material and b) for IDPWB biomass material

7.2.4.6 Effect of the equivalence ratio

Table 7. 7 Operating conditions for equivalence ratio parameter experimental tests

a) For SPWB

Operating Parameters	Equivalence Ratio ER			
	0.2	**0.31**	**0.5**	**0.55**
1- Air Flowrate l/min (kg/hr)	30 (2.17)	30 (2.17)	30 (2.17)	30 (2.17)
2- Reaction Bed Temperature T2, ^{o}C	360	360	360	360
3- Bed Material (Sand) Particle Size, µm	300-425	300-425	300-425	300-425
4- Biomass solid Fuel Particle Size, µm	600-850	600-850	600-850	600-850
5- Static Bed Height Hs, cm	6.225	6.225	6.225	6.225
6- Mass Rate of biomass Feeding, kg/hr	1.74	1.14	0.7	0.64
7- $(MAFR)_{stoichiometric}$ For SPWB	6.2	6.2	6.2	6.2
8- Air superficial velocity U_o, cm/sec	9.25	9.25	9.25	9.25

b) For IDPWB

Operating Parameters	Equivalence Ratio ER			
	0.2	**0.277**	**0.381**	**0.45**
1- Air Flowrate l/min (kg/hr)	44 (3.18)	44 (3.18)	44 (3.18)	44 (3.18)
2- Reaction Bed Temperature T2, ^{o}C	360	360	360	360
3- Bed Material (Sand) Particle Size, µm	300-425	300-425	300-425	300-425
4- Biomass solid Fuel Particle Size, µm	600-850	600-850	600-850	600-850
5- Static Bed Height Hs, cm	6.225	6.225	6.225	6.225
6- Mass Rate of biomass Feeding, kg/hr	2.5	1.81	1.32	1.11
7- $(MAFR)_{stoichiometric}$ For IDPWB	6.352	6.352	6.352	6.352
8- Air superficial velocity U_o, cm/sec	13.56	13.56	13.56	13.56

(a) Producer Gas Composition for Two Biomass Materials

According to the operating conditions which have been shown in Table 7.7 (a) and (b), the results of the effect of ER on the producer gas composition is revealed in Figure 7.25-(a) and (b) for both biomass feedstock SPWB and IDPWB, respectively. ER was changed by changing biomass feed rate at a fixed air flowrate. For SPWB it can be seen that as ER increased in the interval of from 0.2 to 0.31 all producer gases, CO, H_2, CO_2 and CH_4 were decreases from 22% to 18%, 16% to 12%, 8.8 to 7% and 5.8% to 3.5%, respectively. Thereafter, as ER increased in the interval of from 0.31 to 0.55 the gases increased to 22.5%, 16.7%, 10.8% and 4.4% respectively, whereas O_2 increased from 7.2% to 9.8% and then decreased to 3.5%.

For IDPWB the trend of the producer gas composition in ER interval (0.31-0.55) is different compared to SPWB. It can be seen that as ER increased in the interval (0.2 to 0.277) CO, CO_2, H_2 and CH_4 were decreased from 16.5% to 13.5%, 14.7% to 12.8%, 9.6% to 8.2% and 7.7 to 6.1%, respectively, whereas O_2 remained constant at 6.6%. For

increase ER in interval (0.227 to 0.38), the gases were constant, respectively, while O_2 decreased to 5.6%. For the last interval (0.38 to 0.45) as ER increased the gases decreased again from 12.9% to 11.2%, 13.3% to 12.3%, 8.5% to 7.1% and 6.1 to 4.8%, respectively, while O_2 increased a little to 6.2%. For this biomass, the trend of the results are agree with the results of Hg et al. (2016) for sawdust and pigeon pea biomass air gasification for ER interval (0.35 to 0.61) for the former and (0.38 to 0.68) for the latter. In addition, for ER range (0.21 to 0.32), which was studied for the same principle of this study by changing fuel and keeping constant airflow rate, at 770^{o}C. The results of the researchers (Lahijani and Zainal 2011) are in agreement with this study results for the producer gas composition for both biomass material except the CO_2 trend, which increased for all their ER ranges.

There are several explanations for these results. The high gas concentration for both biomass materials at ER= 0.2 compared to others ER, especially for IDPWB, might be attributed to the high amount of biomass fuel feeding for this ER. However, it can be expected that a high amount of volatile matter might be released inside the bed, reaction R2.1, and with partial oxidation environment exothermic homogenous reactions occur producing a high amount of the CO and H_2 compared to CO_2 and CH_4, according to reactions R2.1, R2.2-R2.6. Also within these conditions, the water gas shift reaction R2.8 occurs due to H_2O releasing by R2.5. Furthermore, the high temperature, up to 900^{o}C in the freeboard, and long residence time inside the freeboard section are high enough for tar and high hydrocarbon thermal cracking and homogenous gas reactions, secondary tar reactions, which are indicated by the increase in levels of CO, H_2 and CH_4 (Sudipta 2013) and (W.A.W.K. Ghani1, 2*, R.A. Moghadam1, M.A.M. Salleh1, 2 2012). The gas concentrations, which were released by SPWB, were higher than IPDWB. This is may be because of the high volatile matter of the former biomass as shown in Table 4.4. In addition, the air flowrate, which was used for SPWB was lower than air flowrate for IDPWB, 30l/min for the former and 44l/min for the latter. This low flowrate increased the residence time in the bed and freeboard sections. Also the difference in the chemical composition of each component of lignocellulosic (cellulose, hemicelluloses and lignin) biomass might affect the devolatilisation rates (Chhiti and Kemiha 2013).

For SPWB, the amount of produced CO_2 was much less than H_2 and CO for all investigated ER values. This may be attributed to the dry reforming endothermic reactions of high hydrocarbons, R2.14, in the freeboard section resulting in high

amounts of CO and H_2 and reduction of CO_2. Also, the endothermic Boudouard reaction R2.13 could be expected to enhance in the freeboard section due to the conditions and the availability of the entrained porous char in freeboard (Feng et al. 2011). This condition may also available for IDPWB. This due to the two exothermic reactions Methanation R2.12 and hydrogen gasification R2.11 producing CH_4 and the endothermic tar decomposition reaction that might be occurred in freeboard section (Ghani A.K. et al. 2009). This can be confirmed by the high concentration of CH_4 in producer gas for this ER value 0.2. Furthermore, it can be observed that CH_4 approximately stayed constant at ER interval (0.31-0.55) for SPWB. It can be attributed to the balance of CH_4 consumption, R2.10, and its generation, whereas for IDPWB CH_4 continuously declined at ER interval (0.227-0.45). Likewise, for this biomass the decreasing of biomass feeding along the ER interval may have a high contribution in the decrease of the producer gas composition due to their low volatile matter compared to SPWB.

On the hydrodynamic aspect, for these observed results, it can be interpreted that, according to the ER calculation method, ER was increased as biomass fuel decreased and thereby the mass fraction of the biomass was decreased. As shown in chapter 6, biomass fraction in the bed mixture affect the fluidisation quality, where the bubble phase characteristics affect the particle mixing and segregation in the fluidised bed reactor and thereby affects the performance of the biomass gasifier (Fotovat et al. 2015)**.** Increasing biomass mass fraction is driving to create more homogenous distribution of small bubbles across the bed cross –section leading to improve fluidisation quality and thereby improving gasification performance (Fotovat et al. 2013). According to their fluidisability, the low performance of IDPWB compared to SPWB might be attributed to the higher irregularity in shape and higher aspect ratios of IDPWB particles (refer to Chapter 6).

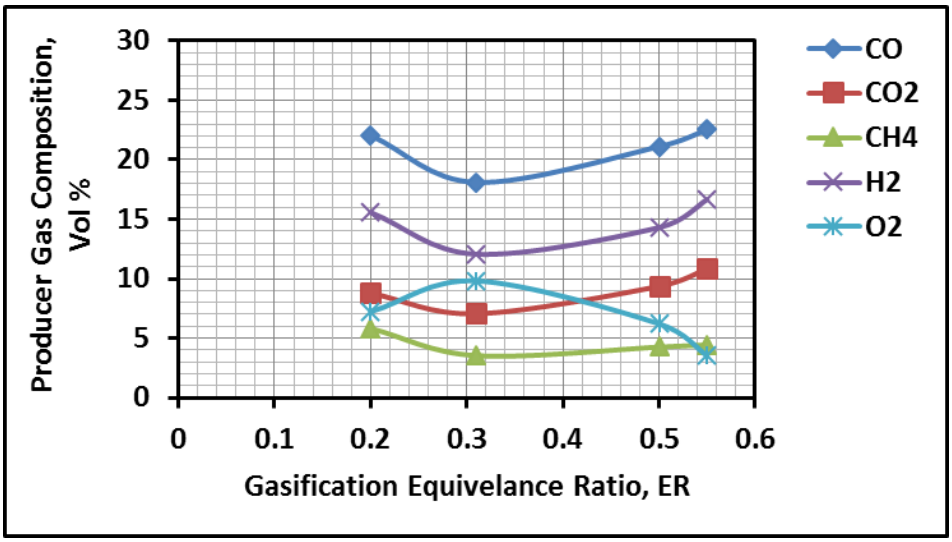

a) SPWB

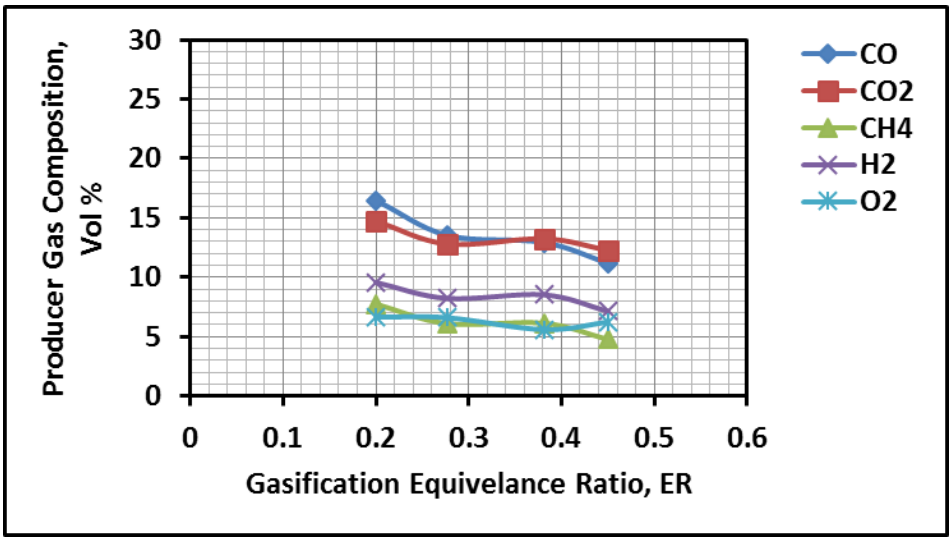

b) IDPWB

Figure 7. 25 Effect of the air ER on the producer gas composition (PGC): a) For SPWB biomass material and b) For IDPWB biomass material

(b) Carbon conversion efficiency, cold-gas efficiency, and producer gas heating value

The effect of the air ER on the performance parameters for two biomass SPWB and IDPWB is provided in Figure 7.26 (a) and (b), respectively. For SPWB, it can be observed that the performance parameters CCE, CGE and LHV were slightly decreased: from 74% to 72%, 60% to 55.7% and 6.2 to 4.6 MJ/Nm^3 db, respectively, as ER increased from 0.2 to 0.31. Whereas, for ER interval (0.31 to 0.55) the performance parameters increased significantly to, 199%, 149%, respectively, except LHV which

increased slightly to 5.9MJ/Nm^{3}db. This increasing can be linked to the increase in combustible gases CO, H_2 and CH_4, in this ER interval, as shown in Figure 7.25-(a).

For IDPWB, as shown in Figure 7.25-(b), in general the average trend was similar compared to SPWB for ER range from 0.2 to 0.381. It can be observed that the performance parameters CCE, CGE and LHV slightly decreased: from 83.9% to 82.1%, 52.6% to 50.2% and 5.6 to 4.5 MJ/Nm^3 db, respectively, as ER increased from 0.2 to 0.277. Whereas CCE and CGE increased gradually to 110.7% and 67.5%, respectively and LHV stayed constant as ER increased to 0.381. Finally, all parameters decreased gradually to 104.8%, 60% and 3.7 MJ/Nm^3, respectively as ER increased to 0.43.

As discussed before, for both biomass materials CCE is a result of carbon conversion, mainly to CO, CO_2 and CH_4. Hence, it was affected significantly by their composition in the producer gas as shown in previous section. For heating value LHV and CGE, it can be observed that the heating value is highly affected by the composition of the combustible gases, mainly CO, H_2 and CH_4.

Finally, it can be seen that for the ER range (from 0.2 to 0.43) the gasifier performance is approximately similar for both feed stock biomass materials SPWB and IDPWB.

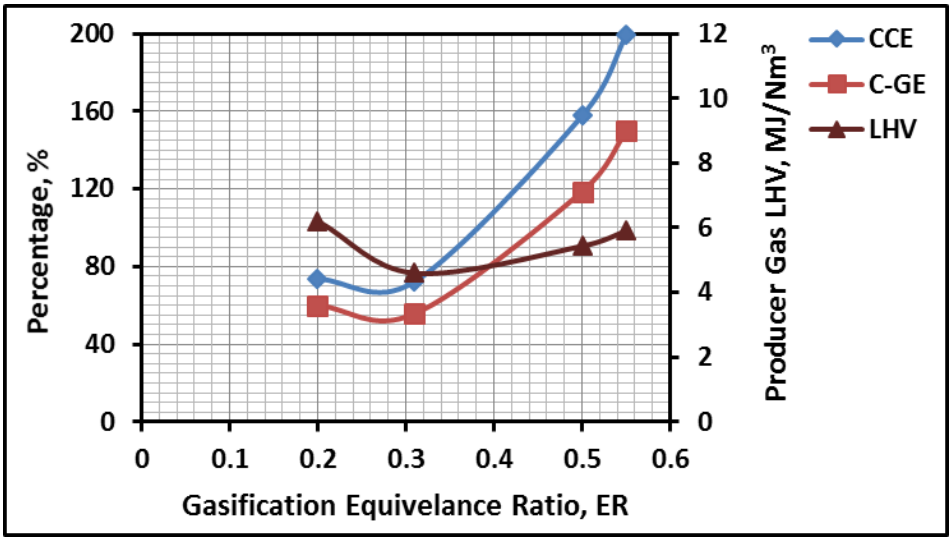

a) SPWB

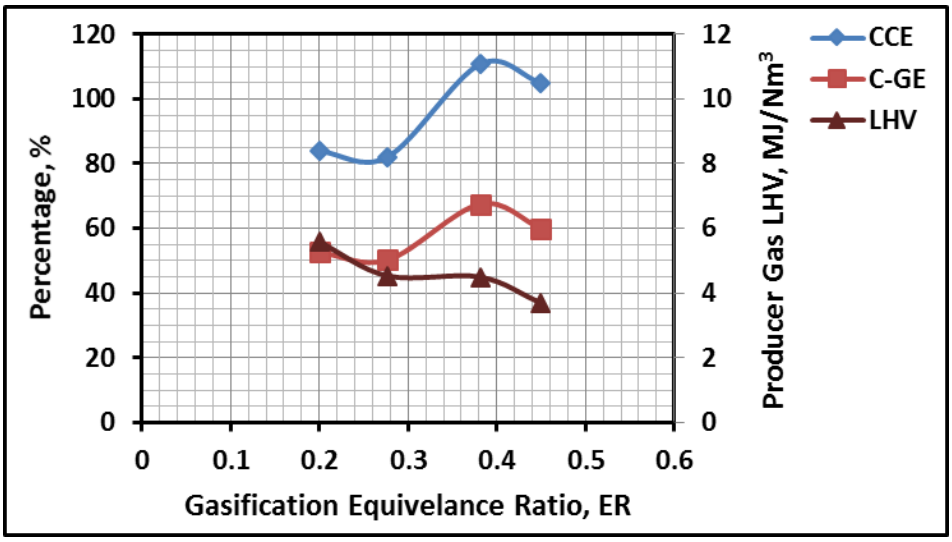

b) IDPWB

Figure 7. 26 Effect of the ER on the CCE, CGE and LHV performance parameters: a) For SPWB biomass material and b) For IDPWB biomass material

(c) Gases ratios

Figure 7.27-(a) and (b) provides the effect of ER on the gases ratio for two biomass materials. It can be shown that for SPWB as ER increased, for its entire interval, the ratios CO/CO_2, H_2/CO_2 and CH_4/CO_2 decreased gradually from 2.5 to 2.1, 1.8 to 1.5 and 0.7 to 0.4, respectively. This can be attributed to high partial oxidation atmosphere at low ER and high oxidation at high ER values leading to rise in CO_2 concentration. H_2/CO ratio revealed approximately constant value= 0.7 at ER interval 0.2-0.5 and increased a little to 0.74 at ER= 0.55. CH_4/CO approximately stayed constant at ER=0.2. For IDPWB Figure 7.26 (b) shows mostly low, gas ratio, less than one. CO/CO_2 ratio decreased gradually from 1.12 to 0.9 along the interval of ER (0.2-0.45), whereas ER did not affect the rest ratios in the interval (0.2-0.38), but they decreased slightly for ER interval (0.38-0.45). This indicates that oxidation reactions are to some extent active at higher ER due to the availability of O_2 compared to the feed fuel(Mohammed et al. 2011).

Overall, it can be concluded that SPWB provided higher CO/CO_2 and H_2/CO_2 and a slightly higher H_2/CO ratio than IDPWB. Furthermore, ratios indicated that the producer gas is rich in combustible gases at low equivalence ratio than high ER.

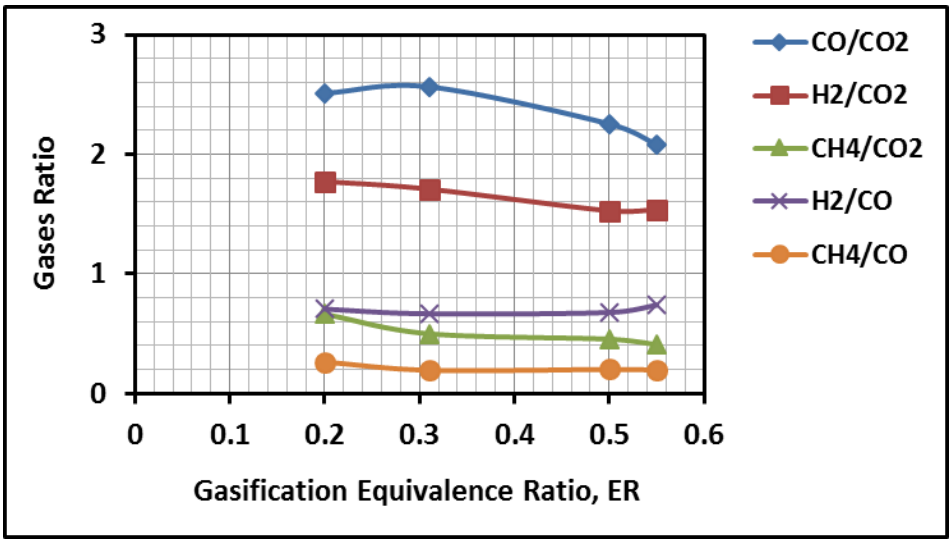

a) SPWB

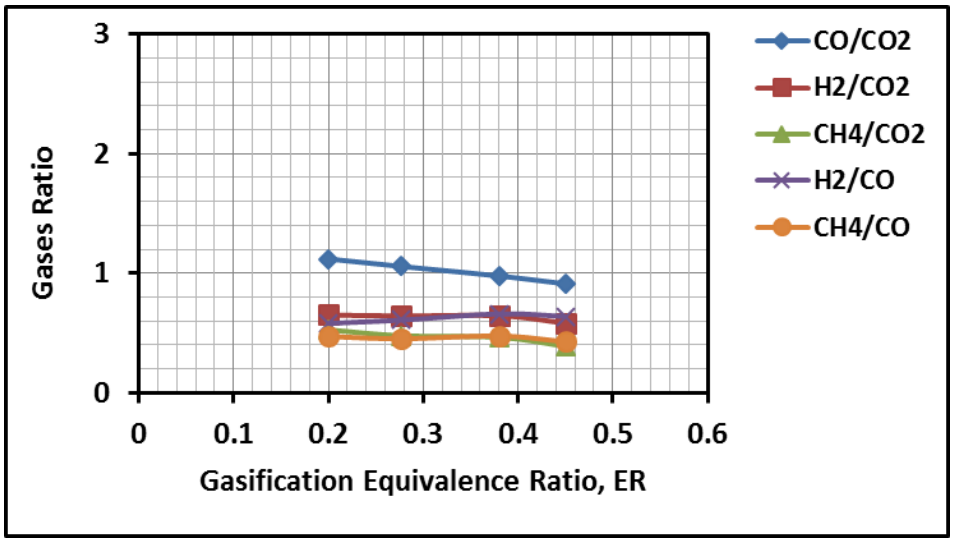

b) IDPWB

Figure 7. 27 Effect of the air ER on the gas ratio: a) For SPWB biomass material and b) For IDPWB biomass material

(d) Producer gas yield (GY)

Figure 7.28-(a) and (b) displays the effect of the Equivalence Ratio ER on the gases yield for two biomass materials. It can be observed that for SPWB, the total gas yield increased exponentially from 1.85 to 4.86Nm^3/kg feed db as ER increased from 0.2 to 0.55. For IDPWB the total gas yield increased gradually from 1.7 to 2.95Nm^3/kg feed db. This finding is in agreement with the previous finding published by(Ramin Radmanesh, Jamal Chaouki 2006) and the results reported by(Lahijani and Zainal

2011). In addition, for both biomass N_2 gas yield increased linearly as ER increased along the range. For SPWB, it increased from 0.75 to 2.04Nm^3/kg feed db where for IDPWB increased from0.77 to 1.73Nm^3/kg feed db. This is due to, as it has been shown in Chapter 5-Section 5.8.6, that mass of input N_2 was equal to mass of output. In addition, for this ER interval and for constant air flowrate the biomass mass rate must decrease as ER increased to achieve a required ER. Therefore, the net result of N_2 yield in Nm^3/kg feed db led to increase as ER increased.

Furthermore, the gas yield observation for each individual gas along the ER range was as follows. For SPWB, as shown in Figure 7.28-(a), in general, there was a gradual increase for CO from 0.41 to 1.1, H_2 from 0.3 to 0.8 and CO_2 from 0.16 to 0.52, CH_4 from 0.11 to 0.22Nm^3/kg feed db along ER range (from 0.2 to 0.55). For IDPWB, as shown in Figure 7.28-(b), in general a slight and an identical increase for CO, CO_2, H_2 and CH_4 from 0.28 to 0.33, 0.25 to 0.36, 0.16 to 0.21Nm^3/kg feed db, respectively, along ER range (from 0.2 to 0.43).

For these observed results it can be interpreted that the increase in gas yield GY can be linked to the resultant of the producer gas composition results, as shown in previous section, and to the calculations of the moles of N_2 gas in producer gas for each kg fuel feed, which decreased as ER increased.

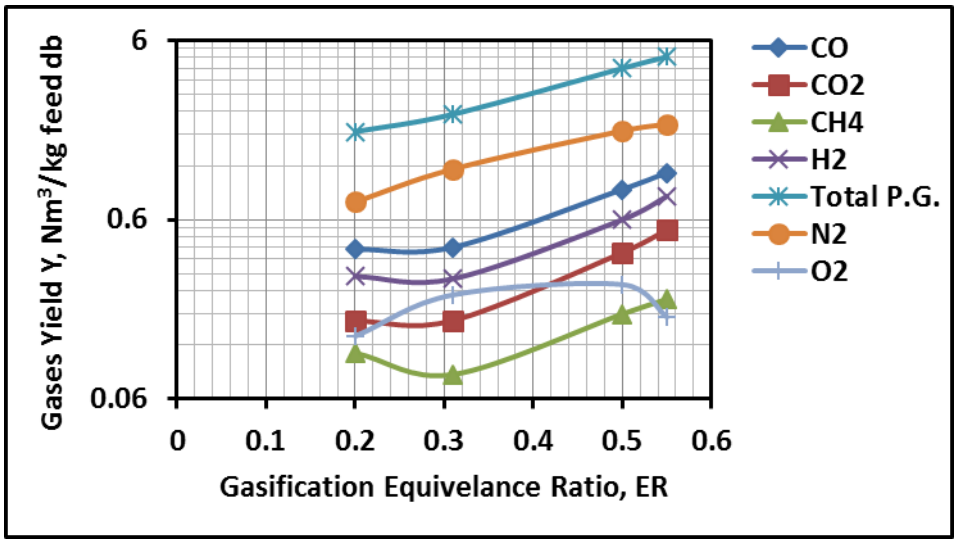

a) SPWB

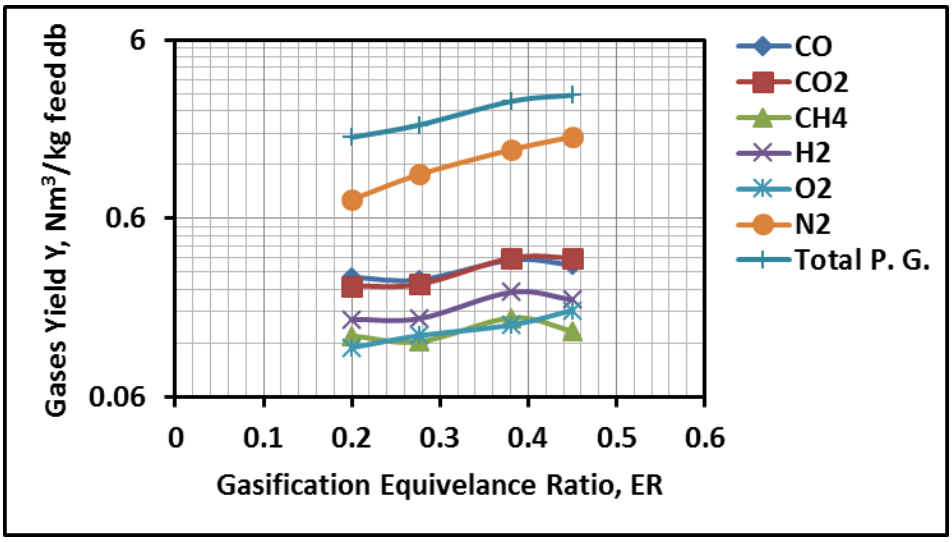

b) IDPWB

Figure 7. 28 Effect of the equivalence ratio ER on gas yield (GY): a) for SPWB biomass material and b) for IDPWB biomass material

7.2.4.7 Effect of the Bed Temperature T2

Table 7. 8 Operating conditions for bed temperature T2 parameter experimental tests:

a) For SPWB

Operating Parameters	**Bed Temperature T2, ºC**	
	360	**465**
1- Air Flowrate l/min	44 (3.18)	44 (3.18)
2- Equivalence Ratio ER	0.43	0.43
3- Bed Material (Sand) Particle Size, µm	300-425	300-425
4- Biomass solid Fuel Particle Size, µm	600-850	600-850
5- Static Bed Height Hs, cm	6.225	6.225
6- Mass Rate of biomass Feeding, kg/hr	1.192	1.192
7- $(MAFR)_{stoichiometric}$ For SPWB	6.2	6.2
8- Air superficial velocity U_o, cm/sec	13.56	13.56

b) For SPWB

Operating Parameters	**Bed Temperature T2, ºC**	
	360	**465**
1- Air Flowrate l/min (kg/hr)	44 (3.18)	44 (3.18)
2- Equivalence Ratio ER	0.381	0.381
3- Bed Material (Sand) Particle Size, µm	300-425	300-425
4- Biomass solid Fuel Particle Size, µm	600-850	600-850
5- Static Bed Height Hs, cm	6.225	6.225
6- Mass Rate of biomass Feeding, kg/hr	1.315	1.315
7- $(MAFR)_{stoichiometric}$ For IDPWB	6.352	6.352
8- Air superficial velocity U_o, cm/sec	13.56	13.56

(a) Producer gas composition for two biomass materials

According to the operating conditions, which have been shown in Table 7.8-(a) and (b), Figure 7.29-(a) and (b) presents the effect of the bed temperature T2 on the producer gas composition for two biomass materials for constant operating conditions. From the Figure, the results revealed that for both biomass the trend of this effect for all gases are similar, except O_2 gas, and CH_4 for SPWB only. The Figure 7.28 (a) shows that as the bed temperature increased from 360ºC to 465ºC the gases CO, H_2, CO_2 increased steadily from 22.5 to 23.8, 2 to 17, 10 to 11 vol %, respectively, whereas CH_4 remained constant at 4% and O_2 decreased slightly from 5 to 4 vol%. For IDPWB, Figure 7.28 (b) shows the gases CO, CO_2, H_2 and CH_4 increased steadily from 13.8% to 15.2%, from 14% to 15.78%, from 9.13% to 10.92%, and from 6.5% to 7.12%, respectively, whereas O_2 decreased from 4.54% to 3.97%. From the observed results it can be interpreted that there are three main factors which might play a role in producer gas composition.

The first factor is the bed temperature T2, which was low in this study. However, according to TGA analysis as shown in TGA Figure 4.15-Chapter 4 this temperature could enhance the release of the most of the volatile matter, which is a comparatively fast process. In addition, it can enhance the exothermic oxidation reaction, mainly partial oxidation with air gasification agent resulting in releasing higher amounts of CO than CO_2 and heat depending on the ER value (Gómez-barea et al. 2011).

The second factor is related to the bed hydrodynamics i.e. the fluidisation quality. The fuel particle position and the residence time, air flow rate, formation of the bubbles (their size and velocity), fuel particle size, and the heat homogeneity in the bed all affect the volatile and char mixing and then reaction with the surrounding gas by secondary reactions. On the other hand for the experiment operating conditions the low mass percent of the biomass, 2.68% at the end of 5 min feeding, inside the bed was not affected the minimum fluidisation velocity value and thereby not affected the fluidisation quality.

The third factor is the secondary conversion of tar and high hydrocarbons by thermal cracking under high temperature conditions. For this study this reaction can be expected due to high freeboard temperature T1=900ºC and enough residence time resulting in high quality of producer gas represented by high composition of combustible gases CO, H_2 and CH_4. High yield of H_2 gas could occur at thermal cracking and low equivalence

ratio conditions according to endothermic reactions R2.15 and R2.16 (Skoulou et al. 2008). In addition, endothermic reaction R2.14 confirm CO_2 reaction with tar and hydrocarbon, specifically in freeboard section, producing additional amount of H_2 and CO. CH_4 production is possibly due to the exothermic Methanation reaction R2.12 and tar cracking R2.15 in freeboard section Gómez-Barea & Leckner (2010). The heterogeneous gasification reactions, mainly char reaction Bouduard R2.13 and water gas R2.7 , inside the bed could occur due to low temperature inside the bed and their slow endothermic reactions (Basu 2006) (Gómez-barea et al. 2011). Overall, it can be concluded that the temperature either bed or freeboard has a significant effect on the producer gas quality, especially with a high bed fluidisation quality due to a heat homogeneity and uniform temperature distribution.

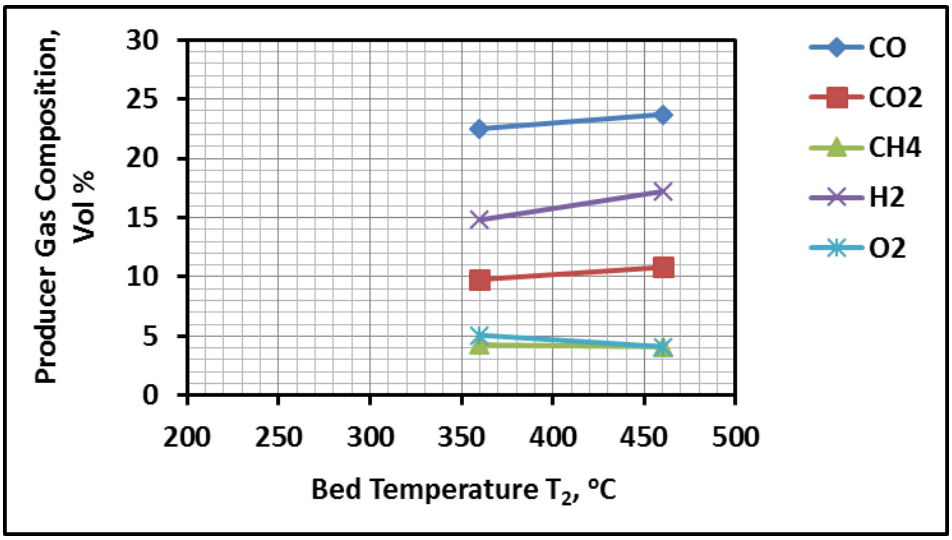

a) SPWB

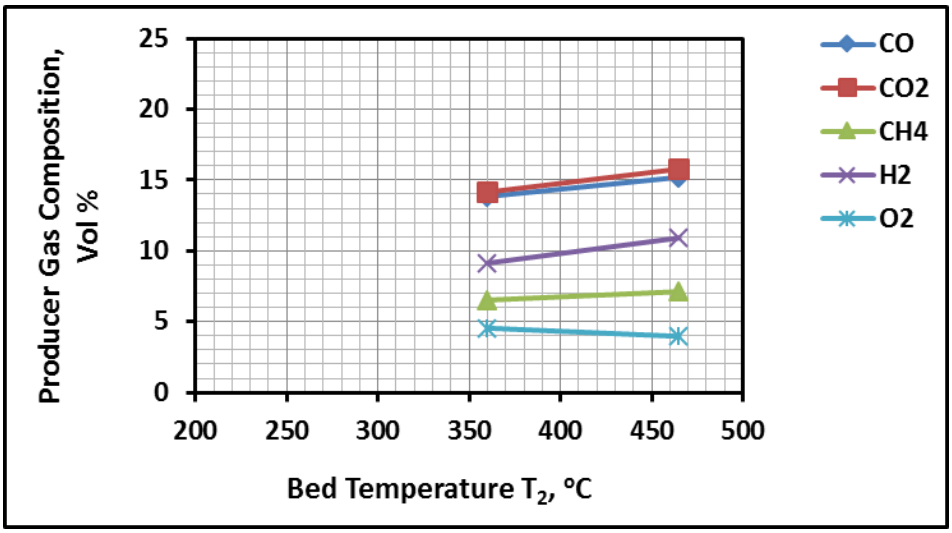

b) IDPWB

Figure 7. 29 Effect of the bed temperature T2 on the producer gas composition: a) for SPWB biomass material and b) for IDPWB biomass material

(b) Carbon conversion efficiency, cold-gas efficiency, and producer gas heating value

The effect of the bed temperature T2 on the performance parameters for two biomass SPWB and IDPWB is indicated in Figure 7.30-(a) and (b), respectively. It can be observed that the performance parameters CCE, LHV and CGE were increased positively as T2 increased from 360ºC to 465ºC, except CCE for SPWB, which decreased slightly from 148% to 145%, due to CH_4 decreased. As discussed before, CCE is a result of carbon conversion to CO, CO_2 and CH_4. Hence, it was affected significantly by their composition in the producer gas as shown in previous section. For heating value and CGE, it can be observed that for SPWB the LHV and CGE increased steadily from 5.66 to 6MJ/Nm^3db and from 107% to 125%, respectively. This higher heating value is due to the high composition of the combustible gases CO, H_2 and CH_4. This producer gas can be classified within a medium LHV level, according to the classification has been shown in Table 2.4, which is suitable for further utilization in internal combustion engines (ICE), turbines for power production and for the chemical formation of methanol and methane (Skoulou et al. 2008).

For IDPWB the producer gas CCE, LHV and CGE increased steadily from 122.3% t0 145.8 %, from 4.8 to 5.4MJ/Nm^3 db and from 75% to 90%, respectively.

Finally, it can be seen that the higher gasifier performance can be achieved by using SPWB as a fuel feedstock biomass compared to IDPWB.

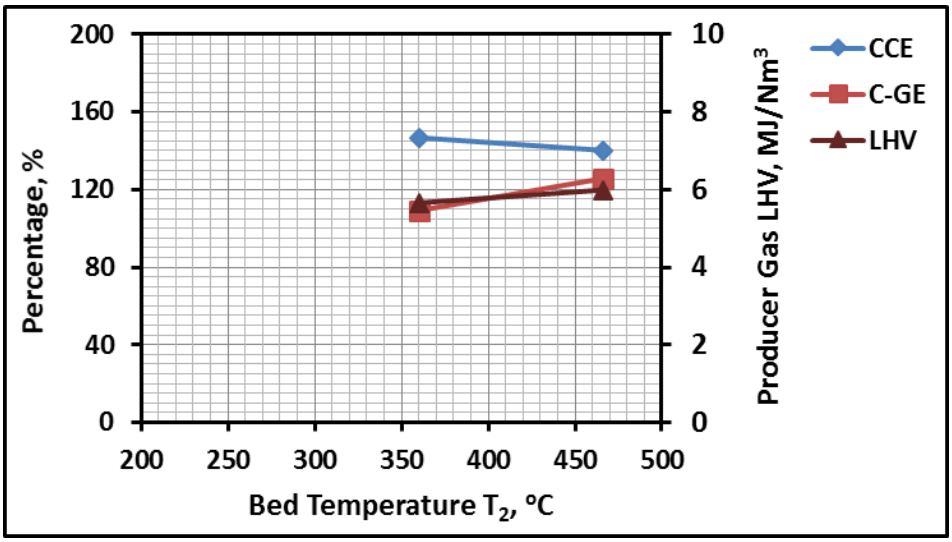

a) SPWB

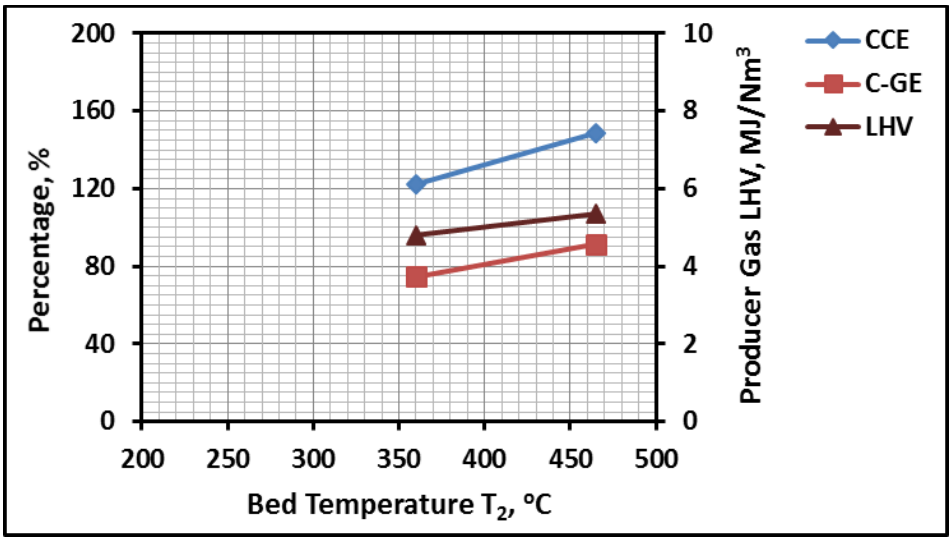

b) IDPWB

Figure 7. 30 Effect of the bed temperature T2 on CCE, CGE and LHV performance parameters: a) for SPWB biomass material and b) for IDPWB biomass material

(c) Gases ratios

Figure 7.31-(a) and (b) provides the effect of bed temperature T2 on the gas ratio for two biomass materials. It can be shown that for both biomass materials, SPWB and IDPWB, the results revealed that there was no significant effect of this range of temperature on the gas ratio, in volume ratio or mole ratio, CO/CO_2, H_2/CO_2, CH_4/CO_2, H_2/CO and CH_4/CO. The value of these ratios are linked to the composition of gases in the producer gas as shown in Section (7.2.4.7-a). However, SPWB shows higher CO/CO_2 and H_2/CO_2 than IDPWB's ratios, approximately 2.5 and 1.5 for the former and 1.0 and 0.6 for the latter, whereas H_2/CO and CH_4/CO_2 are approximately similar, around 0.6 and 0.4, respectively. H_2/CO ratio is an important ratio, which can be used

to specify the producer gas quality and its uses. For this range of bed temperature, it can be seen that there is no significant effect on these ratios.

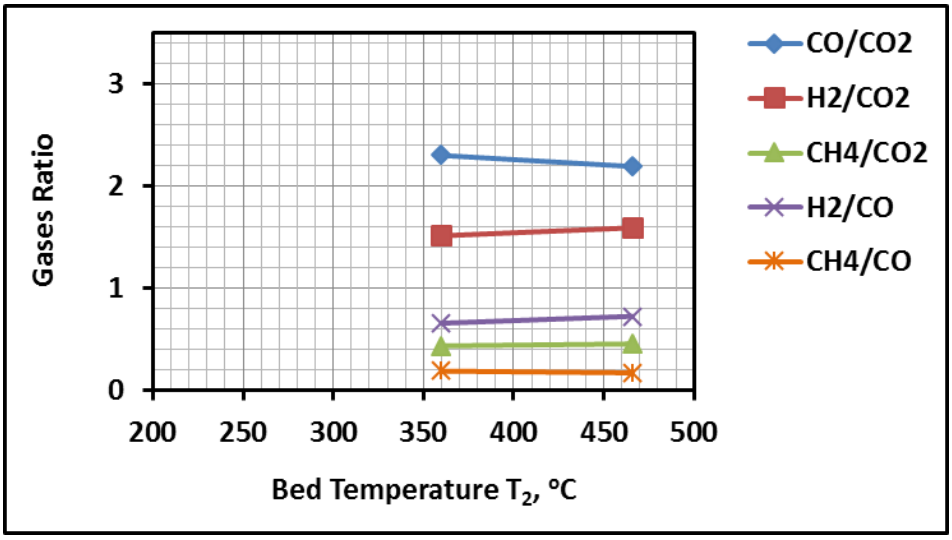

a) SPWP

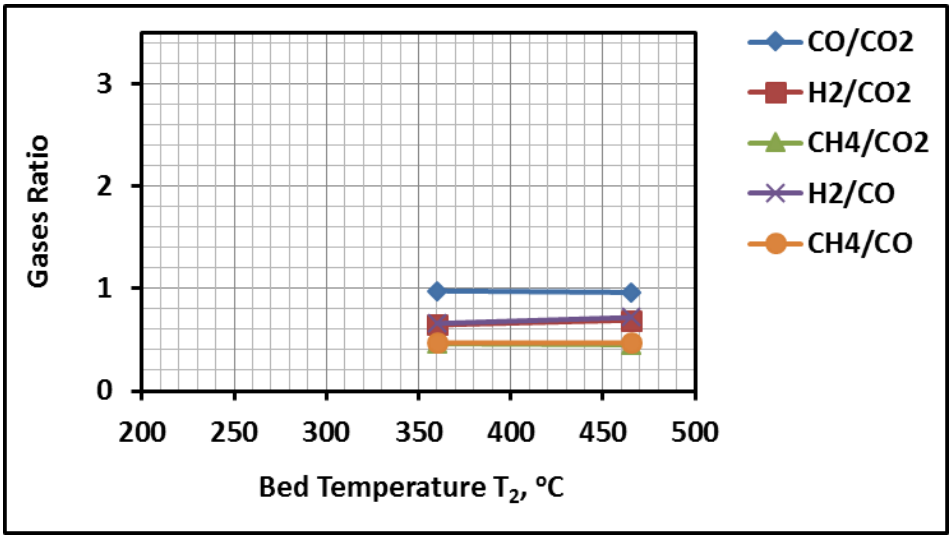

b) IDPWB

Figure 7. 31 Effect of the bed temperature T2 on the gases ratio: a) for SPWB biomass material and b) for IDPWB biomass material

(d) Producer gases yield(GY)

Figure 7.32 (a) and (b) highlights the effect of the bed temperature on the gas yield for two biomass materials. It can be observed that for SPWB, the total gas yield was increased steadily from 3.7 to 4.2Nm^3/kg feed db as bed temperature increased from 360ºC to 465ºC. For IDPWB the total gas yield was increased slightly from 2.8 to 3.1Nm^3/kg feed db. Furthermore, the gas yield observation for each individual gas along the bed temperature range was as follows: For SPWB, a slight increase for CO from

0.84 to 1.0, H_2 from 0.55 to 0.7 and CO_2 from 0.35 to 0.4, whereas N_2 and CH_4 approximately stayed constant on 1.6 and 0.15, respectively. For IDPWB, a slight and identical increase for CO and CO_2 from 0.38 to 0.45, H_2 and CH_4 increased slightly from 0.25 to 0.32 and from 0.15 to 0.2, respectively and N_2 stayed constant on 1.4. All units are in Nm^3/kg feed db. It can be concluded that there is no significant effect of bed temperature on the total producer gas yield and for individual gases for both biomass. Furthermore, SPWB produced higher total producer gas yield than IDPWB. There is possible explanation for these results. The observed increase in total gas yield and individual gas yield can be strongly linked to the change in each gas composition as has been discussed above. Due to a slight difference in the producer gas composition and then gas yield due to a low bed temperatures, so the same difference was revealed due to the thermal cracking of gas-phase hydrocarbon (secondary reactions) in the high temperature freeboard section T1=Tset=900ºC Cao et al. (2006), Mohammed et al. (2011).

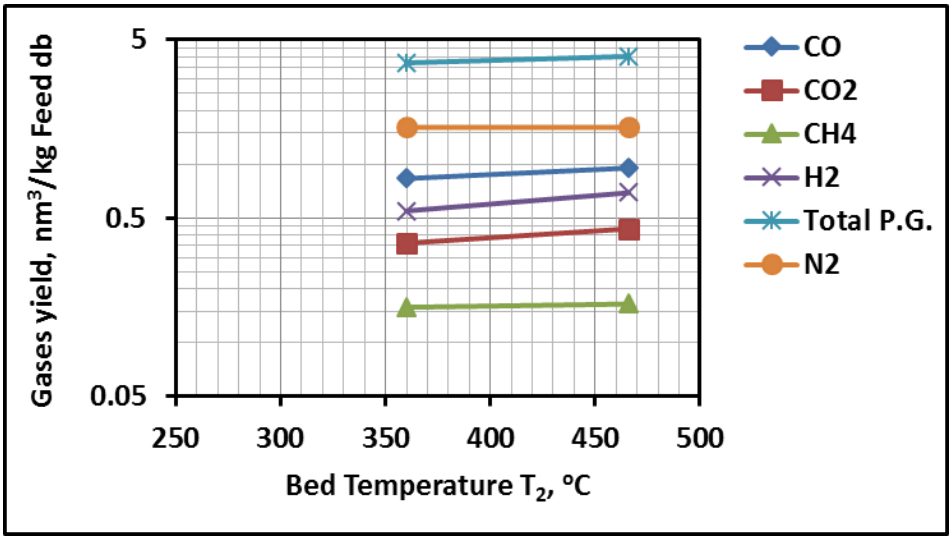

a) SPWB

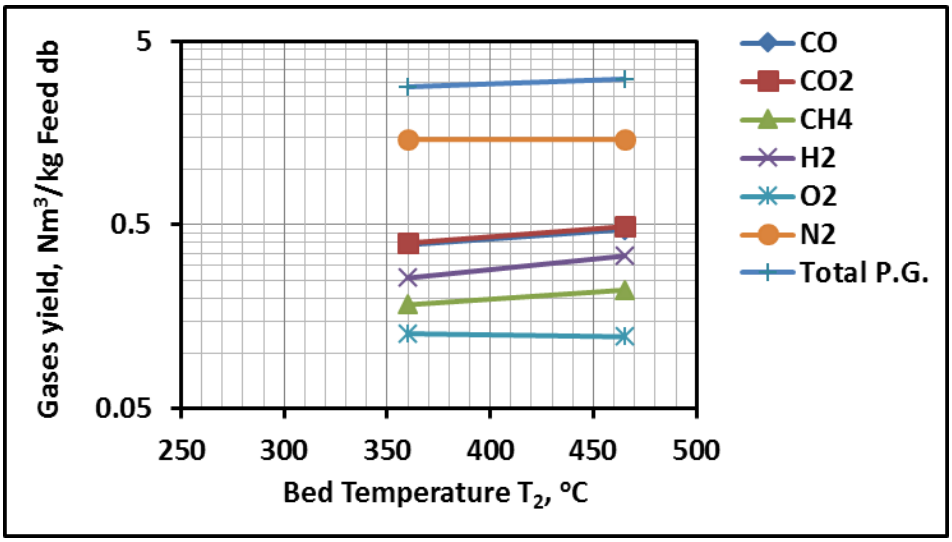

b) IDPWB

Figure 7. 32 Effect of the bed temperature T2 on gas yield (GY): a) for SPWB biomass material and b) for IDPWB biomass material

7.2.4.8 Effect of the number of holes of the distributor plate

Table 7. 9 Operating conditions for holes number of distributor plate parameter experimental tests

a) For SPWB

Operating Parameters	**Holes No of Distributor Plate, N_{orf}**		
	19	**85**	**169**
1- Air Flowrate l/min (kg/hr)	44 (3.18)	44 (3.18)	44 (3.18)
2- Reaction Bed Temperature T2, °C	360	360	360
3- Bed Material (Sand) Particle Size, µm	300-425	300-425	300-425
4- Biomass solid Fuel Particle Size, µm	600-850	600-850	600-850
5- Equivalence Ratio ER	0.42	0.42	0.42
6- Mass Rate of biomass Feeding, kg/hr	1.192	1.192	1.192
7- $(MAFR)_{stoichiometric}$ For SPWB	6.2	6.2	6.2
8- Air superficial velocity U_o, cm/sec	13.56	13.56	13.56

b) For IDPWB

Operating Parameters	**Holes No of Distributor Plate, N_{orf}**		
	19	**85**	**169**
1- Air Flowrate l/min (kg/hr)	44 (3.18)	44 (3.18)	44 (3.18)
2- Reaction Bed Temperature T2, °C	360	360	360
3- Bed Material (Sand) Particle Size, µm	300-425	300-425	300-425
4- Biomass solid Fuel Particle Size, µm	600-850	600-850	600-850
5- Equivalence Ratio ER	0.42	0.42	0.42
6- Mass Rate of biomass Feeding, kg/hr	1.192	1.192	1.192
7- $(MAFR)_{stoichiometric}$ For IDPWB	6.352	6.352	6.352
8- Air superficial velocity U_o, cm/sec	13.56	13.56	13.56

(a) Producer gas composition for two biomass materials

According to the operating conditions, which have been shown in Table 7.9-(a) and (b), Figure 7.33 (a) and (b) presents the influence of the number of holes N_{orf} of the distributor plate on the producer gas composition for two biomass materials. The operating conditions of this effect for both biomass SPWB and IDPWB are presented in Table 7.9 (a) and (b), respectively. The configurations used were 19, 85 and 169 holes, which equate to the open area 0.3, 1.5 and 3cm^2, respectively. From Figure 7.32-(a) and (b), for both biomass, it can be seen that the effect on producer gas composition was as follows: CO initially increased from 15% to 22.8%, when the N_{orf} increased from 19 to 85 and then decreased to 12.6% at N_{orf} =169. While for IDPWB it decreased steadily from 12.5% at 19 N_{orf} to 11.2% at 85 and then to 8.2% at N_{orf} =169. H_2 had a similar trend but lower than the CO trend. It increased slightly from 13.5% to 15.3% for the first period (19 to 85) and then decreased to 10.2% at 169, whereas for IDPWB H_2 decreased slightly from 10% to 5.7%. For CO_2 a trend was obtained for SPWB material similar to CO. It increased from 5.9% to 9.8% and then decreased to 6.6%, while for IDPWB the trend was similar to CO_2 for SPWB. It increased from 4.5% to 12.3% and then decreased to 6.3%. Finally, CH_4 decreased very slightly for SPWB from 5.3% to 4.1% along the N_{orf} range, whereas for IDPWB CH_4 increased from 4.1% to 4.5% for (19 - 85 N_{orf} range) and then approximately stayed constant at 4.6% for (85-169 N_{orf} range). Furthermore, it can be seen that SPWB produced higher gas concentration than IDPWB except CH_4 gas was approximately the same. This is possibly, as shown in Table 4.4, due to the higher characteristics, higher chemical composition (Ultimate and Proximate analysis), of the former material than latter. So for SPWB the maximum producing value for CO, CO_2, and H_2 was attained at N_{orf} =85, whereas for CH_4 at N_{orf} =19. For IDPWB the maximum value for CO_2 and CH_4 was attained at N_{orf} =85, while for CO and H_2 at N_{orf} =19. In all cases, for both biomass materials it can be seen that the distributor N_{orf} =19 had a better effect than N_{orf} =169.

According to the experiment operating conditions and according to this discrepancy in the behaviour of the distributor effect on the gasification results especially for the two-biomass materials, SPWB and IDPWB. N_{orf} =85 was found the optimum distributor plate for the former biomass material and N_{orf} =19 the optimum for the latter. The possible explanations for these results can be attributed to: the high chemical and physical characteristics of SPWB compared to IDPWB especially the shape of their particles. The latter has a high needle shape, high particle aspect ratio and inter-particle

force, which leads to a high cohesion between particles and then a weak associated hydrodynamic behaviour with bed material. Finally, this leads to a weak uniform temperature distribution and low rate of mass and heat transfer and reaction rates. So, because of the high pressure drop due to a low number of orifices the distributor plate of N_{orf} =19 can provide a sufficient pressure driving force to ensure a high solid fluidisation and then attained the homogenous flow structure (Dong et al. 2009). On the other hand the distributor plate of N_{orf} =85 has a low pressure drop but because of the large number of holes will generate large number of small bubbles, the air would be distributed more effectively (Dong et al. 2009) and increase the air residence time in the bed (Yang 2003). However, for N_{orf} =169 the matter is different, where it provided a lowest effect. It can be interpreted that the bubbles coalescence phenomena is more clear for high holes number (more than N_{orf} =85). This high holes number produces a large number of the convergent bubbles due to the small hole pitch. This converge leads to coalesce the bubbles fast and gradually producing larger and larger bubbles along the bed. Finally, these large bubbles will possibly contribute a weak contact between the reactants leading to a low reaction rates. These results lead to infer that there is a limited number of holes should not be exceeded. In addition, the bubble size is an important variable, which affects the fluidised bed gasifier performance through its influence on the hydrodynamic parameters. From Chapter 3- Equation (3.15-b) for the perforated plate the initial bubble diameter d_{bo} increased when the number of orifices N_{orf} decreased and then the bubble region area decreased with increasing N_{orf} as shown in Equation (3.17) and confirmed by (Dong et al. 2009).

All these hydrodynamic effects because of the distributor plate design will affect significantly the gasification producer gas composition quality and the gasifier performance. Although the importance of the distributor plate in the design of fluidised bed gasifier, but any published research in studying the effect of the distributor plate holes number on the gasifier performance has not been found.

Overall, for this range of the distributor plate holes number the results show that N_{orf}=85 has a significant effect on SPWB gasification producer gas composition, whereas for IDPWB is N_{orf} =19, especially for CO and H_2. In addition, there is an optimum and limited number of distributor holes.

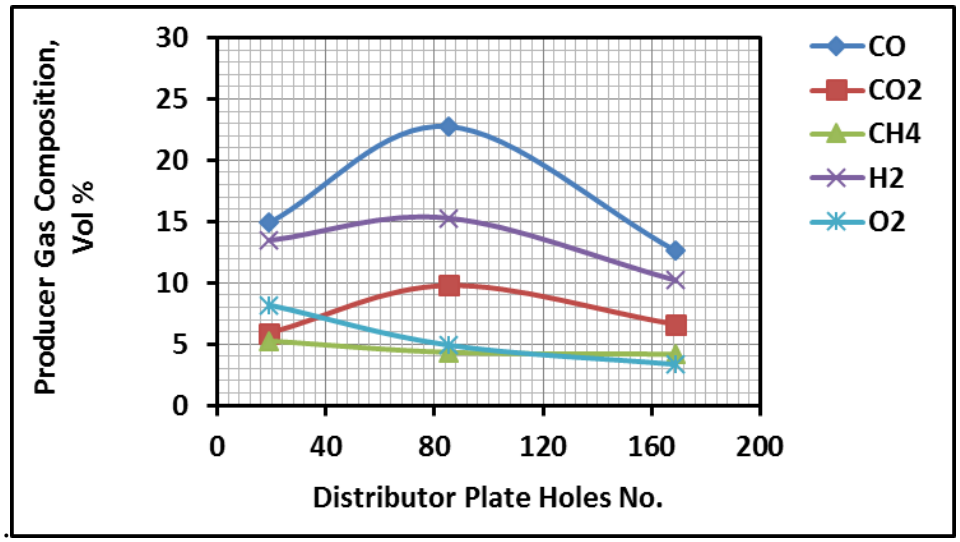

a) SPWB

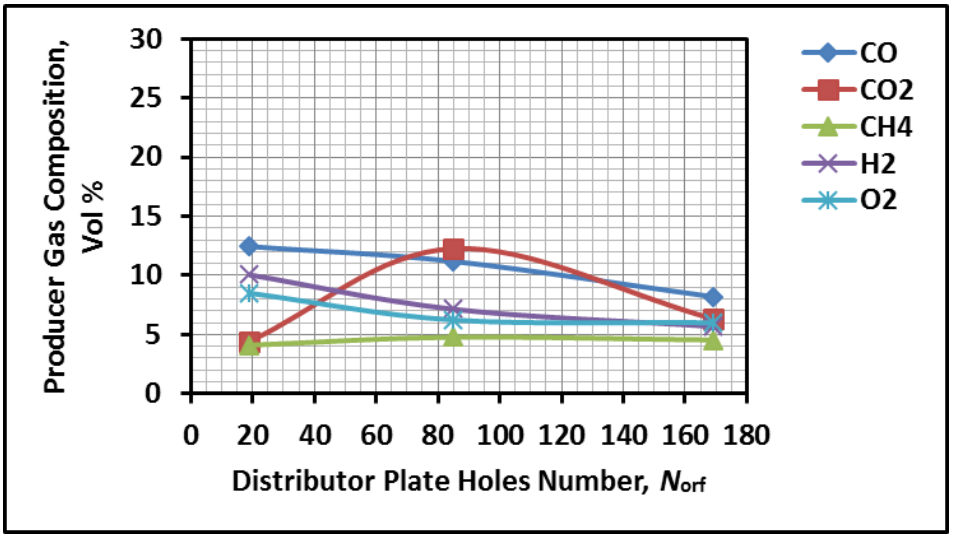

b) IDPWB

Figure 7. 33 Effect of the number of holes of the distributor plate N_{orf} on the producer gas composition: a) for SPWB biomass material and b) for IDPWB biomass material.

(b) Carbon conversion efficiency, cold-gas efficiency, and producer gas heating value

Figure 7.34-(a) and (b) provides the effect of the number of holes of the distributor plate on the performance parameters for two biomass SPWB and IDPWB, respectively. It can be observed that along the range of N_{orf} = (19-85) the performance parameters CCE, LHV and CGE for SPWB were increased from 87% to 150.1%, 5.0 to 5.8 MJ/Nm^{3}db and from 82% to 116.2%, while for the second range (85-169), they decreased to 64.7%, 4.0 MJ/Nm^{3}db and 54.5%, respectively. For IDPWB, only CCE increased from 75.3% to 104.8% in the first range and then decreased to 59.8% at N_{orf} =169. Whereas LHV

and CGE decreased steadily, for the whole range (19-85-169), from 4.0 to 3.1MJ/nm^{3}db and from 60 % to 42.6%, respectively.

Furthermore, it can be seen that for IDPWB the maximum value of CCE achieved at 85, while for LHV and CGE at 19. For SPWB, the maximum value for three performance parameters was achieved at N_{orf} = 85.

These results might be possibly explained that the observed increasing and decreasing of these performance parameters along the three N_{orf} values can be linked to the composition of CO, CO_2, H_2 and CH_4 in the producer gas, as revealed in Figure 7.32 (a) and (b). This is due to the gases, which hold carbon atom, CO, CO_2, and CH_4 represent the carbon conversion CCE in producer gas, whereas the gases CO, H_2 and CH_4 represent the chemical energy conversion, LHV and CGE.

It can be concluded that for SPWB-air gasification the attained results of the heating value of the producer gas, LHV= 5.76 MJ/Nm^3 db at N_{orf} = 85, proved the potential of this biomass to generate energy. In contrast, for IDPWB the attained results, LHV=4.0 MJ/Nm^3 db at N_{orf} = 19, proved the potential of this biomass.

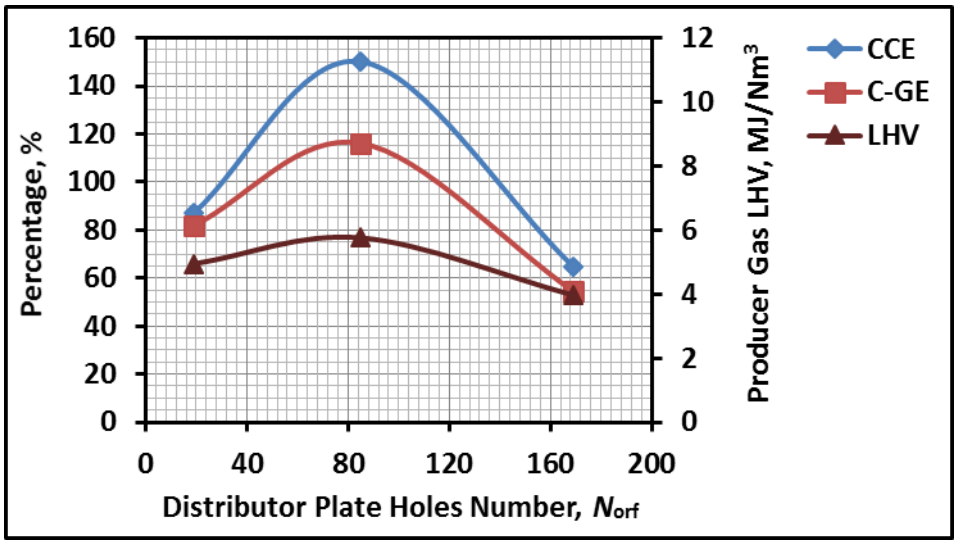

a) SPWB

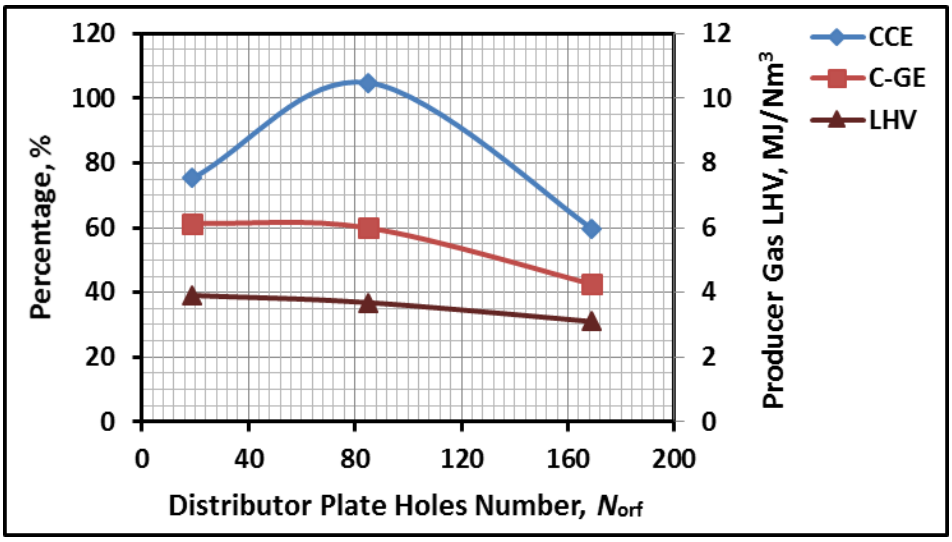

b) IDPWB

Figure 7. 34 Effect of the number of holes of the distributor plate on CCE, CGE and LHV performance parameters: a) for SPWB biomass material and b) for IDPWB biomass material

(c) Gases ratios

Figure 7.35 (a) and (b) provides the effect of the number of holes of the distributor plate (N_{orf}) on the gas ratio for two biomass materials. It can be shown that SPWB implemented maximum CO/CO_2, 2.5, at N_{orf} = 19 and gradually decreased to 1.9 at N_{orf} = 169. This maximum value indicates a high partial oxidation environment. H_2/CO_2 was also significantly decreased from 2.3 at N_{orf} = 19 and approximately levelled off at 1.5 at N_{orf} =85 and N_{orf} = 169. The decrease of the above two ratios indicates the increase of the combustion reactions as the N_{orf} increased. The important ratio in producer gas, H_2/CO and CH_4/CO_2 ratio achieved a maximum value, 0.9 at N_{orf} = 19 and then slightly decreased in a similar trend along the N_{orf} range studied. CH_4/CO ratio shows a maximum value 0.35 at N_{orf} = 19 and 0.5 at169. This ratio indicates a low concentration of CH_4 compared to CO for all distributor plates.

For IDPWB CO/CO_2 and H_2/CO_2, ratios show a similar trend. They decreased steeply from 2.8 and 2.3 at N_{orf} = 19 to 0.9 and 0.58 at N_{orf} = 85, then they increased steadily to 1.3 and 0.9 at N_{orf} = 169, respectively. This sharp decrease indicates that higher combustion reactions occur at N_{orf} = 85 than at N_{orf} = 19. Approximately a similar trend and values can be observed for H_2/CO and CH_4/CO_2 ratios as shown for SPWB. Their values were less than 1.0. CH_4/CO increased slightly from 0.3 to 0.6 along the N_{orf} range studied. This indicates that CH_4 increased slightly as N_{orf} increased compared to CO.

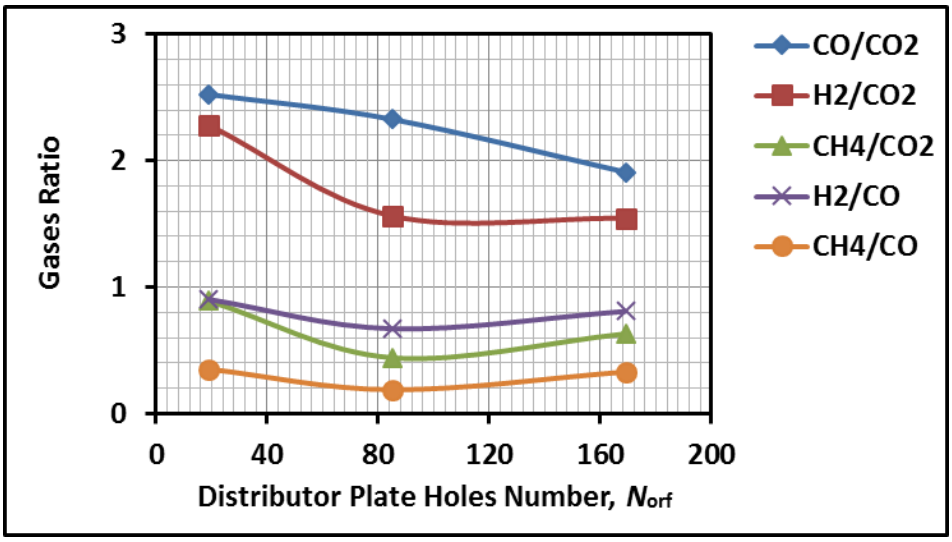

a) SPWB

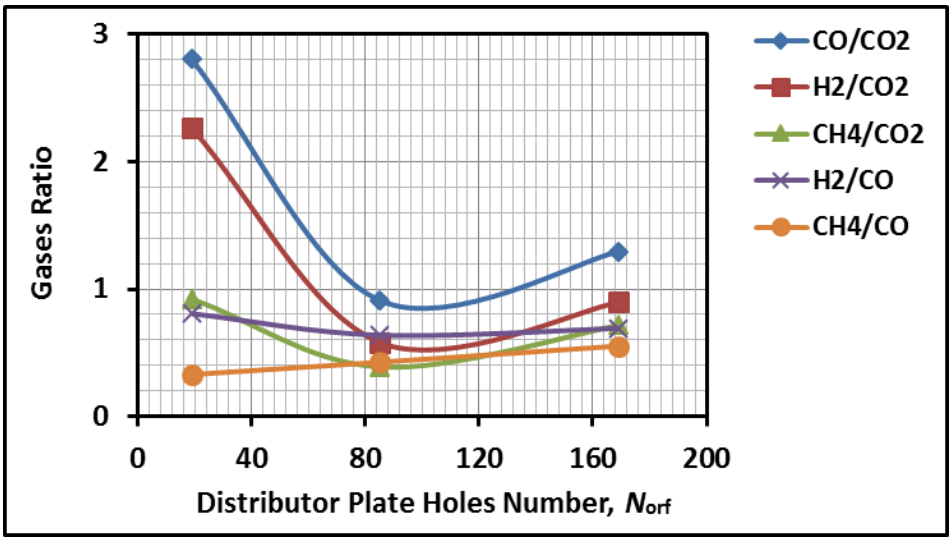

b) IDPWB

Figure 7. 35 Effect of the number of holes of the distributor plate on the gases ratio: a) for SPWB biomass material and b) for IDPWB biomass material

(d) Producer gas yield (GY)

Figure 7.36-(a) and (b) highlights the effect of the number of the holes of the distributor plate on the gas yield for two biomass materials. It can be observed that for SPWB, the total gas yield attained a maximum value, 3.75 Nm^3/kg feed db, at N_{orf} = 85 and the minimum value was 2.55 Nm^3/kg feed db at N_{orf} = 169. Similarly for individual gases CO, H_2, CO_2 and CH_4 the maximum yield was attained at N_{orf} = 85. Their values took a descending sequence as follows: 0.9, 0.6, 0.4 and 0.2 Nm^3/kg feed db, respectively, whereas N_2 stayed constant, 1.6Nm^3/kg feed db.

For IDPWB the maximum value was 3.0Nm^3/kg feed db at N_{orf} = 85 and the minimum value was 2.5Nm^3/kg feed db at N_{orf} = 169. Whereas for the individual gases their yield attained very low values except N_2, which attained a constant yield value, 1.7Nm^3/kg feed db, for all three-distributor plates. The maximum yield values for CO and H_2 were 0.4 and 0.3 nm^3/kg feed db, respectively at N_{orf} = 19, while for CO_2 and CH_4 were 0.4 and 0.2Nm^3/kg feed db, respectively at N_{orf} = 85.

As discussed in Section 7.2.4.8-(a), the yield results completely depend on the producer gas composition. In general, from the Figure7.36-(a) and (b) it can be seen that SPWB achieved gas yield higher than IDPWB for total producer gas and individual gases. This can be linked to the higher producer gas compositions for SPWB as shown in Figure 7.34 (a) compared to producer gas composition for IDPWB as shown in Figure 7.34 (b). Furthermore the best total gas yield that can be achieved for both, SPWB and IDPWB was at distributor plate, N_{orf} = 85.

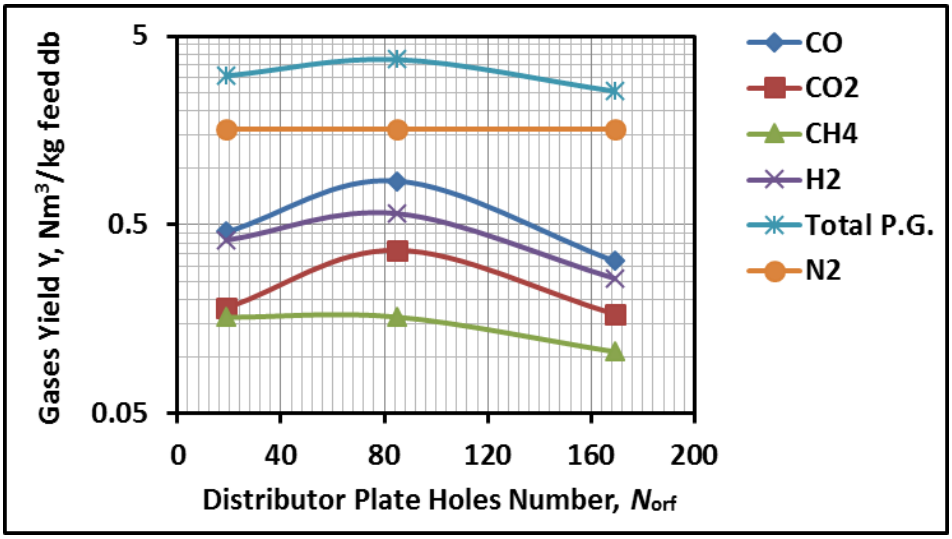

a) SPWB

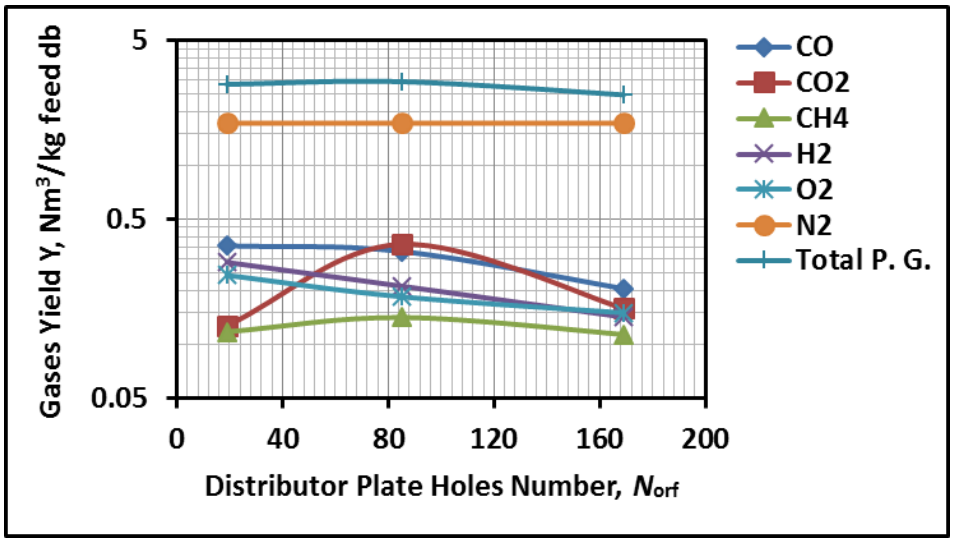

b) IDPWB

Figure 7. 36 Effect of the number of holes of the distributor plate on gases yield: a) for SPWB biomass material and b) for IDPWB biomass material

7.2.5 Material balance

A material balance and carbon species mass balance in the gasification system were undertaken to observe the conversion of biomass material, SPWB and IDPWB, into producer gas as well as the other products as illustrated in Figure 7.37. As described in Chapter 5 reactant materials, biomass fuel and air were fed to the fluidised bed gasifier. The inert material, sand, was used as fluidised bed material. The products were classified as producer gas, tar, traces of particulates and char + sand mixture. The producer gas was represented mainly CO, CO_2, CH_4, H_2 and O_2, which their composition were measured in volume percent, whereas N_2 was calculated by difference. Char in the char-sand mixture represented the unburnt carbon. Tar and particulates represented a condensable volatile material and a fine particles, sand and char, respectively.

For this study the output product streams, producer gas and char only were considered making the total and carbon mass balances of the gasification system. The boundary of this system was laid out using a dashed line as shown in Figure 7.37.

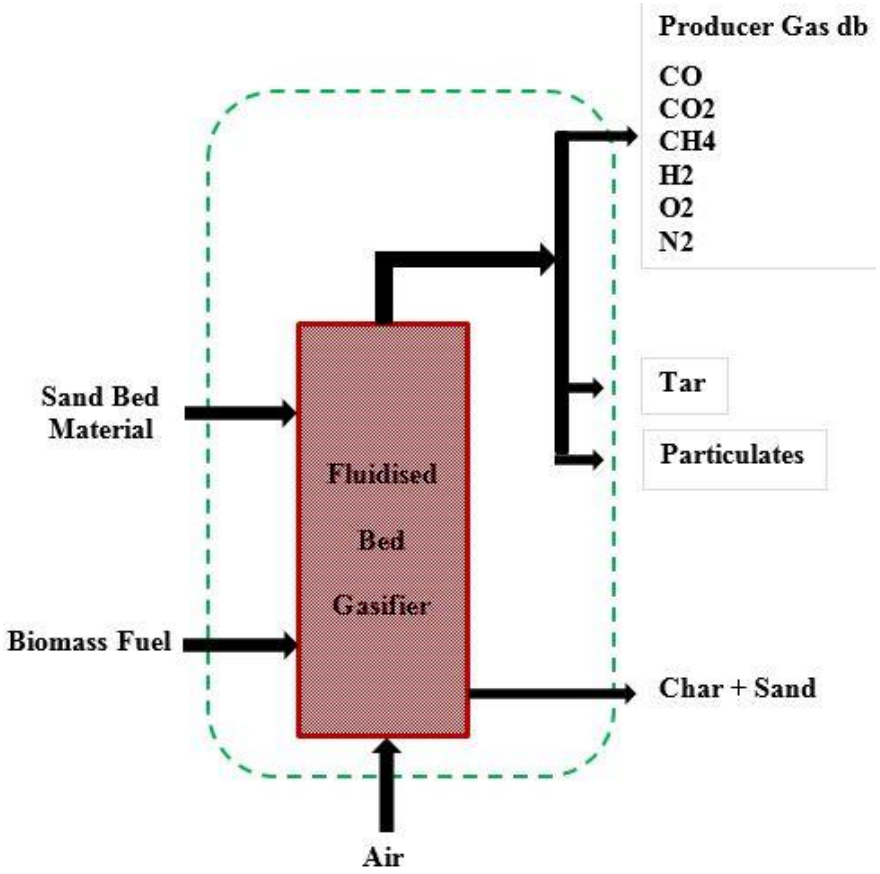

Figure 7. 37 Schematic of the block diagram of the biomass gasification system mass balance

For steady state conditions, the total mass balance in the fluidised bed gasification system was calculated using Equation 7.3a.

$$Total\ Input\ Mass = Total\ Output\ Mass \tag{7.3}$$

$$\left[(\dot{m})_{air} + (\dot{m})_{bio.fuel}\right]_{Input} = \left[(\dot{m})_{p.gas} + (\dot{m})_{char}\right]_{Output} \tag{7.3a}$$

The mass of the input biomass fuel, input inert sand $(m)_{\text{sand}}$ and output char + sand $(m)_{\text{char + sand}}$ mixture were weighed using a laboratory scale balance. The mass rate of air and producer gas were calculated according to Equation 7.4 and Equation 7.8, respectively. All the streams were calculated in mass rate unit, g/min, except the sand in g. Therefore, 1 min as the basis of the calculations was taken. The duration of the experiment time (t) was 5 min. Steady state conditions were assumed

$$(\dot{m})_{air} = V_{air} \times \rho_{air} \times 1000 \tag{7.4}$$

Where V_{air} and ρ_{air} are the input air flowrate (l/min) and air density (1.2 g/cm^3 at ambient temperature). Producer gas mass rate $(\dot{m})_{p.gas}$ can be calculated as follows:

Using Equation (5.9) in Chapter 5, the individual gas yield of each gas was determined using Equation (7.5).

$$Y_i = Y_{P.Gas} \times x_i \tag{7.5}$$

Where Y_i, $Y_{P.Gas}$, x_i are the individual gas yield in (Nm^3/kg fuel feed), yield of producer gas in (Nm^3/ kg fuel feed) and mole fraction of individual gas (i), respectively. This unit of (i) gas yield converted to $(m)_i$ in [mass of (i) gas/ mass feed fuel] unit using Equation (7.6).

$$m_i = y_i \times (Mwt)_i/22.4 \quad (7.6)$$

$$\therefore (\dot{m})_i = m_i * (\dot{m})_{bio.fuel} \quad (7.7)$$

$$\therefore (\dot{m})_{p.gas} = \sum(\dot{m})_i \quad (7.8)$$

Where $(Mwt)_i$, $(\dot{m})_i$ are molecular weight of gas (i) and the mass rate of gas (i) in (g/min), respectively.

Carbon mass balance was performed to observe the conversion of biomass fuel materials, SPWB and IDPWB, to gases and char. Only both biomass fuels were considered as a principal source of the carbon in the input streams. For this study in the output, producer gas and char + sand streams were considered the main source of carbon. According to the mass balance, Equation (7.1), carbon balance was determined using Equation (7.9).

$$(\dot{C})_{bio.fuel} = (\dot{C})_{P.gas} + (\dot{C})_{char+sand} \quad (7.9)$$

Where $(\dot{C})_{bio.fuel}$, $(\dot{C})_{P.gas}$, and $(\dot{C})_{char+sand}$ are the carbon mass rate (g/min) in biomass feed fuel, producer gas and char + sand streams, respectively. These carbon mass rates were determined using Equation (7.10), (7.12) and (7.13), respectively.

$$(\dot{C})_{bio.fuel} = (CC)_{bio.fuel} \times (\dot{m})_{bio.fuel} \quad (7.10)$$

Where $(CC)_{bio.fuel}$ is the carbon mass fraction in biomass feed fuel, using biomass ultimate analysis as shown in Table 4.1.

$$(\dot{C})_i = C_i \times (\dot{m})_{bio.fuel} = [y_i \times 12/22.4] \times (\dot{m})_{bio.fuel} \quad (7.11)$$

$$(\dot{C})_{P.gas} = \sum(\dot{C})_i \quad (7.12)$$

Where $(\dot{C})_i$, C_i are the carbon mass rate and carbon mass of the carbonaceous gas (i), respectively.

$$(\dot{C})_{char+sand} = (CC)_{char+sand} \times (m)_{char+sand}/t \quad (7.13)$$

Where $(CC)_{char+sand}$ and $(m)_{char+sand}$the carbon mass fraction and mass of char + sand mixture stream, respectively.

Equation 7.14 was used to determine the comparison of the total and carbon mass balance parameters between input and output streams.

$$\% \, Error = \left[\frac{Input\ mass - Output\ mass}{Input\ mass}\right] \times 100 \quad (7.14)$$

For each parameter, whose effect has been discussed in Section 7.2.4.2 – 7.2.4.8, the results of the measured and calculated quantities for each experiment for each stream in the total and carbon mass balances are outlined in tables. The data in these tables are presented to show the trend of the each parameter group on the gasification mass balance streams. These tables and figures are shown in Appendix E

The total and carbon mass balances data of the experiment group of the air flowrate parameter for the two biomass materials, SPWB and IDPWB was selected as an example. These data are outlined in Table 7.10 (a) and (b) and Figure 7.38 (a) and (b).

From the table it can be seen that for SPWB for three air flowrates the total mass of the output streams were 80.3, 121.9 and 164.7g/min, which is more than the total mass input streams 73.2, 109.7, and 146.3g/min leading to -9.7, -11.1 and -12.6 % error, respectively. This result will interpreted in the proceeding. IDPWB showed an opposite trend except for 44 l/min, which showed a similar trend to SPWB. For carbon mass balance for SPWB the total balance between input and output streams for three air flow rates were at -59.8, -86.5 and -60.7 % error, respectively, whereas for IDPWB were at -60.8, -14.1 and -12.7, respectively. These higher output carbon mass was due to the high output carbon mass in producer gas which was higher than the total input carbon mass itself. These results will be explained in the next paragraphs.

In Figure 7.38 it can be seen that the total mass input (Biomass fuel + Air) and carbon (carbon input) lines were taken as a reference lines for total mass and carbon balances. Each line can be used to observe the output streams of the total and carbon mass deviations. Furthermore, when the output mass lines follows a downward trend, it indicates that the output mass is less than the input mass and gives positive (+ve) percent error and vice versa. From the Figure 7.38, for both biomass, it can be seen that as the air flowrate increased from 44 to 88 l/min all streams were increased except the char stream of IDPWB was slightly decreased. Furthermore, for SPWB the total output mass of producer gas and char was greater than the total mass input, whereas for IDPWB was lesser. For both biomass the deviation (% error) increased as air flowrate increased. For carbon balance, it can be seen that the total mass of the output carbon was exceeded the total input carbon. This excess for SPWB was higher than IDPWB.

The negative deviation either for total mass balance or carbon balance might be attributed to the following reasons: 1). the biomass screw feeder supplied more biomass quantity than the measured. 2) There were quantities of char residues and soot product from previous experiments that available inside gasifier at the freeboard section. Due to a high temperature and oxidation atmosphere in this section gasification and combustion reactions possibly occurred. These materials in turn led to increase the amount of carbon in producer gas causing high carbon conversion efficiency CCE and cold gas efficiency CGE. 3) The error that may result by the gas analyzer was excluded because it was calibrated for each experiment. 4) The heterogeneity of the residue mixture (char + sand) due to their high-density difference caused no precision carbon content measurement and leading to inaccurate mass balances.

Table 7. 10 Total and carbon mass balances for air flowrate experiments: a) for SPWB and b) for IDPWB

a) SPWB

Air flow, l/min	Stream	Total mass balance, g/min			Carbon mass balance, g/min		
		Input	Output	% Error	Input	Output	% Error
44	Biomass Fuel	20.17	-	-	9.96	-	-
	Air	52.98	-	-	-	-	-
	Producer Gas	-	77.75	-	-	12.66	-
	Char + Sand	-	2.52	-	-	3.26	-
	Total	73.15	80.27	-9.74	9.96	15.92	-59.84
66	Biomass Fuel	30.26	-	-	14.95	-	-
	Air	79.47	-	-	-	-	-
	Producer Gas	-	113.16	-	-	18.19	-
	Char + Sand	-	8.71	-	-	9.69	-
	Total	109.73	121.87	-11.07	14.95	27.88	-86.52
88	Biomass Fuel	40.36	-	-	19.94	-	-
	Air	105.96	-	-	-	-	-
	Producer Gas	-	152.79	-	-	24.61	-
	Char+Sand	-	11.93	-	-	7.44	-
	Total	146.32	164.72	-12.57	19.94	32.05	-60.73

b) IDPWB

Air flow, l/min	Stream	Total mass balance, g/min			Carbon mass balance, g/min		
		Input	Output	% Error	Input	Output	% Error
44	Biomass Fuel	21.92	-	-	9.34	-	-
	Air	52.98	-	-	-	-	-
	Producer Gas	-	75.26	-	-	11.42	-
	Char+Sand	-	3.36	-	-	3.60	-
	Total	74.90	78.62	-4.96	9.34	15.02	-60.81
66	Biomass Fuel	32.87	-	-	14.00	-	-
	Air	79.47	-	-	-	-	-
	Producer Gas	-	104.09	-	-	14.91	-
	Char+Sand	-	2.98	-	-	0.97	-
	Total	112.34	107.08	-4.69	14.00	15.98	-14.14
88	Biomass Fuel	43.84	-	-	18.67	-	-
	Air	105.96	-	-	-	-	-
	Producer Gas	-	135.45	-	-	18.61	-
	Char+Sand	-	2.45	-	-	2.43	-
	Total	149.80	137.90	-7.95	18.67	21.04	-12.68

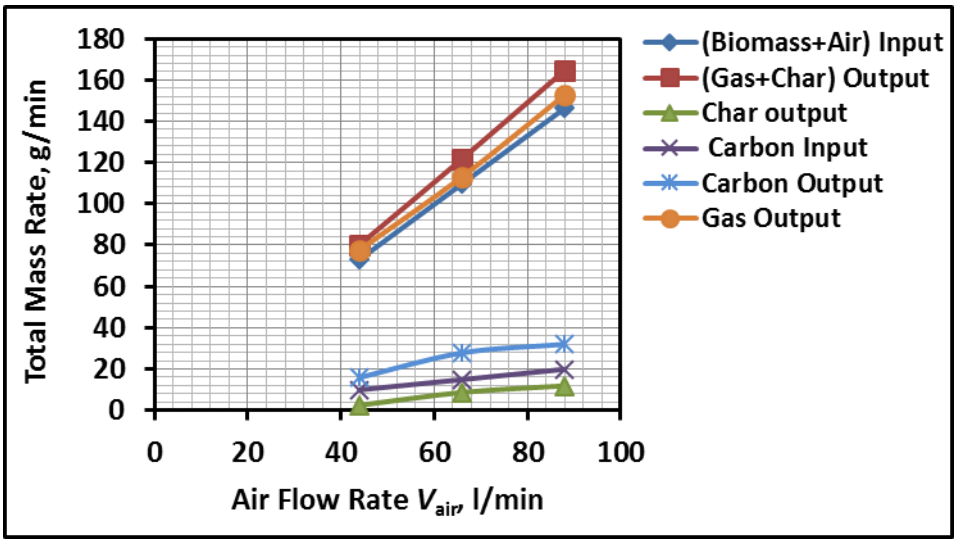

a) SPWB

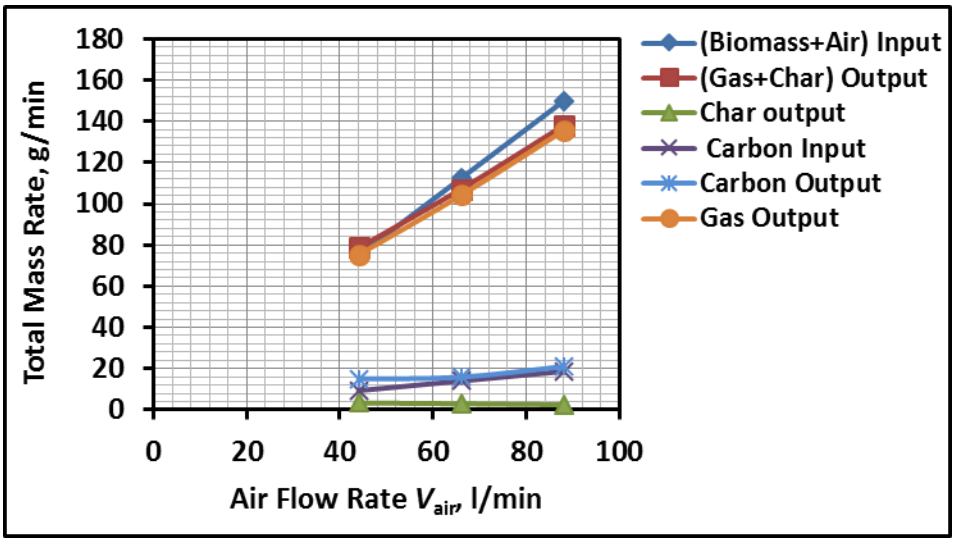

b) IDPWB

Figure 7. 38 Total and carbon mass balances for air flowrate experiments: a) for SPWB and b) for IDPWB

7.3 Summary

This chapter has shown the results of the possibility of the gasification of the two-biomass materials, SPWB and IDPWB, by using an air-blown bubbling fluidised bed gasifier. The results and the effect of the operating and hydrodynamic parameters has been presented and discussed in detail. The air flowrate parameter has shown a negative effect on the performance parameter, especially for IDPWB feedstock, and H_2 gas decreased as flow increased. In addition, it has shown that a high LHV can be produced at low air velocities. The smaller sand particle size has shown a slightly effect higher

than the others on producer gas composition and performance parameter for SPWB, whereas the effect was higher for IDPWB feedstock. In addition, a smaller biomass particle size has shown a more favorable quality producer gas production and upgrade performance parameters. Furthermore, the effects of the static bed height have shown a fluctuating effect on the performance parameters whereas the maximum values at the medium height 0.75D has been concluded. In general, different effects of ER parameter has been detected on the gasification of two biomass feedstocks. This chapter has also shown the positive effect of the bed temperature on all the produced combustible gases composition, in addition to performance parameter. The effect of the number of the holes of the distributor plate has been discussed and it has shown a different effect depending on the biomass type. Finally, the total and carbon mass balance in the biomass gasification system has been conducted to observe the balancing of input and output streams.

Chapter 8

Conclusions and Recommendations for Future Work

8.1 Conclusions

This study is concerned with the investigation of the effect of the hydrodynamic fluidization parameters and operating conditions on the performance of the gasification of the solid biomass fuels in a bubbling fluidised bed reactor. This involved a preliminary design and cold experimental hydrodynamic studies to provide design data for gasification processes.

The main conclusions that found in this research study are summarised and classified into three major groups: a design study, cold fluidisation experimental tests, and biomass gasification experimental trials.

8.1.1 Design Study

The design study has shown an important part of this research for predicting and providing an elementary design data for constructing both cold fluidization and biomass gasification rigs and for conducting their experimental tests as well. From the results of the design study, the following findings have been concluded:

- According to the available facilities the suitable size, represented by the gasifier diameter, of the bubbling fluidised bed gasifier has been specified. For this study, 8.3cm the internal diameter of the gasifier column has been selected.
- The design parameter, minimum fluidization velocity U_{mf}, was highly affected by the particle size of the bed material. This, in turn, specified the minimum requirement of air flowrate, an agent gas for fluidization. These quantities of the air have helped to specify the required quantity of biomass fuel for gasification at a selected equivalence ratio.
- It has indicated that the minimum fluidization velocity was not affected by the static height of the bed material H_s.
- The number of distributor plate holes, N_{orf} affected the air flowrate. It means that for each specific flow rate, there is a specific number of holes. Furthermore, this has a direct effect on the hydrodynamic behaviour of the fluidised bed reactor represented by the pressure drop across the plate and the number of the generated bubbles. For the cold fluidisation experimental tests, N_{orf} =19, 55 and 85 were used, whereas, for the gasification tests, N_{orf} =19, 85 and 169 have been used.

- Finally, from the design results, this design model can predict the gasifier size and some of required hardware, such as biomass screw feeder and air rotameters specifications.

8.1.2 Cold fluidisation experimental tests

The experimental tests on the hydrodynamics of the fluidization of inert sand material, SPWB and IDPWB biomass materials and biomass-inert mixtures have been conducted to study fluidisation material behaviours and to determine the minimum fluidization velocity for each single and mixed materials according to the geometry design results.

The cold experimental tests has shown the following conclusions over the ranges tested within the thesis:

- Fluidization behaviour, bed material or solid fuel reactant, has depended on the type and physical characteristics of the material. By observing the fluidization behaviour the findings have shown that sand bed material has a perfect fluidization ability leading to establishing a smooth hydrodynamic curve (ΔP-U_o), whereas the observed fluidization behaviour of each biomass, SPWB and IDPWB, which are the biomass materials in this study, have shown a weak fluidization behaviour causing an unclear hydrodynamic curve. The indication of this weak fluidization was observed during the formation of the bridging, clustering and channelling features inside the biomass bed column. This was due to their physical characteristics: low particle density, irregular shape, and high particle aspect ratio, moisture content and high inter-particular forces between biomass particles.
- The minimum fluidization velocity for sand bed material U_{mf} has been found from the hydrodynamic curve (ΔP-U_o). Furthermore, it has concluded that U_{mf} was affected by the sand particle size. For three ranges of particle size of the sand material, (300-425) µm, (425-500) µm and (500-600) µm were 10.875, 18.665 and 23 cm/sec, respectively.
- The three static bed heights H_s, 0.5D=4.15, 0.75D= 6.225 and 1D=8.3cm, have no significant effect on the minimum fluidization velocity U_{mf}.
- In order to upgrade their fluidization behaviour, biomass material has been blended with the sand material in a specific weight percent. The finding has shown

that the minimum fluidization velocity can be estimated by their established hydrodynamic curve. In addition, it has been found that when the mass percent increased the U_{mf} has gradually increased.

8.1.3 Air-biomass gasification experimental tests

Experimental tests for air-biomass gasification in the bubbling fluidised bed gasifier have been conducted. The effect of fluidization hydrodynamics and operating conditions parameters on the performance have been investigated. The conclusion can be outlined as follows:

- Uniform axial temperature distribution along the fluidised bed gasifier has not been achieved. This was because that the electric heater element has one temperature set point, which provided a maximum allowable temperature 1020^{o}C at the position 44 cm above the distributor plate. Practically 900^{o}C as the set temperature has been used for all experimental tests. Experiments had shown 551^{o}C, a bed temperature T2 that can be achieved when the gasifier was filled with an 8.3cm static bed height of (300-425) µm particle size of sand material with zero airflows. The best temperature distribution at equilibrium conditions for airflow range (30-100l/min and more) has been obtained at the set-point temperature 900^{o}C and bed temperature T2 at 340-360^{o}C. It is likely that uniform conditions do not occur in real systems, and this result shows that temperature distribution is an important operational consideration.
- For 5 min and more, this biomass feeding time has approximately shown stable conditions of producer gas composition, CO, CO_2, CH_4, H_2 and O_2.
- ***Effect of air flowrate parameter*:** This parameter has shown a significant effect on the producer gas composition and performance parameters (CCE), (CGE), (LHV) and gas yield (Y) at constant equivalence ratio, i.e. the feed rate of feeding biomass increases as air flowrate increases. It has been shown that the trends of the producer gases composition for two biomass, SPWB and IDPWB were similar. H_2, CO_2 and CH_4 decreased as air flowrate increased whereas CO increased. SPWB has produced higher H_2 and CO and lower CO_2 and CH_4 than IDPWB. A low air flowrate of 44 l/min has shown a significant effect providing a highest (CCE), (CGE), (LHV), gas yield (GY) and gas composition for IDPWB.

Within this range of air flowrates, an LHV of producer gas for both biomass has been achieved between 4.0 and 5.3MJ/Nm^3db.

This factor is mainly related to the hydrodynamic fluidization parameters such as bubble size and velocity, which are linked to the bubble fraction in the bed, and the residence time of the gas and biomass particles. In addition, as the air flowrate increase, the biomass mass fraction in the bed increase and thereby the minimum fluidization velocity increase.

- ***Effect of particle size of san bed material***: The effect of this factor has shown that as sand particle size increased the hydrodynamic changes will weaken the gasification performance. These hydrodynamic changes were due to the variations in the values of the minimum fluidization velocity due to the various ranges of sand particle size.

  For SPWB it has been shown that there was no a considerable effect of the sand particle size on the producer gas composition and gasifier performance parameters (CCE), (CGE), (LHV) and (GY), which agrees with published results. While for IDPWB it has been shown that the low range of sand particle size (300-425) µm provided higher performance parameters (CCE), (CGE), (LHV) and (GY) than the other ranges, (425-500) µm and (500-600) µm which provided a similar effect. SPWB has provided 6MJ/Nm^3db (LHV) of producer gas, which is higher than IDPWB.

- ***Effect of the biomass particle size***: This parameter has shown a significant effect on the producer gas composition and performance parameters for both biomass SPWB and IDPWB. In general, the best effect has been achieved by the smallest biomass particle size (300-425) µm due to their high reaction surface area. Three possible reason can be given and confirmed due to this finding, 1) The smaller particles have a faster heating rate, where in the pyrolysis process the control step for smaller particles is reaction kinetics. 2) Whereas for larger is the gas diffusion step. 3) Due to the segregation phenomena of the biomass particles which is faster for small particles than large particles due to the low weight of the former particles.

- ***Effect of the static bed height H_s***: For this study, according to the experiment operating conditions and due to the position of the temperature set point it has been shown that the bed temperature T2 decreased as the bed height increased thereby affecting the gasifier performance. Furthermore, the position of the

biomass feeding point has also affected the gasifier performance. For this range of the three selected bed heights, the static height 6.23cm has shown the best results for both biomass materials, in particular on the performance parameters. This height has achieved two important points, a suitable residence time larger than H_s=4.15cm and lesser than H_s=8.3cm, the feeding point was located within the bed height (in bed feeding point) providing a better mixing and contact of reactants than the on-bed feeding point.

- ***Effect of equivalence ratio ER***: The results have shown that equivalence ratio has a significant effect on the biomass gasification performance. For the range (0.2-0.45) of ER for both biomass materials, SPWB and IDPWB it has been shown that at lowest value of ER=0.2 the highest gas compositions, LHV, have been obtained, whereas the highest values of the (CCE), (CGE), and total and individual gas yield have been achieved at ER=0.45. In addition, it has been shown that the total producer gas yield increases significantly as ER increases due to the rise of the gas yield of each individual gas in the producer gas. Furthermore, in this study the fluidization hydrodynamic has shown a significant effect on the ER effects. This was because of the increase of ER was at constant air flowrate, and decrease biomass mass rate is leading to decreasing in biomass mass fraction inside the bed.
- ***Effect of the bed temperature T2***: The results of this factor have shown that the low bed temperature 360^{o}C and 465^{o}C had a considerable effect on the gasifier performance producing a high producer gas composition, (CCE), (CGE), (LHV) and gas yield (GY). SPWB has shown higher results for these producer gas and performance parameters than IDPWB. Furthermore, it has been illustrated that the increase of the bed temperature T2 from 360 to 465^{o}C does not provide a significant difference in the results.
- ***Effect of the number of holes of the distributor plate N_{orf}***: The results of the consequences of this parameter N_{orf} has revealed that this has a significant effect on the biomass gasification performance. The results have also shown there is a disagreement in its effect on each biomass results. For this range of N_{orf} it has proved that the N_{orf}= 85 is the optimum distributor plate for SPWB, whereas N_{orf}= 19 is the optimum for IDPWB.

- For all factors effects, the results have appeared that SPWB has higher gasification potential in fluidised bed reactor than IDPWB.
- For all factors, the results have shown the highest composition of CO and H_2 in producer gas and the former is greater than the later.

8.2 Recommendations for Future work

The following are the number of possible future studies that can be done within this study:

- A simulation based preliminary design study should be performed for biomass gasification research using a high-performance software such as FLUENT.
- Increase the biomass feeding time, minimum 1/2 hour, to show the maximum equilibrium bed temperature without external heating.
- Modify and improve the performance of the air biomass bubbling fluidised gasifier for optimum gasification conditions with optimisation studies within a broad range of studied parameters or factors (more than 5 points for each factor) to obtain a wider range of gasification conditions.
- To enhance biomass gasification performance and conversion further research work can be conducted under high-temperature conditions in the bed and freeboard sections. This will require multi-temperature set points, particularly in the bed and freeboard sections.
- For a correct material balance for an air-biomass gasification process, an accurate instrument for all input and output streams to their mass rate or volumetric flow rate are needed. For example, the tar measurement, measurement of the total producer gas mass rate and measurement of accumulated particulates, which accompanied producer gas quantification.
- The research study should be conducted to examine the effect of the catalyst materials on the biomass gasification in the bubbling fluidised bed gasifier. This catalyst material can be used with the sand material for a different mass percent or alone according to the physical properties and the potential of the catalyst. In addition, a research study can be conducted to investigate the effect of other gas agents such as CO_2, steam, H_2, etc…or a mixture of them with air.

- For the same conditions of this study, a research study under pyrolysis conditions using N_2 gas as an agent gas for fluidization and for pyrolysis environment conditions can be recommended, i.e. varying the hydrodynamic conditions independently of ER and vice versa.
- To obtain more specific and precise biomass gasification results, high quality instruments with computer control are needed.

References

Abdullah, M.Z., Husain, Z. and Pong, S.L.Y. 2003. Analysis of cold test results for various biomass fuels. *Biomass and Bioenergy* 24, pp. 487–494.

AHMED F. ZABAR, A.B. 2012. Cultivation of date palm in Iraq. *A nnales Universitatis Mariae Curie-Sklodowska L U B L IN – P O L O N IA* XXII(1), pp. 39–53.

Alauddin, Z., Lahijani, P., Mohammadi, M. and Mohamed, A. 2010. Gasification of lignocellulosic biomass in fluidized beds for renewable energy development: A review. *Renewable and Sustainable Energy Reviews* 14(9), pp. 2852–2862.

Ali, H.G. 2010. Development of date palm Cultivation and its Role in Sustainability of Agriculture in Oman. *IV International Date Palm Conference, Abu Dhabi, United Arab Emirate* IV(882), pp. 29–35.

Almeida, A.F., Vieira, M.S., Ribeiro, A.M., Pereira, I.M. and Neto, M.P. 2016. Effect of Air/Biomass Ratio on the Gasification of Olive Bagasse Particles. *International Journal of Environmental Science and Development* 7(4), pp. 269–272.

Anon 2011a. BSI Standards Publication Solid biofuels — Determination of total content of carbon , hydrogen and nitrogen — Instrumental methods.

Anon 2011b. BSI Standards Publication Solid recovered fuels — Methods for the preparation of the test sample from the laboratory sample.

Anon 2011c. Date Palm Cultivation in Iraq. *www.iraqi-datepalm.net*.

Anon No Titlehttp://thefrogpad.weebly.com/general-ecology.html [Online].

Arena, U. 2012. Process and technological aspects of municipal solid waste gasification. A review. *Waste Management* 32(4), pp. 625–639.

Augusta, A., Pécora, B., Vinicius, M., Geris, A., Harold, J. and Arnao, S. 2011. Experimental Study of Gas Distributors for Fluidized Beds Containing Sand-Bagasse Mixtures.

Aznar, M.P., Gracia-Gorria, F.A. and Corella, J. 1992. Minimum and maximum velocities for fluidization for mixtures of agricultural and forest residues with a second fluidized solid. I. Preliminary data and results with sand-sawdust mixtures. *International Chemical Engineering* 32(1), pp. 95–102.

Badday, B.A., Gupta, A. V., Beddai, A.A. and Naik, M.T. 2014. Experimental Study on the Bed Voidage and Minimum Fluidization Velocity of Gas-Solid Fluidization under Different Conditions. *International jornal of Mechanical Engineering* 2(7), pp. 22–26.

Barmina, I., Lickrastina, A., Valdmanis, R., Zake, M., Arshanitsa, A., Solodovnik, V. and Telysheva, G. 2013. Effects of Biomass composition variations on gasification and combustion characteristics. *Engineering for rural development*, pp. 382–387.

Basu, P. 2006. *Combustion and Gasification fluidised Beds*.

Basu, P. 2010. *Biomass Gasification and Pyrolysis-Practical Design and Theory*. Elsevier Ink.

Bauer, W., Werther, J. and Emig, G. 1981. Influence of gas distributor design on the performance of fluidized bed reactor. *Ger. Chem. Eng* 4, pp. 291–298.

British Standards Institution (BSI) 2010. Solid biofuels. Determination of bulk density. (BS EN 15103:2009).

British Standards Institution (BSI) 2014. Plastics — Thermogravimetry (TG) of polymers — Part 1: General principles. *Bs En Iso 11358-1:2014*.

Brown, J. 2006. Biomass Gasification : Fast Internal Circulating Fluidised Bed Gasifier Characterisation and Comparison. *Fuel* 89(2), pp. 384–391.

BS 1377-9 1990. *Soils for civil engineering purposes*.

BS DD CEN/TS 14918 2005. *Solid biofuels - Method for the determination of calorific value*.

Cao, Y., Wang, Y., Riley, J.T. and Pan, W.-P. 2006. A novel biomass air gasification process for producing tar-free higher heating value fuel gas. *Fuel Processing Technology* 87(4), pp. 343–353.

CEN (European Comitte for Standardisation) 2009. EN 15148:2009 Solid biofuels - Determination of the content of volatile matter.

Chhiti, Y. and Kemiha, M. 2013. Thermal Conversion of Biomass , Pyrolysis and Gasification : A Review. *The International Journal of Engineering And Siences (IJES)* 2(3), pp. 75–85. Available at: www.theijes.com.

Chok, V.S. 2009. Effect of Particle and Bed Diameter on Characteristic Velocities in Compartmented Fluidized Bed Gasifier. 09.

Chok, V.S., Gorin, a and Chua, H.B. 2010. Minimum and Complete Fluidization Velocity for Sand-Palm Shell Mixtures , Part I : Fluidization Behavior and Characteristic Velocities Department of Chemical Engineering , University Technology PETRONAS , School of Engineering and Science , Department of . 7(6), pp. 763–772.

Christopher Higman, M. van der B. 2003. *Gasification*. Elsevier Ltd.

Ciferno, J.P. and Marano, J.J. 2002. Benchmarking biomass gasification technologies for fuels, chemicals and hydrogen production. *US Department of Energy. National Energy* (June), p. 58.

Cirad, B.P. 2009. Catalytic Biomass Gasification Process in Fluidized bed Reactor Dottorato di Ricerca in Ingegneria Chimica. *Thesis* (January).

Clarke, K.L., Pugsley, T. and Hill, G. a. 2005. Fluidization of moist sawdust in binary particle systems in a gas-solid fluidized bed. *Chemical Engineering Science* 60(24), pp. 6909–6918.

Cocco, R., Karri, S.B.R. and Knowlton, T. 2014. Introduction to fluidization. *Chemical Engineering Progress* 110(11), pp. 21–29.

Cui, H. and Grace, J.R. 2007. Fluidization of biomass particles: A review of experimental multiphase flow aspects. *Chemical Engineering Science* 62(1-2), pp. 45–55.

Daizo, K. and Levenspiel, O. 1991. Fluidization engineering.

Das, B. and Datta, A. 2014. Effects of Fluidizing Gas Flow Rate and Reactor Diameter on the Hydrodynamics of a Bubbling Fluidized Bed Gasifier.

David Sutton, Brian Kellehr, J.R.H.R. 2001. Review of literature on catalysts for biomass gasification. *Fuel Processing Technology* 73, pp. 155–173.

Demirel, Y. 2012. *Energy: Production, Conversion, Storage, Conservation, and Coupling*.

Devi, L., Ptasinski, K.J. and Janssen, F.J.J.G. 2002. A review of the primary measures for tar elimination in biomass gasification processes. *Biomass and Bioenergy* 24(2), pp. 125–140.

Dong, S., Cao, C., Si, C. and Guo, Q. 2009. Effect of perforated ratios of distributor on the fluidization characteristics in a gas-solid fluidized bed. *Industrial and Engineering Chemistry Research* 48(1), pp. 517–527.

Dora, D.T.K., Panda, S.R., Mohanty, Y.K. and Roy, G.K. 2013. Hydrodynamics of gas-solid fluidization of a homogeneous ternary mixture in a conical bed: Prediction of bed expansion and bed fluctuation ratios. *Particuology* 11(6), pp. 681–688.

Dr. Sami Sadaka, P.E., P.E. 1. Gasification. *Center for Sustainable Environmental Technologies , Iowa State University* (1521 West F. Ave, Nivada, IA 50201).

Eea 2011. Total primary energy consumption by energy source in 2008, EU-27.

Eisentraut, A. and Brown, A. 2012. Technology Roadmap Bioenergy for Heat and Power. *Technology Roadmaps* (2), pp. 1–41.

Emerson Process Management 2012. *X-Stream Gas Analyzers, Instruction Manual*.

En 14774-1 2009. Solid biofuels - Determination of moisture content - Oven dry method - Part 1: Total moisture - Reference method. , pp. 1–8.

Van Den Enden, P.J. and Lora, E.S. 2004. Design approach for a biomass fed fluidized bed gasifier using the simulation software CSFB. *Biomass and Bioenergy* 26(3), pp. 281–287.

Energy research Centre of the Netherlands 2004. Biomass gasification - Tar and particles in product gases - Sampling and analysis. 2, p. 41.

Engineering, C. 2011. The effect of parameters on the performance of a Fluidized bed reactor and Gasifier The effect of parameters on the performance of a Fluidized bed reactor and Gasifier. (209).

Escudero, D. and Heindel, T.J. 2011. Bed height and material density effects on fluidized bed hydrodynamics. *Chemical Engineering Science* 66(16), pp. 3648–3655.

Feng, Y., Xiao, B., Klaus, G., Gong, C. and Jingbo, W. 2011. Influence of Particle Size and Temperature on Gasification Performance in Externally Heated Gasifier. *Smart Grid and Renewable Energy* 02(03), pp. 177–183.

Folkeson, B. 2014. Propensity of various bed materials used in fluidized beds to retain ash-forming elements from biomass fuels.

Formisani, B., Girimonte, R. and Longo, T. 2008. The fluidization process of binary mixtures of solids: Development of the approach based on the fluidization velocity interval. *Powder Technology* 185(2), pp. 97–108.

Formisani, B., Girimonte, R. and Mancuso, L. 1998. Analysis of the fluidization process of particle beds at high temperature. *Chemical Engineering Science* 53(5), pp. 951–961.

Fotovat, F., Abbasi, A., Spiteri, R.J., de Lasa, H. and Chaouki, J. 2015. A CPFD model for a bubbly biomass-sand fluidized bed. *Powder Technology* 275, pp. 39–50.

Fotovat, F., Chaouki, J. and Bergthorson, J. 2013. The effect of biomass particles on the gas distribution and dilute phase characteristics of sand-biomass mixtures fluidized in the bubbling regime. *Chemical Engineering Science* 102, pp. 129–138.

Fremaux, S., Beheshti, S.-M., Ghassemi, H. and Shahsavan-Markadeh, R. 2015. An experimental study on hydrogen-rich gas production via steam gasification of biomass in a research-scale fluidized bed. *Energy Conversion and Management* 91, pp. 427–432.

Gautam, G. 2010. Parametric Study of a Commercial-Scale Biomass Downdraft Gasifier: Experiments and Equilibrium Modeling.

Gauthier, D., Zerguerras, S. and Flamant, G. 1999. Influence of the particle size distribution of powders on the velocities of minimum and complete fluidization. *Chemical Engineering Journal* 74(3), pp. 181–196.

Geldart, D. 1973. Types of gas fluidization. *Powder Technology* 7(5), pp. 285–292.

Ghaly, a., Ergudenler, A. and Ramakrishnan, V. 2015. Effect of Distributor Plate Configuration on Pressure Drop in a Bubbling Fluidized Bed Reactor. *Advances in Research* 3(3), pp. 251–268. Available at: http://www.sciencedomain.org/abstract.php?iid=755&id=31&aid=6538.

Ghani A.K., Moghadam R.A., Salleh M.A. and Alias A.B. 2009. Air Gasification of Agricultural Waste in Fluidized Bed Gasifier: Hydrogen Production Performance. *Energies* 2, pp. 258–268.

Gómez-Barea, a. and Leckner, B. 2010. Modeling of biomass gasification in fluidized bed. *Progress in Energy and Combustion Science* 36(4), pp. 444–509.

Gómez-barea, A., Leckner, B. and Ollero, P. 2011. Methods to improve the performance of fluidized bed biomass gasifiers. *Energy Conversion*, pp. 1–12.

Guevara, D.E. 2010. Bed height and material density effects on fluidized bed hydrodynamics. MSc thesis, Iowa state university, USA.

Gunn, D.J. and Hilal, N. 1997. The expansion of gas-fluidised beds in bubbling fluidisation. *Chemical Engineering Science* 52(16), pp. 2811–2822.

Guo, Q., Chen, X. and Liu, H. 2012. Experimental research on shape and size distribution of biomass particle. *Fuel* 94, pp. 551–555.

Halvorsen, B. 2010. Applications. , p. 16.

Harriott, P. 2003. *Chemical Reactor Design*.

Hilal, N., Ghannam, M.T. and Anabtawi, M.Z. 2001. Effect of Bed Diameter, Distributor and Inserts on Minimum Fluidization Velocity. *Chemical Engineering & Technology* 24(2), pp. 161–165.

Hlavsová, A., Corsaro, A., Raclavská, H., Vallová, S. and Juchelková, D. 2016. The effect of feedstock composition and taxonomy on the products distribution from pyrolysis of nine herbaceous plants. *Fuel Processing Technology* 144, pp. 27–36.

International Energy Agency 2012. Iraq Energy Outlook. , pp. 1–142.

International Energy Agengy 2014. 2014 Key World Energy STATISTICS.

J.S.M.Botterill 1975. *Fluid-bed heat transfer, J*. London: Acadimic Press INC.LTD.

Jangam, S. V., Mujumdar, A.S. and Thorat, B.N. 2009. Design of an Efficient Gas Distribution System for a Fluidized Bed Dryer. *Drying Technology* 27(11), pp. 1217–1228.

Jena, H.M., Roy, G.K. and Biswal, K.C. 2008. Studies on pressure drop and minimum fluidization velocity of gas-solid fluidization of homogeneous well-mixed ternary mixtures in un-promoted and promoted square bed. *Chemical Engineering Journal* 145(1), pp. 16–24.

Jeremiáš, M., Pohořelý, M., Vosecký, M., Skoblia, S., Kameníková, P., Svoboda, K. and Punčochář, M. 2009. Experimental Study of Fluidized-Bed Biomass Gasification with CO 2 + H 2 O Mixtures on Limestone and Silica Sand. *IEC Gasification conference publication*.

Jiliang, M., Xiaoping, C. and Daoyin, L. 2013. Minimum fluidization velocity of particles with wide size distribution at high temperatures. *Powder Technology* 235, pp. 271–278.

Karmakar, M.K., Haldar, S. and Chatterjee, P.K. 2013. STUDIES ON FLUIDIZATION BEHAVIOUR OF SAND AND BIOMASS MIXTURES. *International Journal of Engineering Technology and Advanced Engineering* 3(Special Issue).

Karnik, A., Rangarajan, A. and Tandon, M. 2013. Numerical Investigation of the Effect of Bed Height and Coefficient of Restitution on the Minimum Fluidization Velocity of a Cylindrical Fluidized Bed . (December), pp. 1–5.

Kern, S., Pfeifer, C. and Hofbauer, H. 2013. Gasification of lignite in a dual fluidized bed gasifier - Influence of bed material particle size and the amount of steam. *Fuel Processing Technology* 111, pp. 1–13.

Kim, Y.D., Yang, C.W., Kim, B.J., Kim, K.S., Lee, J.W., Moon, J.H., Yang, W., Yu, T.U. and Lee, U. Do 2013. Air-blown gasification of woody biomass in a bubbling fluidized bed gasifier. *Applied Energy* 112, pp. 414–420.

Kirsanovs, V., Žandeckis, A., Blumberga, D. and Veidenbergs, I. 2014. The influence of process temperature , equivalence ratio and fuel moisture content on gasification process : A review. 2(JUNE).

Klein, A. 2002. Gasification: an alternative process for energy recovery and disposal of municipal solid wastes. *New York* (May), pp. 1–50.

Koppatz, S., Schmid, J.C., Pfeifer, C. and Hofbauer, H. 2012. The E ff ect of Bed Particle Inventories with Di ff erent Particle Sizes in a Dual Fluidized Bed Pilot Plant for Biomass Steam Gasi fi cation.

Kumar, A., Jones, D.D. and Hanna, M. a. 2009. Thermochemical Biomass Gasification: A Review of the Current Status of the Technology. *Energies* 2(3), pp. 556–581.

Kumoro, A., Nasution, D., Cifriadi, A. and Falaah, A. 2014. A New Correlation For The Prediction of Minimum Fluidization of Sand And Irregularly Shape Biomass Mixtures In A Bubbling Fluidized Bed. 9(23), pp. 21561–21573.

Laboratory, N.E.T. (NETL) 2016. -systems/gasification/gasifipedia/water-gas-shift [Online].

Lahijani, P. and Zainal, Z.A. 2011. Gasification of palm empty fruit bunch in a bubbling fluidized bed: A performance and agglomeration study. *Bioresource Technology* 102(2), pp. 2068–2076.

LECO, C. 2008. SC-144DR Sulfur / Carbon Determinator Specification Sheet. 5/08-REV8(209-134-001), pp. 0–1.

Lee, W.-J., Kim, S.-D. and Song, B.-H. 2002. Steam gasification of an australian bituminous coal in a fluidized bed. *Korean Journal of Chemical Engineering* 19(6), pp. 1091–1096.

Legonda, I.A. 2012. Biomass gasification using a horizontal entrained-flow gasifier and catalytic processing of the product gas.

Lettieri, P. and Macrì, D. 2016. Effect of Process Conditions on Fluidization. *KONA Powder and Particle Journal* (October), pp. 1–24.

Lim, M.T. and Alimuddin, Z. 2008. Bubbling fluidized bed biomass gasification—Performance, process findings and energy analysis. *Renewable Energy* 33(10), pp. 2339–2343.

Lu, H., Ip, E., Scott, J., Foster, P., Vickers, M. and Baxter, L.L. 2010. Effects of particle shape and size on devolatilization of biomass particle. *Fuel* 89(5), pp. 1156–1168.

Lv, D., Xu, M., Liu, X., Zhan, Z., Li, Z. and Yao, H. 2010. Effect of cellulose, lignin, alkali and alkaline earth metallic species on biomass pyrolysis and gasification. *Fuel Processing Technology* 91(8), pp. 903–909.

Lv, P.., Xiong, Z.., Chang, J., Wu, C.., Chen, Y. and Zhu, J.. 2004. An experimental study on biomass air–steam gasification in a fluidized bed. *Bioresource Technology* 95(1), pp. 95–101.

Maglinao, A.L., Capareda, S.C. and Nam, H. 2015. Fluidized bed gasification of high tonnage sorghum, cotton gin trash and beef cattle manure: Evaluation of synthesis gas production. *Energy Conversion and Management* 105, pp. 578–587.

Makwana, J.P., Joshi, A.K., Athawale, G., Singh, D. and Mohanty, P. 2015. Air gasification of rice husk in bubbling fluidized bed reactor with bed heating by conventional charcoal. *Bioresource technology* 178, pp. 45–52.

Makwana, J.P., Joshi, A.K., Patel, N.R. and Patel, D. 2016. Effect of Equivalence Ratio on Performance of Fluidized Bed Gasifier Run With Sized Biomass. *International journal of mechanical , aerospace, indusrtial, mechatronic and manufacturing engineering* 10(6), pp. 974–978.

Malvern Instruments 2015. Mastersizer 3000 user manual. November(MAN0474-07-EN-00).

Malvern Instruments Mastersizer 3000-Smarter Particle Sizing, Malvern-Material relationships.

Marque, J.J.P. 2002. Minimum fluidization velocities for gasÁ solid 2D beds Guadalupe Ramos Caicedo *, Mo. *Chemical Engineering and Processing* 41, pp. 761–764.

Marsh, R., Steer, J.M., Fesenko, E., Cleary, V., Rahman, A., Griffiths, A.J. and Williams, K.P. 2008. Biomass and waste co-firing in large-scale combustion systems. *Proceedings of the ICE-Energy* (August), pp. 115–126. Available at: http://orca.cf.ac.uk/7933/.

Miccio, F., Barletta, D. and Poletto, M. 2013. Flow properties and arching behavior of biomass particulate solids. *Powder Technology* 235, pp. 312–321.

Miccio, F., Silvestri, N., Barletta, D. and Poletto, M. 2011. Characterization of Woody Biomass Flowability. *Chemical engineering transactions* 24, pp. 643–648.

Mohammed, M. a. a., Salmiaton, A., Wan Azlina, W. a. K.G., Mohammad Amran, M.S. and Fakhru'l-Razi, A. 2011. Air gasification of empty fruit bunch for hydrogen-rich gas production in a fluidized-bed reactor. *Energy Conversion and Management* 52(2), pp. 1555–1561.

Mohd Salleh, M. a., Nsamba, H.K., Yusuf, H.M., Idris, A. and Ghani, W. a. W.A.K. 2015. Effect of Equivalence Ratio and Particle Size on EFB Char Gasification. *Energy Sources, Part A: Recovery, Utilization, and Environmental Effects* 37(15), pp. 1647–1662.

Molino, A., Chianese, S. and Musmarra, D. 2015. Biomass gasification technology: The state of the art overview. *Journal of Energy Chemistry* 000, pp. 1–16.

Morf, P., Hasler, P. and Nussbaumer, T. 2002. Mechanisms and kinetics of homogeneous secondary reactions of tar from continuous pyrolysis of wood chips. *Fuel* 81(7), pp. 843–853.

Muazu, R.I., Borrion, A.L. and Stegemann, J. a 2015. Fluidised Bed Gasification of Multiple Agricultural Biomass Derived Briquettes. 9(5), pp. 610–616.

Narvaez, I., Orıo, A., Aznar, M.P. and Corella, J. 1996. Biomass Gasification with Air in an Atmospheric Bubbling Fluidized Bed . Effect of Six Operational Variables on the Quality of. *Ind. Eng. Chem. Res.* 35(95), pp. 2110–2120.

Newton, H.W. 1969. R12.3 Fluidized-Bed Reactors 1. *Symposium A Quarterly Journal In Modern Foreign Literatures* 168, pp. 1–44.

Nguyen, M., Duddy, G. and Karam, C. 2015. PAM Review.

Oliveira, T.J.P., Cardoso, C.R. and Ata??de, C.H. 2013. Bubbling fluidization of biomass and sand binary mixtures: Minimum fluidization velocity and particle segregation. *Chemical Engineering and Processing: Process Intensification* 72, pp. 113–121.

Ommen, J.R. Van and Ellis, N. 2010. Fluidization Gas-Solid Fluidized Bed.

Parr instrument company 6100 Calorimeter Operation.

Patel, N. 2014. http://www.slideshare.net/nmpatel92/hot-producer-gas-cleaning-system [Online].

Patil, K., Bower, T., Bellmer, D. and Huhnke, R. 2005. Fluidization Characteristics of Sand and Chopped Switchgrass- Sand Mixtures. *Agricultural Engineering International: the CIGR Ejournal* VII, pp. 1–9.

PETRO, J.J.R. j. d. M. and S.L. 2007. Basic design of a fluidized bed gasifier for rice husk on a pilot scale. *Latin American Applied Research* 37, pp. 299–306.

Piriou, B. 2009. Catalytic Biomass Gasification Process in Fluidized bed Reactor Dottorato di Ricerca in Ingegneria Chimica.

Puig-Arnavat, M., Bruno, J.C. and Coronas, A. 2010. Review and analysis of biomass gasification models. *Renewable and Sustainable Energy Reviews* 14(9), pp. 2841–2851.

Qiaoqun, S., Huilin, L., Wentie, L., Yurong, H., Lidan, Y. and Gidaspow, D. 2005. Simulation and experiment of segregating/mixing of rice husk-sand mixture in a bubbling fluidized bed. *Fuel* 84(14-15), p. 1739.

R. R. Pattipati, C.Y.W. 1981. Minimum Fluidization Velocity at High Temperatures. *Ind. Eng. Chem. Process Des. Dev.* 20, pp. 705–707.

Radwan, A.M. 2012. An overview on gasification of biomass for production of hydrogen rich gas. *Der Chemica Sinica* 3(2), pp. 323–335.

Ramin Radmanesh, Jamal Chaouki, and C.G. 2006. Biomass Gasification in a Bubbling Fluidized Bed Reactor: Experiments and Modeling. *AICHE* 52(12), pp. 405–410.

Rao, T.R. and Bheemarasetti, J.V.R. 2001. Minimum fluidization velocities of mixtures of biomass and sands. *Energy* 26(6), pp. 633–644. Available at: http://linkinghub.elsevier.com/retrieve/pii/S0360544201000147\npapers3://publication/doi/10.1016/S0360-5442(01)00014-7.

Rapagnà, S., Mazziotti, G. and Rapagna, S. 2008. Devolatilization of wood particles in a hot fluidized bed : Product yields and conversion rates Product yields and conversion rates. (December).

Ravaghi-ardebili, Z., Manenti, F., Pirola, C. and Soares, F. 2014. Influence of the Effective Parameters on H 2 : CO Ratio of Syngas at Low-Temperature Gasification. 37, pp. 253–258.

Rhodes, M. 2008. *Introduction to Particle Technology: Second Edition*.

Ross, D., Noda, R., Horio, M., Kosminski, A., Ashman, P. and Mullinger, P. 2007. Axial gas profiles in a bubbling fluidised bed biomass gasifier. 86, pp. 1417–1429.

Sadaka, S. 2010. Gasification, producer gas and syngas. *Agriculture and Natural Resources*.

Sadaka, S.S., Ghaly, a. E. and Sabbah, M. a. 2002. Two phase biomass air-steam gasification model for fluidized bed reactors: Part II - Model sensitivity. *Biomass and Bioenergy* 22(6), pp. 463–477.

Sampaio, D.P. 2013. Effect of the Geometry of a Gas Distributor (Tuyere Type) on Fluidization of a Binary Mixture Biomass-Sand. *22nd International Congress of Mechanical Engineering (COBEM 2013)* (Cobem), pp. 6439–6448.

Sau, D.C., Mohanty, S. and Biswal, K.C. 2007. Minimum fluidization velocities and maximum bed pressure drops for gas–solid tapered fluidized beds. *Chemical Engineering Journal* 132(1-3), pp. 151–157.

Seo, M.W., Goo, J.H., Kim, S.D., Lee, J.G., Guahk, Y.T., Rho, N.S., Koo, G.H., Lee, D.Y., Cho, W.C. and Song, B.H. 2014. The transition velocities in a dual circulating fluidized bed reactor with variation of temperatures. *Powder Technology* 264, pp. 583–591.

Sethupathy, S.B. (Velammal E.C. and E. Natarajan (Institute for Energy Studies, Anna University, C. 2012. Hydrodynamic study on gasification of biomass in a fluidized bed gasifier. *International Journal of Engineering Science and Technology* 4(01), pp. 316–323.

Shao, Y., Ren, B., Jin, B., Zhong, W., Hu, H., Chen, X. and Sha, C. 2013. Experimental flow behaviors of irregular particles with silica sand in solid waste fluidized bed. *Powder Technology* 234, pp. 67–75.

Sharma, A.M., Kumar, A., Patil, K.N. and Huhnke, R.L. 2013. Fluidization characteristics of a mixture of gasifier solid residues, switchgrass and inert material. *Powder Technology* 235, pp. 661–668.

Siedlecki, M., de Jong, W. and Verkooijen, A.H.M. 2011. Fluidized bed gasification as a mature and reliable technology for the production of bio-syngas and applied in the production of liquid transportation fuels-a review. *Energies* 4(3), pp. 389–434.

Skoulou, V., Koufodimos, G., Samaras, Z. and Zabaniotou, A. 2008. Low temperature gasification of olive kernels in a 5-kW fluidized bed reactor for H2-rich producer gas. *International Journal of Hydrogen Energy* 33(22), pp. 6515–6524.

Subramani, H.J., Mothivel Balaiyya, M.B. and Miranda, L.R. 2007. Minimum fluidization velocity at elevated temperatures for Geldart's group-B powders. *Experimental Thermal and Fluid Science* 32(1), pp. 166–173.

Subramanian, R. 2004. Flow through Packed Beds and Fluidized Beds. *... University,[cited February 2007], http://www. ...*, pp. 1–6. Available at: http://web2.clarkson.edu/projects/subramanian/ch301/notes/packfluidbed.pdf.

Sudipta, R.M.& S.G.& 2013. Cracking of tar by steam reforming and hydrogenation. , pp. 103–111.

Teaters, L.C., Tech, V., Battaglia, F. and Tech, V. 2014. On the Computational Modeling of Unfluidized and Fluidized Bed Dynamics. *Journal of Fluids Engineering* 136(October 2014), pp. 1–7.

Technical committee CEN/TC 2005. Solid biofuels - Determination of ash content. *Management*, pp. 1–140.

Tilay, A., Azargohar, R., Gerspacher, R., Dalai, A. and Kozinski, J. 2014. Gasification of Canola Meal and Factors Affecting Gasification Process. *BioEnergy Research*, pp. 1–13.

Tzeng, L.M. 2007. Characterization of a Bubbling Fluidized Bed Biomass Gasifier.

University of Florida 2015. Fluidization: A Unit Operation in Chemical Engineering. (March 13 2015), pp. 1–13. Available at: http://www.che.ufl.edu/unit-ops-lab/experiments/FB/FB-manual.pdf.

Vassilev, S. V., Baxter, D., Andersen, L.K. and Vassileva, C.G. 2010. An overview of the chemical composition of biomass. *Fuel* 89(5), pp. 913–933.

W.A.W.K. Ghani1, 2*, R.A. Moghadam1, M.A.M. Salleh1, 2, A.T. 2012. Gasification Performance of Rice Husk in Fluidized Bed Reactor: A Hydrogen-Rich Production. *Journal of Energy & Environment* 4(1), pp. 7–11.

WATLOW 2013. *Ceramic Fiber Heaters*.

Wilk, V., Schmid, J.C. and Hofbauer, H. 2013. Influence of fuel feeding positions on gasification in dual fluidized bed gasifiers. *Biomass and Bioenergy* 54, pp. 46–58.

Xiao, R., Jin, B., Zhou, H., Zhong, Z. and Zhang, M. 2007. Air gasification of polypropylene plastic waste in fluidized bed gasifier. *Energy Conversion and Management* 48(3), pp. 778–786.

Yang, W. 2003. *Handbook of fluidization and fluid-particle systems*. CRC press.

Zhang, Y., Zhong, W. and Jin, B. 2011. Experimental and Theoretical Study on Fluidization of Stalk-Shaped Biomass Particle in a Fluidized Bed. *International Journal of Chemical Reactor Engineering* 9, pp. 1–23.

Zhong, W., Jin, B., Zhang, Y., Wang, X. and Xiao, R. 2008. Fluidization of biomass particles in a gas-solid fluidized bed. *Energy and Fuels* 22(6), pp. 4170–4176.

APPENDIX A

Gasifier Design Procedure and Steps

A.1 Design steps calculation

To show the procedure and algorithm of the fluidized bed gasifier design, the following steps were built and performed:

- **Step 1: Given input data:**

The following data should be given as an input data to calculate the design parameters in the next steps:

1- Inside diameter of the fluidised bed reaction section in **cm**, ***D***. This value can be given as desired, but at the same time will limit the gasifier size.
2- Diameter of the selected particle size of the solid bed material in **cm,** d_p.
3- The value of the ambient temperature in℃**,** T_{amb}.
4- The value of the atmospheric pressure in ***Pascal unit,*** P_{amb}.
5- A selected value of the equivalence ratio from applicable range for solid biomass gasification, ***ER.***
6- Viscosity and density of the gasifying gas at required temperature and pressure in $gm/cm.s$, μ_f and gm/cm^3, ρ_f, respectively. These two physical properties can be calculated for air from equations (A.1) and (A.2).

$$\mu_f = \frac{1.458 \times 10^{-6} T^{1.5}}{(T+110.4)} \quad \text{(A.1)}$$

Where, T is air temperature in ^oK

$$\rho_f = \frac{P \times Molwt}{R \times T} \quad \text{(A.2)}$$

For P= Pressure in Pascal unit, T= absolute temperature in ^oK, the value and units of universal gas constant R is 8.314 (m^3) (Pa) (K^{-1}) (mol^{-1})

7- Gravitation accélération g, cm/s^2 .
8- Particle density of the solid bed material in gm/cm^3, ρ_s.
9- Sphericity of the solid bed particles in ***dimensionless units,*** $\emptyset_s$**.**
10- Void fraction (porosity) of the solid bed material in ***dimensionless units,*** ε_s.
Porosity can be calculated from equation (A.3) or may be given.

$$Porosity = \varepsilon_s = 1 - \frac{bulk\ density}{particle\ density} \quad \text{(A.3)}$$

- **Step 2: Selection of static bed height,** H_s

In this step a several values of the height of the static bed H_s is selected as desired and required by putting it in a loop with a certain step.

- **Step 3:**

1- From Equation (3-2), the porosity of the solid bed material at minimum fluidisation conditions ε_{mf} is calculated.

2- From Equation (3-1) the gas velocity at minimum fluidisation conditions U_{mf} was calculated.

3- The terminal velocity of the solid particle U_t, which represents a maximum value of the superficial gas velocity, is calculated either by equation (3.6a) for U_{t1} if Reynold number at this velocity Re_{Ut1} is less than 0.4 or by Equation (3.6b) for U_{t2} if Reynold number at this velocity Re_{Ut2} is greater than 0.4 and less than 500.

4- The minimum slugging velocity $U_{b,ms}$ is calculated from Equation (3.7).

- **Step 4: Selection of superficial gas velocity, U_o.**

After Step 3 the superficial gas velocity U_o value can be suggested and selected from the range

$$U_{mf} < U_o < U_t, \ and$$
$$U_{mf} < U_o < U_{ms},$$

To see the effect of the gas velocity value on many design parameters, several U_o values were selected by making a loop with a certain step starting from U_{mf} as initial value up to U_{ms} velocity or any value within the required range as a final value. In this loop many values of the gas superficial velocity will be obtained within one value of the static height H_s in the main loop as shown in step 3. Five values of the static height were selected in terms of the static height to diameter H_s/D ratios, **0.5*D*, 1*D*, 1.5*D*, 2*D*** and **3*D***, respectively.

- **Step 5: Calculation of the fraction of the solid bed in bubble phase, δ**:

This parameter can be calculated by the following parameters:

1- From equation (3.16) bubble rise velocity U_b can be calculated.

2- To calculate U_b it is required to calculate the bubble diameter at a certain height of fluidised bed d_b from equation (3.14).

3- From equation (3.10), (3.15b) and (3.13b), d_{bm}, d_{bo} and H_{max} should be calculated, respectively to calculate d_{bo}.

4- Eventually, δ can be calculated from Equation (3.17).

- **Step 6: Calculations of the height of the expansion bed:**

The expansion height of the solid bed material, $\boldsymbol{H_{exp}}$ and its height at the minimum fluidisation conditions, $\boldsymbol{H_{mf}}$ can be calculated from Equations (3.21) and (3.22).

- **Step 7: Calculation the mass of the solid bed material, W_s for a certain static height H_s.**

This mass can be calculated from either Equation (3.21) or Equation (3.24).

- **Step 8: Calculations of the TDH and the total height of the gasifier, H_{total}.**

From Equations (3.31b) or (3.32) or (3.34) the total disengaging height TDH can be calculated. From Equation (3.36) the total height of the gasifier above distributor plate can be calculated.

- **Step 9: Calculations of the design parameters of the distributor plate.**

1- From Equation (3.39), the pressure drop across the bed can be calculated, ΔP_{bed} in N/m^2.

2- The pressure drop across the plateΔP_{ditr} can be calculated from Equation (3.38).

3- The total pressure drop across the gasifier column can be calculated by Equation (3.41).

4- 1.5mm diameter of the orifice (hole) of the perforated distributor plate d_{orf} was recommended to select (Basu 2006) to avoid the falling of the solid particles inside the air-box. Also, 6mm was recommended as a thickness of the distributor plate, t_{dist} to avoid the material defects at high temperature.

5- The drag coefficient of the gas flow through the holes C_d was calculated from Equation (3.43).

6- The gas velocity through the orifice U_{orf} was calculated by Equation (3.42).

7- From the above design parameters the number of the orifices (holes), N_{orf}, can be calculated from Equation (3.44a).

8- The number of the holes per unit cross-sectional area of the distributor plate, which is called orifice or hole density N_{den}, is calculated by Equation (3.45).

9- The triangular layout of the holes distribution is recommended and the pitch P_{pitch} of this layout is calculated by Equation (3.46b).

- **Step 10: Gasification equivalence ratio selecting , ER, and solid biomass mass flow-rate $\dot{m}_{bio}$ calculations:**

1- The required value of the gasification equivalence ratio *ER* should be selected from a recommended range, usually between 0.2 and 0.55.

2- From the ultimate analysis of the solid biomass material the stoichiometric air fuel ratio, $[MAFR]_{stoichio}$ can be estimated by Equation (3.27).
3- The actual air fuel ratio, $[MAFR]_{actual}$ was calculated from Equation (3.26).
4- The air gas volumetric flow rate $\dot{V}_{air}$ was calculated from Equation (3.30).
5- At the ambient temperature and pressure and for ideal gas the air mass flowrate $\dot{m}_{air}$ was calculated from the Equation (3.29).
6- From actual air-fuel ratio $[MAFR]_{actual}$ and air mass flow-rate $\dot{m}_{air}$ the solid biomass mass flowrate $\dot{m}_{biomass}$ was calculated from Equation (3.28).

A.2 The geometry drawing of the gasifier components (sections):

According to the design results and gasification process requirements, the suggested design and geometry drawing specifications of the gasifier components were prepared. The schematic of the whole rig, geometry and detail specifications for each component are shown in the next sections. The whole rig of the assembled fluidised bed gasifier has been shown in Figure 3.6. All components (Sections) are titled and pointed by giving a number for each one and were specified and drawn in details as shown below. The gasifier pipe, flange specifications are as follows:

- **Gasifier pipe:**
  Pipe material: Stainless-Steel type 316L.
  Pipe nominal size: 3
  Inside Pipe Diameter: 82.8mm.
  Outside pipe diameter: 88.9mm.
  Pipe thickness: 3.05mm.

- **Flange:**
  Flange Type: Open-Flat Face Flange
  Flange material: Stainless-Steel type-316L.
  Flange outside diameter: 170mm.
  Flange inside diameter: ≈ 90mm.
  No. of Flange holes: 6.
  Diameter of the hole: 10mm.
  Flange thickness: 6mm.

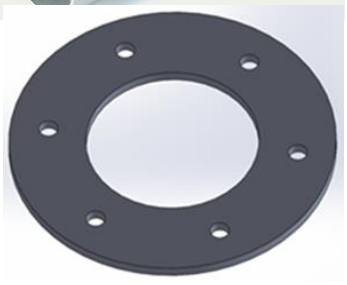

The geometric shape and specifications of each section of the gasifier are shown as follows:

A.2.1 Gases Outlet Top Section – No (1)

The geometric shape of this section is shown in Figure (A.1). The specifications of this section are shown in details as follows:

Gasifier pipe specifications: As shown in Section A.2 - gasifier pipe.
Flange specifications: As shown in Section A.2 - Flange.
No of flanges: 1
Connection pipe specification: Stainless-Steel
Outlet vertical pipe length: 50mm.
Outlet horizontal pipe length: 200mm.

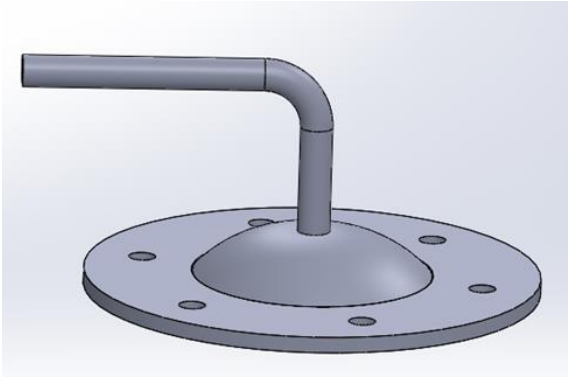

Figure A. 1 Geometry of the gas out let-top section.

A.2.2 Free-board section – Part I-No (2)

The geometric shape of this section is shown in figure (A.2). The specifications of this section are shown in details as follows:

Gasifier pipe specifications: As shown in Section A.2, gasifier pipe.
Flange specifications: As shown in Section A.2, Flange.
No of flanges: 2.
Pipe length: 700mm.

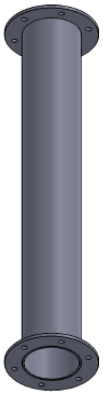

Figure A. 2 Geometry of the free-board section – Part I

A.2.3 Free-board section – Part II No (3)

The geometric shape of this section is shown in figure (A.3). The specifications of this section are shown in details as follows:

Gasifier pipe specifications: As shown in Section A.2, gasifier pipe.
Flange specifications: As shown in Section A.2, Flange.
No of flanges: 2
Pipe length: 1000mm.

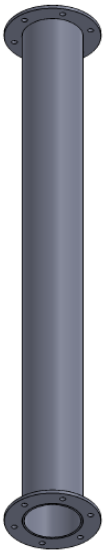

Figure A. 3 Geometry of the free-board section – Part II

A.2.4 Fluidisation reaction section – No (4)

The geometric shape of this section is shown in Figure (A.4). The specifications of this section are shown in details as follows:

Gasifier pipe specifications: As shown in Section A.2, gasifier pipe.
Flange specifications: As shown in Section A.2, Flange.
No of flanges: 2
Pipe length: 325mm.
There are 3 holes in the pipe:

- Bed material feeding-250mm length from porous plate distributor surface.
- Biomass material feeding - 40mm length from plate distributor surface.
- Solid material outlet (sand + char) – at plate distributor level.

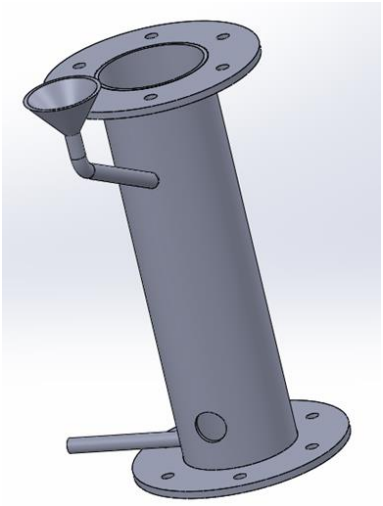

Figure A. 4 Geometry of the fluidized bed section.

A.2.5 Distributor plate section – No (5)

The geometric shape of this section is shown in figure (A.5). The specifications of this section are shown in details as follows:

Material of the plate: Similar to flange specifications
No. of the orifices (holes) for air distribution: depend on the superficial velocity values (calculated).
Diameter of the orifice (hole): 1.5mm or 2mm.

The holes of the distributor plate lie within inside pipe diameter border: 83mm.
Holes arrangement: Triangular
Pitch length: depends on the number of the holes (calculated).

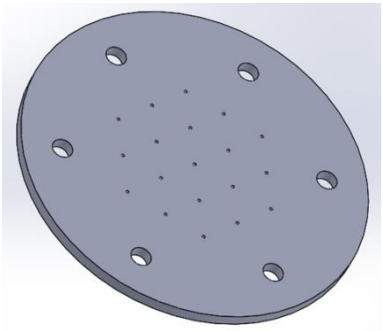

Figure A. 5 Geometry of the distributor plate section.

A.2.6 Air box (plenum) section – No (6)

The geometric shape of this section is shown in Figure (A.6). The specifications of this section are shown in details as follows:

Gasifier pipe specifications: As shown in Section A.2, gasifier pipe.
Flange specifications: As shown in Section A.2, Flange.
No. of flanges: 2, top only.
Pipe length: 300mm.
Inlet air pipe length: 300mm.
Inside diameter of the air supply pipe: 25.4mm.
Thickness of the air pipe: 2mm.
Length of the solid waste pipe: 150mm.
Inside diameter of the solid waste pipe: 11mm.
Thickness of the solid waste pipe: 0.5mm.

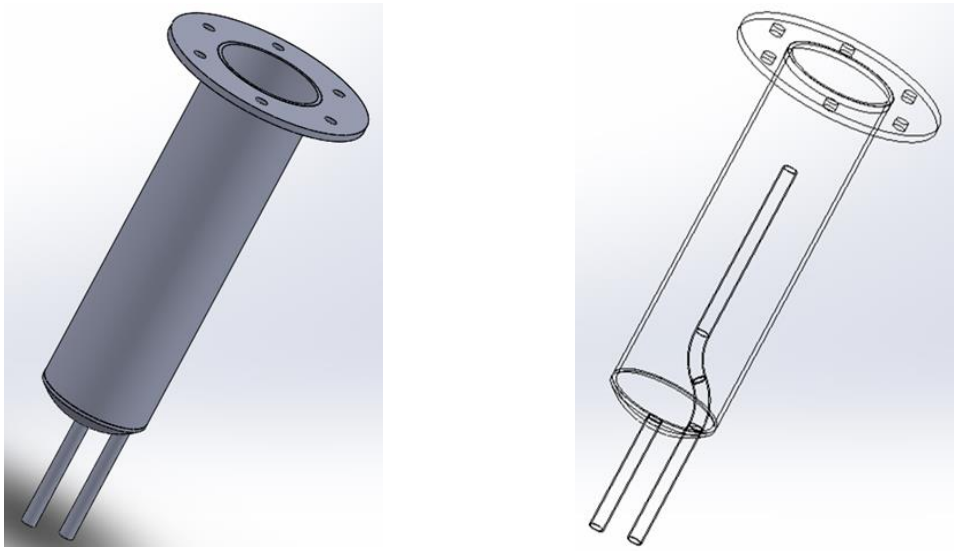

Figure A. 6 Geometry of the air box (plenum) section

The geometric shape of the assembled of the whole bubbling fluidised bed gasifier is shown in Figure A.7 as shown below:

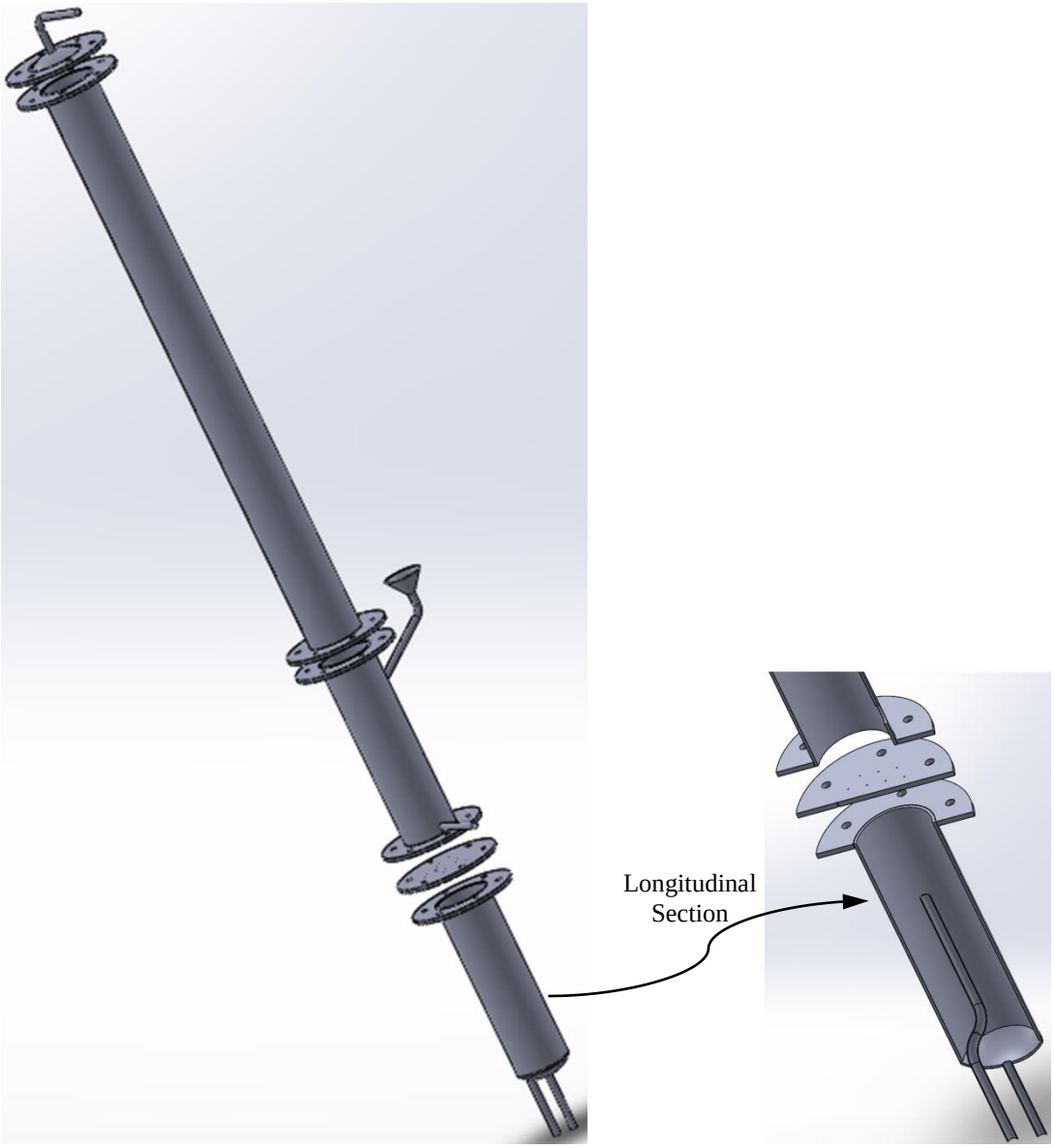

Figure A. 7 Geometry of the assembled fluidized bed gasifier

APPENDIX B

Matlab Program for Design of the Bubbling Fluidised Bed

```
% Design programme For Bubbling Fluidised Bed Reactor
clear all;
clc;
display (' enter the values of the required parameters')
% dp = input( ' enter the value of particle diameter,in ( cm ) dp
=')
% TR = input( ' enter the value of reaction temperature TR =')
% PR =  input( ' enter the value of the reactor pressure PR =')
% ER =  input( ' enter the value of the equivalence ratio ER =')
% VR = input( ' enter the value of the gas volumetric flow rate VR
=')
% g  = input( ' enter the value of the gravitational acceleration in
(cm/s2)g=')
% mg = input( ' enter the value of the viscosity of the gasifying
fluid in (g/cm.s) mg =')
% pc =  input( ' enter the value of the density of the solid
catalyst particles in (g/cm3) pc =')
% pg =  input( ' enter the value of the density of the gas in
(g/cm3) pg =')
% SPH=  input( ' enter the value of the spherity of the particles
SPH =')
% D  = input( ' Enter the value of the column rector bed diameter in
cm D= ')
TC=20
TK=273.15+TC
P1=101.325*10^3
dp=0.0396;
g=980;
mg=1.458*((TK^1.5)/(TK+110.4))/(10^5)
pc=2.65;
pg=(P1/((287.058)*TK))/1000
target=pg
SPH=0.78;
D=8.3;
Es=0.42;

for i=1:1:5
    j=1
Hs= input(' Hs= ')
target(j,i)=Hs

display ( ' Umf and Ut calculations ')
display ( ' 1- calculation of the epsilon at the minimum
fluidisation condition Emf= ');
Emf = 0.586*(SPH^(-0.72))*((mg^2/(pg*g*(pc-
pg)*dp^3))^(0.029))*((pg/pc)^(0.021))
j=j+1
target(j,i)= Emf
display (' 2- calculation of the minimum fluidization velocity in
(cm/s) Umf = ')
Umf1=((( SPH *dp)^2)*(g*(pc-pg))*(Emf^3))/(150*mg*(1-Emf))
j=j+1
target(j,i)=Umf1
Ar=(pg*g*(pc-pg)*(dp)^3)/(mg^2)
j=j+1
target(j,i)=Ar
Remf=(((33.7)^2+(0.0408*Ar))^0.5)-33.7
j=j+1
target(j,i)=Remf
Umf=(Remf*mg)/(pg*dp)
```

```
j=j+1
target(j,i)=Umf

display ( '3- Calculation of the terminal velocity ( maximum
superficial velocity) in (cm/s) Ut =');
Remf1 = pg*Umf1*dp/mg
j=j+1
target(j,i)=Remf1
Ut1=(g*(pc-pg)*dp^2)/(18*mg)
j=j+1
target(j,i)=Ut1
ReUt1=pg*Ut1*dp/mg
j=j+1
target(j,i)= ReUt1
    Ut2 =(((1.788*(1/100))*((g*(pc-pg))^2)/(pg*mg))^(1/3))*dp
    j=j+1
    target(j,i)=Ut2
    ReUt2= pg*Ut2*dp/mg
    j=j+1
    target(j,i)=ReUt2
    display( ' Remf should be Remf < 10( ref R12, 20(ref Kunii&
Leven)
               and ReUt1 < 0.4 or 0.4< ReUt2 <500 ')
    display (' 4- Calculation of the entering (suggestion )
superficial
               velocity in ( cm/s ) Uo')
    display (' calculation of the cross-sectional area of the bed
               reactor in ( cm2 ) Ac ')
    Ac= 22*D^2/(7*4)
   display ( ' Calculation of the minimum slugging velocity in m/s,
Ums ')
   Ums=(Umf/100)+ 0.07*((g*D/10000)^0.5)
   Umscm=Ums*100
   j=j+1
   target(j,i)= Umscm
   dbmassum=(2/3)*D


    display (' Uo should be between Umf & Ut and Umf and Ums,' )
    k=1;
    for Uo= Umf:5:60

  targetUo(k,1)=Uo


    j=j+1
    target(j,i)= Uo

     display (' Method I, Let ZH= Hexp/Hmf ' )
     ZHassum=1.2
     Uoassum= (((ZHassum-
1)*((Umf/100)^0.937)*((pg*1000)^0.126)/(10.978*((pc*1000)^0.376)*((d
p/100)^1.006)))^(1/0.738))+(Umf/100);
    ZH= 1+ (((10.978)*(((Uo-
Umf)/100)^0.738)*((pc*1000)^0.376)*((dp/100)^1.006))/(((Umf/100)^0.9
37)*((pg*1000)^0.126)))
    display ( ' Calculation of the maximum bed height below which
the
               bed will be freely bubbling in cm, Zmax. D in cm ')
```

```
      Zmax=((D- 2.51*(D^0.2))/(0.13*(D^0.47)))
     ZmaxR=Zmax/D
     Hmax=2*D
     j=j+1
     target(j,i)=Hmax
     Zs = 60*(D^0.175)
     ZsR=Zs/D


    display (' 5- calculation of the bubble velocity Ub in ( cm/s ),
Ub= ')
     dbo=0.347*[Ac*(Uo-Umf)/Norf]^0.4
     j=j+1
     target(j,i)=dbo
     dbm= 0.652*(Ac*(Uo-Umf))^0.4
     j=j+1
     target(j,i)=dbm
     targetUo(k,i+1)=target(j,i)
     Dbmax= (2/3)*D

     db= dbm-(dbm-dbo)*exp(-0.3*Hs/(2*D))
     j=j+1
     target(j,i)=db
     display (' 6- calculation of the fraction of bed in bubble phase
S')
     Ub= Uo-Umf+(0.71)*(g*db)^0.5
     j=j+1
     target(j,i)=Ub
     a=0.255
     S= (Uo-Umf)/(( Ub- Umf)*(1+a))
     j=j+1
     target(j,i) =S
     Rexpstatic=(1-Es)/((1-S)*(1-Emf))
     j=j+1
     target(j,i) =Rexpstatic
     Hexp1=Rexpstatic*Hs
     j=j+1
     target(j,i)=Hexp1

     Rexpmf=1/(1-S)
     j=j+1
     target(j,i) =Rexpmf
     Hmf=Hs*(1-Es)/(1-Emf)
     j=j+1
     target(j,i)=Hmf
     Hexp2=(Rexpmf)*Hmf
     j=j+1
     target(j,i) =Hexp2
     display ( ' 7- calculation the mass of the solid bed material
Ws, in
                 grams ')
     Ws= Hs* Ac* (1-Es)*pc
     Ws2=Hexp1*Ac*(1-S)*(1-Emf)*pc
     j=j+1
     target(j,i)= Ws2
     display ( ' Design of the Freeboard Section ' )
     display ( ' Calculation of the TDH in m ')
     TDH0=13.8*db/100
     j=j+1
     target(j,i)=TDH0
     Uom=Uo/100
```

```
    gm=g/100
    TDH1= (Uom^2*1000)/gm
    j=j+1
    target(j,i)=TDH1
    dbs= dbm-(dbm-dbo)*exp(-0.3*Hs/D)
    dbsmeter= 1.13*dbs/100
    TDH2= (4.47)*(dbsmeter^0.5)
    j=j+1
    target(j,i)=TDH2
    display ( ' Calculation of volumetric flowrate, Vo, in cm3/s ')
    Volmetric=Ac*Uo
    j=j+1
    target(j,i)=Volmetric
    TDH3= (D^( 1-(0.115)*Uo-0.587))*(4.46*Volmetric)
    TDH3= TDH3/100
    j=j+1
    target(j,i)=TDH3
    display ( ' Calculation of the total height of the Reactor in
meter,
                Htotl ')
    Hmaxm=Hmax/100
    Htotal0= TDH0+Hmaxm+0.3
    j=j+1
    target (j,i)=Htotal0
    Htotal1= TDH1+Hmaxm+0.3
    j=j+1
    target (j,i)=Htotal1
    Htotal2= TDH2+Hmaxm+0.3
    j=j+1
    target(j,i)=Htotal2
    Htotal3= TDH3+Hmaxm+0.3

    display ( ' Distributor Design Steps ')
    display ( ' Calculation of the BED pressure drop, DPBED in N/m2
')
    display (' let Epsexp= (1-E)')
    Epsexp=((1-S)*(1-Emf));

    DPBED= Epsexp*Hexp1*0.01*(g*0.01)*(pc*1000)
    j=j+1
    target(j,i)=DPBED
    DPBED2= Epsexp*Hexp1*0.01*(g*0.01)*(pc-pg)*1000
    display ( ' Calculation of the DISTRIBUTOR pressure drop, DPDIST
in
                N/m2 ')
    DPDIST= 0.3*DPBED
    j=j+1
    target(j,i)=DPDIST
    DPtotal=DPBED+DPDIST
    j=j+1
    target(j,i)=DPtotal
    display ( ' Let CD = 0.8 ')
    display ( ' Select diameter of the orifice (hole) in distribute
                plate value in m, dor ')
    display ( ' Select  of the orifice (hole) in distribute plate
value
                in m, dor ')
    display ( ' enter the value of dor, dor = ')
    dor=0.0015
    display ( ' Select thickness of the porous distributor plate
value
```

```
                in m, ThickPD ')
    display ( ' enter the value of ThickPD, ThickPD= ')
    display ( ' ratio of ThickPD/dor should be > 0.09')
    ThickPD=0.006
    CD=0.82*((ThickPD/dor)^0.13)
    j=j+1
    target (j,i)=CD
    display ( ' Calculation of the velocity through the orifice in
m/s,
                Uor. pgor density of the gas at orifice in kg/m3 ')
     pgor=pg*1000
    Uor=CD*((2*DPDIST/pgor)^0.5)
    j=j+1
    target (j,i)=Uor
    display ( ' calculate N the number of orifice in the plate and
NPm2
                the number per unit area m2')
    N= ((D/ (100*dor))^2)* (pg*1000/pgor)*(Uo/(100*Uor))
    j=j+1
    target(j,i)=N

    NPm2= 4*10000*N/((22/7)*(D^2))
    j=j+1
    target(j,i) =NPm2
    display (' This is the number of holes in the plate at assomed
dor
               You can assume another and another')
    display (' From assumed CD & dor one can calculate the thickness
of
               the plate distributor in ( m ), ThickPD');
    ThickPD= dor*(CD/0.82)^(1/0.13)
    j=j+1
    target(j,i)=ThickPD
    display (' You can compare this thickness value to that which
can be
               obtained by Fig 4,Handbook of fluidization, p.160 ');
    display (' Calculate the pitch distant in ( m ), PITCH, for
               triangular layout ');
    PITCH = (2/((3^(0.5))*NPm2))^0.5
    j=j+1
    target(j,i)=PITCH
    display (' Calculations of the actual compressor power
consumption
               in kW ')
    Pexit=101.325*10^3
    P2=(DPtotal+ Pexit)
    Q2=Volmetric/1000000
    Gama=1.4
    Eff=0.85
    Powerid= (Gama/(Gama-1))*P2*Q2*(1-(P1/P2)^((Gama-1)/Gama))
    Poweract=Powerid/Eff
    j=j+1
    target(j,i)=Poweract
    TCi=20
    TC1=273.15+TCi
    T2comp=TC1+((TC1/Eff)*(((P2/P1)^((Gama-1)/Gama))-1))
    j=j+1
    target(j,i)=T2comp

    plot (targetUo(:,2),targetUo(:,1))
```

```
     plot (targetUo(:,2),targetUo(:,1))
%     plot (N,Uo)


%     for t=1:j;
%         target1(1,t)=target(1,t);
%     end
%    target1
% end
    display ( ' Equvalence Ratio and Mass Flowrate of The Biomass
                Calculations ' );
    ER=0.2
    display( ' From the Ultimate Analysis of The Biomass Entere the
               following ');
    C = 49.4
    Su = 0.02
    H = 5.9
    N2gas=0
    O = 40.68
    RStoic = 8.89*(C+0.375*Su)+26.5*(H)-3.3*O
    RACTU = ER* RStoic

    AirV = Uo*Ac/(10^6)
    TR=20+273.15
    Airkg = (P1)*AirV*29/((8.3145)*TK)
    FedBios = Airkg/(RACTU)
    FedBioh = FedBios*60
    j=j+1
   target(j,i)=FedBioh
   k=k+1
    end

end
```

APPENDIX C

Analysis of Particle Size Distribution for Three Sand Ranges (500-600), (425-500) and (300-425) µm, respectively

Analysis

Created by: Malvern Instruments Ltd
Last edited: 13/04/2012 16:12:51

Malvern

Measurement Details

Sample Name	Average of 'Mohammed sand 500-600'	**Measurement Date Time**	23/07/2014 15:55:54
Operator Name	Malvern	**Analysis Date Time**	23/07/2014 15:55:54
SOP File Name	Fine Sand.msop	**Result Source**	Averaged

Analysis

Particle Name	Sand	**Particle Refractive Index**	1.540
Dispersant Name	Water	**Dispersant Refractive Index**	1.330
Particle Absorption Index	0.010	**Laser Obscuration**	6.40 %
Weighted Residual	1.83 %	**Scattering Model**	Mie
Analysis Model	General Purpose	**Analysis Sensitivity**	Normal

Result

Concentration	0.4963 %	**Span**	0.449
Uniformity	0.137	**Result Units**	Volume
Specific Surface Area	3.878 m^2/kg	**Dv (10)**	471 µm
D [3,2]	582 µm	**Dv (50)**	592 µm
D [4,3]	598 µm	**Dv (90)**	737 µm

Frequency (compatible)

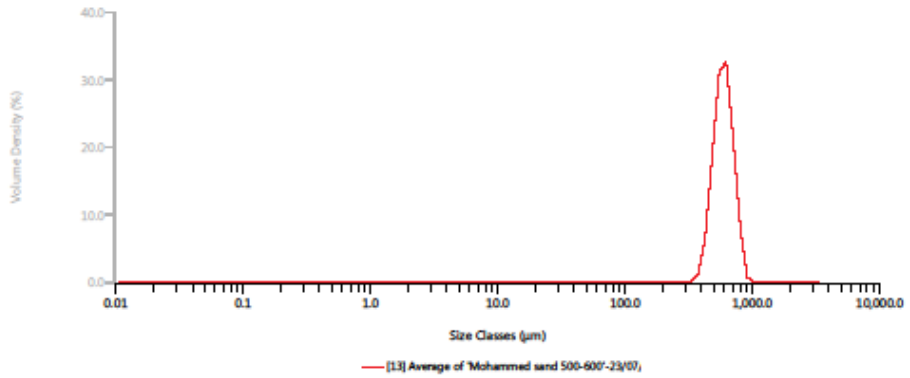

Size (µm)	% Volume In	Size (µm)	% Volume In	Size (µm)	% Volume In	Size (µm)	% Volume In	Size (µm)	% Volume In	Size (µm)	% Volume In
0.0100	0.00	0.0679	0.00	0.460	0.00	3.12	0.00	21.2	0.00	144	0.00	976	0.00
0.0114	0.00	0.0771	0.00	0.523	0.00	3.55	0.00	24.1	0.00	163	0.00	1110	0.00
0.0129	0.00	0.0876	0.00	0.594	0.00	4.03	0.00	27.4	0.00	186	0.00	1260	0.00
0.0147	0.00	0.0995	0.00	0.675	0.00	4.58	0.00	31.1	0.00	211	0.00	1430	0.00
0.0167	0.00	0.113	0.00	0.767	0.00	5.21	0.00	35.3	0.00	240	0.00	1630	0.00
0.0189	0.00	0.128	0.00	0.872	0.00	5.92	0.00	40.1	0.00	272	0.00	1850	0.00
0.0215	0.00	0.146	0.00	0.991	0.00	6.72	0.00	45.6	0.00	310	0.04	2100	0.00
0.0244	0.00	0.166	0.00	1.13	0.00	7.64	0.00	51.8	0.00	352	0.75	2390	0.00
0.0278	0.00	0.188	0.00	1.28	0.00	8.68	0.00	58.9	0.00	400	4.86	2710	0.00
0.0315	0.00	0.214	0.00	1.45	0.00	9.86	0.00	66.9	0.00	454	15.27	3080	0.00
0.0358	0.00	0.243	0.00	1.65	0.00	11.2	0.00	76.0	0.00	516	26.89	3500	
0.0407	0.00	0.276	0.00	1.88	0.00	12.7	0.00	86.4	0.00	586	28.21		
0.0463	0.00	0.314	0.00	2.13	0.00	14.5	0.00	98.1	0.00	666	17.65		
0.0526	0.00	0.357	0.00	2.42	0.00	16.4	0.00	111	0.00	756	6.30		
0.0597	0.00	0.405	0.00	2.75	0.00	18.7	0.00	127	0.00	859	0.04		

Software Version: 3.00
Malvern Instruments Ltd - www.malvern.com
Page 1 of 1

Malvern

Figure C. 1 Image of the Malvern analysis results for sand particle size range (500-600) µm

Analysis

Created by: Malvern Instruments Ltd
Last edited: 20/10/2011 11:30:50

Malvern

Measurement Details

Sample Name	Average of 'Mohammed sand 425-500 ii'	**Measurement Date**	23/09/2013 11:28:47
Operator Name	Malvern	**Analysis Date Time**	23/09/2013 11:28:47
Sop Name	Fine Sand.msop	**Result Source**	Averaged

Analysis

Particle Name	Sand	**Particle Refractive Index**	1.540
Dispersant Name	Water	**Dispersant Refractive Index**	1.330
Particle Absorption Index	0.010	**Laser Obscuration**	8.21 %
Weighted Residual	0.74 %	**Scattering Model**	Mie
Analysis Model	General Purpose	**Analysis Sensitivity**	Normal
Scattering Model	Mie		

Result

Concentration	0.5650 %	**Span**	0.484
Uniformity	0.151	**Result Transformation Type**	Volume
Specific Surface Area	4.427 m^2/kg	**Dv 10**	407 µm
D[3,2]	510 µm	**Dv 50**	520 µm
D[4,3]	527 µm	**Dv 90**	658 µm

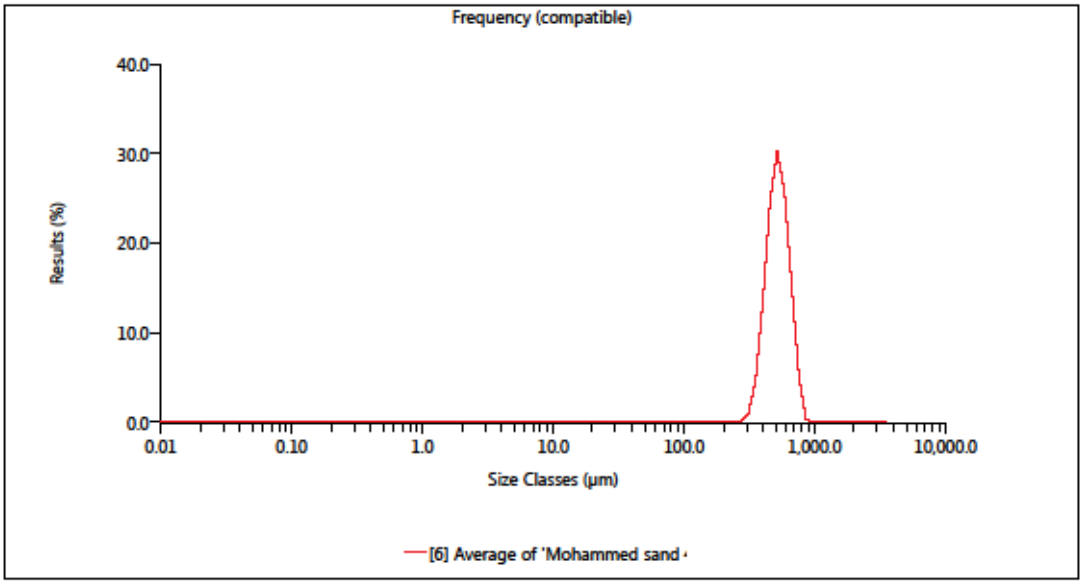

Malvern

Figure C. 2 Image of the Malvern analysis results for sand particle size range (425-500) µm.

Analysis

Created by: Malvern Instruments Ltd
Last edited: 20/10/2011 11:30:56

Malvern

Measurement Details

Sample Name sand >300 & <425	**Measurement Date** 19/09/2013 13:34:32
Operator Name Malvern	**Analysis Date Time** 19/09/2013 13:34:32
Sop Name Coal.msop	**Result Source** Measurement

Analysis

Particle Name Sand	**Particle Refractive Index** 1.540
Dispersant Name Water	**Dispersant Refractive Index** 1.330
Particle Absorption Index 0.010	**Laser Obscuration** 9.15 %
Weighted Residual 0.44 %	**Scattering Model** Mie
Analysis Model General Purpose	**Analysis Sensitivity** Normal
Scattering Model Mie	

Result

Concentration 0.5218 %	**Span** 0.503
Uniformity 0.146	**Result Transformation Type** Volume
Specific Surface Area 5.355 m²/kg	**Dv 10** 334 µm
D[3,2] 421 µm	**Dv 50** 429 µm
D[4,3] 436 µm	**Dv 90** 550 µm

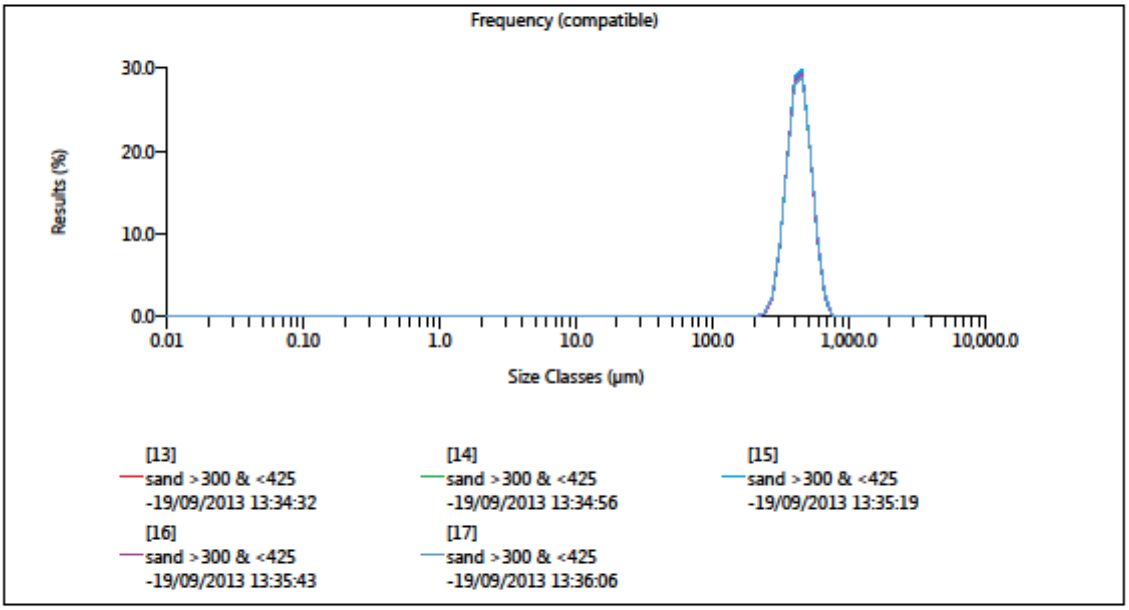

Malvern Instruments Ltd
www.malvern.com
Page 1 of 2

Malvern

Figure C. 3 Image of the Malvern analysis results for sand particle size range (300-425) µm

APPENDIX D

Results and Discussion of the Rest Results of Chapter 6

D.1 Comparison of three materials, sand, SPWB and IDPWB

Figure D.1 shows photographically a comparison of the behaviour of air fluidisation for three single materials, sand, SPWB and IDPWB for each air flowrate from 10 l/min to 120 l/min. For each flowrate, three images for those three materials were arranged starting from the left-hand side, respectively. This image comparison can be used to show the differences of three materials in their fluidisation behaviour. As discussed in previous sections, the biomass materials SPWB and IDPWB have a poor fluidisation ability compared to sand material. This is because of the high density of sand material, which classify them within the Geldert B group. This group can be easily fluidised. In contrast, because of their low density, these two biomass materials are not classified within Geldert B group. It means that are not easily fluidised.

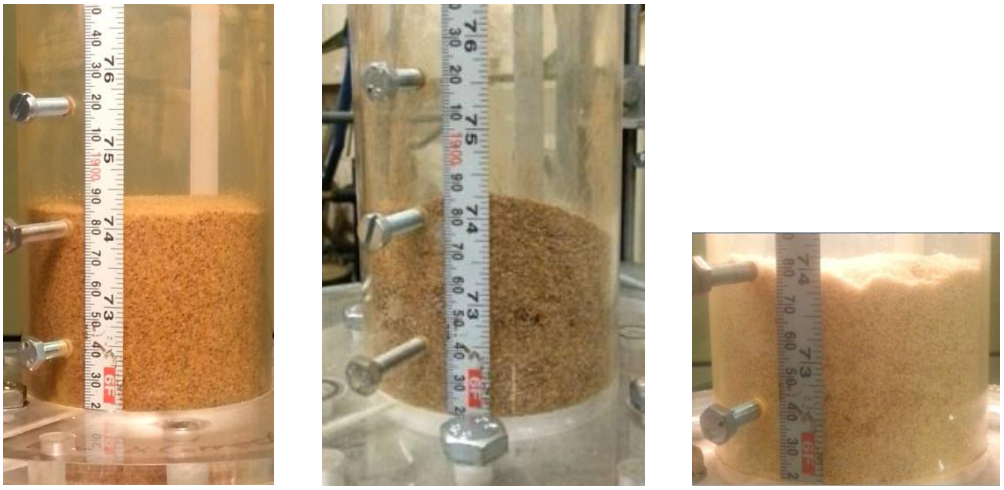

Uo=10 l/min

Uo= 20 l/min



Uo- 30 L/min



Uo= 40 l/min



Uo= 50 l/min



Uo= 60 l/min



Uo= 70 l/min

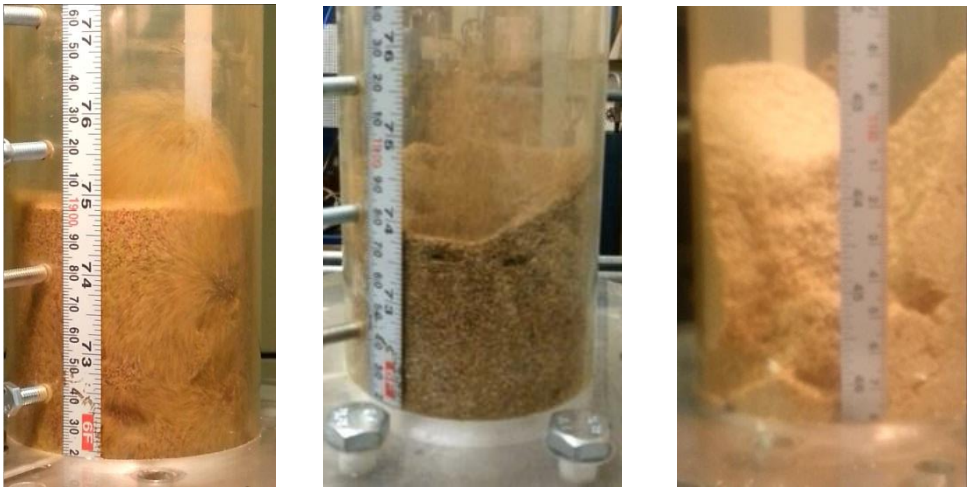

Uo= 80 l/min

Uo= 90 l/min

Figure D. 1 Images for air fluidisation behavior comparison of three single materials, sand, IDPWB and SPWB for descending velocities from 0.0 to 110 l/min

D.2 Air fluidization behaviour for sand–biomass mixture bed

D.2.1 Experiment of: 2cm SPWB (1180-1500) µm / 8.3cm sand (500-600) µm

Figure D.2 shows the image sequence of the bed fluidization behavior for the mixture of 2.075cm sawdust biomass (1180-1500) µm/8.3cm sand (500-600) µm. This ratio was 2.69% weight percent of SPWB biomass in the mixture. At zero to 50 l/min of air

flowrate the mixture bed appears as a stagnant bed and looks a same shape. The dispersion and distribution density of the biomass along the bed was poor. As observed at 70 l/min a few small bubbles appeared at the bottom half of the bed. One small hole appeared at the bed surface. At air flowrates from 80-120 l/min most of the biomass was transferred to the bed surface because of the bubble effect and the low biomass density. Bubbles size became larger and faster along the bed especially at high flowrates, 110 and 120 l/min. Also the bed had visibly expanded. After biomass segregation, fluidization behavior of the bed appeared as fluidization behavior of the sand material only. In addition, due to high air velocities, some biomass particles escaped from the top of the bed surface and projected into the freeboard section. This is may be due to the high difference between their particle size and for the same weight of biomass the number of large particles is fewer than when smaller particles are used. In this weight percent the bridges and caves due to biomass material were not observed. Additionally, in some sides of the column and especially near the wall some of the bed mixture was not affected by the fluidisation because some of biomass particles were observed to be stagnant. This can be attributed to the non-uniform distribution of distributor plate holes near the plate edge creating a dead area; thereafter no air bubbles were observed. Therefore, for this point it can be concluded that a high fluidisation quality and uniformity can be obtained by covering the plate area by holes wherever possible. In addition, the low biomass fraction as shown in this case has low effect on the fluidisation quality.

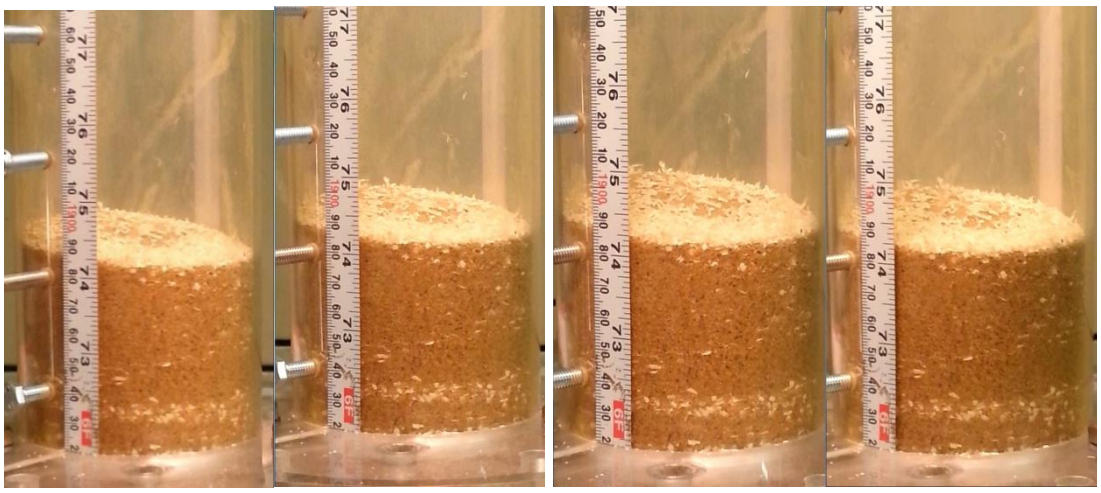

Uo= 0.0-10 l/min Uo= 20 l/min Uo= 30 l/min Uo= 40 l/min

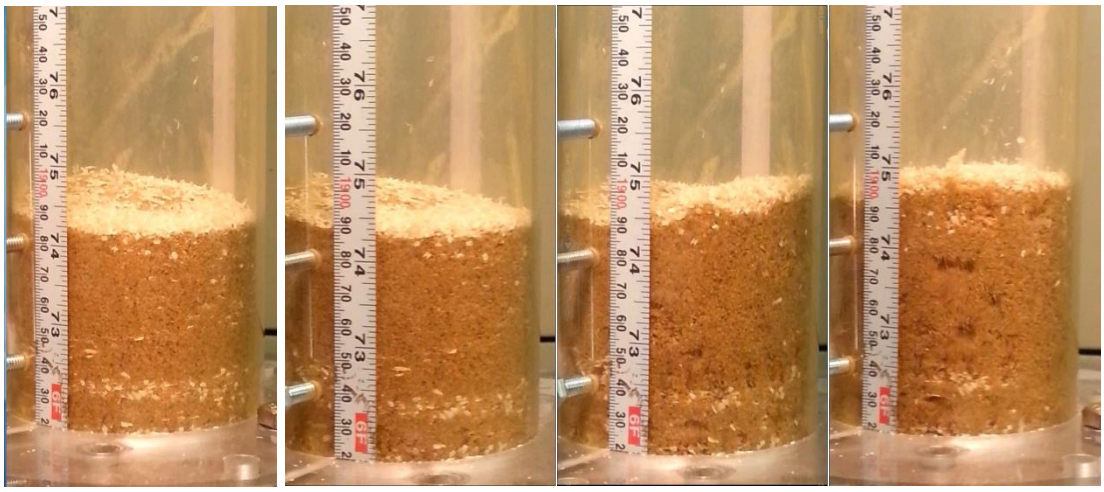

Uo= 50 l/min Uo= 60 l/min Uo= 70 l/min Uo= 80 l/min

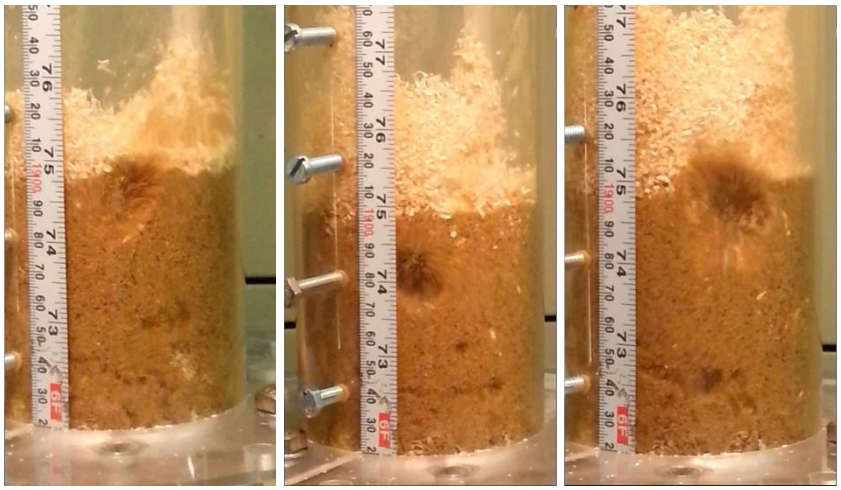

Uo= 100 l/min Uo= 110 l/min Uo= 120 l/min

Figure D. 2 Images of the cold fluidization of 2 cm SPWB (1180-1500) µm/ 8.3cm Sand (500-600) µm mixture

D.2.2 Experiment of: 2cm SPWB (500-600) µm / 8.3cm sand (500-600) µm

The cold hydrodynamic fluidization experiment was conducted for 2.68 weight percent of sawdust biomass (500-600) µm-sand (500-600) µm mixture to show the effect of biomass particle size on the hydrodynamics of fluidization and compared to the previous experiment. This mixture was represented by a height ratio of 2 cm biomass to 8.3 cm sand. Materials were mixed well and poured in the plastic fluidized column. The bed mixture took the shape as shown in Figure D.3 (image 1 for 0.0 l/min). It shows that this biomass particle size (white color) was approximately

distributed and dispersed more homogenous and dense along the bed comparing to previous large particle size. Some of them assembled at the top of the bed surface. It can be also seen that there was not any changes in the shape of the bed column when the air velocity increased from 0 l/min to 60 l/min. At 70 l/min= 21.57cm/sec small air bubbles were seen. They moved upward slowly and burst slightly at the top bed surface as shown in the image. These small bubbles created small holes at the bed surface, confirming that air channels were formed. The image of 80 l/min=24.66 cm/sec shows that the bubbles became more clear and faster than before along the bed. The distribution of biomass particles were changed along the bed, segregated and pushed upward and jammed at the bed surface. A slight expansion of the bed was observed. As shown in the images for air flowrates from 90 l/min to 120 l/min and by experiment observation the bubbles gradually became more clear, larger and faster. Due to high velocity, air bubbles action and their low density comparing to the sand, most of the biomass particles went up faster to the top bed surface. Because of the bubble burst intensity at the surface, some of the biomass particles were pushed to the freeboard and a quantity of them stayed projected into the freeboard according to the force balance theory. Systematically as velocity increased, the bed became more fluidized and behaved as if a sand material only. These phenomena were more clearly at high velocities, 110 l/min and 120 l/min, than previous velocities as shown in images of Figure D.3. From these observations, it can be concluded that for low biomass concentration in biomass-sand mixtures the bed fluidization behavior is more close to the single sand material behavior. However, this behavior gives a good fluidization quality and homogeneity. Comparing to (1180-1500)μm biomass particle size, (500-600) μm was dispersed and distributed more effectively and densely along the bed. In addition, for the same biomass mass percent mixture, the fluidisation of bed mixture was not highly affected by biomass particle size.

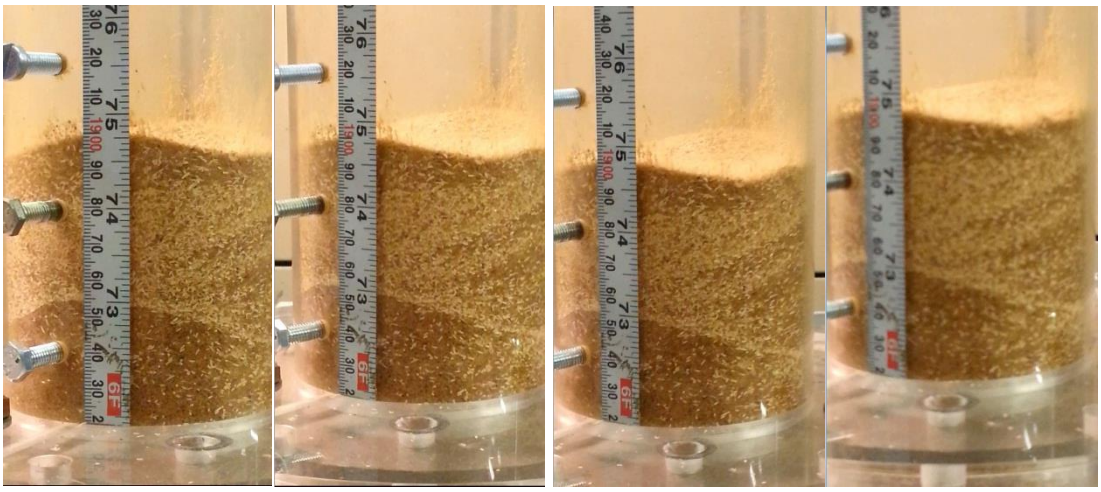

Uo= 0-40 l/min Uo= 50 l/min Uo= 60 l/min Uo= 70 l/min

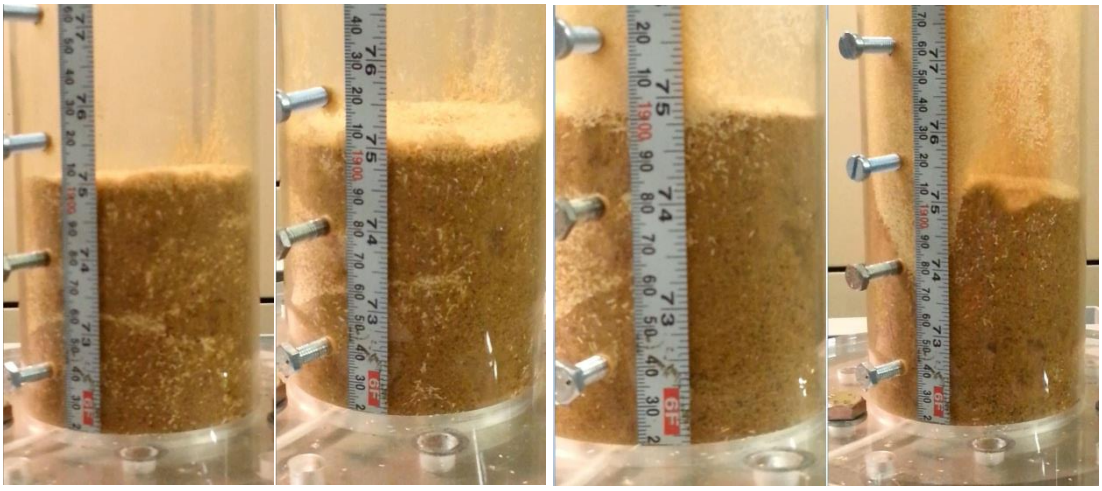

Uo= 80 l/min Uo= 90 l/min Uo= 100 l/min Uo= 110 l/min

Uo= 110 l/min Uo=120 l/min Uo=120 l/min

Figure D. 3 Images of the cold fluidization of 2.07cm SPWB (500-600) µm/ 8.3cm Sand (500-600) µm mixture

D.2.3 Experiment of: 8.3cm SPWB (1180-1500) µm/ 8.3 cm and (500-600) µm

Figure D.4 shows the sequence of the bed fluidization behavior for the mixture of 8.3cm sawdust biomass (1180-1500) µm/ 8.3 sand (500-600) µm. This ratio was 9.93 weight percent of SPWB. The bed materials were well mixed and poured in the column. The bed took the shape as shown in Figure D.4 (image 1 for 0.0 l/min). In addition, the density of the biomass distribution is approximately uniform. This is because of high biomass weight percent, 9.93 %, comparing to 2.69% for the same height 8.3cm of sand. As shown in Figure D.4 (image 1 &2) for air velocities from 0 l/min to 60 l/min there was not any changes in bed shape, neither for biomass distribution nor for bed height. No any bubbles were observed at these velocities. At 70 l/min airflow rate, bubbles could not be observed clearly, but a small hole was observed at the bed surface. This hole indicates that a few numbers of bubbles were available creating a small diameter of air channel along the bed. At 80 l/min air flowrate, a few bubbles appeared at the bottom of the bed at one side of the bed surface. At 100 l/min of air, the bubbles were increased along the bed and caused cracking in the side bed surface. Due to a bed expansion, the top surface of the bed became more level. As the air flowrate increased up to 150 l/min, as shown in Figure D.4 (images for 110-150l/min) the cracking of the bed, bed bridges and cavities inside the bed and bed expansion were increased and became larger. In addition, biomass particles were slowly transferred and segregated upward and accumulated at the top bed surface. Overall, for this biomass weight percent at these high velocities such as 150 l/min, a clear fluidization behavior compared to single-sand material cannot be observed. There was no violent fluidization and mixing in the bed, no bubble bursting at the top bed surface and then no clear and fast transfer of biomass particles to the freeboard section. It can be noticed for a short period of time many changes in the bed body may occur due to bridges, and channels breaks. Approximately, 17.5 cm average bed height was recorded at 150 l/min air flowrate.

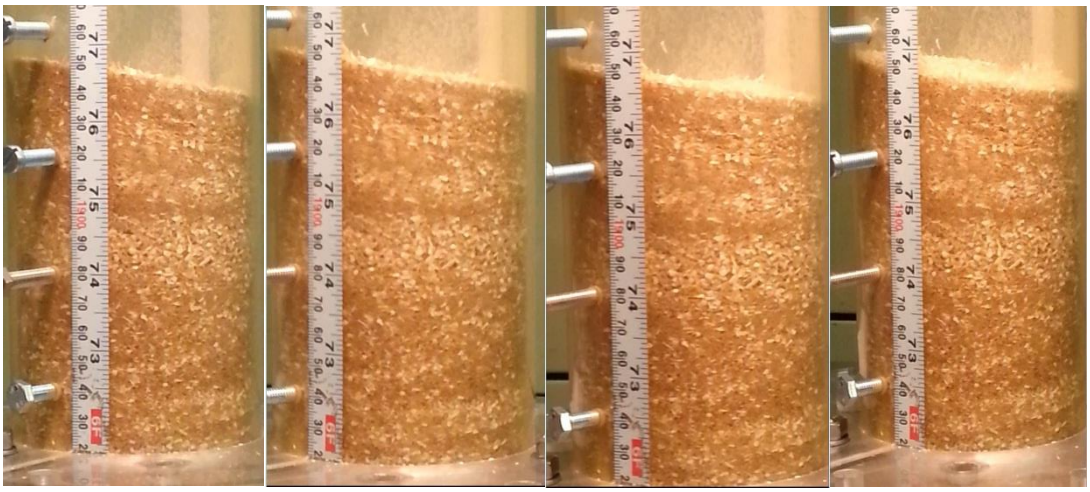

Uo= 0 l/min Uo= 50 l/min Uo= 70 l/min Uo= 80 l/min

Uo=90 l/min Uo= 100 l/min Uo=110 l/min Uo=120 l/min

Uo=130 l/min Uo= 140 l/min Uo= 150 l/min Top view, Uo=140 l/min

Figure D. 4 Images of the cold fluidization of 8.3cm SPWB (1180-1500) µm/ 8.3cm Sand (500-600) µm mixture

D.2.4 Experiment of 8.3cm SPWB (500-600) µm/ 8.3 cm and (500-600) µm

Figure D.5 shows the sequence of the bed fluidization behavior for the mixture of 8.3cm SPWB (500-600) µm/ 8.3cm Sand (500-600) µm. This ratio is equivalent to 9.93 weight percent of sawdust biomass. The bed materials were well mixed then poured in the column. The bed took the shape as shown in Figure D.5 - image 1 for zero l/min. The biomass distribution is approximately looking more dens comparing to previous bed of large biomass particle size (1180-1500) µm for the same weight percent. In addition, it is more dense compared to the previous bed of the same biomass particle size (500-600) µm for less biomass weight percent, 2.68%. For the former, this is because of the same biomass weight percent the number of small particles is larger than large particles, thereafter for the same unit area the number of small particles size was considerably occupied comparing to large particles. For the latter, because of the high biomass weight percent, 9.93 %, compared to 2.68% has a high dispersion and distribution density. In addition, the biomass distribution is looking more clear and uniform along the bed.

In this experiment, the hydrodynamic fluidization behavior and the bed changes because of air velocity increase are considerably similar to the bed behavior of the mixture shown in Figure D.3. Comparing to the previous experiment, the biomass dispersion along the bed appeared more dense and clear. This is because of the small biomass particle range (500-600) µm compared to biomass size in previous experiment, 1180-1500 µm. The fluidization bubbles were observed at 80 l/min. So, for this experiment the same conclusions as shown in previous experiment can be obtained.

Uo=0-40 l/min

Uo= 50 l/min

Uo= 70 l/min

Uo= 80 l/min

Uo=90 l/min

Uo= 100 l/min

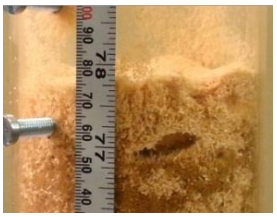

Uo= 110 l/min

Uo= 120 l/min

Top view, Uo= 120 l/min

Figure D. 5 Images of the cold fluidization of 8.3cm SPWB (500-600)µm/ 8.3cm Sand (500-600) µm mixture

APPENDIX E

Total Mass and Carbon Balances for All Experimental Tests

E.1 Gas analysis test

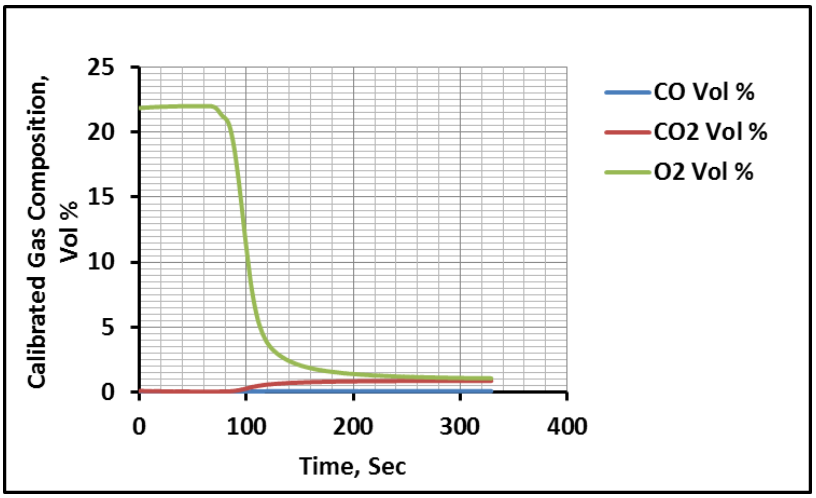

a)

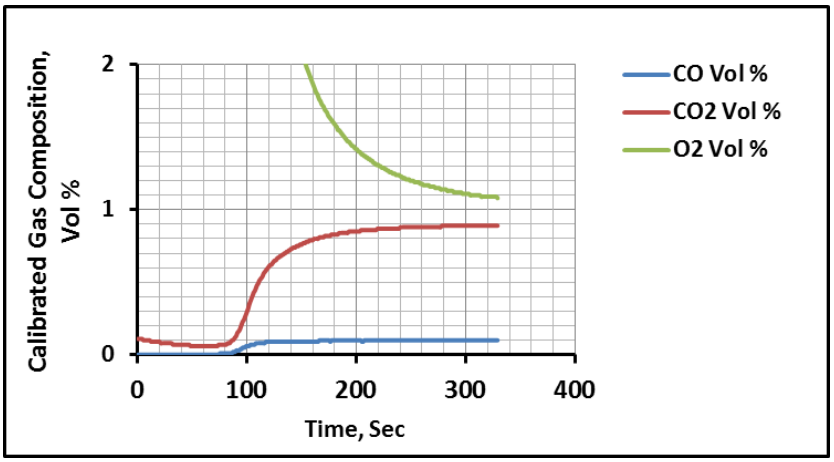

b)

Figure E. 1 Composition-time analyzing behaviour for standard gas mixture CO_2= 1%, O_2= 1% and CO= 0.1%: a) for normal scale and b) for enlargement scale

E.2 Total mass and carbon balances for all experimental tests

E.2.1 Air flow rate experimental tests group

Table E. 1 Total and carbon mass balances for air flowrate experiments: a) for SPWB and b) for IDPWB

a) SPWB

Air flow, l/min	Stream	Total mass balance, g/min			Carbon mass balance, g/min		
		Input	Output	% Error	Input	Output	% Error
44	Biomass Fuel	20.17	-	-	9.96	-	-
	Air	52.98	-	-	-	-	-
	Producer Gas	-	77.75	-	-	12.66	-
	Char+Sand	-	2.52	-	-	3.26	-
	Total	73.15	80.27	-9.74	9.96	15.92	-59.84
66	Biomass Fuel	30.26	-	-	14.95	-	-
	Air	79.47	-	-	-	-	-
	Producer Gas	-	113.16	-	-	18.19	-
	Char+Sand	-	8.71	-	-	9.69	-
	Total	109.73	121.87	-11.07	14.95	27.88	-86.52
88	Biomass Fuel	40.36	-	-	19.94	-	-
	Air	105.96	-	-	-	-	-
	Producer Gas	-	152.79	-	-	24.61	-
	Char+Sand	-	11.93	-	-	7.44	-
	Total	164.33	164.72	-12.57	19.94	32.05	-60.73

b) IDPWB

Air flow, l/min	Stream	Total mass balance, g/min			Carbon mass balance, g/min		
		Input	Output	% Error	Input	Output	% Error
44	Biomass Fuel	21.92	-	-	9.34	-	-
	Air	52.98	-	-	-	-	-
	Producer Gas	-	75.26	-	-	11.42	-
	Char+Sand	-	3.36	-	-	3.60	-
	Total	74.90	78.62	-4.96	9.34	15.02	-60.81
66	Biomass Fuel	32.87	-	-	14.00	-	-
	Air	79.47	-	-	-	-	-
	Producer Gas	-	104.09	-	-	14.91	-
	Char+Sand	-	2.98	-	-	0.97	-
	Total	112.34	107.08	-4.69	14.00	15.98	-14.14
88	Biomass Fuel	43.84	-	-	18.67	-	-
	Air	105.96	-	-	-	-	-
	Producer Gas	-	135.45	-	-	18.61	-
	Char+Sand	-	2.45	-	-	2.43	-
	Total	149.80	137.90	-7.95	18.67	21.04	-12.68

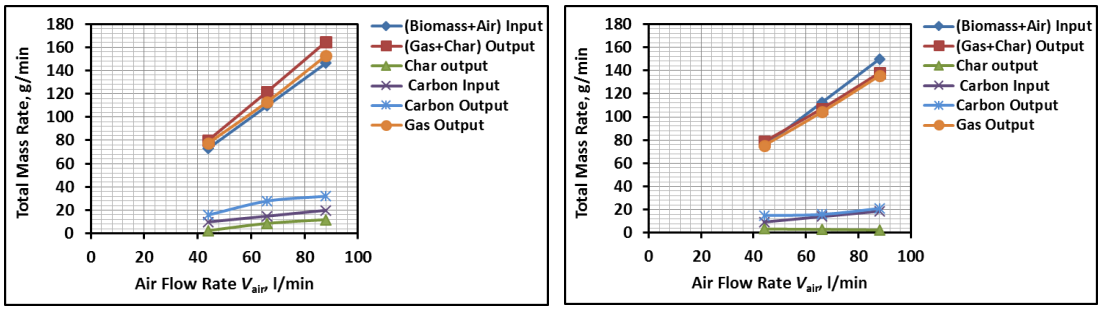

a) SPWB b) IDPWB

Figure E. 2 Total and carbon mass balances for air flowrate experiments: a) for SPWB and b) for IDPWB

E.2.2 Sand particle size experimental tests group

Table E. 2 Total and carbon mass balances for sand particle size experiments: a) for SPWB and b) for IDPWB

a) SPWB

Sand P.S, µm	Stream	Total mass balance, g/min			Carbon mass balance, g/min		
		Input	Output	%Error	Input	Output	%Error
(300-425)	Biomass Fuel	19.86	-	-	9.81	-	-
	Air	52.98	-	-	-	-	-
	Producer Gas	-	77.64	-	-	12.64	-
	Char+Sand	-	3.63	-	-	0.82	-
	Total	72.84	81.27	-11.57	9.81	13.46	-37.20
(425-500)	Biomass Fuel	34.21	-	-	16.90	-	-
	Air	90.31	-	-	-	-	-
	Producer Gas	-	132.45	-	-	21.60	-
	Char+Sand	-	6.01	-	-	4.99	-
	Total	124.52	138.47	-11.20	16.90	26.59	-57.31
(500-600)	Biomass Fuel	43.34	-	-	21.60	-	-
	Air	114.39	-	-	-	-	-
	Producer Gas	-	168.15	-	-	28.06	-
	Char+Sand	-	4.01	-	-	4.66	-
	Total	157.73	172.16	-9.15	21.60	32.72	-52.83

b) IDPWB

Sand P.S, µm	Stream	Total mass balance, g/min			Carbon mass balance, g/min		
		Input	Output	%Error	Input	Output	%Error
(300-425)	Biomass Fuel	21.92	-	-	9.34	-	-
	Air	52.98	-	-	-	-	-
	Producer Gas	-	68.07	-	-	6.24	-
	Char+Sand	-	3.36	-	-	3.61	-
	Total	74.90	71.43	4.63	9.34	9.85	-5.45
(425-500)	Biomass Fuel	37.61	-	-	16.02	-	-
	Air	90.91	-	-	-	-	-
	Producer Gas	-	108.33	-	-	10.71	-
	Char+Sand	-	3.72	-	-	0.00	-
	Total	128.52	112.05	12.82	16.02	10.71	33.14
(500-600)	Biomass Fuel	46.36	-	-	19.75	-	-
	Air	112.06	-	-	-	-	-
	Producer Gas	-	131.25	-	-	14.76	-
	Char+Sand	-	2.45	-	-	0.00	-
	Total	158.41	133.70	15.60	19.75	14.76	25.25

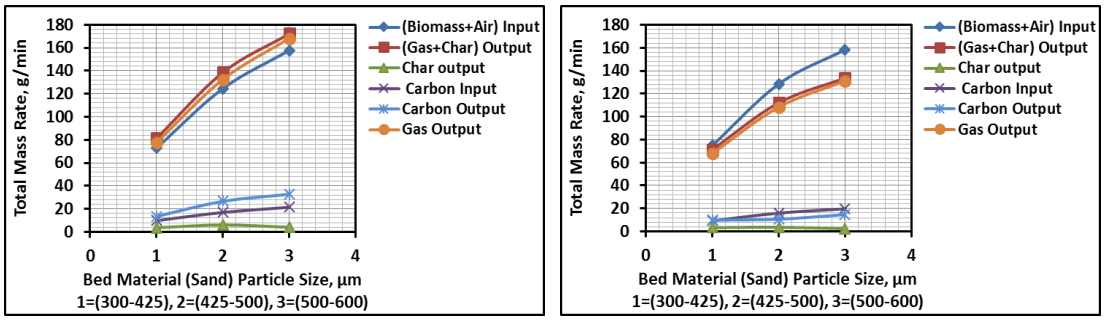

a) SPWB b) IDPWB

Figure E. 3 Total and carbon mass balances for sand particle size experiments: a) for SPWB and b) for IDPWB

E.2.3 Biomass particle size experimental tests group

Table E. 3 Total and carbon mass balances for biomass particle size experiments: a) for SPWB and b) for IDPWB

a) SPWB

Biomass P.S, µm	Stream	Total mass balance, g/min			Carbon mass balance, g/min		
		Input	Output	%Error	Input	Output	%Error
(300-425)	Biomass Fuel	10.68	-	-	5.28	-	-
	Air	36.12	-	-	-	-	-
	Producer Gas	-	47.96	-	-	5.76	-
	Char+Sand	-	2.13	-	-	0.89	-
	Total	46.80	53.71	-14.76	5.28	6.65	-25.98
(600-850)	Biomass Fuel	10.68	-	-	5.28	-	-
	Air	36.12	-	-	-	-	-
	Producer Gas	-	55.45	-	-	9.34	-
	Char+Sand	-	3.15	-	-	1.89	-
	Total	46.80	64.80	-38.43	5.28	11.23	-112.82
(1000-1180)	Biomass Fuel	10.68	-	-	5.28	-	-
	Air	36.12	-	-	-	-	-
	Producer Gas	-	45.79	-	-	5.28	-
	Char+Sand	-	5.98	-	-	3.13	-
	Total	46.80	51.07	-9.11	5.28	8.41	-59.43

b) IDPWB

Biomass P.S, µm	Stream	Total mass balance, g/min			Carbon mass balance, g/min		
		Input	Output	%Error	Input	Output	%Error
(300-425)	Biomass Fuel	21.92	-	-	9.34	-	-
	Air	52.98	-	-	-	-	-
	Producer Gas	-	85.51	-	-	12.66	-
	Char+Sand	-	1.32	-	-	6.61	-
	Total	74.90	86.82	-15.92	9.34	19.27	-106.33
(600-850)	Biomass Fuel	21.92	-	-	9.34	-	-
	Air	52.98	-	-	-	-	-
	Producer Gas	-	75.84	-	-	8.66	-
	Char+Sand	-	3.56	-	-	3.61	-
	Total	74.90	79.40	-6.03	9.34	12.27	-31.37
(1000-1180)	Biomass Fuel	21.92	-	-	9.34	-	-
	Air	52.98	-	-	-	-	-
	Producer Gas	-	74.29	-	-	6.70	-
	Char+Sand	-	4.48	-	-	5.39	-
	Total	74.90	78.77	-5.16	9.34	12.09	-29.51

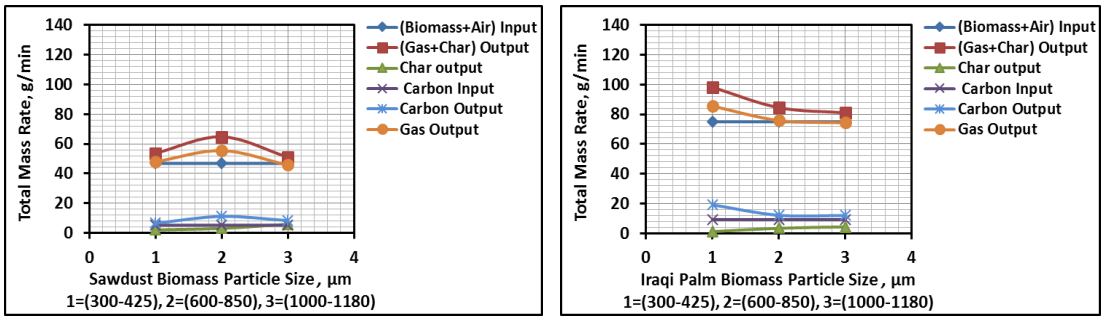

a) SPWB b) IDPWB

Figure E. 4 Total and carbon mass balances for biomass particle size experiments: a) for SPWB and b) for IDPWB

E.2.4 Static bed height experimental tests group

Table E. 4 Total and carbon mass balances for static bed height experiments: a) for SPWB and b) for IDPWB

a) SPWB

H_s, cm	Stream	Total mass balance, g/min			Carbon mass balance, g/min		
		Input	Output	%Error	Input	Output	%Error
4.15	Biomass Fuel	20.17	-	-	9.96	-	-
	Air	52.98	-	-	-	-	-
	Producer Gas	-	74.86	-	-	11.22	-
	Char+Sand	-	2.27	-	-	3.64	-
	Total	73.15	77.13	-5.44	9.96	14.86	-49.17
6.225	Biomass Fuel	20.17	-	-	9.96	-	-
	Air	52.98	-	-	-	-	-
	Producer Gas	-	82.13	-	-	14.73	-
	Char+Sand	-	3.64	-	-	0.82	-
	Total	73.15	85.77	-17.25	9.96	15.55	-56.11
8.3	Biomass Fuel	20.17	-	-	9.96	-	-
	Air	52.98	-	-	-	-	-
	Producer Gas	-	80.04	-	-	12.91	-
	Char+Sand	-	2.59	-	-	1.76	-
	Total	73.15	82,63	-12.96	9.96	14.67	-47.25

b) IDPWB

H_s, cm	Stream	Total mass balance, g/min			Carbon mass balance, g/min		
		Input	Output	%Error	Input	Output	%Error
4.15	Biomass Fuel	21.92	-	-	9.34	-	-
	Air	52.98	-	-	-	-	-
	Producer Gas	-	77.76	-	-	13.3	-
	Char+Sand	-	0.90	-	-	0.00	-
	Total	74.90	78.66	-5.02	9.34	13.3	-42.48
6.225	Biomass Fuel	37.61	-	-	16.02	-	-
	Air	90.91	-	-	-	-	-
	Producer Gas	-	80.67	-	-	13.71	-
	Char+Sand	-	3.36	-	-	3.61	-
	Total	128.52	84.03	-12.18	16.02	17.32	-85.46
8.3	Biomass Fuel	46.36	-	-	19.75	-	-
	Air	112.06	-	-	-	-	-
	Producer Gas	-	78.88	-	-	12.47	-
	Char+Sand	-	1.34	-	-	6.36	-
	Total	158.41	80.22	-7.10	19.75	18.83	-101.65

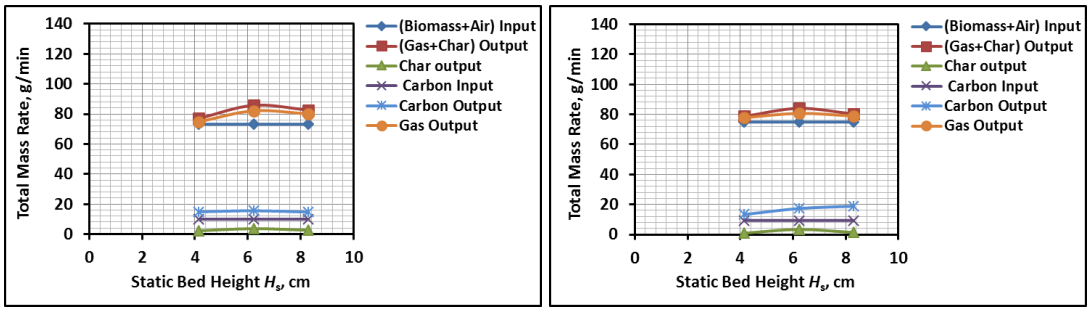

a) SPWB **b)** IDPWB

Figure E. 5 Total and carbon mass balances for static bed height experiments: a) for SPWB and b) for IDPWB

E.2.5 Equivalence ratio experimental tests group

Table E. 5 Total and carbon mass balances for equivalence ratio experiments: a) for SPWB and b) for IDPWB

a) SPWB

ER	Stream	Total mass balance, g/min			Carbon mass balance, g/min		
		Input	Output	%Error	Input	Output	%Error
0.2	Biomass Fuel	29.00	-	-	14.33	-	-
	Air	36.12	-	-	-	-	-
	Producer Gas	-	59.92	-	-	10.56	-
	Char+Sand	-	8.5	-	-	9.47	-
	Total	65.12	68.17	-4.68	14.33	20.03	-39.79
0.31	Biomass Fuel	19..00	-	-	9.39	-	-
	Air	36.12	-	-	-	-	-
	Producer Gas	-	51.16	-	-	6.78	-
	Char+Sand	-	6.05	-	-	5.57	-
	Total	55.12	57,21	-3.79	9.39	12.35	-31.56
0.5	Biomass Fuel	11.63	-	-	5.75	-	-
	Air	36.12	-	-	-	-	-
	Producer Gas	-	55.56	-	-	9.07	-
	Char+Sand	-	3.09	-	-	2.29	-
	Total	47.76	58.61	-22.73	5.75	11.36	-97.63
0.55	Biomass Fuel	10.68	-	-	5.28	-	-
	Air	36.12	-	-	-	-	-
	Producer Gas	-	57.99	-	-	6.74	-
	Char+Sand	-	2.31	-	-	1.88	-
	Total	46.80	60.29	-28.81	5.28	8.62	-63.32

b) IDPWB

ER	Stream	Total mass balance, g/min			Carbon mass balance, g/min		
		Input	Output	%Error	Input	Output	%Error
0.2	Biomass Fuel	41.71	-	-	17.77	-	-
	Air	52.98	-	-	-	-	-
	Producer Gas	-	86.73	-	-	14.90	-
	Char+Sand	-	15.10	-	-	6.58	-
	Total	94.69	101.83	-7.54	17.77	21.48	-20.88
0.277	Biomass Fuel	30.14	-	-	12.84	-	-
	Air	52.98	-	-	-	-	-
	Producer Gas	-	74.33	-	-	10.54	-
	Char+Sand	-	8.28	-	-	5.09	-
	Total	82.61	82.61	0.62	12.84	15.63	-21.74
0.381	Biomass Fuel	21.14	-	-	9.34	-	-
	Air	52.98	-	-	-	-	-
	Producer Gas	-	73.05	-	-	10.34	-
	Char+Sand	-	3.56	-	-	3.61	-
	Total	76.61	76.61	-2.28	9.34	13.95	-49.39
0.45	Biomass Fuel	18.55	-	-	7.90	-	-
	Air	52.98	-	-	-	-	-
	Producer Gas	-	67.96	-	-	8.79	-
	Char+Sand	-	0.97		-	2.88	
	Total	71.53	68.93	3.63	7.90	11.67	-47.72

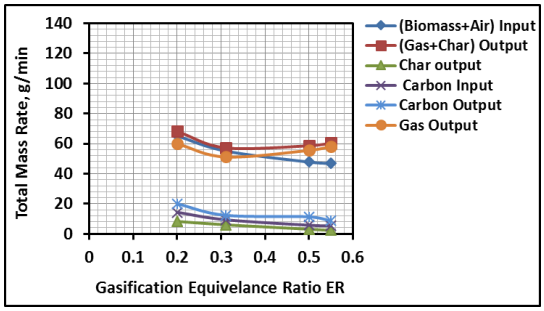

a) SPWB

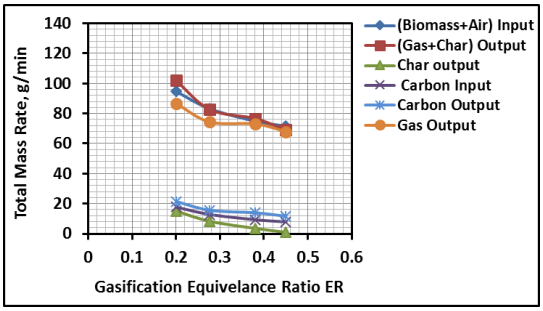

b) IDPWB

Figure E. 6 Total and carbon mass balances for equivalence ratio experiments: a) for SPWB and b) for IDPWB

E.2.6 Bed temperature T2 experimental tests group

Table E. 6 Total and carbon mass balances for bed temperature T2 experiments: a) for SPWB and b) for IDPWB

a) SPWB

T2, °C	Stream	Total mass balance, g/min			Carbon mass balance, g/min		
		Input	Output	%Error	Input	Output	%Error
360	Biomass Fuel	19.86	-	-	9.91	-	-
	Air	52.98	-	-	-	-	-
	Producer Gas	-	83.38	-	-	14.40	-
	Char+Sand	-	3.63	-	-	0.82	-
	Total	72.84	87.01	-19.45	9.91	15.22	-53.54
465	Biomass Fuel	19.86	-	-	9.91	-	-
	Air	52.98	-	-	--	-	-
	Producer Gas	-	88.95	-	-	13.76	-
	Char+Sand	-	1.30	-	-	0.55	-
	Total	72.84	90.25	-23.90	9.91	14.31	-44.42

b) IDPWB

T2, °C	Stream	Total mass balance, g/min			Carbon mass balance, g/min		
		Input	Output	%Error	Input	Output	%Error
360	Biomass Fuel	21.92	-	-	9.34	-	-
	Air	52.98	-	-	-	-	-
	Producer Gas	-	75.26	-	-	11.42	-
	Char+Sand	-	3.36	-	--	3.61	-
	Total	74.90	78.62	-4.96	9.34	15.03	-60.93
465	Biomass Fuel	21.92	-	-	9.34	-	-
	Air	52.98	-	-	-	-	-
	Producer Gas	-	82.03	-	-	13.89	-
	Char+Sand	-	3.386	-	-	2.77	-
	Total	74.90	85.41	-14.04	9.34	16.67	-78.50

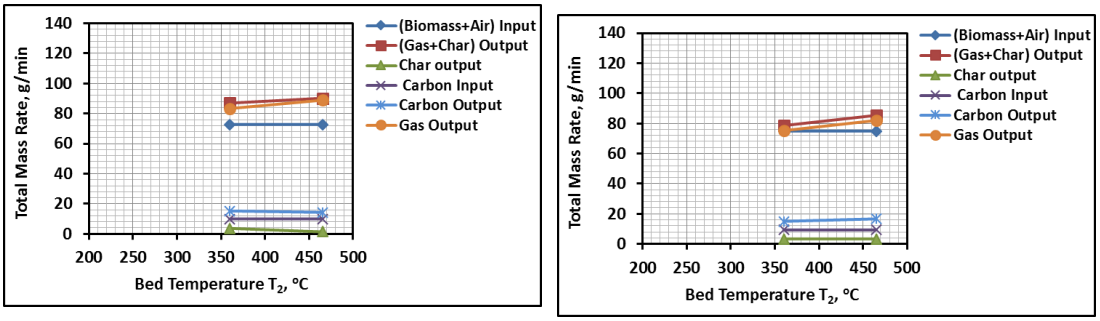

a) SPWB b) IDPWB

Figure E. 7 Total and carbon mass balances for bed temperature T2 experiments: a) for SPWB and b) for IDPWB

E.2.7 Holes number of distributor plate experimental tests group

Table E. 7 Total and carbon mass balances for distributor holes number experiments: a) for SPWB and b) for IDPWB

a) SPWB

N_{orf}	Stream	Total mass balance, g/min			Carbon mass balance, g/min		
		Input	Output	%Error	Input	Output	%Error
19	Biomass Fuel	19.87	-	-	9.81	-	-
	Air	52.98	-	-	-	-	-
	Producer Gas	-	68.71	-	-	8.54	-
	Char+Sand	-	5.8	-	-	6.96	-
	Total	72.85	74.51	-2.28	9.81	15.5	-60
85	Biomass Fuel	19.87	-	-	9.81	-	-
	Air	52.98	-	-	-	-	-
	Producer Gas	-	84.14	-	-	14.4	-
	Char+Sand	-	3.66	-	-	1.19	-
	Total	72.85	87.80	-20.52	9.81	15.93	-62.31
169	Biomass Fuel	19.87	-	-	9.81	-	-
	Air	52.98	-	-	-	-	-
	Producer Gas	-	58.97	-	-	6.35	-
	Char+Sand	-	3.33	-	-	4.1	-
	Total	72.85	62.3	-14.48	9.81	10.45	-6.45

b) IDPWB

N_{orf}	Stream	Total mass balance, g/min			Carbon mass balance, g/min		
		Input	Output	%Error	Input	Output	%Error
19	Biomass Fuel	18.55	-	-	7.9	-	-
	Air	52.98	-	-	-	-	-
	Producer Gas	-	61.31	-	-	5.95	-
	Char+Sand	-	6.84	-	-	3.99	-
	Total	71.53	68.15	4.73	7.9	9.94	-25.83
85	Biomass Fuel	18.55	-	-	7.9	-	-
	Air	52.98	-	-	-	-	-
	Producer Gas	-	67.96	-	-	8.79	-
	Char+Sand	-	3.33	-	-	2.9	-
	Total	71.53	71.29	0.34	7.9	11.69	-48.01
169	Biomass Fuel	18.55	-	-	7.9	-	-
	Air	52.98	-	-	-	-	-
	Producer Gas	-	56.19	-	-	7.9	-
	Char+Sand	-	1.95	-	-	2.81	-
	Total	71.53	62.3	18.71	7.9	10.71	-35.62

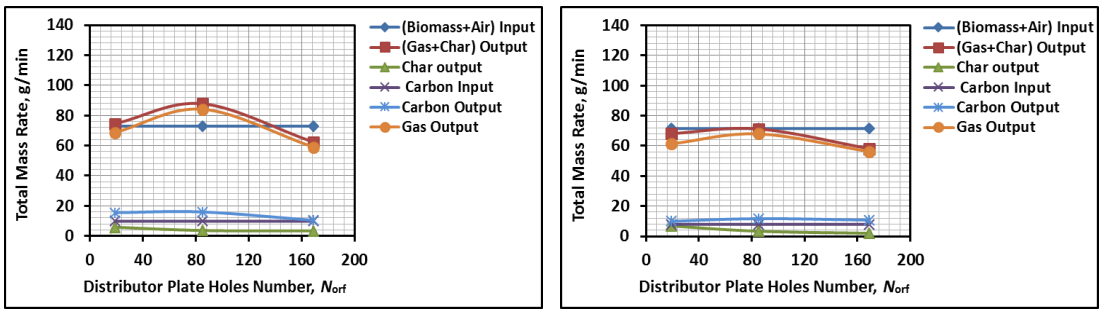

a) SPWB b) IDPWB

Figure E. 8 Total and carbon mass balances for distributor holes number experiments: a) for SPWB and b) for IDPWB